Autophagy in *Plasmodium falciparum* intraerythrocytic stages

Andrew Michael Tomlins BSc

Submitted in fulfilment of the requirements for the Degree of PhD

Institute of Infection, Immunity and Inflammation

College of Medical, Veterinary and Life Sciences

University of Glasgow

September 2012

Abstract

Apicomplexan parasites of the genus *Plasmodium* are the causative agents of malaria, which along with tuberculosis and AIDS contributes to half of all human deaths from infectious disease. Five different *Plasmodium* species are known to cause malaria infections in humans with approximately 220 million new infections attributed each year. The major species in regards to disease severity and prevalence *is P. falciparum*. Great effort has been applied to eradication of malaria but this disease remains a major global health and economic burden. A major obstacle to eradication efforts is the widespread resistance to commonly used therapies. Improving our understanding of resistance mechanisms and identifying novel drug targets are essential weapons in the fight against malaria. A sound understanding of the basic biology of *Plasmodium* parasites is therefore vital.

Autophagy is a cellular process believed to be conserved amongst all eukaryotes but has not yet been characterised in *P. falciparum*. Exploring this process in *P. falciparum* might lead to the elucidation of exploitable drug targets for future therapeutic intervention strategies. Autophagy is a homeostatic process facilitating the lysosomal turnover of long-lived proteins and cellular components. It can also be upregulated in response to triggers such as nutrient deprivation and during periods of cellular remodelling. It would seem likely that *P. falciparum* might rely on autophagy during the multiple differentiation events needed throughout its complex life cycle and when adapting to changes in cellular environments with varying nutrient availabilities.

A number of proteins are known to be involved in autophagy in other organisms. This study aimed to explore the potential process of autophagy in *P. falciparum* via the characterisation of a major autophagy-related protein, ATG8. This protein is commonly used as a marker for autophagy in other organisms as its expression level, lipidation state and localisation are indicative of an active autophagic process. A bioinformatic screen of the *P. falciparum* genome revealed genes likely to encode ATG8 and other autophagy-related proteins. The putative ATG8 (*Pf*ATG8) was shown to be a functional homologue of the ATG8 of *Saccharomyces cerevisiae*, the reference organism for autophagy and was also

found to be differentially expressed during the intraerythrocytic development of *P. falciparum*. In order to benefit further characterisation of *Pf*ATG8, transgenic *P. falciparum* lines were generated in which fluorescently tagged *Pf*ATG8 fusion proteins were expressed. These were used to demonstrate that *Pf*ATG8 is post-translationally modified via lipid conjugation, similar to ATG8 in other organisms. Through the expression of a truncated version of a fluorescently tagged *Pf*ATG8, this lipid modification was shown to be entirely dependent on the C-terminal glycine residue of *Pf*ATG8, as has been demonstrated for other ATG8 homologues. However, in contrast to ATG8 homologues in other organisms, *Pf*ATG8 did not appear to be involved in a canonical autophagic process. Attempts to influence *Pf*ATG8 expression, lipidation or localisation through methods known to manipulate autophagy in other organisms failed to illicit a response. It was instead found that *Pf*ATG8 specifically localises to the apicoplast of *P. falciparum*, likely via association with the organelle's outer membrane(s). When the apicoplast was disrupted, *Pf*ATG8 was seen to associate with apicoplast-targeted vesicles. The properties displayed by *Pf*ATG8 in the intraerythrocytic stages of *P. falciparum*, led to the hypothesis that it may play a role in apicoplast homeostasis, potentially via participation in the relatively enigmatic processes behind delivery of apicoplast-targeted proteins and lipids to the developing organelle. This is in starck contrast to the ATG8 homologue in the closely related parasite *Toxoplasma gondii*, which has been reported to function in mitochondrial homeostasis. Deletion of the *Pfatg8* gene was not possible, even when the fluorescently tagged copy of the *Pf*ATG8 protein was co-expressed by the parasites. This suggested that the *Pf*ATG8 protein may have an essential role in the survival of *P. falciparum* erythrocytic stages.

The apparent parasite-specific role for *Pf*ATG8 not observed for human ATG8 homologues coupled with the potential essentiality of this role may prove to be exploitable for therapeutic design.

Author's declaration

I, Andrew Michael Tomlins hereby declare that I am the sole author of this thesis and performed all of the work presented, with the following exceptions. This work has not been submitted for any other degree.

Chapter 1:

Figure 1.6 was compiled from microscopic images collected by Dr. P. McMillan (University of Melbourne, Australia).

Chapter 3:

The initial identification of potential homologues to components of the ATG8 and ATG12 conjugation pathways in *P. falciparum* shown in Figure 3.1 was performed by Dr. R. Williams (University of Strathclyde, UK).

The construct *Lm*ATG12-pCM186 was provided by Dr. R. Williams.

cDNA was made by Dr. E. Patzewitz (University of Nottingham, UK).

Generation of the construct His-*Pf*ATG8-pET28a(+), His-*Pf*ATG8 expression and purification (as shown in purification A in Figure 3.6) was performed by Dr. W. Proto (University of Glasgow, UK).

Chapter 4:

The constructs *Pfhsp*86-pDONRP2R-P3 and eYFP-pDONR221 were provided by Dr. E. Patzewitz. The construct mCherry-pDONR221was provided by Dr. W. Proto.

Culturing of 3D7 *P. falciparum* parasites in preparation for time course experiments was performed by Bruno Luukinen.

Acknowledgements

Firstly I would like to sincerely thank Prof. Sylke Müller and Prof. Jeremy Mottram for giving me the opportunity to study and grow here in Glasgow. Being a part of the Müller lab has been crucial to my development both as a scientist and on a personal level. I am grateful for the opportunities presented to me and I hope that I have made the most of them. Also Prof. Graham Coombs must be acknowledged for facilitating time spent at the University of Strathclyde, along with his invaluable input and support.

I would also like to thank former and current members of the Müller and other labs, in particular Janet, Will, Roderick and Ellie, who have put up with both my 'quick questions' and protracted ramblings. The excellent working environment in the GBRC is made possible not only by the excellent facilities but more so by the intelligence, openness and humour of all that work here.

I would like to thank my parents and my sister Christine for inspiration, encouragement and keeping my room clean in my absence. I think that I have got my money's worth from Glasgow and the Premier Inn has done well out of my Mum and Dad. Your support has been the linchpin to everything I have done and I hope that I've done (/are doing) you proud.

I would finally like to thank Chanelle, for putting her life on hold for 4 years to keep me happy. I will forever be indebted to you for your tireless love and support, not to mention your feigned interest in what I do! Now we can start anew. X

For materials used in this study, I would like to thank the European *Saccharomyces cerevisiae* Archive for Functional Analysis (EuroScarf) for the use of wild type and mutant yeast lines and yeast expression vectors used in complementation experiments.

I would also like to thank Prof. Daniel J. Klionsky, University of Michigan, USA, for the use of the anti-aminopeptidase antibody used in complementation experiments.

I would also like to thank Prof. Geoffrey McFadden, University of Melbourne, Australia, for the use of the Gateway destination vectors used in transfection of *P. falciparum*.

I would also like to thank Prof. Alan Cowman, Walter and Eliza Hall Institute of Medical Research, Melbourne, Australia, for the use of the pCC-4 construct used in knockout attempts.

I would finally like to thank Dr. Gordon Langsley, Institut Cochin, Paris, France, for the use of peptide antibodies against *Pf*ATG8 and *Pf*Rab7.

Table of contents

List of tables

List of figures

Definitions / abbreviations

µ	Micro
µg	Microgram
µl	Microlitre
µm	Micrometer
µM	Micromolar
µmol	Micromoles
3' UTR	Three prime untranslated region
5-FC	5-Fluorocytosine
5' UTR	Five prime untranslated region
AIDS	Acquired immunodeficiency syndrome
Amp	Ampere
AmpR	Ampicillin resistance cassette
AP1	Aminopeptidase 1
atg	Autophagy-related gene
ATG	Autophagy-related gene product (protein)
ATP	Adenosine triphosphate
att	Recombination site in Multisite Gateway vectors
BCDH	*P. falciparum* branched chain alpha-keto acid dehydrogenase acyltransferase subunit
BLA	Blasticidin-S-HCl
BLAST	Basic logical alignment search tool
bp	Base pairs
BSA	Bovine serum albumin
BSD	Blasticidin-S-deaminase
°C	Degrees Celsius
ccdB	Cytotoxic protein ccdB (gene)
CDC	Centers for Disease Control and Prevention
Ch	*Cryptosporidium hominis*
Cm	*Cryptosporidium muris*
CmR	Chloramphenicol resistance cassette
CQ	Chloroquine
C-terminal	Carboxyl terminal
cDNA	Complementary DNA
Cvt	Cytoplasm to vacuole targeting
Da	Daltons
DABCO	1,4-diazabicyclo[2.2.2]octane
ddH_2O	Double distilled water
DEPC	Diethylpyrocarbonate
DHFR	Dihydrofolate reductase
DIC	Differential interference contrast
DMSO	Dimethyl sulphoxide
DNA	Deoxyribonucleic acid
DNase	Deoxyribonuclease
DTT	Dithiothreitol
DV	Digestive vacuole
EBSS	Earle's balanced salt solution
ECL	Enhanced chemiluminescence
EDTA	Ethylene diamine tetraacetic acid
EGTA	Ethylene glycol tetraacetic acid

EMBL-EBI	European Molecular Biology Laboratory – European Bioinformatics Institute
ER	Endoplasmic reticulum
EuroScarf	European *Saccharomyces cerevisiae* Archive for Functional Analysis
f	Femto
FITC	Fluoresceine-isothiocyanate
FKBP	(FKBP12) - 12 kDa FK506-and rapamycin-binding protein
fmoles	femtomoles
fwd	Forward
G	Glycine
g	Gram
g	Gravitational acceleration
gDNA	Genomic deoxyribonucleic acid
GFP	Green fluorescent protein
Gway	Gateway
hDHFR	Human dihydrofolate reductase
HEPES	4-(2-Hydroxyethyl)-piperazineethanesulphonic acid
His	Poly-histidine
HRP	Horseradish peroxidase
Hs	*Homo sapiens*
IC_{50}	Concentration at which 50 % growth inhibition occurs
IMAC	Immobilized metal ion affinity chromatography
IPTG	Isopropyl-O-D-thiogalactopyranoside
KanR	Kanamycin resistance cassette
k	Kilo
kb	Kilobases
kDa	Kilo Daltons
KO	Knockout
Kpsi	Kilo pounds per square inch
l	Litre
LacI	Repressor of the Lac operon
LacZ	ß-galactosidase encoding gene
LB	Luria Bertani
Lm	*Leishmania major*
LMP	Low melting point
m	Meter
M	Molar
MACS	Magnet activated cell sorting
mbar	Millibar
MES	2-(*N*-morpholino)ethanesulfonic acid
mg	Milligram
min	Minute
ml	Millilitre
mM	Millimolar
n	Nano
Nc	*Neospora caninum*
ng	Nanogram
NIH	National Institutes of Health (US)
Ni-NTA	Nickel-nitriloacetic acid
nm	Nanometer
nM	Nanomolar
N-terminal	Amino terminal
OD_{600}	Optical density at 600 nm

ORF	Open reading frame
p	Pico
PAGE	Polyacrylamide gel electrophoresis
Pc	*Plasmodium chabaudi chabaudi*
Pb	*Plasmodium berghei*
*Pb*DT 3'	*Plasmodium berghei* dihydrofolate reductase-thymidylate synthase 3' untranslated region
PBS	Phosphate buffered saline
PCR	Polymerase chain reaction
PEG 3350	Polyethylene glycol 3350
Pf	*Plasmodium falciparum*
*Pf*CAM 5'	*Plasmodium falciparum* calmodulin 5' untranslated region
*Pf*hrpII 3'	*Plasmodium falciparum* histidine-rich protein II 3' untranslated region
*Pfhsp*86	*Plasmodium falciparum* heat shock protein 86 (gene)
*Pf*hsp86 5'	*Plasmodium falciparum* heat shock protein 86 5' untranslated region
Phage F1	Origin of single stranded replication
Pk	*Plasmodium knowlesi*
PMSF	Phenylmethyl sulphonyl fluoride
pmol	Picomoles
pUC ori	origin of double stranded replication
Pv	*Plasmodium vivax*
Py	*Plasmodium yoelii*
R	Pearson's coefficient of correlation
RBC	Red blood cell
rev	Reverse
RNA	Ribonucleic acid
RNase	Ribonuclease
Sc	*Saccharomyces cerevisiae*
SC medium	Selective medium (-uracil)
S.D.	Standard deviation
SDS	Sodium dodecyl sulphate
sec	Seconds
S.E.M.	Standard error of the mean
Ta	*Theileria annulata*
TAE	Tris-acetate buffer containing EDTA
Tb	*Trypanosoma brucei*
TB	Terrific Broth
TBE	Tris-borate buffer containing EDTA
TE	Tris buffer containing EDTA
TEMED	N,N,N',N'-tetramethylethylenediamine
Tg	*Toxoplasma gondii*
UK	United Kingdom
U.S.A	United States of America
UV	Ultraviolet
V	Volt
v/v	Volume per volume
w/v	Weight per volume
WHO	World Health Organisation
X-Gal	5-bromo-4-chloro-indolyl-ß-D-galactopyranoside
YNB	Yeast nitrogen base
YPD medium	Yeast extract peptone glucose medium

1 Introduction to malaria and autophagy

1.1 Malaria and *Plasmodium falciparum*

Malaria is one of the most important public health concerns globally with around half of the world's population, 3.3 billion people, at risk. It is found in over 100 countries mainly in sub-Saharan Africa, but also in other tropical regions (Figure 1.1). In 2010, approximately 220 million new cases were reported, leading to an estimated 655,000 deaths, 90 % of which were in Africa (World Health Organisation (WHO)(a)). Most fatalities occur in vulnerable groups – children under 5 years old, pregnant women and immune-compromised individuals (Desai *et al.*, 2007).

Malaria is caused in humans by infection with one (or more) of five species of protozoan parasites of the genus *Plasmodium*; *P. falciparum*, *P. vivax*, *P. ovale*, *P. malariae* and *P. knowlesi*. *Plasmodium* parasites are transmitted to humans by female *Anopheles* mosquitoes. About 30 – 40 species of *Anopheles* mosquito can act as a vector for the human malaria *Plasmodium spp*. (Centers for Disease Control and Prevention (CDC)). As the sexual development of the parasite occurs in the mosquito vector, malaria endemic areas only occur in regions where *Anopheles* mosquitoes are found. Disease burden is therefore intrinsically linked to mosquito populations and transmission rates. These can be greatly influenced by environmental factors such as rain fall, resulting in a malaria 'season' coinciding with periods when rainfall is high and mosquito breeding rates are high. As well as seasonal variations in transmission and infection rates, expansion of mosquito environments, such as following flooding, or large scale movement of humans, can both have a large effect on transmission and infection rates. This can be particularly heightened when individuals from non-endemic areas, who will have poor immunity due to lack of exposure, move into a malaria endemic region. Crucially, environmental factors also affect the ability of *Plasmodium* parasites to execute sexual development, with environmental temperature known to be a controlling factor in developmental transition (Ogwan'g *et al.*, 1993). This contributes to the fact that malaria is not endemic in many regions where *Anopheles* mosquitoes are present. Recently, vector control strategies appear to be having an impressive impact on disease control (Karunamoorthi, 2011).

Typical clinical symptoms of malaria include high fever, malaise, myalgia and vomiting (CDC). These symptoms will be absent for the first 10 – 15 days after the actual inoculation event and then often occur in bouts every 24 – 72 hours, depending on the species of parasite responsible for infection. More severe symptoms are associated with infection by *P. falciparum*. These can include severe anaemia, acute renal failure, pulmonary oedema and coma, resulting from infection of the central nervous system. These severe disease outcomes are largely the result of the ability of the *P. falciparum* parasite to cause the adhesion of infected and uninfected red blood cells in small capillaries, resulting in the disruption of blood flow to vital organs (Franke-Fayard *et al.*, 2010).

As well as being a major health concern, malaria represents a major economic burden in endemic regions. Malaria has been calculated to be responsible for a 1 % reduction of gross domestic product in some endemic countries (WHO(a)). Loss of working productivity, combined with the requirement for up to 40 % of total public health expenditure to be dedicated to tackling malaria, contribute to the fact that malaria disproportionately affects the poorest countries of the world.

Malaria mortality rates have fallen by 25 % globally since 2010 (WHO(b)). Improving diagnostic, treatment and preventative methods, including insecticide spraying and use of bed nets have contributed to this decrease. Malaria is currently the focus of improved elimination and global eradication efforts (Alonso *et al.*, 2011, Feachem and Sabot, 2008). However, resistance to commonly used treatment therapies is a growing problem (Volkman *et al.*, 2012) and no vaccine for malaria is currently available for widespread employment (Schwartz *et al.*, 2012). With a limited repertoire of available anti-malarial drugs and no decision on the implementation of a malaria vaccine until 2015 (WHO(c)), it seems that eradication will not be achievable without further advances in these areas.

Web resources used for this section include:-

WHO(a) (http://www.who.int/features/factfiles/malaria/index/en) [Last accessed 14/09/2012].

WHO(b) (http://www.who.int/topics/malaria/en) [Last accessed 14/09/2012].

WHO(c) (http://www.who.int/mediacentre/factsheets/fs094/en/index.html) [Last accessed 14/09/2012].

CDC (http://www.cdc.gov/malaria/about/index) [Last accessed 14/09/2012].

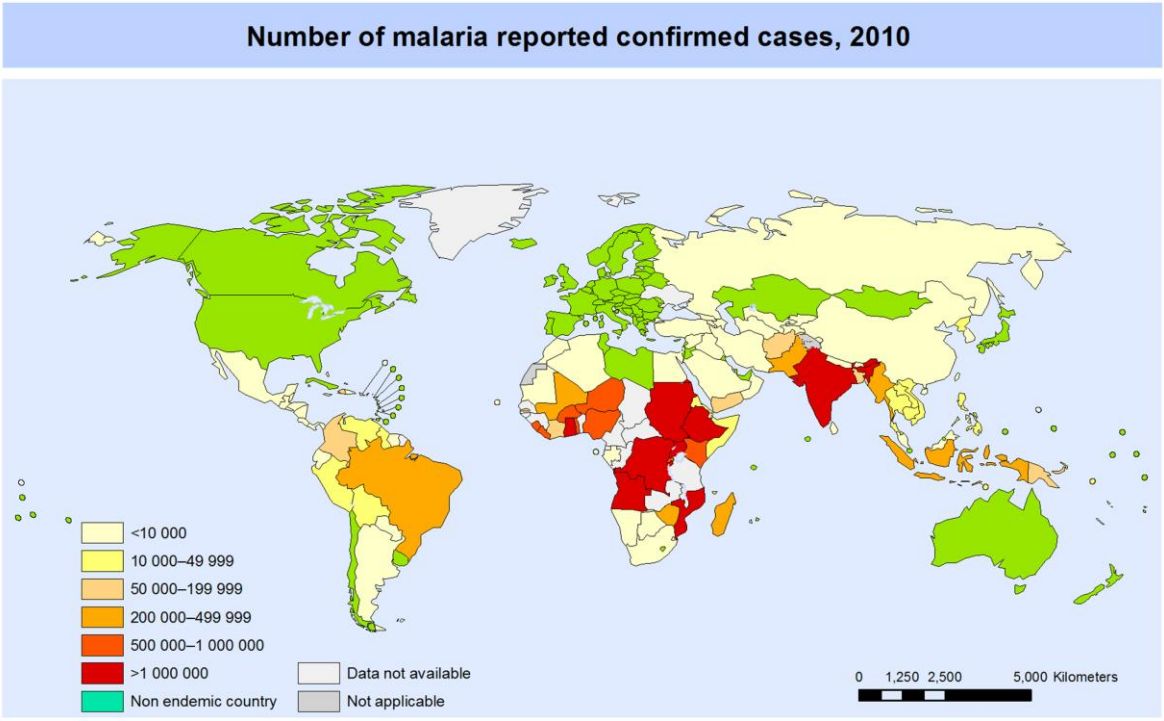

Figure 1.1: Global malaria prevalence in 2010.

Malaria is endemic in over 100 countries, primarily in sub-Saharan Africa, South and South East Asia and South America. Malaria has been eliminated from 28 countries including the United States of America in 1951 (WHO, 2011). Countries shaded red have a high prevalence of malaria. Countries shaded green have no communicable transmission of malaria.

Printed with permission from the World Health Organisation. (Original legend reads 'The boundaries and names shown and the designations used on this map do not imply the expression of any opinion whatsoever on the part of the World Health Organisation concerning the legal status of any country, territory, city or area or of its authorities, or concerning the delimitation of its frontiers or boundaries').

1.1.1 Exoerythrocytic development

The life cycle of *Plasmodium spp*. is complex, involving developmental transitions in both the *Anopheles* mosquito and the mammalian host. The life cycle can be roughly divided into the asexual cycle, which takes place in the mammalian host, and the sexual stages of development, which take place in the mosquito vector (Figure 1.2). Upon taking a blood meal from an infected

mammal, a female *Anopheles* mosquito will acquire female macrogametocytes and male microgametocytes that circulate in the mammalian host's peripheral blood (Alano, 2007). The sudden change in environment triggers rapid cellular remodelling and exit from host erythrocytes. The male microgametocyte converts into up to 8 motile flagellated microgametes, which are capable of fertilizing a female macrogamete, which emerges from its erythrocyte in an enlarged spherical form. The zygote, which forms following fertilization, is capable of surviving in the hostile environment of the mosquito gut, where it develops further, firstly into a tetraploid motile ookinete, and then into an oocyst following meiosis (Sinden *et al.*, 1985). The motility of the ookinete facilitates traversal of the peritrophic membrane and a layer of midgut cells, enabling the development of the oocyst on the basal lamina (Matuschewski, 2006). Approximately 12 days later the oocyst has developed into a sporoblast, in which sporozoites form through multiple rounds of asexual proliferation. Sporozoites then actively egress from the sporoblast and enter the haemolymph system and eventually make their way into the salivary glands following penetration of the surrounding acinar cells (Matuschewski, 2006).

Upon reaching the salivary glands, sporozoites mature into an invasion competent form capable of gliding motility. This is an actin-dependent motility mechanism that allows transit across a substrate (Morahan *et al.*, 2009). This motility facilitates transit through the skin, away from the bite site, where sporozoites are introduced in varying numbers during salivation of a feeding mosquito (Hellmann *et al.*, 2011, Singer and Frischknecht, 2012). Sporozoites must then reach the liver where they invade hepatocytes and reside within the replication-permissive intravacuolar niche of the parasitophorous vacuole (PV) (Matuschewski, 2006). The route they take is still not completely clear (Baldacci and Menard, 2004). They can either enter the bloodstream or lymphatic circulation in order to reach the liver. These processes may or may not involve the penetration of additional cell types, such as immunocompetent cells in the lymphatic system (Krettli and Dantas, 2000). Once at the liver, sporozoites are sequestered via interaction of their predominant surface protein, circumsporozoite protein, with subsets of heparan sulphate proteoglycans abundant on liver endothelial cells (Baldacci and Menard, 2004). Sporozoites sequestered in the liver can then invade hepatocytes, likely after penetration of

specialised macrophages called Kupffer cells, which line the liver sinusoid. Once residing within a PV inside a hepatocyte, sporozoites differentiate and undergo massive asexual multiplication over 5 – 15 days, depending on species, to form up to 30,000 erythrocyte-infective merozoites (Mikolajczak *et al.*, 2011). The liver stages of *P. vivax* and *P. ovale* are capable of differentiating into dormant hypnozoite forms, which can cause relapses of disease many years after the initial infection (Markus, 2012). The mechanism of merozoite release may also differ according to species. In *P. berghei* and *P. yoelii*, breakdown of the PV precedes the release of merosomes, large membrane-bound vesicles containing multiple merozoites, which ensures that the released merozoites reach the bloodstream before being exposed to the host immune response (Sturm *et al.*, 2006). This process has not yet been elucidated in *P. falciparum* (Prudencio *et al.*, 2006).

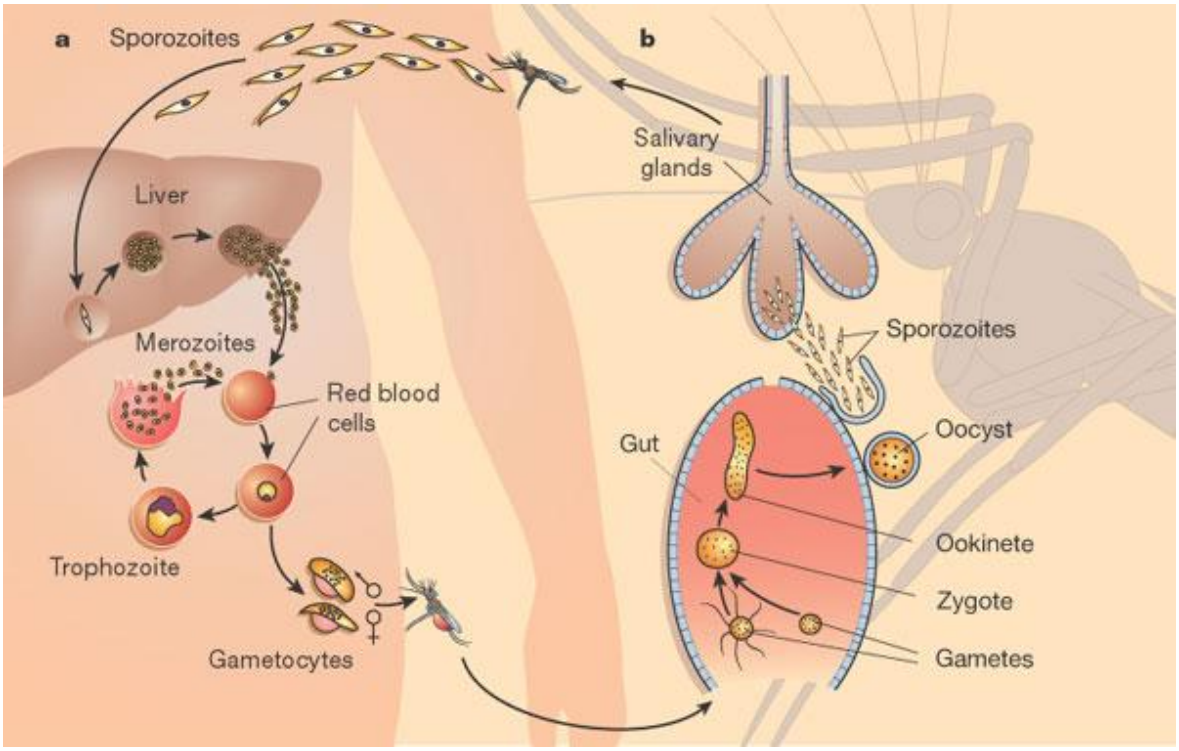

Figure 1.2: Life cycle of *Plasmodium spp*. (taken from (Wirth, 2002)).

(a) Sporozoites injected into the skin by a feeding female *Anopheles* mosquito make their way to the liver where they invade hepatocytes. Asexual development leads to the release of tens of thousands of erythrocyte-infective merozoites into the bloodstream. Invasion of erythrocytes allows further asexual multiplication to form about 20 newly infective merozoites. A population of asexual erythrocytic stage parasites switch to develop into sexual gametocyte forms.

(b) Gametocytes circulate in the bloodstream and are taken up into the midgut of a feeding mosquito. Following further differentiation into gametes, they fertilize each other to form a zygote. The zygote differentiates further into a motile ookinete and then an oocyst, in which asexual multiplication generates sporozoites. Sporozoites then travel to the mosquito salivary glands ready to be injected into another mammalian host.

Printed with permission from the Nature Publishing Group.

1.1.2 Intraerythrocytic development

Merozoites begin the asexual, intraerythrocytic cycle by invasion and multiplication within circulating erythrocytes. *P. falciparum* parasites are able to cause rosetting; clustering of infected and uninfected erythrocytes and interaction with blood vessel endothelial cells (Chen *et al.*, 1998). This is associated with more severe disease outcomes (Rowe *et al.*, 1997). Erythrocytes are often considered to be cellular bags of haemoglobin specialised for the transport of O_2 and CO_2 around the mammalian body (Tilley *et al.*, 2011). Haemoglobin is a metalloprotein which is modified to oxyhaemoglobin, which transports O_2 from the lungs to the rest of the body and carbaminohaemoglobin, which transports CO_2 back to the lungs (Klinken, 2002). Merozoites can invade an

erythrocyte within seconds (Boyle *et al.*, 2010, Cowman and Crabb, 2006). Development within an erythrocyte again varies according to species. *P. falciparum* parasites progress through ring, trophozoite and schizont stages, before forming on average 20 new merozoites within 48 hours of the initial invasion event (Tilley *et al.*, 2011). While residing in host erythrocytes, parasites avoid the display of their antigens via major histocompatibility complexes that would usually be the case in other cell types. However, in balance they must contend with the lack of host cell endocytic and secretory pathways which might be exploited to target host cell contents to the resident parasite. Intraerythrocytic parasites counter this potential obstacle by remodelling the host erythrocyte with parasite-derived tubular networks to both expand the effective surface area of interaction between parasite and host cell and to facilitate the export and import of extracellular factors (Hanssen *et al.*, 2010, Silvie *et al.*, 2008). The characteristic amoeboid appearance of trophozoite stage parasites is shown in Figure 1.3. While within the erythrocyte, *Plasmodium* parasites consume around 75 % of the erythrocyte's haemoglobin, primarily as a source of nutrients but also as a way of regulating osmotic integrity and as a way of generating space for development (Abu Bakar *et al.*, 2010). Continuation of the intraerythrocytic cycle can be almost perpetual (Cox, 2010) and is responsible for the majority of the disease pathology (Tilley *et al.*, 2011). The completion of the parasite life cycle occurs with the differentiation of a subset of erythrocytic asexual parasites into the sexual gametocyte stages (Reininger *et al.*, 2012). Male and female gametocytes are characterised by the presence of a sub-pellicular membrane complex analogous to the inner membrane complex seen in other Apicomplexan parasites (Dearnley *et al.*, 2012). The gametocytes of *P. falciparum* transition through 5 distinct stages before reaching a point at which, following ingestion by a feeding *Anopheles* mosquito, microgametes and macrogametes can be formed (Baker, 2010).

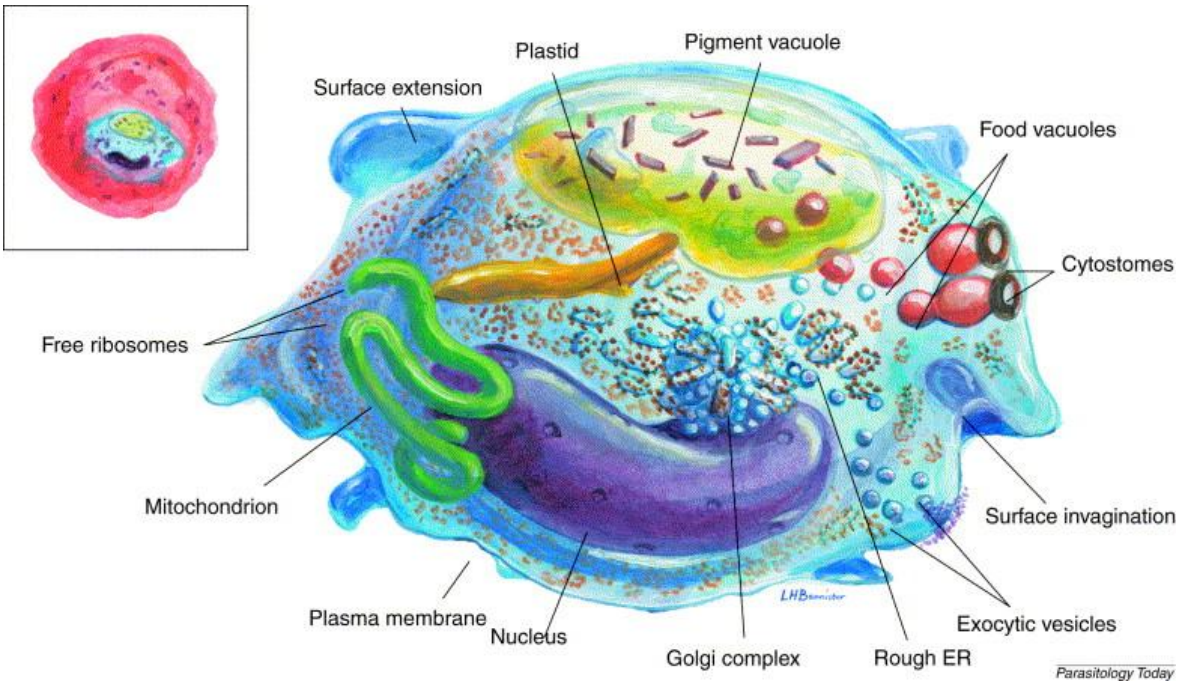

Figure 1.3: Schematic representation of a trophozoite stage *P. falciparum* parasite. (taken from (Bannister *et al.*, 2000)).

The trophozoite stage parasite resides within a host erythrocyte and is surrounded by a parasitophorous vacuole (not shown). An amoeboid form with surface extensions and invaginations increases the area of interaction with the host erythrocyte. The parasite ingests host erythrocyte cytosol and digests haemoglobin, generating haemozoin pigment crystals as waste. The nucleus, mitochondrion, apicoplast and other organelles develop as the parasite undergoes multiplication via schizogony.

Printed with permission from the Elsevier Publishing Group.

1.1.3 Cellular differentiation and organelle biology

The ring, trophozoite, schizont and merozoite stages that constitute the erythrocytic asexual cycle are characterised by their differing cellular architecture, organellar composition and metabolism, underpinned by differential gene expression (Bozdech *et al.*, 2003, Otto *et al.*, 2010). A great deal of cellular remodelling is needed concurrently and at each transitional stage of parasite development along with tightly controlled temporal protein expression (Florens *et al.*, 2002). This is typified by the *de novo* biogenesis of stage-specific organelles and their subsequent loss upon transition to downstream stages of development. Merozoites and other parasite stages possess a core set of organelles common to most eukaryotes, such as a nucleus, endoplasmic reticulum, a simplified Golgi network and a single mitochondrion (Tilley *et al.*, 2011). The parasite also possesses an apicoplast, a remnant plastid

derived from secondary endosymbiosis (McFadden *et al.*, 1996). At various stages the parasite also develops a variety of parasite-specific organelles. In intraerythrocytic parasites a lysosome-like compartment called the digestive vacuole (DV) is formed (Abu Bakar *et al.*, 2010), while in merozoite stage parasites a set of apical organelles can be found. These are composed of the rhoptries, micronemes, exonemes and dense granules and are essential for the invasion of host cells (Bannister and Mitchell, 2009).

1.1.3.1 Apical organelles and invasion

The apical organelles give Apicomplexan parasites their name (Cowman and Crabb, 2006). Late in schizogony, proteins needed for invasion of new erythrocytes are expressed and packaged into the apical organelles ready for release when merozoites egress from an erythrocyte and invade another (Figure 1.4) (Srivastava *et al.*, 2010). It remains uncertain quite how the micronemes and rhoptries are generated *de novo* each asexual cycle; the precursors from which these organelles are generated have yet to be identified (Baumeister *et al.*, 2010). Compartmentalisation of these different proteins allows the tightly controlled release of specific proteins exactly when they are needed during the complex and rapid, parasite controlled process of invasion (Cowman and Crabb, 2006, Preiser *et al.*, 2000).

Merozoites must first recognise invasion-competent erythrocytes, a process that is low in affinity and reversible to avoid adherence to other types of cell, including already infected erythrocytes (Pei *et al.*, 2007). Stronger interactions then precede merozoite reorientation so that their apical end is in contact with the selected erythrocyte (Crosnier *et al.*, 2011), causing a deformation of the erythrocyte membrane as they do so (Mitchell *et al.*, 2004). Invasion of the erythrocyte is then mediated by the formation of a tight junction complex, a component of which is an actin-myosin motor which actively drives the merozoite forward into the erythrocyte (Angrisano *et al.*, 2012). Invasion into the erythrocyte in this manner, without rupture of the erythrocyte membrane, leaves the invaded merozoite enclosed within a membrane called the parasitophorous vacuole, apparently derived from both parasite and host lipids (Preiser *et al.*, 2000). Following invasion, these organelles are lost as the

parasite converts to a ring stage. The process(es) involved in the turnover of apical organelles remains largely unknown (Jayabalasingham *et al.*, 2010).

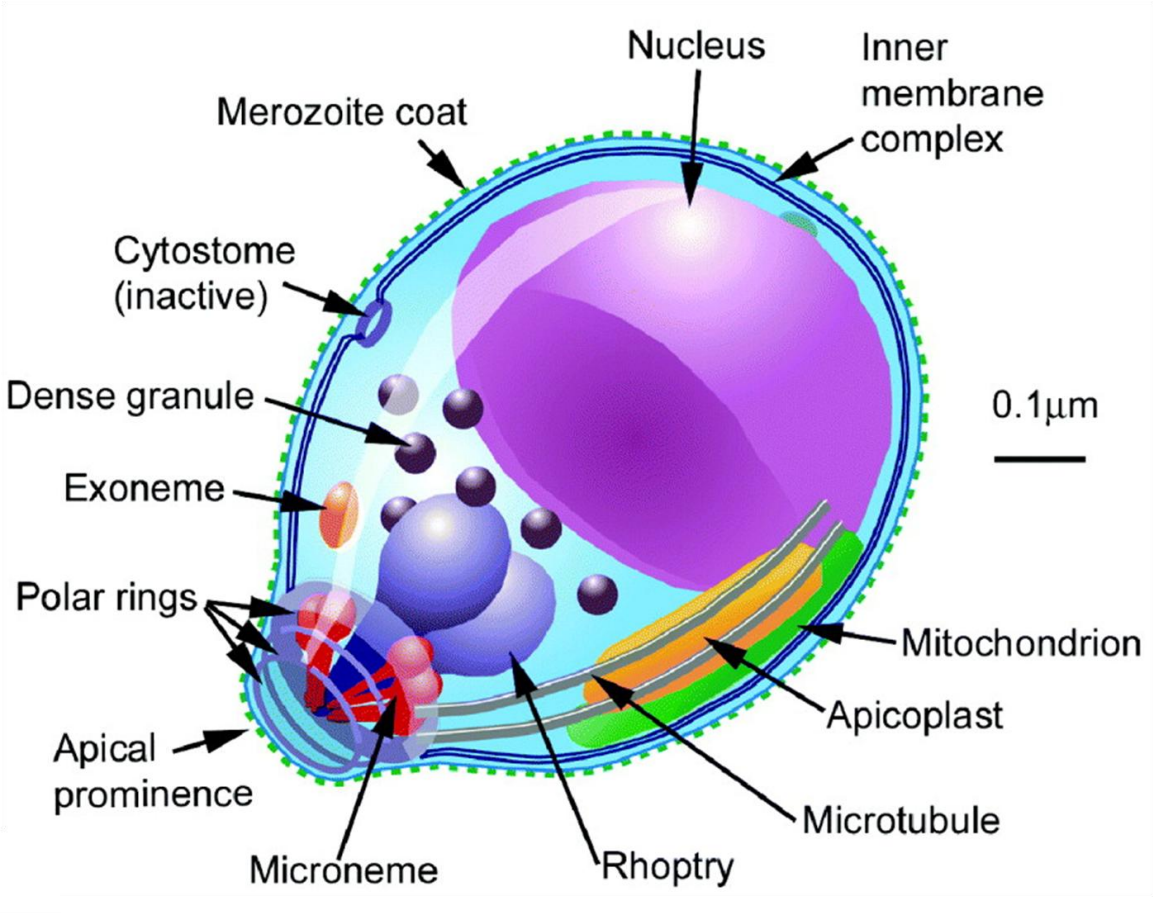

Figure 1.4: Schematic representation of a merozoite stage *P. falciparum* parasite (taken from (Bannister and Mitchell, 2009)).

The merozoite stage parasite is released from host hepatocytes or erythrocytes following multiplication via schizogony. Merozoites are polarised and possess a complement of apical organelles not maintained in the intraerythrocytic stages. The micronemes, rhoptries, exonemes and dense granules localise to the apical prominence and the whole cell is surrounded by a proteinaceous merozoite coat.

1.1.3.2 Digestive vacuole and nutrient acquisition

Similarly to other parasitic eukaryotes, *Plasmodium* parasites possess a full complement of biosynthetic pathway components for only 6 non-essential amino acids, and can not generate any of the 9 essential amino acids they need *de novo* (Payne and Loomis, 2006). The nutrient-rich environment of the parasite's host appears to have allowed the loss of non-essential biosynthetic pathways

while concurrent expansion of the mechanisms of amino acid acquisition, either from host cells or the extracellular environment, appears to have fulfilled the amino acid requirements of *Plasmodium* parasites (Istvan *et al.*, 2011). Haemoglobin degradation has been shown to be one such important mechanism and is sufficient to provide intraerythrocytic parasites with the nutrients needed to make all 20 amino acids except for isoleucine (Liu *et al.*, 2006).

Plasmodium parasites invade host red blood cells and feed on haemoglobin. The toxic by-product of haemoglobin breakdown, Fe(II)-protoporphyrin IX, is sequestered into a cyclic dimer. These dimers link and assemble via an ordered bio-crystallisation process (Hempelmann *et al.*, 2003), forming insoluble haemozoin crystals which are predominantly found in a specialised organelle called the digestive vacuole (DV) (Kapishnikov *et al.*, 2012). Compartmentalisation of this process into the DV allows for control of the production and detoxification of Fe(II)-protoporphyrin IX. The *Plasmodium* DV is distinct from lysosomes and the vacuole of yeast, as it does not contain other hydrolases commonly found in lysosomes and appears to be specialised solely for haemoglobin degradation (Goldberg *et al.*, 1990).

The origin(s) of the DV remain unresolved. It is thought to be formed by the fusion of haemoglobin-containing vesicles derived from the cytostome, a microtubule-supported focus of membrane invagination and vesicle formation unique to protozoa (Abu Bakar *et al.*, 2010). It has also been suggested that the initial formation of the DV is mediated by a single event distinct from macropinocytosis or phagocytosis in that it does not require actin polymerisation (Elliott *et al.*, 2008). This event, termed the ‘big gulp’ involves the folding over of the flattened early ring stage parasite to envelop a portion of host erythrocyte cytosol equivalent to up to 40 % of the parasite volume. This forms the DV which then expands following the fusion of haemoglobin-containing vesicles derived from either the cytostome or from smaller scale ‘gulps’. Either mechanism requires the breakdown of the nascent DV’s inner membrane, acidification of its lumen and the delivery of haemoglobin degrading enzymes before DV maturity is made evident by the presence of distinctive haemozoin crystals (Abu Bakar *et al.*, 2010). However, a degree of haemoglobin degradation has also been observed in haemoglobin-containing vesicles prior to or in the absence of fusion with the DV (Abu Bakar *et al.*, 2010, Hempelmann *et al.*,

2003). Parasites appear to digest haemoglobin until late in intraerythrocytic development and when merozoites egress from an erythrocyte, remnants of the DV remain as part of the residual body (Dluzewski *et al.*, 2008). The routes of DV formation and haemoglobin uptake from host erythrocyte cytosol are summarised in Figure 1.5.

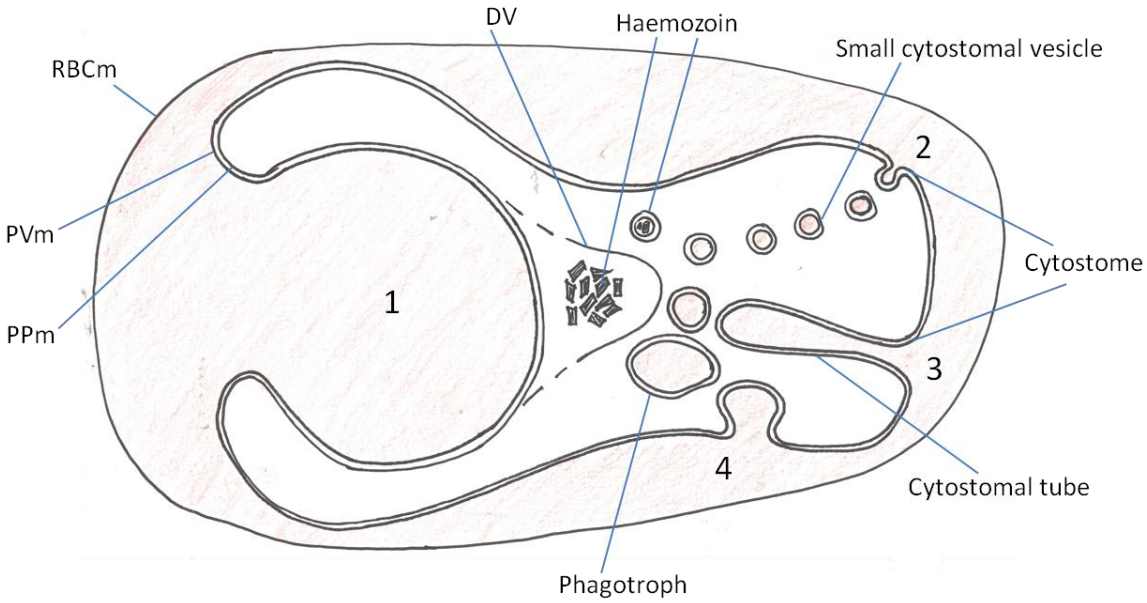

Figure 1.5: Schematic representation of haemoglobin uptake.

1. Early ring stage parasites have been proposed to engulf a large proportion of host cell contents in an initial 'big gulp'.

2. The predominant uptake mechanism in late rings and trophozoite stage parasites is via the cytostome, a structure from which small haemoglobin-containing vesicles (sHVs) bud and traffic to the digestive vacuole (DV), which is formed following either the big gulp or from fusion of multiple sHVs. Degradation of haemoglobin has also been shown to occur in sHVs before fusion with the DV.

3. Cytostomes also contribute, in part, to haemoglobin uptake via the formation of cytostomal tubes. These elongated tubular invaginations of both the parasitophorous vacuole membrane (PVm) and parasite plasma membranes (PPm) either fuse directly with the DV, forming a corridor between the DV and host cytosol, or pinch of at either end before trafficking to the DV.

4. An additional uptake mechanism predominant in the later stages of development involves the formation of large haemoglobin-containing vesicles or phagotrophs following a process similar to that which instigates the big gulp.

1.1.3.3 Mitochondrion and apicoplast

Plasmodium parasites possess only a single mitochondrion with a 6 kb genome (Waller and McFadden, 2005). In other organisms, one of the major but certainly not the only role of mitochondria is the oxidation of substrates in the tricarboxylic acid (TCA) cycle, which feeds electrons into the electron transport chain and hence provides energy in the form of ATP via a process known as

oxidative phosphorylation (McBride *et al.*, 2006). However, asexual *Plasmodium* parasites appear to feed the majority of glucose acquired from the host blood serum into glycolysis, bypassing the TCA cycle as the pyruvate generated is converted into lactate rather than acetyl-CoA (Sherman, 2005). Therefore the mitochondrion in *Plasmodium spp.* is thought to have been maintained due to its involvement in processes distinct from energy production (van Dooren *et al.*, 2006). It has been suggested that mitochondrion of erythrocytic stage parasites primarily functions in pyrimidine biosynthesis (Painter *et al.*, 2007).

The genome of the *Plasmodium* mitochondrion is one of the smallest yet sequenced and encodes only 3 protein-coding genes, along with 20 rRNAs (Sherman, 2005). As such, the majority of mitochondrial proteins are nuclear-encoded and must be trafficked back to the mitochondrion by one of a number of mechanisms (van Dooren *et al.*, 2006). All proteins passing beyond the outer membrane of the mitochondrion have to pass through the translocator of the outer membrane (TOM) complex. An N-terminal leader sequence can target a nuclear-encoded protein for translocation via TOM, after which additional signal motifs within the protein can then direct it to different locations within the mitochondrion (Macasev *et al.*, 2004). To continue on to the matrix of the mitochondrion, translocation of the inner membrane via the translocator of the inner membrane (TIM) complex is required (Pfanner and Wiedemann, 2002). To be integrated into the inner membrane, proteins possessing additional signal motifs can either be inserted into the membrane directly via TIM22 and so called tiny-TIM proteins (Rehling *et al.*, 2003), or from the matrix after translocation by TIM complexes via the activity of Oxa1 (Pfanner and Geissler, 2001). While a number of the proteins known to contribute to these processes appear to be conserved in *Plasmodium spp.* our understanding of mitochondrial targeting and import of nuclear-encoded proteins in *P. falciparum* is limited (van Dooren *et al.*, 2006).

Along with most Apicomplexan parasites, *Plasmodium spp.* possess a remnant plastid termed the apicoplast (Foth and McFadden, 2003). This organelle is bound by 4 membranes as a result of its origin by secondary endosymbiosis (Nair and Striepen, 2011). Apicomplexans, along with other chromalveolates arose from the uptake of a eukaryotic algal symbiont, possessing a photosynthetic chloroplast, by an ancestral eukaryotic protist (Botte *et al.*, 2011). The

membranes of the apicoplast in *Plasmodium spp.* therefore represent, working from host cytosol to apicoplast lumen, the phagosomal membrane of the host, the plasma membrane of the engulfed alga, the outer chloroplast membrane and finally the inner chloroplast membrane (Lim and McFadden, 2010).

The apicoplast of *P. falciparum* resembles its ancestral chloroplast in its semi-autonomous nature facilitated by its own 35 kb genome and protein expression machinery but crucially has lost photosynthetic abilities (Wilson *et al.*, 1996). It has been shown to contain components of isoprenoid biosynthesis, iron/sulphur cluster assembly, fatty acid, haem and lipoic acid biosynthetic pathways (DeRocher *et al.*, 2012). Fatty acid synthesis and isoprenoid precursor synthesis appear to only occur within the apicoplast (Nair and Striepen, 2011), with the former being shown to be essential to development of liver stage parasites (Vaughan *et al.*, 2009, Yu *et al.*, 2008) and the later for blood stage parasites (Yeh and DeRisi, 2011).

While the apicoplast appears to encode as few as 64 genes, many of which are rRNAs and tRNAs, up to 1,000 proteins might localise to the apicoplast (Foth *et al.*, 2003, Waller and McFadden, 2005). Therefore transport of nuclear-encoded proteins into the organelle is an essential requirement for its function and presumably parasite survival (Waller *et al.*, 1998). Recent identification of a nuclear-encoded endoplasmic reticulum associated protein degradation system (ERAD)-like complex, that is targeted to the second outermost apicoplast membrane has improved understanding of how nuclear-encoded proteins are targeted to the apicoplast lumen (Spork *et al.*, 2009). Most nuclear-encoded, apicoplast-targeted proteins possess an N-terminal bipartite leader sequence so called because the first part encodes an ER signal peptide and the second part encodes an apicoplast transit peptide (Tonkin *et al.*, 2008). The signal peptide directs the protein into the secretory pathway by translocation across the ER membrane via the Sec61 complex (Waller *et al.*, 2000). Following cleavage of the signal peptide during co-translational import into the ER, apicoplast-targeted vesicles are then believed to transfer these proteins to the space between the outermost and third membrane of the apicoplast (Lim *et al.*, 2009). The transit peptide directs the protein across the 3 innermost membranes of the apicoplast (Spork *et al.*, 2009). The ERAD-like complex facilitates translocation of the third outermost membrane, while a translocator of the inner chloroplast

membrane (TIC) complex facilitates entry into the apicoplast lumen (Kalanon *et al.*, 2009). Translocation of the second innermost membrane might be achieved through an as yet unidentified translocator of the outer chloroplast membrane (TOC) complex, or via an additional ERAD-like complex (Tonkin *et al.*, 2008). Upon entry to the apicoplast lumen the transit peptide is then cleaved by a protease similar to the stromal processing peptidase of plant chloroplasts (van Dooren *et al.*, 2002). As well as the large number of luminal apicoplast-targeted proteins, a smaller number of nuclear-encoded proteins are targeted to the outer membrane(s) of the apicoplast, however identification of these proteins is made difficult by the frequent absence of a bipartite leader sequence (Lim *et al.*, 2009). The exact route(s) by which these proteins reach their target membranes remains unresolved.

Both the mitochondrion and apicoplast must be inherited by each daughter merozoite as it forms late in schizogony. This unusual and complicated multiplication strategy places the need for organelle division processes distinct from the binary fission observed in most other organisms (van Dooren *et al.*, 2006). The processes responsible for this exquisitely controlled action are poorly understood in *Plasmodium spp*. but a link with nuclear division and a dynamin-related protein have been identified in *T. gondii* (Striepen *et al.*, 2000, van Dooren *et al.*, 2009). Through the use of fluorescence and immunoelectron microscopy, the expansion and segmentation of the mitochondrion and apicoplast has been observed during the intraerythrocytic development of *P. falciparum* (Hopkins *et al.*, 1999, van Dooren *et al.*, 2005). This appears to be an adaptation to division by schizogony that is not shared in similar organisms that divide by more simple fission (Ferguson *et al.*, 2005). The characteristic elongation, branching and segmentation of the mitochondrion and apicoplast in *P. falciparum* are represented in Figure 1.6. Little is known about either the mitochondrion or the apicoplast in *Plasmodium* parasites outside of the intraerythrocytic stages (van Dooren *et al.*, 2006). When asexual stages differentiate into the gametocyte stages, the mitochondrion has been observed to undergo extensive morphological changes, while the apicoplast remains small (Okamoto *et al.*, 2009). Despite these differences, the close association between the two organelles, as that observed in asexual stages, appears to be maintained (van Dooren *et al.*, 2006).

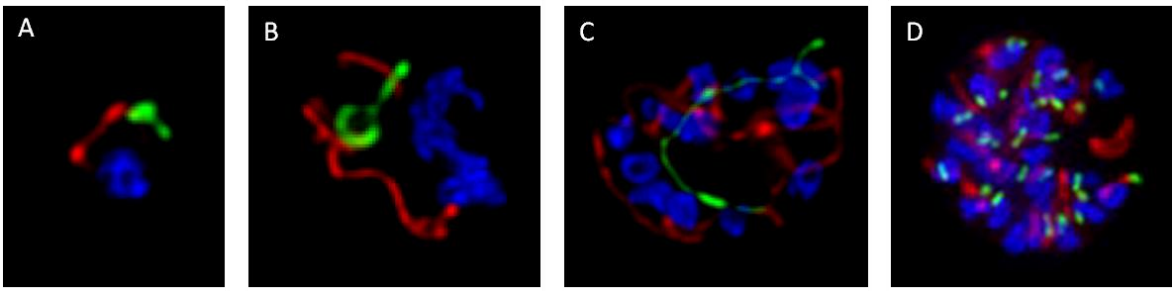

Figure 1.6: Development of the apicoplast and mitochondrion during intraerythrocytic development. (Figure is composed of data generated by Dr. P. McMillan).

(A) An early trophozoite stage with a single nucleus. The apicoplast (green) and mitochondrion (red) are single copy organelles often seen in close proximity.

(B) A late trophozoite stage with an expanded nucleus. The mitochondrion elongates early in intraerythrocytic development. The apicoplast begins to elongate in a similar but slightly delayed manner.

(C) An early schizont stage with multiple nuclei. The mitochondrion and apicoplast are highly elongated and are beginning to form branches, often closely associated with individual nuclei.

(D) A late schizont / segmenter stage with > 20 nuclei. The apicoplast and mitochondrion segment and distribute into forming merozoites. The residual body is devoid of apicoplast or mitochondrial material following egress.

Blue shows DNA staining by Hoechst 33258, red shows the mitochondrion labelled with MitoTracker Cmx-Ros and green shows the apicoplast reported by *Pf*LipDH1-GFP.

1.2 Autophagy

1.2.1 The process of autophagy

Organisms must rely on both the continuous biosynthesis and degradation of cellular components in order to maintain homeostasis (Vellai and Takacs-Vellai, 2010). Not only does protein degradation provide the building blocks for new protein synthesis and energy generation in times of starvation but it is also vital for the removal of non-functional, damaged and potentially harmful proteins. Degradation of cellular components is performed by two different but potentially overlapping mechanisms (Korolchuk *et al.*, 2010, Wong and Cuervo, 2010).

Short-lived and aberrantly folded proteins are primarily degraded via the ubiquitin-proteosome system (UPS) (Liu *et al.*, 2010). This process involves the post-translational modification of a target protein via the conjugation of ubiquitin, a small but abundant protein, through a tightly controlled cascade of protein:protein interactions (Varshavsky, 2012). The ubiquitination cascade is facilitated by 3 types of protein – ubiquitin-activating (E1), ubiquitin-conjugating (E2) and ubiquitin ligase (E3) enzymes. The eventual conjugation of free ubiquitin to the target protein takes 2 forms - monoubiquitination or multi-monoubiquitination, while the conjugation of free ubiqiutin to ubiquitin already conjugated to the target protein is referred to as polyubiquitination (Hochstrasser, 2009, Komander and Rape, 2012). Among roles in cell cycle progression, signal transduction, DNA repair and inflammation, ubiquitination demarcates the target protein for degradation via the 26S proteosome, a large protein complex which cleaves the unfolded target protein or peptide into shorter peptides which can then be broken down further (Liu *et al.*, 2010, Wong and Cuervo, 2010). Other mediators of protein degradation including caspases, calpains and separases, may also act upstream of the UPS, predestining a protein for degradation (Varshavsky, 2012).

Long-lived proteins, along with macromolecules and organelles are primarily degraded via a different mechanism, relying on the process of autophagy (Levine and Deretic, 2007). The term autophagy is used to refer to a range of catabolic processes which converge on the degradation of cellular components in the lytic

compartment i.e. the lysosome or food vacuole in yeast and plants (Inoue and Klionsky, 2010). This can be achieved by three routes (Figure 1.7) (Yang and Klionsky, 2009). The major pathway, macroautophagy, involves the engulfment of cellular components into a double-membraned vesicle termed the autophagosome. This sequesters cytosolic proteins, protein aggregates and in some cases whole or portions of organelles (Baba *et al.*, 1994). Autophagosomes then traffic sequestered cargo to the lytic compartment, where after fusion of the outer membrane and collapse of the inner membrane, lytic enzymes initiate the breakdown of cargo (Dennis and Mercer, 2009). The second pathway, microautophagy, involves the invagination of the lytic compartment membrane to form an autophagic tube (Li *et al.*, 2012b). Vesicles bud from this tube into the lumen of the lytic compartment and are then degraded by the same route as autophagosomes (Kunz *et al.*, 2004). The third process, chaperone mediated autophagy (CMA), involves the translocation of single unfolded proteins across the lytic compartment membrane via specific chaperone and transporter proteins (Li *et al.*, 2011b). The specificity of CMA target proteins relies on the recognition of a KFERQ-related consensus peptide sequence by a chaperone protein complex (Dice, 1990). Interaction between the chaperone:target complex and a lysosomal receptor then promotes the translocation of the target with the help of additional chaperones in the lumen of the lytic compartment (Agarraberes *et al.*, 1997).

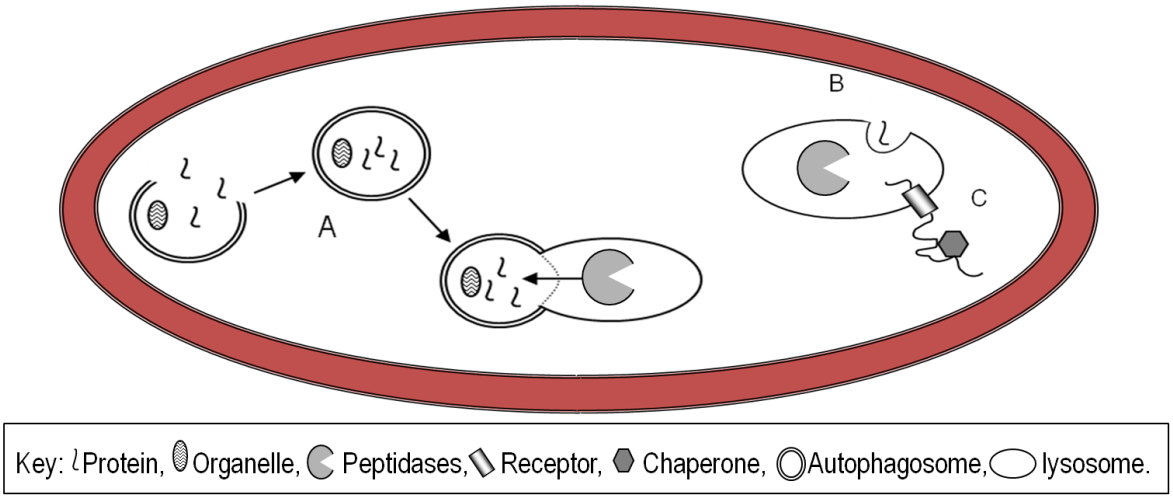

Figure 1.7: Schematic representation of the three variations of autophagy.

(A) Macroautophagy – Cytosolic components are engulfed by a double-membraned autophagosome and delivered to the lytic compartment via fusion of the autophagosome outer membrane and breakdown of the inner membrane.

(B) Microautophagy – Cytosolic components are engulfed by invagination of the lytic compartment limiting membrane.

(C) Chaperone-mediated autophagy – Specific cytosolic components are recruited to the lytic compartment and, via interaction with chaperone proteins, are translocated across the lytic compartment limiting membrane.

All of these degradation processes result in the conversion of cellular components into smaller macromolecules and amino acids, which can then be utilised in the generation of new proteins. These processes contribute to the maintenance of intrinsic cellular homeostasis by removing damaged, redundant or toxic proteins and replenishing the pool of available amino acids. This ongoing process is often referred to as basal autophagy (Hara *et al.*, 2006, Pattison *et al.*, 2011, Xia *et al.*, 2010). However, autophagic activity can be upregulated to mediate response to cellular stresses, such as when countering invading pathogens (Birmingham *et al.*, 2006, Singh *et al.*, 2006), in adaption to an environment of nutrient starvation (Mizushima *et al.*, 2004) or at times of cellular differentiation (Alvarez *et al.*, 2008, Besteiro *et al.*, 2006). The regulation of an autophagic response is therefore important for initiating a rapid response to stress(es) but must also be tightly controlled to prevent unnecessary turnover of cellular components (Chang *et al.*, 2009, He and Klionsky, 2009). Aberrant control of autophagy is linked to many human diseases and has therefore been the focus of intense study over recent years (Behrends *et al.*, 2010, Levine and Kroemer, 2008).

It was long regarded that autophagy (primarily macroautophagy) represented bulk, non-specific catabolic processes, while ubiquitination represented a process mediating the breakdown of specific targets at specific time points (Yoshimori, 2004). However, increasing evidence points towards the involvement of macroautophagy in the degradation of specific protein cargos (Johansen and Lamark, 2011, Noda *et al.*, 2010, Pankiv *et al.*, 2007). Forms of specific autophagy, where organelles are inclusively and exclusively incorporated into an autophagosome have also been described, for example mitophagy of mitochondria (Kim *et al.*, 2007), pexophagy of peroxisomes (Bellu and Kiel, 2003), xenophagy of intracellular pathogens (Levine, 2005) and 'chlorophagy' of chloroplasts in plant leaves (Izumi *et al.*, 2010). While large gaps in our knowledge of autophagy still exist, a great deal is now known following extensive study in yeast and mammalian cells and increasingly in other organisms (Duszenko *et al.*, 2011, Inoue and Klionsky, 2010, Kiel, 2010, Mizushima *et al.*, 2010).

1.2.2 Macroautophagy

Of the three forms of autophagy, macroautophagy has attracted the most attention in the research community. This process is referred to as autophagy from hereafter. In yeast, over 30 proteins have been identified to play a role in autophagy and have subsequently been named autophagy-related (ATG) proteins (Klionsky *et al.*, 2003, Yang and Klionsky, 2009). Many of these proteins have been found to have homologues in mammals and other higher eukaryotes (Levine and Klionsky, 2004). For clarity, the nomenclature used to describe ATGs in yeast is used throughout this study. Many other proteins in yeast and other organisms involved in or complementary to autophagy have been named according to their roles in other processes (Jager *et al.*, 2004, Lin and Zhong, 2011). ATG proteins can be grouped according to their function and role during autophagy. ATG1, 13, 17, 20, 24, 29 and 31 are involved in the signalling processes which control induction of autophagosome formation. ATG3, 4, 5, 7, 8, 10, 12 and 16 are involved in the two conjugation pathways responsible for ATG8 lipidation and drive autophagosome expansion and completion. ATG2, 6, 9, 14, 18, 23 and 27 are involved in autophagosomal nucleation and the membrane dynamic events surrounding autophagosome formation. ATG11 plays roles in both the induction of autophagosome formation and in the recognition of autophagic

cargo. ATG15 plays a role in the lysosomal breakdown of autophagosomes and their contents. ATG22 plays a role in the recycling of autophagic cargo. ATG19 and 21 play specific roles in cargo recognition and the membrane dynamic events of the cytoplasm to vacuole targeting (Cvt) pathway, a specific type of autophagy found in yeast. ATG25, 26, 28 and 30 play specific roles in cargo recognition during pexophagy. ATG32 and 33 play specific roles in cargo recognition during mitophagy (Inoue and Klionsky, 2010).

Different models for autophagosome biogenesis have been put forward, with membrane fusion and fission events forming the basis of each (Krick *et al.*, 2011). It remains undetermined if there is a definitive membrane source that contributes to the formation of autophagosomes (Tooze and Yoshimori, 2010). It appears that under differing circumstances the ER (Axe *et al.*, 2008), Golgi (Ohashi and Munro, 2010), plasma membrane (Ravikumar *et al.*, 2010) and mitochondria (Hailey *et al.*, 2010) can all contribute to autophagosome biogenesis. It has also been suggested that lipids reversibly-destined for autophagosome biogenesis might first enter a pool of tubular/vesicular structures referred to as the ATG9 reservoir (Mari *et al.*, 2010). In yeast, autophagosomes are generated from a single focus called either the pre-autophagosomal structure or the phagophore assembly site (PAS) (Suzuki *et al.*, 2001), while in mammalian cells autophagosomes form from multiple isolation membranes (IMs) also called phagophores (Tooze and Yoshimori, 2010). Once nucleation of the pre-autophagosomal membrane has been initiated a series of interactions between proteins and lipids drives the expansion and curvature of the membrane to form a nascent double-membraned autophagosome (Figure 1.8) (Kraft and Martens, 2012).

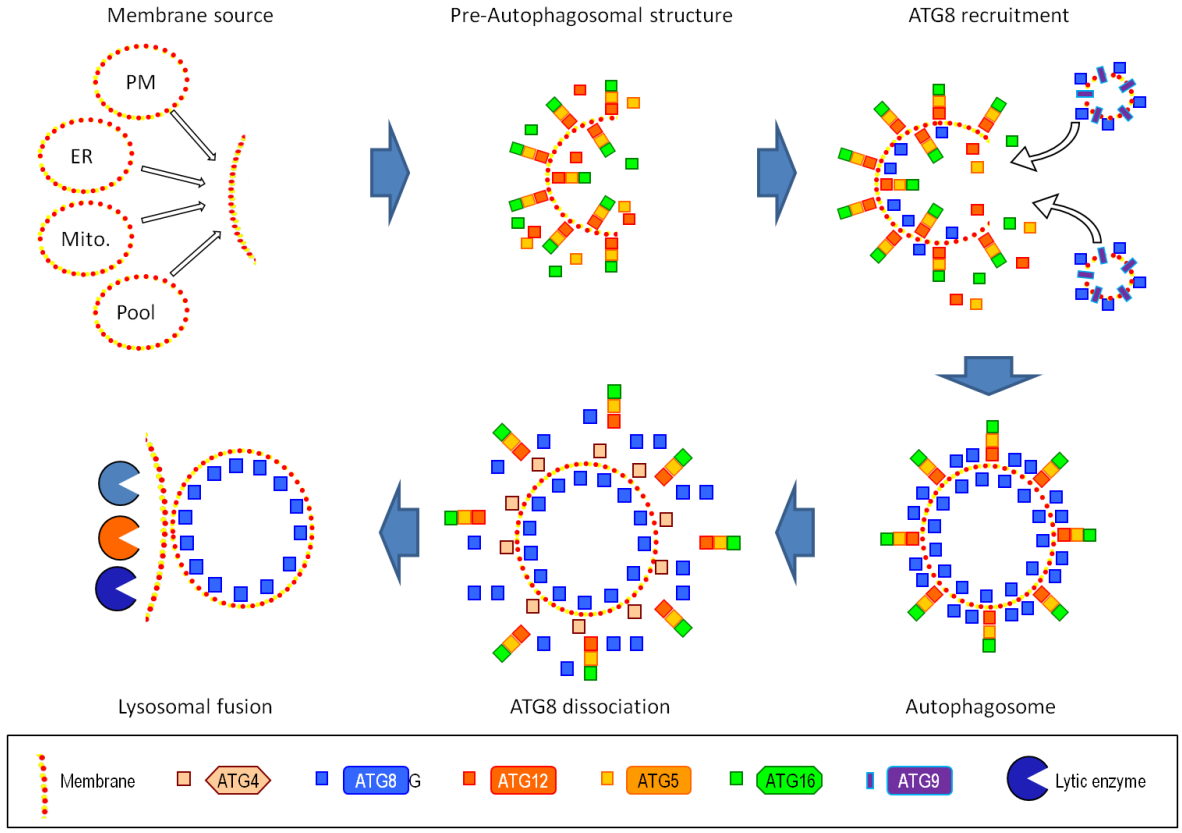

Figure 1.8: Schematic representation of autophagosome formation.

Clockwise from top left: A membrane source is acquired from a pre-existing membranous structure (e.g. the ER or mitochondria), the plasma membrane or a vesicular pool donated to autophagy; initiation of autophagosome formation requires, amongst others, the recruitment of the ATG5:ATG12:ATG16 complex; via its E3-like activity, this complex promotes ATG8 lipidation to phosphatidylethanolamine (PE), recruiting additional membrane material possibly in an ATG9-dependent manner; as the autophagosome completes, ATG8 is the predominant ATG protein trapped inside, along with autophagic cargo, as it is still conjugated to PE; the ATG5:ATG12:ATG16 complex dissociates from the completed autophagosome and ATG4 cleaves ATG8 from PE on the outer face; fusion of the autophagosome outer membrane with the membrane of the lytic compartment precedes breakdown of the autophagosome inner membrane and contents.

A complete autophagosome contains autophagic cargo destined for the cell's lytic compartment. Cargo can be non-specifically engulfed or, through various protein:protein interactions, specific protein or organelle cargoes might be selectively engulfed via their interaction with ATG8, which remains conjugated to the autophagosome inner face throughout expansion and completion of the autophagosome (Noda *et al.*, 2008). Autophagosomes are known to fuse with endocytic vesicles prior to fusion with the lytic compartment, forming an amphisome (Berg *et al.*, 1998). Autophagosomes and amphisomes are thought to be directed to the lytic compartment via interaction with the microtubule network, again through interaction with ATG8, this time conjugated to the outer face of the autophagosome (Geeraert *et al.*, 2010, Pankiv *et al.*, 2010). Fusion

of the autophagosome with the lysosome (or vacuole in yeast and plants) is mediated by endosomal sorting complexes (Raiborg and Stenmark, 2009) and results in the formation of an autophagolysosomes, characterised by a reduced internal pH and the presence of lytic enzymes (Kimura *et al.*, 2007).

1.2.3 Autophagosome biogenesis

The formation of autophagosomes requires upstream signalling and regulation of this signalling has been a recent focus of autophagy research (Inoue and Klionsky, 2010, Moretti *et al.*, 2007). ATG8 has been shown to be upregulated by autophagy induction in yeast, with 8 - 20 times more protein detected following starvation of nitrogen (Huang *et al.*, 2000, Kirisako *et al.*, 1999). This upregulation determines the size of autophagosomes rather than their frequency (Inoue and Klionsky, 2010, Xie *et al.*, 2008), showing that the initiation of autophagosome biogenesis occurs upstream of ATG8. Current knowledge suggests that initiation of autophagosome biogenesis is regulated through ATG1, a serine/threonine kinase which forms a complex with ATG13 and other proteins depending on its phosphorylation state (Kamada *et al.*, 2000).

The ATG1 complex receives signals relating to, among other triggers, cellular nutrient levels and via interaction with multiple other proteins, promotes the recruitment of ATG proteins to the site(s) of autophagosome biogenesis (Mizushima, 2010). Initiation of autophagosome formation is inhibited by the target of rapamycin (TOR), the so called master regulator of autophagy (Kohli and Roth, 2010), which acts upstream of ATG1.

ATG1 activity promotes the localisation of the phosphoinositide 3-kinase class III (PI3K) complex to membranes destined to contribute to autophagosomes by a poorly understood mechanism (Juhasz *et al.*, 2008). It also plays a role in the shuttling of ATG9 between autophagic and peripheral membranes (Reggiori *et al.*, 2004a), which in turn is believed to facilitate the expansion of autophagic membranes by the acquisition of lipids (Reggiori *et al.*, 2005). PI3K forms a complex with other proteins including ATG6 and the vacuolar protein sorting protein Vps15 and through its lipid kinase activity it phosphorylates phosphatidylinositol to generate phosphatidylinositol (3)-phosphate (PI3P) in autophagic membranes (Simonsen and Tooze, 2009). Enrichment of PI3P in

autophagic membranes is described as the nucleation step of autophagosome biogenesis and promotes recruitment of the autophagosome marker protein ATG8 along with other components of the ATG8 and ATG12 conjugation pathways (Zhong *et al.*, 2009), likely through interaction with additional PI3P-binding proteins such as ATG18 (Nair *et al.*, 2010).

The ATG8 and ATG12 conjugation pathways control the expansion and completion of the autophagosome (Chen and Klionsky, 2011). These two proteins show limited sequence similarity with ubiquitin, but do show structural similarities and are the focus of a ubiquitination-like conjugation cascade involving E1, E2 and E3-like proteins (Figure 1.9) (Geng and Klionsky, 2008, Ichimura *et al.*, 2000).

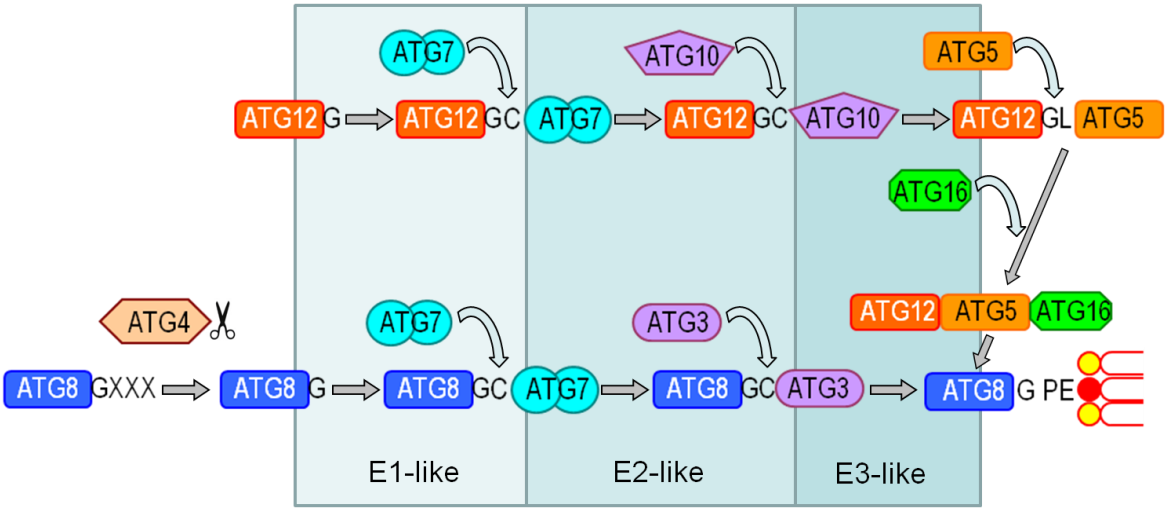

Figure 1.9: Schematic representation of the ubiquitination-like conjugation pathways of ATG8 and ATG12.

The proteins ATG8 and ATG12 both possess ubiquitin-like folds in their core. They undergo ubiquitination-like conjugation pathways sharing ATG7 as an E1-like protein. ATG10 acts as an E2-like protein in the conjugation of ATG12, which is finally conjugated to ATG5. The ATG12-ATG5 complex recruits ATG16 and forms a tetramer. This tetrameric complex acts in an E3-like manner in the conjugation of ATG8, transferring it from ATG3, its E2-like protein, not to another protein but to phosphatidylethanolamine (PE).

ATG12 is activated by the E1-like enzyme ATG7 when a labile thioester bond forms between the C-terminal glycine residue of ATG12 and a catalytic cysteine of ATG7 (Tanida *et al.*, 1999). ATG12 is then transferred to the E2-like enzyme ATG10, forming the same bond with the catalytic cysteine of ATG10 (Shintani *et al.*, 1999). ATG12 is then transferred to ATG5 with which it forms a stable isopeptide bond between its C-terminal glycine and the ε-amino group of a lysine in ATG5 (Mizushima *et al.*, 1998). The ATG12:ATG5 complex then acts as an E3-

like enzyme in the conjugation pathway of ATG8 (Hanada *et al.*, 2007), following interaction between it and its E1-like and E2-like enzymes ATG7 and ATG3, respectively (Taherbhoy *et al.*, 2011). The ATG12:ATG5 complex promotes the transfer of ATG8 from ATG3, not to another protein but rather to phosphatidylethanolamine (PE), a phospholipid found in autophagic and other membranes (Ichimura *et al.*, 2000). This is directed by another protein, which interacts with the ATG12:ATG5 complex, ATG16 (Fujita *et al.*, 2008). While the final bond between ATG12 and ATG5 appears to be irreversible (Hanada *et al.*, 2007), the isopeptide bond between ATG8 and PE can be cleaved by the cysteine peptidase ATG4 (Tanida *et al.*, 2004). ATG4 is first required to process the C-terminus of ATG8 by cleaving the residue(s) beyond the reactive glycine, a post-translational modification that renders ATG8 lipidation-competent (Kirisako *et al.*, 2000). It can then also deconjugate ATG8 to release it from the membrane, which may also require other ATG proteins for the strict control of this function (Chen and Klionsky, 2011). As with earlier steps in initiation and nucleation of autophagosomes, quite how the proteins of the ATG8 and ATG12 conjugation pathways promote autophagosome biogenesis is poorly understood (Chen and Klionsky, 2011). ATG8 has been shown to promote tethering and hemifusion of membranes *in vitro* (Nakatogawa *et al.*, 2007) and it has been suggested that through interaction with another protein, Shp1, and resultant recruitment of cdc48, an AAA-type ATPase, ATG8 might function to bring about the final steps of autophagosome expansion and closure (Krick *et al.*, 2010).

1.2.4 ATG8 and autophagy in diverse eukaryotes

While subsets of ATG homologues have been identified in all eukaryotic genomes analysed, there is increasing evidence that the ability to perform autophagy is in fact, not maintained in all eukaryotes. For example, while a small number of potential genes encoding ATG homologues have been identified in *Giardia lamblia* and *Cyanidioschyzon merolae*, the protein products of these genes are likely to participate in other cellular processes, in the absence of a full complement of core autophagy components (Rigden *et al.*, 2009). It is also known that in organisms with either a full complement of homologues to core autophagic machinery or with characterised autophagic processes, ATG homologues also contribute to distinct cellular processes. For example, in the yeast *Pichia pastoris*, ATG8 has been shown to play a role in vesicular membrane

dynamics during the adaptation to methanol consumption (Tamura *et al.*, 2010). This role does not rely on the ATG8 conjugation pathway and the protein does not need to be lipidated. In *Schizosaccharomyces pombe,* ATG8 has been shown to participate in vacuolar function in relation to stress response, again independent to its role in autophagy (Mikawa *et al.*, 2010). In mammalian cells, ATG12 has been shown to conjugate to ATG3, the E2-like enzyme of ATG8, with which it contributes to mitochondrial homeostasis (Radoshevich *et al.*, 2010). It has recently been demonstrated that in mammalian cells performing xenophagy, a homologue of ATG8 can become lipidated to non-classical autophagic membranes without ATG1 complex signalling or ATG9-dependent recruitment of the PI3K complex (Kageyama *et al.*, 2011). When ATG9 or ATG14 were genetically ablated, ATG8 was seen to localise to a single-membraned vesicle, enveloping an invading *Salmonella typhimurium* bacterium and the formation of a double-membraned xenophagosome seen in wild type cells was absent. ATG8 has also been shown to become lipidated at non-autophagosomal membranes and is only released to a lipidation-competent form through the activity of ATG4 (Nakatogawa *et al.*, 2012a). Its function, if any at these non-autophagic membranes has not been determined.

These instances show that ATG8 and likely other ATG proteins can have far reaching roles distinct from autophagy and that in some organisms, such roles might be in fact be the only reason for their conservation. Whether ATG proteins contribute to autophagic or distinct processes in *Plasmodium spp*. has not yet been explored. Recent studies into related organisms have shed light on an autophagic process in each. In *Toxoplasma gondii*, an ATG8 homologue has been shown to participate in both basal and starvation-induced autophagy (Besteiro *et al.*, 2011). It was shown that when *Tg*ATG8 lipidation was blocked via depleting *Tg*ATG3, mitochondrial homeostasis was disrupted and growth was inhibited. This suggests that in *T. gondii*, *Tg*ATG8 and autophagy may have roles in both response to nutrient starvation and in maintaining mitochondrial integrity. More recently, mitophagy mediated by *Tg*ATG8 has also been suggested to contribute to an apoptosis-independant, autophagic programmed cel death mechanism in amino acid-starved *T. gondii* tachyzoites (Ghosh *et al.*, 2012). The requirement and maintainance of programmed cell death mechanisms in unicellular eukaryotes remains controversial but the potential invovlvement of *Tg*ATG8 in

such a process indicates that ATG8 homologues can play unexpected roles in diverse eukaryotes. Whether a programmed cell death mechanism exists in *P. falciparum* remains to be determined.

In *Trypanosoma brucei*, three ATG8 homologues have been identified and characterised (Proto, 2010), with one being found to display ATG12-like characteristics. The two *de facto* ATG8 homologues appear to be involved in processes relating to cell death under starvation conditions (Li *et al.*, 2012a). In *Trypanosoma cruzi*, an ATG8 homologue was found to complement yeast *Sc*ATG8 and was processed by two ATG4 homologues to expose its C-terminal glycine (Alvarez *et al.*, 2008). This ATG8 homologue was found to localise to autophagosomes in response to starvation and during the differentiation of epimastigotes. In *Leishmania major*, homologues of ATG8, ATG3 and ATG4 have been shown to participate in canonical autophagy in response to starvation. Autophagy was also shown to be upregulated during the differentiation from promastigotes to infective metacyclic promastigotes (Besteiro *et al.*, 2006). Genetic ablation of one of two ATG4 homologues was found to reduce the parasite's ability to differentiate into metacyclic promastigotes, indicating that autophagy is needed for differentiation. Interestingly, the repertoire of ATG8 homologues in *L. major* is vastly expanded in comparison to other organisms, with 25 *atg*8 genes identified (Williams *et al.*, 2009). Examples of the 4 families of ATG8 homologues appear to play different roles, with members of 2 families apparently participating in a process other than autophagy (Williams *et al.*, 2009). It has recently been shown that *L. major* also possesses an active ATG12 conjugation system, which is required for ATG8-dependent autophagosome biogenesis (Williams *et al.*, 2012). Genetic ablation of ATG5 prevented autophagosome formation which resulted in morphological defects, mitochondrial dysfunction, reduced viability and decreased ability to differentiate. These findings show that in many parasitic eukaryotes, the involvement of ATG8 in an autophagic process appears to be conserved. However they also indicate that in many of these organisms, ATG8 is involved in processes such as organelle maintenance, differentiation and viability, either in relation to its role in autophagy, or due non-canonical roles.

1.3 Rationale for study

At present it is proving difficult to interpret how the fight against malaria is progressing. While at first glance it would appear that worldwide incidence is actually on the decline, the rapid emergence of populations of parasites resistant to therapeutics used in the field is a great worry. In the absence of an effective malaria vaccine, and without promise for delivery of such a vaccine in the near future, there is a clear requirement on therapeutics for the treatment of malarial infections, particularly in the individuals who are most at risk of serious or fatal disease. Our knowledge of basic parasite biology remains fairly limited, despite decades of dedicated research. However, in this, the post genomic era for human malarial parasites, great leaps forward in our understanding of parasite biology are now being achieved. Our understanding of resistance mechanisms and the factors that might promote development of resistance is becoming more detailed (Summers *et al.*, 2012). Our knowledge of how anti-malarial drugs actually work is also improving (Bouquet *et al.*, 2012), facilitating the development of chemically designed therapeutics (Mullie *et al.*, 2012). However, without the identification of additional drug targets, new 'designer' drugs based on compounds to which resistance in the field has already developed, will have a limited input into attempts to eradicate malaria. Gaining additional knowledge of parasite biology is therefore crucial, as identifying potential weaknesses in the parasite's armour, provides a platform from which to identify potential drug targets.

Autophagy is well established as a stress response as well as being involved in homeostatic processes in a number of organisms. It has also more recently been shown to be involved in cellular remodelling and differentiation. As *Plasmodium* parasites switch between invertebrate and mammalian hosts and the different tissues, cells and environments within each, they perform elaborate and vast changes to their cellular structure, contents and metabolism. It would seem likely that an autophagic process might contribute to these crucial steps in the parasite life cycle.

At the onset of this study it was not known whether an autophagic process was conserved in the malaria parasite *Plasmodium falciparum*. It is becoming increasingly evident that the canonical autophagic process has been modified or

built upon in a species-specific manner in a number of organisms. It is also apparent that a number of fundamental biological processes are performed differently in *P. falciparum* intraerythrocytic stages than in its human host. Therefore, understanding the process of autophagy in *P. falciparum* will add to our overall understanding of parasite biology and could uncover a weakness or difference to human biology. Identifying such differences could aid the elucidation of novel therapeutic targets in *P. falciparum*.

1.4 Aims of this study

Autophagic membranes are mostly devoid of any transmembrane proteins and proteins peripheral to the outer membrane of autophagosomes have proven difficult to identify (Fengsrud *et al.*, 2000). Due to the recruitment of ATG8 to autophagic membranes early in autophagosome biogenesis and the fact that this protein remains conjugated to PE on the inner face of an autophagosome until after lysosomal fusion, ATG8 is commonly used as a marker for autophagosomes (Kabeya *et al.*, 2000, Kirisako *et al.*, 1999, Weidberg *et al.*, 2010). The lipidation state of ATG8 is also commonly used as a measure of autophagic flux, particularly when autophagosome turnover is blocked (Kabeya *et al.*, 2004, Mizushima and Yoshimori, 2007). As such, ATG8 commonly constitutes the focus of research during the early examination of autophagy in various organisms (Koopmann *et al.*, 2009, Perez-Perez *et al.*, 2010, Williams *et al.*, 2009).

Preceding this study, an initial bioinformatic screen had identified a potential ATG8 homologue in *P. falciparum*. This study therefore intended to build upon this initial screen and characterise the potential ATG8 homologue in the intraerythrocytic stages of *P. falciparum*. Aims therefore included:-

- Identify potential homologues to components of the autophagic machinery already characterised in yeast and other organisms.

- Characterise the potential homologue of ATG8, a commonly used marker for autophagy. This would involve:-

    - Analysis of its function.

- Analysis of its expression in intraerythrocytic parasite stages.
- Analysis of its post-translational modification.
- Analysis of its localisation in intraerythrocytic parasite stages.
- Analysis of how these three aspects are altered in response to manipulation of the processes responsible for regulation of autophagy in other organisms.
- Analysis of its essentiality to parasite viability or development.

- Place knowledge gained about the potential homologue of ATG8 into the context of parasite biology and how this relates to what is known about ATG8 and autophagy in other organisms.

The results of this study are organised into 3 chapters. Chapter 3 details the identification of a homologue to ATG8 (*Pf*ATG8) and the analysis of its function and expression. Chapter 4 details the attempts made generate *P. falciparum* lines in which the endogenous copy of *Pfatg*8 has been genetically ablated or replaced with a tagged version. Chapter 5 details the analysis of *Pf*ATG8 localisation and explores the possible role(s) of *Pf*ATG8 in *P. falciparum* intraerythrocytic stages.

2 Materials and methods

2.1 Consumables, biological and chemical reagents

Ambion	RETROscript reverse transcription for real time PCR kit, Turbo DNA-free
BDH	Saponin
Bio-Rad	Bradford protein assay reagent, Gene Pulser electroporation cuvette (0.2 cm), Precision Plus dual-colour protein standard, Certified Megabase agarose, CHEF DNA marker (*Hansenula wingei*), InstaGene Matrix
Blood transfusion service	Human full blood
BOC	Malaria culture gas (3 % CO_2, 1 % O_2, 96 % N_2)
Clontech	Mouse monoclonal anti-His antibody, Mouse monoclonal anti-mCherry antibody
Eurogentec	Oligonucleotides, antisera generation programmes
Fisher Scientific	Gelcode Blue Safe protein stain, 10 x Phosphate buffered saline (PBS), Reddy mix PCR mastermix, 96 well plates, imidazole (low absorbance), Protran Nitrocellulose, Restore western stripping buffer, 500 ml 0.2 µm Stericup filter units, 0.2 µm syringe filters, Sodium hydrogen carbonate, Reagent reservoirs, disposable filtration columns
Glasgow Royal Infirmary	Ancotil (5-FC)
Greiner	Aspiration pipettes, 50 ml pipettes, 25, 75 and 175 cm^2 tissue culture flasks
GE Healthcare	Gene images AlkPhos direct labelling and detection system, Gene images CDP-Star detection module, Hypercassettes (18 x 24 cm), Hyperfilm ECL, Hybond N+ membrane, PD-10 de-salting columns
Jacobus pharmaceuticals	WR99210
Kodak	Autoradiography film
Life Technologies	LysoSensor green DND-153, LysoSensor green DND-189, MitoTracker green-FM, Novex tricine gels and buffer kit, goat monoclonal anti-mouse Alexa 594-conjgated antibody, blasticidin-S-HCl, Accuprime *Pfx* SuperMix, Albumax II, gel cassettes, EBSS, Gateway multi-site cloning kit, glycogen, agarose, low melting point (LMP) agarose, chemically competent *E. coli* TOP10 and *ccdB* Survival T1 cells, gentamycin, POROS MC nickel column, RPMI 1640 (with 25mM HEPES, L- glutamine, without NaHCO3), SYBR Safe, TRIzol reagent
Lonza (UK)	TaKaRa *Ex-Taq* polymerase
Melford	Benzamidine, leupeptin, E64, kanamycin, ampicillin, carbenicillin, isopropyl-O-dithiogalacopyranoside (IPTG), dithiothreitol (DTT), proteinase K

Merck-Millipore	Chloramphenicol, BugBuster extraction reagent, YeastBuster extraction reagent, Immobilon western blot detection kit
Miltenyi	LS+ Columns
Nalgene	1.0 ml cryotubes
New England Biolabs	T4 ligase and buffer, 1 kb DNA ladder, 100 b DNA ladder, 6 x DNA loading dye, all restriction endonucleases and associated buffers
Novagen	Benzonase, chemically competent *E. coli* BLR (DE3), pET28a(+) vector
PAA	Gentamycin, amino acid-limited RPMI (custom)
Promega	Anti-mouse IgG (HRP conjugated), anti-rabbit IgG (HRP conjugated), pGEM-T Easy vector system II
Qiagen	QIAprep Hispeed maxiprep extraction kit, QIAprep spin DNA miniprep Kit, QIAquick gel extraction kit, QIAamp DNA mini kit, QIAquick PCR purification kit, Ni-NTA resin
Roche	Bovine Serum Albumin (BSA)
Sigma	All chemicals unless otherwise stated
StrataGene	Chemically competent *E. coli* XL10-Gold, chemically competent *E. coli* StrataClone Solo Pack, StrataClone Blunt PCR cloning kit
Thermo Scientific	Restore Plus western blot stripping buffer, AminoLink coupling resin, LabTek II chamber slides (Nunc)
VWR	Giemsa stain, Vivaspin protein concentrators
Wallac	Betaplate Scintillant, Printed Filter Mat A filter membranes
Zeiss	Imersol microscopy oil

2.2 Equipment

Applied Systems	Delta Vision Core microscope, SoftWoRx software
Beckman Coulter	Avanti J-26 XP centrifuge with JA25.50 rotor (used for spins at 48,000 *g*) and F10BCL rotor (used for spins at 4,400 *g*)
Bio-Rad	Gel tanks, Gene Pulser Xcell electroporator, Power Pac 300, Power Pac Basic, PowerPac HC, Transblot semi-dry transfer cell, GelDoc 2000 (Mitsubishi P91 printer) CHEF-DR-III system, Biologic DuoFlow purification system, BioFrac collector, 583 Gel dryer (KNF vacuum pump)
Constant Systems	One shot cell disrupter
Eppendorf	Microcentrifuge 5415D with F45-24-11 rotor (used for spins at 16,000 *g*), BioPhotometer 6131 000.055 (DPU-414 thermal printer)
Fisher	Microcentrifuge Accuspin MicroR with 13-100-515 rotor (used for spins at 13,000 *g* and 16,000 *g*), water bath
GE Healthcare	Vacu Gene Pump, Vacu Gene XL
G Storm	GS4 4 block PCR machine
Grant	Heat block QBT2, water bath
GraphPad	GraphPad Prism software
GRI	DR-88M transilluminator

Hamamatsu	C4742 CCD camera
Hansal	Impulse sealer
Hawksley	BS.748 Neubauer chamber
Heidolph	Reax top whirly mixer, Rotamax 120 shaker
HT	CH4103 Shaking incubator
Hybaid	Mini 10 incubator
Kühner	Shaking incubator ISF-1-W
Life Technologies	250 EX power pack, Vector NTI software
Millipore	Quantum ddH_2O system
Miltenyi	Vario MACS magnet system
Molecular Devices	Versamax microplate reader
Motic	BA400 microscope
Perkin Elmer	1450 microbeta scintillation counter, Openlab software
Photometrics	CoolSNAP HQ^2 camera
Prestige medical	2100 classic autoclave
Sigma	Sigma 6K 15 centrifuge with 11150 rotor (used for spins at 1,000 *g*)
Thermo Scientific	Sorvall ST-16R centrifuge with TX-400 rotor (used for spins at 400 *g* and 1,800 *g*), NanoDrop 1000, Holten Maxi Safe hood
TomTec	Mach III harvester (GAST and Charles Austin Dymax 30 pumps)
UVP	HB-1000 hybridization oven, UV cross linker
Wallac	1295-012 heat sealer
Zeiss	AxioSkop 2 mot plus microscope

2.3 Buffers, solutions and media

2.3.1 General buffers

1 x PBS	140 mM NaCl, 3 mM KCl, 10 mM Na_2HPO_4, 1.8 mM KH_2PO_4, pH 7.4
Potassium phosphate (pH 7.2)	5 mM KH_2PO_4, 5 mM K_2HPO_4 (in 28:72 ratio from 0.5 M stocks)

2.3.2 DNA analysis

6x DNA loading dye	0.25 % (w/v) bromophenol blue, 0.25 % (w/v) xylene cyanol FF, 0.25 % (w/v) orange-G, 40 % (w/v) sucrose
20 x SSC	300 mM Trisodium citrate, 3 M NaCl, pH 7-8
Southern depurination	0.25 N HCl
Southern denaturing	1.5 M NaCl, 0.5 M NaOH
Southern neutralisation	3 M NaCl and 0.5 M Tris (pH 7.0)
Southern hybridisation	Gene images AlkPhos hybridization buffer, 0.5 M NaCl, 4 % (w/v) blocking reagent
Southern primary wash buffer	2 M Urea, 0.1 % (w/v) SDS, 50 mM sodium phosphate pH 7.0, 150 mM NaCl, 1 mM $MgCl_2$, 0.2 % (w/v) blocking reagent
Southern secondary wash buffer	50 mM Tris base, 100 mM NaCl, 2 mM $MgCl_2$

TE	10 mM Tris-HCl, 1 mM EDTA, pH 8.0
1 x TAE	40 mM Tris-acetate, 1 mM EDTA, pH 8.0

2.3.3 Protein analysis

Coomassie stain	Gelcode Blue Safe reagent
Destaining solution	20 % (v/v) Methanol, 10 % (v/v) acetic acid
Protein loading buffer	62.5 mM Tris / HCl pH 6.8, 2 % (w/v) SDS, 10 % (v/v) glycerol, 0.001 % (w/v) bromophenol blue, 5 % (v/v) 2- mercaptoethanol
Bulk lysis buffer	50 mM TRIS, 500 mM NaCl, 10 % glycerol in PBS supplemented with 5 µg/ml RNase A, 1 mM PMSF, 1 mM benzamidine, 2 µg/ml leupeptin, 10 µM E-64, 2 mM 1,10-phenanthroline, 4 µM pepstatin A
Running gel buffer	375 mM Tris-base pH 8.9, 0.1 % SDS (w/v), 5-15 % (v/v) acrylamide
1x SDS-PAGE running buffer	25 mM Tris, 192 mM glycine, 0.1 % (w/v) SDS
Stacking gel buffer	122 mM Tris-HCl pH 6.7, 0.1 SDS (w/v), 5 % acrylamide
Towbin buffer	25 mM Tris, 192 mM glycine, 20 % (v/v) Methanol

2.3.4 Bacteria culture

Ampicillin	100 mg/ml in ddH_2O (1000 x stock)
Chloramphenicol	34 mg/ml in ethanol (1000 x stock)
Kanamycin	50 mg/ml in ddH_2O (1000 x stock)
Luria Bertani (LB) medium	10 g/l Tryptone, 5 g/l yeast extract, 5 g/l NaCl
LB agar	1.5 % (w/v) agar in LB medium
Terrific Broth medium	12 g/l Tryptone, 24 g/l yeast extract, 0.4 % (v/v) glycerol, 9.4 g/l K_2HPO_4, 2.2 g/l KH_2PO_4 pH 7.2
TfB I	100 mM RbCl, 50 mM $MnCl_2$ x 4 H_2O, 30 mM potassium acetate, 10 mM $CaCl_2$ x 2 H_2O, 15 % (v/v) glycerol
TfB II	10 mM MOPS, 10 mM RbCl, 75 mM $CaCl_2$ x 2 H_2O,15 % (v/v) glycerol

2.3.5 Yeast culture

YPD medium	20 g/l bacteriological peptone, 10g/l yeast extract, 20 g/l glucose, (20g/l bacteriological agar for YPD agar) in ddH_2O
SC medium	7g/l YNB without amino acids, 1.92 g/l Kaiser medium supplement, 20 g/l glucose, (20 g/l bacteriological agar for SC agar) in ddH_2O
Induction medium	1.9 g/l YNB without amino acids or ammonium sulphate, 20 g/l glucose, 20 % glycerol in ddH_2O
Transformation buffer	100 mM lithium acetate, 10 mM Tris / HCl, 1 mM EDTA

PLATE buffer	40 % PEG 3350 in transformation buffer
Kaiser medium supplement	SC, -Ura (DSCK102, Formedium)

2.4 *P. falciparum* culture

5-FC (Ancotil)	4 mM in blood wash medium
Blasticidin-S-HCl (BLA)	10 mg/ml in blood-wash medium
Blood-wash medium	15.9 g/l RPMI 1640 (with 25 mM HEPES and L-glutamine), 0.1 % (w/v) sodium bicarbonate, 10 mM glucose, 200 µM hypoxanthine, 20 µg/ml gentamycin, pH 7.4
Complete RPMI 1640 medium	Blood wash medium supplemented with 0.5 % (w/v) Albumax II
Amino acid limited medium	Complete RPMI 1640 medium except RPMI 1640 replaced with amino acid free RPMI and supplemented with 50 mg/l L-Isoleucine, 65.2 mg/l L-Cystine 2 HCl, 15 mg/l L-Methionine, 300 mg/l L-Glutamine and 20 mg/l L-Glutamic Acid
Earle's balanced salt solution (EBSS)	5.33 mM KCl, 26.19 mM NaHCO3, 117.24 mM NaCl, 1.01 mM $NaH_2PO_4.H_2O$
EBSS+G	As above plus 11mM D-glucose
IC_{50} Medium	RPMI 1640 medium without hypoxanthine
Cytomix	120 mM KCl, 0.15 mM $CaCl_2$, 2 mM EGTA, 5 mM $MgCl_2$, 10 mM K_2HPO_4 / KH_2PO_4 pH 7.6, 25 mM HEPES pH 7.6
Freezing solution	30 % (v/v) glycerol in PBS
Parasite lysis buffer	1 % Triton X-100 in PBS supplemented with 5 µg/ml RNase A, 1 mM PMSF, 1 mM benzamidine, 2 µg/ml leupeptin, 10 µM E-64, 2 mM 1,10-phenanthroline, 4 µM pepstatin A
WR99210	Stock solution: 20 mM in dimethylsulphoxide Working solution: 20 µM in blood wash medium

2.5 Bacteria strains

BLR (DE3) (Novagen) Used for *Pf*ATG8 expression:
F- ompT hsdSB(rB- mB-) gal dcm (DE3) 6(srl-recA)306::Tn10 (TetR)

JM109 (Promega) Used for pGEM-T Easy cloning:
*rec*A1, *end*A1, *gyr*A96, *thi*, *hsd*R17 (rK-,mK+), *rel*A1, *sup*E44, Δ(*lac-pro*AB), [F', *tra*D36, *pro*AB, *lac*I^qZΔM15]

SoloPack® (StrataGene) Used for pSCBamp/kan cloning:
Tet_r Δ(mcrA)183 Δ(mcrCB-hsdSMR-mrr)173 endA1 supE44 thi-1 recA1 gyrA96 relA1 lac Hte [F´ proAB $lacI_q$ZΔM15 Tn10 (Tet_r) Amy Cam_r]

One Shot® Top10 (Life Technologies) Used for Gateway cloning:
F- mcrA 6(mrr-hsdRMS-mcrBC) \80lacZ6M15 6lacX74 recA1 ara2139 6(ara-leu)7697 galU galK rpsL (StrR) endA1 nupG

'Homemade Top10' Used for all other cloning:
See above

2.6 *P. falciparum* strains

3D7 The Netherlands

D10 Papua New Guinea

2.7 Molecular methods

2.7.1 Determination of DNA concentrations

Concentrations of DNA were determined by measuring absorbance with a NanoDrop spectrophotometer (Thermo Scientific, UK) reading at 260 nm (Gallagher, 2001). 260/280 and 260/230 ratios were used as an indicator of DNA purity according to manufacturer's guidelines.

2.7.2 Agarose gel electrophoresis

For separation of DNA, agarose or low melting point (LMP) agarose were heated and dissolved to the required concentration (0.8 – 1 % (w/v)) in 1 x TAE buffer and SYBR Safe was added to 0.5 µg/ml before casting of gels. DNA samples were mixed with 6 x DNA loading dye and separation was performed bathed in 1 x TAE at 5 – 10 V/cm^2 gel. To determine the size of separated bands 1 kb or 100 b ladders were run alongside samples where appropriate. Ladder and sample bands were visualised with a transilluminator.

2.7.3 Ethanol precipitation of DNA

DNA was concentrated for transfection into *P. falciparum* by ethanol precipitation with sodium acetate (Russell, 2001). For each transfection 75 µg plasmid DNA in ddH_2O was mixed with 3 x volumes of ice cold ethanol, 0.1 x volumes of 3 M sodium acetate pH 5.2 and 20 µg of glycogen. DNA was allowed to precipitate at - 20 °C overnight (16 h) before centrifugation at 16,000 *g* at 4 °C for 10 min. The supernatant was removed and the pellet was washed in 100 µl ice cold 70 % ethanol before a second spin. Under sterile conditions, the supernatant was removed and the pellet allowed to air-dry (~ 1 h) prior to resuspension in 30 µl ddH_2O.

2.7.4 Restriction endonuclease digests

All restriction endonucleases were purchased from New England Biolabs, UK (N.E.B.). Digests were performed according to manufacturers' guidelines with appropriate buffer (and BSA) at 37 °C in an incubator to avoid evaporation and condensation. Typically 200 – 300 ng of plasmid DNA was digested in order to determine ligation results.

2.7.5 Polymerase chain reaction

Polymerase chain reaction (PCR) was used to amplify DNA products from genomic DNA or plasmid sequences. One hundred ng of gDNA or cDNA and 1 ng plasmid DNA was used as a template with 132 nM of each appropriate primer and either *Pfx* SuperMix (Life Technologies, UK), Reddy mix (Fisher, UK) or *Ex-Taq* (Lonza, UK) according to manufacturer's guidelines. A GS4 PCR machine (G Storm, UK) was used to run the following programme, which was modified if needed.

Step 1: 95°C, 5 min
Step 2: 95°C, 30 sec
Step 3: annealing temperature between 40 – 60°C, 30 sec
Step 4: 60°C, 1.5 min per 1,000 base pairs to be amplified
Repeat steps 2-4 for 30 cycles
Step 5: 60°C, 10 min
Step 6: Store at 10°C

2.7.6 Oligonucleotides

Oligonucleotide primers were ordered from Eurogentec, UK and were resuspended to 3.2 µM in ddH_2O before use in PCRs or sequencing reactions. Oligonucleotides generated for this study are listed below. For the majority of sequencing reactions, standard M13F and M13R primers were used.

2.7.6.1 Amplification of genes encoding potential ATG homologues in *P. falciparum*

*Pf*ATG3 fwd ATGAGTGACCAAATAAATGTCAAAC
*Pf*ATG3 rev TCATAATCCTGCATTGCTATCC
*Pf*ATG4 fwd ATGTCTAAAGAAATGAAAAACTTTG
*Pf*ATG4 rev TTATAACACAACTAATCCTGAATC
*Pf*ATG5 fwd ATGGAGATAGGTTATATGGAAGTAC
*Pf*ATG5 rev TTAATAGGGGGGTATACGTATG
*Pf*ATG7 fwd ATGAAAAAAAAATTCGAAGAG
*Pf*ATG7 rev TCATTCCAATATTATAACATCATTC
*Pf*ATG8 fwd ATGCCATCGCTTAAAGACG
*Pf*ATG8 rev TTATCCTAGACAACTCTCACAAC
*Pf*ATG10 fwd ATGTTACCTTACATTATAAATTTTC
*Pf*ATG10 rev TTATGTATTTTTTTTTTTTTTTTC
*Pf*ATG12 fwd ATGACAGAGAATTATATACAGTATATAC
*Pf*ATG12 rev TTAATATGCTGGCGTAAAAC

2.7.6.2 Yeast complementation

Yeast-*Pf*ATG8 fwd (***Bam*HI**) GCGC**GGATCC**ATGCCATCGCTTAAAGACGAAG
Yeast-*Pf*ATG8 rev (***Pst*I**) GCGC**CTGCAG**TTATCCTAGACAACTCTCACAACTATATTC

2.7.6.3 Recombinant His-*Pf*ATG8 expression

His-*Pf*ATG8 fwd (***Nhe*I**) A**GCTAGC**CCATCGCTTAAAGACGAA
His-*Pf*ATG8 rev (***Xho*I**) G**CTCGAG**TTATCCTAGACAACTCTCACA

2.7.6.4 Gateway cloning

Gway-EP fwd (***att*B4**)
GGGGACAACTTTGTATAGAAAAGTTGCGGGAAAAATAAAAAGTTGAACAC
Gway-EP rev (***att*B1r**)
GGGGACTGCTTTTTTGTACAAACTTGCTATAAATAAAAATGTAAGTAC
Gway-*Pf*ATG8 fwd (***att*B2r**)
GGGGACAGCTTTCTTGTACAAAGTGGTTCCATCGCTTAAAGACGAAG
Gway-*Pf*ATG8 rev (***att*B3**)
GGGGACAACTTTGTATAATAAAGTTGCTTATCCTAGACAACTCTCACAACTATATTC
Gway-*Pf*ATG8ΔG rev (***att*B3**)
GGGGACAACTTTGTATAATAAAGTTGCTTATAGACAACTCTCACAACTATATTC

2.7.6.5 Knockout cloning

*Pfatg*8 5' flank fwd (***Sac*II**) GCGC**CCGCGG**GTTGCCTGTGTTATAATTTACAACC
*Pfatg*8 5' flank rev (***Spe*I**) GCGC**ACTAGT**CACTTAGAAAGAAGGTGTGAAATTC
*Pfatg*8 3' flank fwd (***Nco*I**) GCGC**CCATGG**CGATTACGAATATAATAGTGTCAATGTG
*Pfatg*8 3' flank rev (***Avr*II**) GCGC**CCTAGG**GAGAAATTATTTGTAGAGAAAAGTTTG
EP fwd (***Sac*II**) GCGC**CCGCGG**GTTGTGTGGAATTGTGAGCG
*Pb*DT 3'UTR rev (***Spe*I**) **ACTAGT**CGCTACGTACTGCAGGG

2.7.6.6 PCR analysis of the *Pfatg*8 locus

(**1**)ORF fwd ATGCCATCGCTTAAAGACG
(**2**)ORF rev CATCTTTTCAAAACAACAAAATG
(**3**)Genomic fwd GGAGGTAATAAAAATGTGAAG
(**4**)Genomic rev ATTCGTTGAATATTTAACAAATC
(**5**)pCC-4 fwd CCAATAGATAAAATTTGTAGAG
(**6**)pCC-4-rev TTATTAAATCTAGAATTCATATCG
(**7**)CD fwd ATCCCTTCCTTACTACAGATTAGG
(**8**)CD rev ATCAGATTGTTGGTTGAAGAAGG

2.7.7 Gateway cloning

To generate *P. falciparum* expression constructs Life Technologies' Multisite Gateway technology was used. This is based on the site specific recombination system of bacteriophage lambda (Landy, 1989). The technology allows the simultaneous cloning of 3 DNA fragments in a defined order and orientation into a final destination vector in a 2 step process. The first step requires the cloning of PCR products into donor vectors. This resembles the integration of the lambda phage into its *E. coli* host genome during the lysogenic cycle. The second step, which resembles the excision of the lambda genome at the onset of the lytic cycle, involves the combination of DNA fragments from 3 donor vectors into a single destination vector (Hartley *et al.*, 2000). Standard entry clones were used for intermediate cloning steps. Two destination vectors were used in the generation of *P. falciparum* expression constructs. pHBlR-3/4 and pCHDR-3/4 are derived from pHBcam (van Dooren *et al.*, 2005, Waller *et al.*, 2000) and have key modifications for use in *P. falciparum*, amongst which a Rep20 element promotes inheritance of episomal plasmid into daughter merozoites by promoting segregation via interaction with chromosome ends (O'Donnell *et al.*, 2002). These constructs have been successfully used in sequential transfections in *P. falciparum* due to their different selectable markers (van Dooren *et al.*, 2005).

2.7.7.1 Gateway entry clones

PCR fragments generated by *Pfx* SuperMix were purified by gel extraction using Qiagen's QIAquick gel extraction kit and were recombined with the appropriate donor vector via the BP reaction according to the manufacturer's guidelines (Life Technologies, UK). Briefly, 50 fmoles of purified PCR product was mixed with 1 µl vector and 2 µl BP Clonase II for overnight incubation at 25 °C. The following

morning, 1 µl Proteinase K was added for 10 min incubation at 37 °C prior to transformation of SoloPack cells using 2 or 4 µl of the mixture. Clones selected with 50 µg/ml kanamycin were analysed by restriction digest to test for presence of insert and potentially successful clones were sequenced to confirm correct recombination of PCR fragments. Plasmid maps of the three Gateway intermediate vectors used are shown in Figure 2.1.

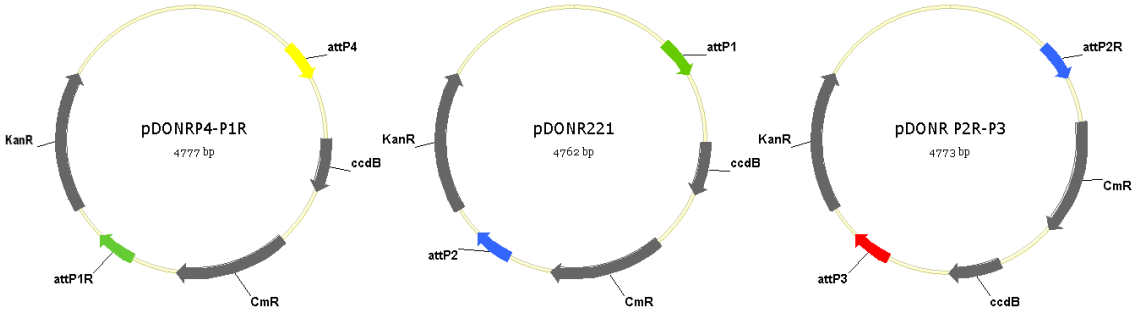

Figure 2.1: Plasmid maps of empty Gateway intermediate vectors.

(left) pDONR P4-P1R was used as an intermediate vector for 5' UTR elements. The *ccdB* death gene and chloramphenicol resistance cassette (CmR) replaced by the insert sequence are shown.

(middle) pDONR 221 was used as an intermediate vector for mCherry / eYFP elements. The *ccdB* death gene and CmR replaced by the insert sequence are shown.

(right) pDONR P2R-P3 was used as an intermediate vector for ORF elements. The *ccdB* death gene and CmR replaced by the insert sequence are shown.

2.7.7.2 Gateway expression clones

Sequenced entry clones were recombined with an appropriate destination vector to generate *P. falciparum* expression constructs according to the manufacturer's guidelines (Life Technologies, UK). Briefly, 10 fmoles of each entry clone was mixed with 20 fmoles of the appropriate destination vector and 2 µl LR Clonase II Plus for overnight incubation at 25 °C. The following morning, 1µl Proteinase K was added for 10 min incubation at 37 °C prior to transformation of SoloPack cells using all of the mixture. Clones selected with 100 µg/ml ampicillin were analysed by restriction digest to test for presence of insert and potentially successful clones were sequenced to confirm correct recombination of DNA fragments. Plasmid maps of the two Gateway destination vectors used are shown in Figure 2.2.

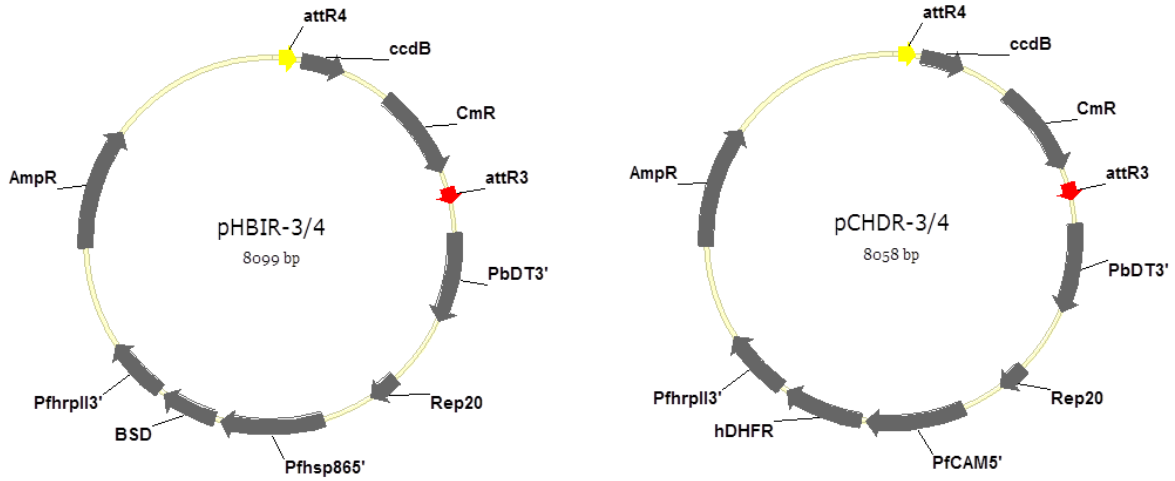

Figure 2.2: Plasmid maps of empty Gateway destination vectors.

(left) pHBIR-3/4 (*Hsp*86 5' UTR driving blasticidin S deaminase with Rep20 in a head to tail (-) orientation with the *att*R3/R4 cassette), showing key regulatory elements. Recombination between entry clones and *att*R3 and *att*R4 sites results in the replacement of the lethal *ccd*B gene. Parasites transfected with pHBIR-3/4-based constructs were selected with blasticidin.

(right) pCHDR-3/4 (Calmodulin 5' UTR driving human DHFR with Rep20 in a head to tail (-) orientation with the *att*R3/R4 cassette), showing key regulatory elements. Recombination between entry clones and *att*R3 and *att*R4 sites results in the replacement of the lethal *ccd*B gene. Parasites transfected with pCHDR-3/4-based constructs were selected with WR99210.

2.7.8 Subcloning into intermediate vectors

To ensure efficient digestion of PCR products and to facilitate sequencing of PCR reactions before cloning into expression or transfection vectors, PCR products were first cloned into appropriate intermediate vectors.

Ex-Taq (Lonza, UK) was used as the DNA polymerase to amplify the *Pfatg*8 3' flank used in the generation of knockout constructs. PCR products contained single deoxyadenosine overhangs at their 3'-ends and so were cloned into the pGEM-T Easy vector using the pGEM-T Easy Vector kit (Promega, UK) according to the manufacturer's guidelines. Briefly, ~ 25 ng of purified PCR product was mixed with 5 µl buffer, 1 µl vector and 1 µl ligase and allowed to mix overnight. Half or all of the ligation mixture was then used to transform JM109 cells and clones were subjected to blue / white screening by adding 0.5 mM IPTG and 80 µg/ml X-Gal to Luria Bertani medium (LB) agar, which also contained 100 µg/ml ampicilin. Inserts were sequenced from minipreps generated from white colonies (see 2.7.12) and excised by restriction digest. A plasmid map of pGEM-T Easy is shown in Figure 2.3.

In all other PCRs intended for subsequent cloning steps, *Pfx* SuperMix (Life Technologies, UK) was used as the DNA polymerase. PCR products were blunt ended and so were cloned into pSC-B amp/kan via the StrataClone Blunt PCR cloning kit (StrataGene, UK) according to manufacturer's guidelines. Briefly, ~ 50 ng of purified PCR product was mixed with 3 µl buffer and 1 µl vector and allowed to mix for 5 min before transforming SoloPack cells with half or all of the ligation mixture. Inserts from white colonies subjected to blue / white screening by adding 80 µg/ml X-Gal to Luria Bertani medium (LB) agar, which also contained 100 µg/ml ampicillin, could then be sequenced and excised by restriction digest. A plasmid map of pSC-B-amp/kan is shown in Figure 2.3.

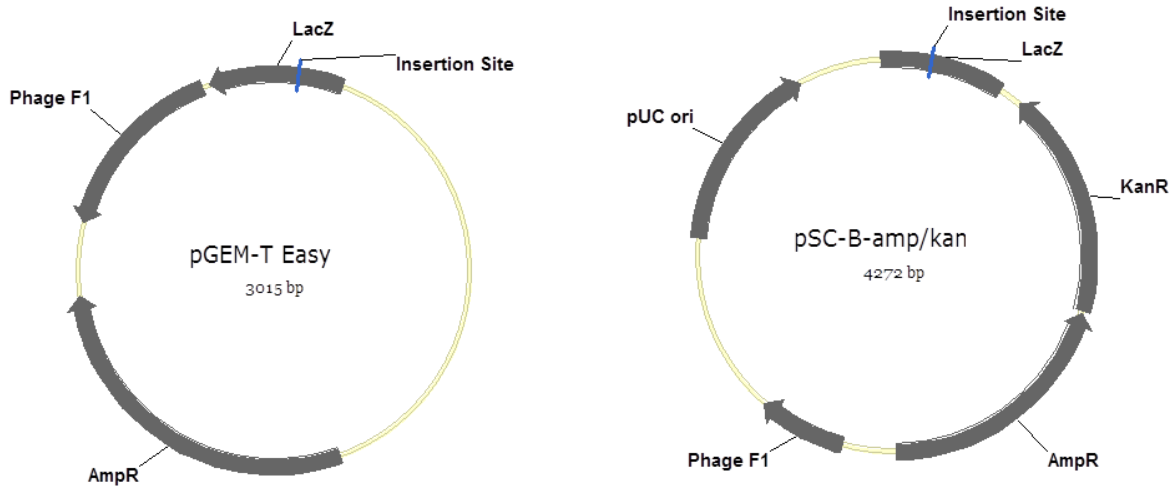

Figure 2.3: Plasmid maps of intermediate vectors.

(left) pGEM-T Easy was used for subcloning of 3' homologous flanks before ligation into pCC-4. The site where PCR products with single deoxyadenosine overhangs insert is shown. Insertion disrupts the Lac operon component LacZ, which allows blue / white screening.

(right) pSC-B-amp/kan was used for all other subcloning steps. The site where blunt ended PCR products insert is shown. Insertion disrupts the Lac operon component LacZ, which allows blue / white screening.

2.7.9 Cloning into transformation / transfection vectors

Inserts were excised from intermediate vectors with appropriate restriction enzymes and were purified by gel extraction using Qiagen's QIAquick kit. Purified insert DNA was mixed with 50 ng digested vector in 1:1 and 3:1 insert to vector ratios. Ligations were performed with 1 µl T4 DNA ligase (N.E.B.) in 1 x ligation buffer overnight at room temperature in total volume of 15 µl. Half or all of the ligation mixture was used to transform BLR (DE3) for *E. coli* expression constructs or Top10 for all *S. cerevisiae* expression and *P. falciparum* knockout

constructs. Plasmid maps of bacterial (pET28a(+)) and yeast (pCM186) expression vectors are shown in Figure 2.4. A plasmid map of pCC-4, used for genetic knockout in *P. falciparum* is shown in Figure 5.1.

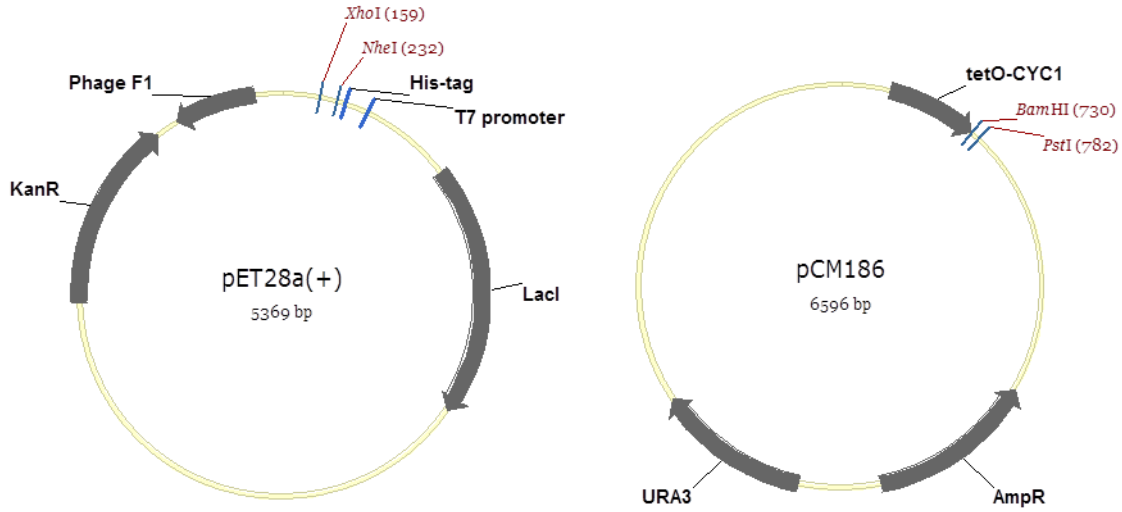

Figure 2.4: Plasmid maps of *E. coli* and *S. cerevisiae* expression vectors.

(left) pET28a(+) was used to express His-tagged *Pf*ATG8 in *E. coli*. *Nhe*I and *Xho*I restriction sites used for directional cloning are indicated. The inserted sequence is in frame with a sequence encoding an N-terminal poly-histidine tag and is under control of the T7 promoter.

(right) pCM186 was used to express *Pf*ATG8 in *S. cerevisiae*. *Bam*HI and *Pst*I restriction sites used for directional cloning are indicated. The URA3 cassette encoding orotidine 5-phosphate decarboxylase, used for selection in yeast is shown. The inserted sequence is under control of the hybrid tetracycline-responsive (tetO-CYC1) promoter (Gari *et al.*, 1997).

Constructs for transfection or transformation, generated for this study, along with the oligonucleotides and intermediate vectors used in their generation are detailed in Table 2.1.

Table 2.1: Constructs generated for this study (see following page).

***Pf*ATG8-pCM186 was used for complementation studies in *S. cerevisiae* lacking *Sc*ATG8 (see 3.2.4).**

His-*Pf*ATG8-pET28a(+) was used for the recombinant expression of His-*Pf*ATG8 in *E. coli* (see 3.2.5).

The expression constructs EP-mC-A8, EP-mC-A8ΔG, 86-mC-A8, EP-eY-A8, EP-eY-A8ΔG and 86-eY-A8, 86-eY-A8ΔG were used for expression of fluorescent fusion proteins of *Pf*ATG8 or the truncated form *Pf*ATG8ΔG in *P. falciparum* (see 4.2.1). A second version of EP-mC-A8 was generated using the destination vector pHB1R-3/4 (selected with BLA) so that colocalisation studies could be performed (see 4.2.7).

***Pfatg*8-pCC-4 was used in attempts to knockout the endogenous *Pfatg*8 ORF (see 5.2.1-2).**

***mCherry-Pfatg*8-pCC-4 was used in attempts to replace the endogenous *Pfatg*8 ORF (see 5.2.3).**

Construct	Purpose (selection)	Oligonucleotides	Intermediate vector	Gene Insert
*Pf*ATG8-pCM186	Expression of *Pf*ATG8 in *S. cerevisiae* (Uracil)	(Yeast-*Pf*ATG8 fwd - Yeast-*Pf*ATG8 rev)	pSCBamp/kan	PF10_0193 4-375 bp (ORF)
His-*Pf*ATG8-pET28a(+)	Expression of His-*Pf*ATG8 in *E. coli* (Amp)	(His-*Pf*ATG8 fwd - His-*Pf*ATG8 rev)	(Genrated by Dr. W. Proto)	PF10_0193 4-375 bp (ORF)
86-mC-A8	Expression of mCherry-*Pf*ATG8 in *P. falciparum* (WR)	(Gway-*Pf*ATG8 fwd - Gway-*Pf*ATG8 rev)	*Pfhsp*86 5'UTR-pDONRP4-P1R + mCherry-pDONR221 + *Pfatg8*-pDONRP2R-P3 into pCDHR-3/4	PF10_0193 4-375 bp (ORF)
EP-mC-A8	Expression of mCherry*Pf*ATG8 in *P. falciparum* (WR)	(Gway-EP fwd - Gway-EP rev) and (Gway-*Pf*ATG8 fwd - Gway-*Pf*ATG8 rev)	*Pfatg8* 5'UTR-pDONRP4-P1R + mCherry-pDONR221 + *Pfatg8*-pDONRP2R-P3 into pCDHR-3/4	PF10_0193 4-375 bp (ORF)
EP-mC-A8ΔG	Expression of mCherry-*Pf*ATG8ΔG in *P. falciparum* (WR)	(Gway-EP fwd - Gway-EP rev) and (Gway-*Pf*ATG8 fwd - Gway-*Pf*ATG8ΔG rev)	*Pfatg8* 5'UTR-pDONRP4-P1R + mCherry-pDONR221 + *Pfatg8*ΔG-pDONRP2R-P3 into pCDHR-3/4	PF10_0193 4-372 bp (truncated)
86-eY-A8	Expression of eYFP-*Pf*ATG8 in *P. falciparum* (WR)	(Gway-*Pf*ATG8 fwd - Gway-*Pf*ATG8 rev)	*Pfhsp*86 5'UTR-pDONRP4-P1R + eYFP-pDONR221 + *Pfatg8*-pDONRP2R-P3 into pCDHR-3/4	PF10_0193 4-375 bp (ORF)
86-eY-A8ΔG	Expression of eYFP-*Pf*ATG8ΔG in *P. falciparum* (WR)	(Gway-*Pf*ATG8 fwd - Gway-*Pf*ATG8ΔG rev)	*Pfhsp*86 5'UTR-pDONRP4-P1R + eYFP-pDONR221 + *Pfatg8*ΔG-pDONRP2R-P3 into pCDHR-3/4	PF10_0193 4-372 bp (truncated)
EP-eY-A8	Expression of eYFP-*Pf*ATG8 in *P. falciparum* (WR)	(Gway-EP fwd - Gway-EP rev) and (Gway-*Pf*ATG8 fwd - Gway-*Pf*ATG8 rev)	*Pfatg8* 5'UTR-pDONRP4-P1R + eYFP-pDONR221 + *Pfatg8*-pDONRP2R-P3 into pCDHR-3/4	PF10_0193 4-375 bp (ORF)
EP-eY-A8ΔG	Expression of eYFP-*Pf*ATG8ΔG in *P. falciparum* (WR)	(Gway-EP fwd - Gway-EP rev) and (Gway-*Pf*ATG8 fwd - Gway-*Pf*ATG8ΔG rev)	*Pfatg8* 5'UTR-pDONRP4-P1R + eYFP-pDONR221 + *Pfatg8*ΔG-pDONRP2R-P3 into pCDHR-3/4	PF10_0193 4-372 bp (truncated)
EP-mC-A8	Expression of mCherry-*Pf*ATG8 in *P. falciparum* (BLA)	(Gway-EP fwd - Gway-EP rev) and (Gway-*Pf*ATG8 fwd - Gway-*Pf*ATG8 rev)	*Pfatg8* 5'UTR-pDONRP4-P1R + mCherry-pDONR221 + *Pfatg8*-pDONRP2R-P3 into pHB1R-3/4	PF10_0193 4-375 bp (ORF)
Pfatg8-pCC-4	genetic knockout of *Pfatg8* (BLA)	(*Pfatg8* 5' flank fwd - *Pfatg8* 5' flank rev) and (*Pfatg8* 3' flank fwd - (*Pfatg8* 3' flank rev)	pSCBamp/kan (5'Flank), pGEM-T Easy (3'Flank)	PF10_0193 -1979--1369 bp (5') and 546-1183 bp (3')
mCherry-Pfatg8-pCC-4	genetic replacement of *Pfatg8* (BLA)	(EP fwd - *Pb*DT 3'UTR rev) and (*Pfatg8* 3' flank fwd - *Pfatg8* 3' flank rev)	pSCBamp/kan (5'Flank), pGEM-T Easy (3'Flank)	*Pfatg8* 5'UTR-*mCherry-Pfatg8-Pb*DT3'UTR (5') and PF10_0193 546-1183 bp (3')

2.7.10 Preparation of chemically competent *E. coli*

A 5 ml pre-culture was grown overnight in LB medium and used to inoculate 500 ml fresh medium the next morning. Cells were grown at 37 °C in a shaking incubator until the OD_{600} of the culture reached 0.5. The bacteria culture was subsequently cooled on ice for 15 min before being transferred into sterile centrifuge tubes. Cells were centrifuged at 4,400 *g* for 10 min at 4 °C. The supernatant was discarded and the cells were resuspended in 30 ml TfB I. The cells were incubated on ice for 15 min before centrifugation at 4,400 g for 5 min. The supernatant was again discarded and the cells were resuspended in 6 ml TfB II. The cells were aliquoted into 1.5 ml tubes and shock frozen on dry ice. Chemically competent cells were stored at – 80 °C. This was performed by A. McIntosh.

2.7.11 Transformation of chemically competent *E. coli*

Plasmid DNA, Gateway or ligation reactions were added to aliquots of chemically competent *E. coli*, which had been allowed to thaw on ice. Cells were incubated on ice for 20 min before heat shock at 42 °C for 35 – 50 sec according to manufacturer's guidelines. Following recovery on ice for 2 min, 200 µL LB medium was added and cells were incubated at 37 °C with gentle shaking for 1 h. Typically 50 and 200 µL of the transformation mixture was then spread onto LB agar plates containing the appropriate antibiotics (100 µg/ml ampicillin, 50 µg/ml kanamycin or 34 µg/ml chloramphenicol) and IPTG or X-Gal when necessary.

2.7.12 Isolation of plasmid DNA from transformed *E. coli*

For isolation of plasmid DNA for transfection of *P. falciparum*, QIAprep Hispeed maxiprep extraction (Qiagen, UK) kits were used according to manufacturer's guidelines. Briefly, sequenced clones were used to inoculate 5 ml starter cultures of Terrific Broth (TB) with the appropriate antibiotic for 8 h incubation at 37 °C with gentle shaking. These were then diluted 1:100 to 500 ml overnight cultures of TB with the appropriate antibiotic for overnight incubation. The following morning cultures were divided into 2 x 250 ml and *E. coli* cells were pelleted by centrifugation at 4,400 *g* for 15 min at 4 °C. Plasmid DNA was then

extracted according to the provided protocol and eluted into 2 x 200 µl ddH_2O. Typical yield was ~ 500 µg of plasmid DNA.

For isolation of plasmid for all other cloning steps, Qiagen's QIAprep spin DNA miniprep Kit was used according to manufacturer's guidelines. Briefly, single colonies picked from selective LB agar plates were used to inoculate a 5 ml LB overnight culture with the appropriate antibiotic for overnight incubation at 37 °C with gentle shaking. The following morning 1 ml of culture was used to make a glycerol stock (mixed thoroughly with 0.5 ml 50 % glycerol and stored at - 80 °C) while the remaining *E. coli* cells were pelleted by centrifugation at 4,400 *g* for 5 min at 4 °C. Plasmid DNA was then extracted according to the provided protocol and eluted into 40 µl ddH_2O. Typical yield was ~ 10 µg of plasmid DNA.

2.7.13 Reverse transcription

Reverse transcription of RNA was performed using the RETROscript reverse transcription for real time PCR kit (Ambion, UK) according to the manufacturer's guidelines. Prior to reverse transcription, parasite RNA was treated with Turbo DNA-free (Ambion, UK) according to manufacturer's instructions to remove any traces of contaminating DNA. Ten µg of extracted RNA was used in a 50 µl reaction for this treatment. Of the DNase treated RNA, 10 µl corresponding to 1 - 2 µg of RNA was used for the generation of cDNA. Reverse transcription was performed following the two step RT-PCR protocol with heat denaturation step according to manufacturer's instructions. The cDNA was stored at – 20 °C. This was performed by Dr. E. Patzewitz.

2.7.14 Southern blot analysis

To analyse the genotype of *P. falciparum* lines transfected with pCC-4-based constructs, 1.5 µg of isolated DNA was analysed by Southern blotting (see 2.10.6 for DNA isolation). DNA was digested overnight at 37 °C with *Spe*I (N.E.B., UK) according to the manufacturer's guidelines. The following morning an additional 1 µl of *Spe*I was added for further 6 h incubation. Digested DNA was separated by electrophoresis in 0.7 % agarose at 20 V for ~ 20 h. Separated DNA was then depurinated in 0.25 M HCl for 10 min, denaturated in 1.5 M NaCl and 0.5 M NaOH for 30 min and neutralised in 3 M NaCl and 0.5 M Tris (pH 7.0) for 30 min. DNA

was then transferred to Hybond N+ nitrocellulose membrane using VacuGene XL apparatus (GE Healthcare, UK) at 50 mbar for 1.5 h whilst being bathed in 20 x SSC. Lanes were marked with pencil and DNA crosslinked to the membrane in a UV crosslinker at 700 x 100 µJ/cm^2. Membranes were prehybridised in hybridisation buffer for 20 min at 55 °C before addition of the appropriate probe. Probes were generated from DNA fragments either amplified from gDNA or pCC-4 plasmid DNA by PCR using *Pfx* SuperMix (*Pfatg8*-specific and *CD*, respectively) or from restriction digests of *Pfatg*8-pCC-4 plasmid DNA (3' flank (*Nco*I-HF and *Avr*II) and *BSD* (*Bam*HI and *Hind*III-HF)). Fragments were purified by gel extraction before probes were generated using the Gene Images AlkPhos direct labelling kit (GE Healthcare, UK) according to the manufacturer's guidelines. Probes were added to prehybridised membranes in 10 ml hybridisation buffer for incubation overnight at 55 °C. The following morning membranes were washed for 3 x 10 min in primary wash buffer at 55 °C and then transferred to a clean container for 2 x 10 min washes with secondary wash buffer at room temperature. The membrane was covered in CDP Star detection solution (GE Healthcare, UK) for 5 min incubation at room temperature after which excess detection solution was removed and the membranes were sealed in plastic sheet and exposed to Hyperfilm autoradiography films (GE Healthcare, UK). To strip membranes of bound probe in order to re-probe, membranes were bathed in 0.5 % SDS at 60 °C for 2 h and were prehybridised and probed as detailed above.

2.8 Biochemical methods

2.8.1 Bradford assay

The concentration of protein samples was determined by Bradford assay (Bradford, 1976). Ten µl of bovine serum albumin (BSA) (Roche, UK) solutions of known concentrations or sample protein solutions were mixed with 250 µl Bradford protein assay reagent (Bio-Rad, UK) diluted 1:5 in ddH_2O and absorbance of each sample was read at 595 nm. BSA standards were used to generate a standard curve from which the concentrations of sample protein solutions were calculated.

2.8.2 Phospholipase D incubation

Protein extracted from wild type or parasite lines expressing mCherry-*Pf*ATG8 (see 2.10.8 for parasite protein extraction) was incubated with phospholipase D from *Streptomyces chromofuscus* (PLD) to evaluate the lipidation state of *Pf*ATG8 or mCherry-*Pf*ATG8. PLD was resuspended in ddH_2O to 10 units per µl and was stored at - 20 °C. Twenty µg of protein extract was incubated with the indicated units of PLD at 30 °C for 1 h. Samples were then mixed with protein loading buffer and were separated by SDS-PAGE or 6 M urea SDS-PAGE.

2.8.3 Sodium dodecyl sulphate polyacrylamide gel electrophoresis (SDS-PAGE)

Separation of proteins was performed by SDS-PAGE according to Laemmli (Laemmli, 1970). Gels were prepared with 5 % polyacrylamide stacking gel and resolving gel of either 7.5 % polyacrylamide for separation of mCherry-*Pf*ATG8 and aminopeptidase-1(AP1) or 15 % polyacrylamide for separation of *Pf*ATG8. Gels were poured into 1 mm plastic cassettes (Life Technologies, UK). For each gel, 6 ml of resolving gel was made by mixing resolving gel buffer with ddH_2O and 30 % acrylamide/bis-acrylamide and was polymerised by addition of 35 µl ammonium persulphate (20 % (w/v)) and 10 µl N,N,N',N'-tetramethylethylenediamine (TEMED). Butanol was layered above the resolving gel while it set to ensure a smooth transitional surface and was then removed and thoroughly washed with ddH_2O. Two ml stacking gel was made by mixing stacking gel buffer with ddH_2O and 30 % acrylamide/bis-acrylamide and was added to the set resolving gel after addition of 20 µl ammonium persulphate and 8 µl TEMED and an appropriate comb was inserted. Parasite protein extract or recombinant protein extract were denatured by mixing with protein loading buffer and boiling for 10 min before 20 µg of parasite or varying amounts of recombinant protein was loaded per lane. Six µl of Precision Plus Protein Dual Colour ladder (Bio-Rad, UK) was loaded into 1 lane of each gel. Proteins were separated by electrophoresis in 1 x SDS-PAGE running buffer at 20 mA (after penetration of resolving gel this was increased to 40 mA) at a maximum of 200 V. When urea gels were necessary, resolving and stacking gels were prepared with the addition of 6 M urea and run as described. Warming of solutions to 50 °C was needed to dissolve urea.

2.8.4 Staining of SDS-PAGE gels with Coomassie blue

Following separation by SDS-PAGE, proteins were visually detected by staining with Coomassie (Gelcode Blue Safe). Gels were carefully removed from cassettes and washed briefly in ddH_2O. They were then covered in Coomassie for 1 h with gentle rocking and destained by 3 x 5 min washes in ddH_2O and multiple 1 h washes in destain at room temperature until background staining had been removed.

2.8.5 Western blot analysis

Following SDS-PAGE, separated proteins were transferred to Protran nitrocellulose membranes (Fisher, UK) using a semi-dry method. A Transblot (Bio-Rad, UK) system was used to transfer at 23 V for 40 min (increased up to 1 h if multiple gels were transferred) with the gels, membrane and filter membrane stacks all moistened in Towbin buffer. After transfer, confirmed by visible ladder bands on the membrane, membranes were washed briefly in ddH_2O and proteins stained for 5 min with Ponceau S solution. Membranes were then washed briefly 3 times with ddH_2O to remove excess Ponceau S and allow a digital image to be taken. Lanes were marked with pencil when appropriate. Bound Ponceau S was then removed by 2 x 5 min washes in 0.1 % Tween 20 (v/v) in PBS before being blocked overnight at 4 °C in 5 % (w/v) milk powder in PBS with gentle rocking. The following morning membranes were washed briefly in 0.1 % Tween 20 (v/v) in PBS before addition of primary antibodies, diluted in 2 % milk powder (w/v) in PBS. Membranes were incubated in primary antibodies for 1.5 h at room temperature with gentle rocking before being washed 3 x 10 min in 0.1 % Tween 20 (v/v) in PBS. Membranes were then incubated with secondary antibodies diluted in 2 % milk powder (w/v) in PBS for 1 h at room temperature with gentle rocking before being washed as above. Horseradish peroxidase (HRP)-conjugated secondary antibodies were detected using the Immobilon western detection kit (Millipore, UK) and exposed to autoradiography film (Kodak, UK). Antibodies used are detailed in Table 2.1.

For loading controls, antisera raised against *P. falciparum* branched chain alpha-keto acid dehydrogenase acyltransferase subunit (BCDH) were used (Storm *et al.*, 2011). Membranes were first stripped by incubation in Restore Plus western

blot stripping buffer (Thermo Scientific, UK) for 15 min at 37 °C before being washed 3 times with ddH_2O and blocked again in 5 % (w/v) milk powder in PBS at room temperature for 2 h. Membranes were then re-probed with anti-BCDH antisera as detailed in Table 2.2.

Table 2.2: List of antibodies and dilutions used in western blotting.

Target	SDS-PAGE	Primary	Type	Dilution	Source	Secondary	Type	Dilution	Source
Recombinant PfATG8	15%	Anti-His	Monoclonal	1:10,000	BD Biosciences	Goat anti-mouse (H+L)-HRP	Polyclonal	1:10,000	Promega
Endogenous PfATG8	15 % (±6 M urea)	Anti-PfATG8	Antisera	1:1,000	This study	Goat anti-rabbit (H+L)-HRP	Polyclonal	1:10,000	Promega
mCherry-PfATG8	7.50%	Anti-mCherry	Monoclonal	1:1,000	Clontech	Goat anti-mouse (H+L)-HRP	Polyclonal	1:10,000	Promega
BCDH	7.5 % / 15 %	Anti-BCDH	Antisera	1:5,000	This lab	Goat anti-rabbit (H+L)-HRP	Polyclonal	1:10,000	Promega
AP1	7.50%	Anti-AP1	Antisera	1:1,000	(Klionsky, D)	Goat anti-rabbit (H+L)-HRP	Polyclonal	1:10,000	Promega

2.8.6 Yeast complementation

A yeast line YBL078c (EuroScarf, Germany) was transformed with the constructs *Pf*ATG8-pCM186 or *Lm*ATG12-pCM186 (as described in (Williams *et al.*, 2009)) according to the lithium acetate method (Gietz and Woods, 2006). A protocol published online as part of a yeast transformation kit was followed (http://www.sigmaaldrich.com/etc/medialib/docs/Sigma/Bulletin/yeast1bul.Par.0001.File.tmp/yeast1bul.pdf [Last accessed 14/09/2012]). In brief, yeast cultures were grown in YPD medium at 30 °C until saturation (OD_{600} > 2). Half of one ml of saturated culture was used to inoculate a fresh 25 ml YPD culture, which was incubated under the same conditions until OD_{600} was between 1.0 and 1.2. At this point the cells were pelleted by centrifugation at 1,000 *g* at room temperature for 5 min. The pelleted cells were washed with 25 ml ddH_2O before being resuspended in 0.5 ml transformation buffer and kept on ice before transformation.

To prepare plasmid DNA for transformation, 1 µg of plasmid was mixed with 10 µl of 10 mg/ml salmon sperm DNA, which had previously been boiled for 10 min and returned to ice. To this DNA mixture, 100 µl of competent cells and 600 µl of PLATE buffer were added. The transformation mixture was incubated for 30 min at 30 °C with gentle shaking before heat shock treatment at 42 °C for 15 min. Transformed cells were pelleted by centrifugation at 16,000 *g* at room temperature for 30 sec. The transformation supernatant was removed and the cells were washed with 500 µl ddH_2O before being finally resuspended in 500 µl

ddH_2O. Fifty and 200 µl of the resuspended cells were plated onto SC agar and were incubated at 30 °C for ~ 3 days until colonies were visible. Single colonies were picked and restreaked onto fresh SC agar plates to ensure isolation of successful transformants.

Single colonies of transformed lines or a wild type line, Y00000 (EuroScarf, Germany), were used to inoculate an SC or YPD medium culture, respectively. These cultures were allowed to grow to saturation at 30 °C. Two ml of each saturated culture was used to inoculate a fresh 100 ml SC or YPD culture, which was incubated under the same conditions until the OD_{600} reached 1.0. At this point each culture was divided in half and yeast cells were pelleted by centrifugation at 1,000 *g* at room temperature for 5 min. One pellet was stored at - 20 °C as the non-induced sample. The other pellet was washed 3 times in 10 ml of Induction medium before being resuspended in 100 ml Induction medium for an additional 16 h incubation at 30 °C. After this incubation, cells were pelleted by centrifugation as above and the pellet was stored at - 20 °C as the induced sample.

For extraction of yeast protein, a One Shot cell disruptor (Constant Systems, UK) was used to mechanically lyse wild type and transformed cells. Pelleted yeast cells were resuspended in 10 ml bulk lysis buffer and were disrupted twice at 35 kpsi. The soluble protein fraction was collected from the supernatant following centrifugation at 48,000 *g* at 4 °C for 45 min and was concentrated using a Vivaspin 20 centrifugation column with a 10 kDa molecular weight cut-off (VWR, UK), until approximately 1 ml remained. The concentration of protein in concentrated non-induced and induced samples was determined by Bradford assay. Twenty µg of protein collected from wild type or transformed lines was separated by 7.5 % SDS-PAGE and western blots were performed as detailed in Table 2.2.

2.8.7 Recombinant His-*Pf*ATG8 expression

In order to determine optimal conditions for His-*Pf*ATG8 expression in *E. coli* a trial of expression temperatures and durations was performed. A 10 ml starter culture of LB supplemented with 50 µg/ml kanamycin and 34 µg/ml chloramphenicol was inoculated with BLR (DE3) cells transformed with His-

*Pf*ATG8-pET28a(+) for incubation overnight at 37 °C. An aliquot of 1.6 ml of the overnight culture was used to inoculate a fresh 80 ml LB culture while the remainder was used to generate glycerol stocks. The 80 ml culture was incubated at 37 °C until OD_{600} reached 0.6, at which point 1 ml was collected as the pre-induced sample by centrifugation at 16,000 *g* at 4 °C for 5 min before being frozen as a pellet. The remaining culture was induced by addition of 1 mM IPTG and was split into 4 x 20 ml cultures for incubation at 15, 20, 30 and 37 °C. One ml samples were collected from each culture at 2, 4, 6 and 16 h post induction as above. At 16 h post induction the remaining cultures were harvested by centrifugation at 4,400 *g* at 4 °C for 15 min before being frozen as a pellet. All pellets generated from 1 ml samples were treated with BugBuster protein extraction solution (Merck, UK) in order to generate soluble and insoluble protein fractions according to manufacturer's guidelines. In brief, pellets were resuspended in 100 µl BugBuster supplemented with 1 mM benzamidine, 20 µM leupeptin, 4 µM pepstatin A and 1 mM PMSF. After thorough mixing on a rocker for 15 min at room temperature, samples were pelleted by centrifugation at 16,000 *g* at 4 °C for 15 min. Supernatants were collected as the soluble protein fraction and 12 µl of each was mixed with 3 µl protein loading buffer for separation by 15 % SDS-PAGE. Each pellet was resuspended in 30 µl protein loading buffer and 30 µl ddH_2O and 5 µl was loaded per lane for separation as above as the insoluble protein fraction.

Once the expression trial of recombinant His-*Pf*ATG8 had been analysed, all His-*Pf*ATG8 expressions were performed at 20 °C for 16 h. Two individual 20 ml LB starter cultures were inoculated with BLR (DE3) cells transformed with His-*Pf*ATG8-pET28a(+) and incubated overnight at 37 °C. Ten ml of these overnight cultures were used to inoculate 2 x 500 ml LB cultures which were incubated at 37 °C and were induced with 1 mM IPTG when OD_{600} was between 0.6 and 1.0. At this point the cultures were cooled to 20 °C and pellets were generated 16 h later by centrifugation at 4,400 *g* at 4 °C for 15 min and stored at - 20 °C. Soluble protein fractions were extracted from pellets by mechanical disruption using a Cell Disruptor (Constant Systems, UK) on a One Shot setting. Pellets were resuspended in 20 ml bulk lysis buffer and disrupted twice at 15 kpsi. The soluble protein fraction was collected from the supernatant following centrifugation at 48,000 *g* at 4 °C for 45 min.

2.8.8 Purification of His-*Pf*ATG8

Two methodologies were used for purification of recombinantly expressed proteins. Metal chelating affinity purification using nickel (Ni^{2+}) charged resin columns was used to purify His-tagged proteins of interest (Crowe *et al.*, 1994). This was achieved by either a simple 'bench-top' or a semi-automated immobilized metal affinity chromatography (IMAC) 'IMAC' method as detailed below.

2.8.8.1 'Bench-top' purification

For bench-top purification of His-*Pf*ATG8 or His-*Pf*LiplA1, supernatants containing soluble protein were transferred to a fresh 50 ml tube to which 1 ml Ni-NTA resin (Qiagen, UK), washed free of ethanol, was added for incubation overnight at 4 °C on a rocker. The mixture was then transferred to disposable filtration columns and the flow through collected and stored at - 20 °C. The packed resin was then washed with 10 ml volumes of 40 mM, 60 mM and 80 mM imidazole in bulk lysis buffer, with the flow through of each being collected and stored at - 20 °C. His-tagged protein was then eluted from the packed resin in 1 ml 250 mM imidazole in bulk lysis buffer and then 1 ml 500 mM imidazole in bulk lysis buffer. Aliquots of each elution were made and then stored at - 20 °C. One final wash was performed with 1 M imidazole in bulk lysis buffer. Ten µl of each elution and wash and 1 µl of the initial flow through (mixed with 9 µl ddH_2O) was then mixed with 3 µl of protein loading buffer and proteins were separated by 15 % SDS-PAGE.

2.8.8.2 'IMAC' purification

For purification using a semi-automated protocol, supernatants containing soluble protein were first filtered through a 0.2 µm syringe filter (Fisher Scientific, UK). A POROS MC nickel column of 1.7 ml volume (Life Technologies, UK) was initially washed in ddH_2O, stripped using 50 mM EDTA and 1 M NaCl in ddH_2O, recharged using 0.1 M nickel sulphate (pH 5) in ddH_2O and equilibrated with bulk lysis buffer using a Biologic DuoFlow System (Bio-Rad, UK). Soluble protein was then loaded onto the column and flow through was collected and stored at - 20 °C. The column was washed with 10 mM and then 20 mM imidazole in bulk lysis buffer to remove weakly bound contaminants. His-*Pf*ATG8 was then

eluted in 20 x 1 ml fractions of a constant gradient of 20 - 500 mM imidazole in bulk lysis buffer. Ten µl of peak elution fractions (monitored by UV absorbance spectra) and each wash and 1 µl of the initial flow through (mixed with 9 µl ddH_2O) was then mixed with 3 µl of protein loading buffer and proteins were separated by 15 % SDS-PAGE. If His-*Pf*ATG8 purified by either method was not immediately separated by SDS-PAGE, then PD10 de-slating columns (GE Healthcare, UK) were used to buffer exchange into either 5 M MES (pH 5.5) or bulk lysis buffer for storage. The concentration of proteins in purified fractions was determined by Bradford assay.

2.8.9 Generation of anti-*Pf*ATG8 antisera

Approximately 125 µg of purified His-*Pf*ATG8 was used per injection during an 87 day inoculation programme in a rabbit host in order to acquire antisera containing antibodies specific for *Pf*ATG8. Two rabbits were used per programme and were each injected 4 times. To further purify His-*Pf*ATG8 for inoculation, 200 µl of His-*Pf*ATG8 from a bench-top purification was separated in a single well by 15 % SDS-PAGE. Proteins were Coomassie-stained and gel slices equivalent to ~ 125 µg were collected. The antisera generation programme was performed by Eurogentec (Belgium). Antisera collected from small, large and final bleeds were tested by western blotting of recombinant and parasite protein extracts for reactivity against His-*Pf*ATG8 and *Pf*ATG8, respectively.

2.8.10 Purification of anti-*Pf*ATG8 antisera

Antisera collected from rabbits following inoculation with His-*Pf*ATG8 was affinity purified against recombinant His-*Pf*ATG8 or His-*Pf*LiplA1 protein preparations. His-*Pf*ATG8 was expressed in BLR (DE3) cells and purified by the bench-top method as previously described. His-*Pf*LiplA1 was expressed at 37 °C for 4 h and protein was extracted and purified by the same methods as His-*Pf*ATG8. Two ml AminoLink coupling resin (Thermo Scientific, UK) was washed and approximately 2 mg of purified recombinant protein was bound during overnight incubation at 4 °C. Two ml of antisera was then purified according to the manufacturer's guidelines and was eluted into 500 µl fractions. Eluted antisera fractions along with unpurified and flow through fractions were tested

by western blotting of purified recombinant His-*Pf*ATG8 protein and parasite extracts separated by 15 % SDS-PAGE.

2.9 Bioinformatic methods

2.9.1 Homologue identification

Protein sequences from *S. cerevisiae* strain S288c (unless stated otherwise) were used as queries in order to identify genes in *P. falciparum* 3D7 that encode potential homologues to ATGs and other proteins complementary to autophagy. Protein sequences retrieved from the UniProtKB/Swiss-Prot database were submitted to BLASTp searches of the *P. falciparum* 3D7 genome available online at PlasmoDB (http://plasmodb.org/plasmo/ [Last accessed 14/09/2012]) and predicted translations of hits were aligned back to query sequences using AlignX (Life Technologies, UK). Predicted translations of hits were then submitted to BLASTp (WU-BLAST2) searches of the *S. cerevisiae* strain S288c proteome available online at (http://yeastgenome.org/cgi-bin/blast-sgd.pl [Last accessed 14/12/2012]).

2.9.2 Sequence alignment of ATG8 homologues

The protein sequence of *Sc*ATG8 was used as a query in order to identify genes in other *Plasmodium spp.* that encode potential ATG8 homologues. Predicted translations of hits were aligned with the predicted translation of *Pfatg*8 along with other known ATG8 homologues and *Sc*ATG8 using the pair-wise alignment program EMBOSS Needle (EMBL-EBI, UK). The predicted translation of *Pfatg*8 was then aligned with the protein sequences of *Sc*ATG8 and human ATG8 homologues using ClustalW2 (EMBL-EBI, UK). The conservation of known key residues was analysed in each alignment.

2.9.3 Structural modelling

Protein sequences of known ATG8 homologues and the predicted translation of *Pfatg*8 were submitted to the online I-TASSER server (Zhang, 2008) and models retrieved with the highest confidence score (indicating the significance of alignment) were selected as the best models. I-TASSER is regarded as one of the best public protein structure prediction servers following Critical Assessment of

protein Structure Prediction (CASP) experiments over the last decade (http://predictioncenter.org/index.cgi [last accessed 12/06/2012]).

2.9.4 Model alignment

Alignment of structural models generated by I-TASSER and solved structures retrieved from (http://www.rcsb.org/pdb/home/home.do [Last accessed 14/09/2012]) was performed using TM-align (Zhang and Skolnick, 2005). The TM scores produced were used as a measure of relatedness between two different proteins or as a measure of accuracy between a model and its corresponding solved structure.

2.9.5 Densitometry of western blots

Densitometry of western blots was performed using ImageJ software available from the National Institutes of Health (U.S.A.) (NIH), according to L. P. Miller 2010 (http://lukemiller.org/index.php/2010/11/analyzing-gels-and-western-blots-with-image-j [last accessed 14/09/2012]). Briefly, the intensity of bands of BDCH loading controls was used to normalise the intensities of bands of either *Pf*ATG8 or mCherry-*Pf*ATG8 in each lane. These were then expressed as either a percentage of the first band in time course experiments (see Figure 3.9 and Figure 3.14) or as a ratio of the lower band to the upper band when analysing the lipidation state of mCherry-*Pf*ATG8 (see Figure 3.13 and others).

2.9.6 Statistical analysis

Statistical analysis was performed using GraphPad Prism software (Graphpad, U.S.A.). Data groups were first tested for normal distribution (when applicable). To determine if two groups of data were significantly different, an unpaired Student t-test was performed. Data presented graphically was generated in GraphPad Prism and Excel (Microsoft, U.S.A.).

2.9.7 Analysis of correlation by generation of Pearson's coefficient

The degree of overlap between signals from either fluorescent fusion proteins or Alexa Fluor 488/594-conjugated antibodies was analysed using SoftWoRx

(Applied Precision, UK). The degree of correlation was represented by a coefficient score based on Pearson's coefficient (*r*) (Adler and Parmryd, 2010, Manders *et al.*, 1993).

2.10 Culturing of *P. falciparum*

Erythrocytic stages of *P. falciparum* strains D10 and 3D7 were cultured according to Trager and Jenson (Trager and Jensen, 1976). All work with live parasites was performed under a Holten Maxi Safe 2010 category 2 tissue culture hood (Thermo Scientific, UK) and all medium and buffers were filter sterilised (0.2 µm) before use. Parasites were grown in sterile tissue culture flasks at 37 °C and individual flasks were gassed with 3 % CO_2, 1 % O_2 and 96 % N_2 before sealing. Erythrocytes from whole blood were isolated by repeated washes in blood wash medium until no trace of white blood cells were seen in Giemsa-stained thin smears. Erythrocytes were stored at 4 °C for no longer than 4 weeks. Erythrocytes were added to cultures at 5 % haematocrit unless stated otherwise and were given fresh culture medium every 24 h after careful aspiration of old medium. Cultures were diluted with fresh erythrocytes to ensure the parasitaemia remained below 10 %. If cultures were not transferred to new flasks during dilutions, for example whilst waiting for recovery of parasites after transfection, transfer to new flasks was performed once every 2 weeks.

2.10.1 Giemsa staining of thin smears

In order to calculate parasitaemia of cultures, thin blood smears were stained with Giemsa to allow identification of parasites. A small amount of sedimented infected erythrocytes was pipetted onto glass slide and smeared to achieve a thin film of cells. Slides were allowed to air dry and then fixed in 100 % methanol for 1 min and then stained for 5 min in Giemsa (1:25 dilution in H_2O). Excess stain was washed off with H_2O and slides allowed to air dry. Slides were then examined using a 100 x oil immersion lens light microscope (Motic, Germany). Parasitaemia was calculated as the proportion of infected erythrocytes to uninfected erythrocytes with around 1,000 cells being counted in total.

2.10.2 Freezing parasites

Parasites were frozen as stabilates in liquid nitrogen for long term storage. Cultures of at least 4 % ring stages were centrifuged at 400 *g* at room temperature for 5 min to allow aspiration of medium. Pelleted infected erythrocytes were resuspended in 1 x volume of cold RPMI complete and 2 x volumes of cold 30 % (v/v) glycerol in PBS and carefully mixed. Six hundred µl were transferred to 1.5 ml cryovials and were incubated on ice for 10 min before being transferred to liquid nitrogen.

2.10.3 Thawing parasites

Stabilated parasites were thawed using increasingly isotonic buffers. Frozen cryovials were thawed at 37 °C for 1 min and then kept on ice. Cells were transferred to sterile tubes and 0.2 x volumes of 12 % (w/v) NaCl in PBS were added. Cells were incubated at room temperature for 5 min before 10 x volumes of 1.8 % (w/v) NaCl in PBS was added step-wise. After further incubation at room temperature for 5 min, 10 x volumes of 0.9 % (w/v) NaCl and 0.2 % (w/v) glucose in PBS was added step-wise. After a final incubation at room temperature for 5 min infected erythrocytes were pelleted by centrifugation at 400 *g* for 5 min at room temperature. The supernatant was aspirated and the pellet resuspended with 200 µl uninfected erythrocytes in 8 ml RPMI complete and transferred to fresh flasks. Cultures were fed daily and when parasitaemia reached 1 %, 300 µl uninfected erythrocytes and appropriate selective drug(s) were added.

2.10.4 Synchronising parasites

Parasites were synchronised to ring stages using sorbitol according to Lambros and Vanderberg (Lambros and Vanderberg, 1979). Cultures of at least 1 % ring stages were centrifuged at 400 *g* at room temperature for 5 min to allow aspiration of medium. Pelleted infected erythrocytes were resuspended in 5 x pellet volumes of 5 % sorbitol (w/v) in 10 mM potassium phosphate (pH 7.2) and incubated for 5 min at 37 °C. Infected erythrocytes were again pelleted to allow aspiration of supernatant. Pelleted infected erythrocytes were then resuspended in culture medium to 5 % haematocrit and transferred to a fresh culture flask.

2.10.5 Isolation of parasites

Parasites were isolated from erythrocytes by using saponin (Christopher, 1939). Cultures were resuspended in culture medium and 0.1 x volumes of 2 % saponin (w/v) in PBS added for 5 min incubation at 4 °C. Freed parasites were pelleted by centrifugation at 1,800 *g* for 5 min at 4 °C. The supernatant was aspirated and parasites repeatedly washed in PBS until the supernatant was visually clear of any haemoglobin. Pelleted parasites, isolated from erythrocytes were then used for DNA, RNA or protein extraction.

2.10.6 Large scale isolation of *P. falciparum* DNA

Parasite DNA was extracted from pelleted parasites using Qiagen's QIAamp DNA mini kit according to the manufacturer's guidelines for extraction from blood or body tissue. Briefly, the parasite pellet was resuspended in PBS supplemented with Proteinase K. Buffer AL was added and samples were incubated at 56 °C for 10 min. Ethanol was added to precipitate DNA and samples were transferred to the provided spin columns. Following washing steps DNA was eluted in 2 x 200 µl of ddH_2O. Parasites pelleted from a 25 ml culture of 5 % parasitaemia gave a typical yield of ~ 15 µg DNA.

2.10.7 Extraction of RNA

RNA was extracted from parasites as previously described (Smith *et al.*, 1998). Pelleted parasites were resuspended in 10 x volumes of TRIzol reagent (Life Technologies, UK) and stored at – 80 °C until RNA extraction. After defrosting, RNA was extracted by addition of 0.2 x volumes of chloroform. Samples were mixed by shaking for 15 sec followed by 2 min incubation at room temperature and subsequent centrifugation at 13,000 *g* at 4 °C for 15 min. The aqueous phase was transferred to a clean 1.5 ml tube and 0.7 x volumes of isopropanol were added. The RNA was precipitated at 4 °C overnight. The following morning samples were centrifuged at 13,000 *g* at 4 °C for 30 min. The supernatant was removed and the RNA pellet washed with 70 % ethanol. Samples were again centrifuged at 13,000 *g* at 4 °C for 15 min and the supernatant removed. The RNA pellet was air dried before being resuspended in an appropriate volume of DEPC-treated RNase free water (20 - 40 µl) by heating to 60 °C for 10 min. RNA was stored at - 80 °C. This was performed by Dr. E. Patzewitz.

2.10.8 Extraction of protein

P. falciparum protein was extracted from pelleted parasites by a process of sequential freeze thaw cycles. Pellets were resuspended in ~ 100 µl cold, freshly prepared parasite lysis buffer and mixed thoroughly by pulse vortexing for 3 x 30 sec. Samples were then frozen on dry ice and thawed at room temperature. Thawed samples were again mixed by pulse vortexing and repeated pipetting (with a p200 tip (Greiner, UK)). This process was repeated twice more and then the samples were left on ice for 20 min before centrifugation at 16,000 *g* for 5 min at 4 °C. Soluble protein in the supernatant was transferred into a fresh tube and subjected to Bradford assay to determine protein concentration. Samples were aliquoted into ~ 25 µg aliquots and stored at – 20 °C. The remaining parasite pellets were also stored at – 20 °C.

2.10.9 Transfection of parasites

Parasites were transfected when between 2 and 4 % ring stages according to Crabb and Cowman (Crabb *et al.*, 2004). Infected erythrocytes were pelleted by centrifugation at 400 *g* for 5 min at room temperature to allow culture medium to be aspirated. Infected erythrocytes were then resuspended in 10 x volumes cytomix and spun again. Seventy five µg of precipitated plasmid DNA which was previously resuspended in 30 µl ddH_2O was diluted with 370 µl cytomix and was kept on ice. Two hundred µl of pelleted infected erythrocytes were carefully mixed with the 400 µl of DNA and transferred to a 2 mm electroporation cuvette (Bio-Rad, UK) and electroporated at 310 V and 950 µF using a Gene Pulser Xcell electroporator (Bio-Rad, UK). A typical time constant was ~ 12 msec. Electroporated cells were immediately transferred to a fresh flask containing 300 µl of uninfected erythrocytes and 8 ml RPMI complete pre-warmed to 37 °C and the electroporation cuvette was washed with 1 ml RPMI complete to give a total final volume of ~ 10 ml. Six hours after transfection, cultures were fed as described above. The following day cultures were fed again with RPMI complete supplemented with the appropriate selective drug(s). Transfected cultures were fed daily for 1 week and then every second day until parasites were detected in Giemsa-stained thin smears.

2.10.10 Cloning by limiting dilution

Clonal lines of *P. falciparum* transgenic strains were generated by limiting dilution (Kirkman *et al.*, 1996). Parasitaemia was determined by analysing Giemsa-stained thin smears and haematocrit was calculated by using a Neubauer chamber (Hawksley, UK). Cultures were diluted to 1.25 parasites / ml at 1 % haematocrit and 200 µl was added per well of a 96 well plate in duplicate. Plates were placed in an incubation chamber, gassed and incubated at 37 °C. Culture medium was replaced every 5 days for 15 days, after which medium was replaced every 2 days for a maximum of 21 days in total. Parasite growth was monitored after the second feed by analysis of Giemsa-stained thick smears and cultures showing growth of parasites were transferred to 2 ml cultures at 1 % haematocrit. Growth was monitored and cultures were bulked up to 10 ml at 5 % haematocrit before stabilates were made and DNA was isolated by using InstaGene Matrix reagent (Babiker *et al.*, 1998) according to manufacturer's guidelines (Bio-Rad, UK). This is referred to as small scale *P. falciparum* DNA isolation.

2.10.11 Determination of IC_{50}

The concentration of various drugs at which 50 % of parasites are killed was measured by [^{3}H]-hypoxanthine incorporation according to Desjardins *et al.* (Desjardins *et al.*, 1979). Cultures were diluted to 0.5 % parasitaemia and 2 % haematocrit in IC_{50} medium. Serial dilutions starting from 2 x the desired starting drug concentration were prepared in 100 µl IC_{50} medium for each well in a 96 well plate. To each well 100 µl of diluted cultures were added and plates were placed in an incubation chamber, gassed and incubated at 37 °C for 48 h. To each well 0.4 µCi of [^{3}H]-hypoxanthine was then added in 30 µl IC_{50} medium. The plates were gassed and incubated at 37 °C for a further 24 h before being frozen at – 20 °C. In parallel, wells were set up which contained uninfected erythrocytes only as a measure of background incorporation and infected erythrocytes without drug were used as growth controls. Plates were allowed to thaw for at least 3 h after which material was harvested onto Printed Filter Mat A filter membranes (Wallac, UK) using a Mach III harvester system (TomTec, U.S.A.). Membranes were dried and then soaked in 4 ml Betaplate scintillant

before reading in a 1450 Microbeta scintillation counter (Perkin Elmer, UK) for 1 min per well. IC_{50} values were determined using GraphPad Prism software.

2.10.12 Magnetic enrichment of late stage parasites

Cultures were enriched for late stage parasites by magnetic separation (Ahn *et al.*, 2008, Trang *et al.*, 2004) with a Vario MACS magnet and LS+ columns (Miltenyi, UK). Infected erythrocytes were pelleted by centrifugation at 400 *g* at room temperature for 5 min to allow aspiration of culture medium. Pelleted infected erythrocytes were resuspended in 4 x volumes of 0.5 % BSA, 2 mM EDTA in PBS and applied to a mounted LS+ column that had been rinsed with 5 ml 0.5 % BSA, 2 mM EDTA in PBS. Cells were allowed to flow through the column under gravity under the resistance of a 0.6 mm needle. Bound infected erythrocytes were then washed with multiple 1 ml volumes until eluate was colourless. Columns were then unmounted from the magnet and infected erythrocytes enriched for late stage parasites were eluted in 1 ml 0.5 % BSA, 2mM EDTA in PBS, pelleted by centrifugation at 400 *g* for 1 min at room temperature and then prepared for fluorescence light microscopy. Typically, enrichment resulted in ~ 90 % parasitaemia of early trophozoite to segmenter stage parasites.

2.10.13 Preparation of slides for live microscopy

Infected erythrocytes were imaged by fluorescence light microscopy in EBSS supplemented with 11 mM glucose (EBSS+G). When enrichment of late stage parasites was not performed, for each slide prepared, 0.5 ml culture was resuspended and incubated with 100 µg/ml Hoechst 33258 at 37 °C for 5 min. Infected erythrocytes were then pelleted by centrifugation at 400 *g* for 1 min at room temperature. The supernatant was removed and infected erythrocytes were resuspended in 1 ml EBSS+G and pelleted as above. The supernatant was removed and infected erythrocytes were resuspended in ~ 30 µl EBSS+G. Five µl was dropped onto a glass slide and covered with a number 1 thickness cover slip. Images were taken from slides for no longer than 30 min after application of the cover slip. Where cultures were enriched for late stage parasites, the 1 ml elution was centrifuged at 400 *g* for 1 min at room temperature to allow removal of the supernatant. The pelleted infected erythrocytes were then washed once with 1 ml EBSS+G before incubation in 0.5 ml EBSS+G with 100 µg/ml Hoechst

33258 at 37 °C for 5 min. Samples were then washed and slides prepared as detailed above.

2.10.14 Preparation of slides for Immunofluorescence assay

The subcellular localisation of proteins was detected by immunofluorescence (IFA) microscopy using the antibodies detailed in Table 2.3. LabTek II 8 well chamber microscope slides (Thermo Scientific, UK) were used in the preparation of infected erythrocytes for microscopy. Slides were coated in poly-L-lysine prior to addition of infected erythrocytes reduced to 2.5 % haematocrit. Once dry, slides were fixed with 2 % paraformaldehyde and 0.0075 % glutaraldehyde in PBS for 20 min, permeabilised with 0.1 % Triton X-100 in PBS for 10 min and reduced with 0.1 mg/ml sodium borohydride in PBS for 10 min. Slides were washed with PBS between each treatment. Slides were blocked overnight in 3 % BSA in PBS at 4 °C in a moist container. The following morning, blocking solution was replaced with fresh 3 % BSA in PBS containing primary antibody and slides were incubated for 1.5 h at room temperature. Unbound antibodies were removed by 3 x washes in 0.05 % Tween 20 in PBS before application of secondary antibodies in 3 % BSA in PBS for 1 h incubation at room temperature. For the final 5 minutes of the incubation, Hoechst 33528 was added to a final concentration of 0.5 µg/ml. Unbound antibodies were removed by washing as above and slides were mounted in 2.5 % DABCO, 50 % glycerol in PBS under a number 1 thickness cover slip. Cover slips were fixed in place using black nail polish and allowed to settle before microscopy.

Table 2.3: Antibodies used in IFA analysis .

	Target	Antibody	Type	Raised	Dilution	Source
PRIMARY	PfATG8	Anti-PfATG8	Antisera	Rabbit	1:1,000	This study
	PfATG8	Anti-PfATG8	Peptide	Guinea pig	1:3,000	Dr. G. Langsley
	PfRab7	Anti-PfRab7	Peptide	Rat	1:300	Dr. G. Langsley
	mCherry-PfATG8	Anti-mCherry	Monoclonal	Mouse	1:1,500	Clontech

	Target	Antibody	Type	Raised	Dilution	Source
SECONDARY	Anti-PfATG8	Anti-Rabbit Alexa Fluor 488/594	Polyclonal	Goat	1:1,500	Life Technologies
	Anti-PfATG8	Anti-Guinea pig Alexa Fluor 488	Polyclonal	Goat	1:6,000	Life Technologies
	Anti-PfRab7	Anti-Rat Alexa Fluor 594	Polyclonal	Goat	1:3,000	Life Technologies
	Anti-mCherry	Anti-Mouse Alexa Fluor 488	Polyclonal	Goat	1:1,500	Life Technologies

2.10.15 Microscopic analysis of live and IFA slides

In total, three microscopes were used in the analysis of live and fixed parasites. A Motic BA400 microscope was used for calculating the parasitaemia of Giemsa-stained thin smears at 100 x magnifications and the haematocrit using a Neubauer chamber slide at 20 x magnifications. For the analysis of live and fixed parasites an AxioSkop 2 mot plus microscope, using Openlab software and a Hamamatsu C4742 CCD camera was used. To facilitate quantification of colocalisation a deconvolving Delta Vision Core microscope, using SoftWoRx software and a CoolSNAP HQ^2 camera was used. Images were captured at 100 x magnification using differential interference contrast (DIC) microscopy. GFP fusion proteins, MitoTracker Green-FM, ER Tracker, LysoSensor probes and Alexa Fluor 488-conjugated secondary antibodies were detected using a FITC filter (excitation at 461 nm, emission at 489 nm). mCherry-*Pf*ATG8, LysoTracker and Alexa Fluor 594-conjugated secondary antibodies were detected using an mCherry filter (excitation at 563 nm, emission at 588 nm). Hoechst 33258 was detected using a DAPI filter (excitation at 381 nm, emission at 399 nm). Images collected were deconvolved (where possible) on a conservative setting and layered using Photoshop Elements 9 (Adobe, U.S.A.). ImageJ was used to stack individual images in order to generate 3D reconstructions. Analysis of colocalisation between signals from FITC and mCherry or mCherry and DAPI filters was performed using SoftWoRx software as were measurements of vesicle size.

3 Bioinformatic and biochemical characterisation of an ATG8 homologue in *P. falciparum*.

3.1 Introduction

At the onset of this study, autophagy in *Plasmodium spp*. had only briefly been eluded to in published literature (Bonilla *et al.*, 2007). Bonilla and co-workers showed that antibodies raised against a peptide of rat ATG8 detected proteins that could have represented a *Plasmodium* homologue of ATG8 and that these proteins were more abundant in parasites in which vacuolar plasmepsins were genetically ablated. They suggested that *P. falciparum* possesses an active autophagy system, which targets autophagic cargo to the digestive vacuole. It was predicted, due to the high degree of conservation of ATG proteins in all eukaryotes examined, that the genome of *P. falciparum* would be found to encode ATG homologues. However, ATG-encoding genes had not been identified and whether any ATG proteins were expressed during the intraerythrocytic stages of parasite development was not known. This study therefore started from the ground up in regards to exploring the potential presence of an autophagic process in these parasite stages. Therefore, initial bioinformatic scrutinisation of the *P. falciparum* 3D7 genome was required to determine if *atg* genes might be present in the parasite genome. To achieve this, a series of basic local alignment search tool (BLAST) searches were performed to analyse the parasite genome for genes that might encode proteins sharing sequence identity to the repertoire of ATG proteins in the reference organism *S. cerevisiae*. Following identification of any potential homologues, further analysis and characterisation of these hits was expected to help to determine whether autophagy exists during the intraerythrocytic stages of *P. falciparum*.

3.2 Results

3.2.1 Bioinformatic screening of autophagy homologues

The protein sequences of a number of ATGs and proteins complementary to autophagy and the Cvt pathway in *S. cerevisiae* were used to probe the predicted proteome of 3D7 *P. falciparum* for potential homologues. Protein sequences retrieved from (http://www.ncbi.nlm.nih.gov/protein [Last accessed

14/09/2012]) for *S. cerevisiae strain* S288c (unless otherwise stated) were submitted to the online BLASTp function available at PlasmoDB (http://www.plasmodb.org [Last accessed 14/09/2012])) and hits with the smallest sum of probability (P value) were recorded. In order to analyse the percentage identity and similarity between queries and hits at the amino acid level, primary amino acid sequences were aligned using AlignX (Life Technologies). In some cases the size of the potential homologue and its protein query were vastly different, with the potential *P. falciparum* homologue often being much longer. In such cases the percentage similarity and identity between the query and hit were negatively affected. If the percentage of identity was found to be less than 10 %, hits from the initial screen with higher P values were analysed until a hit considered to represent the most likely potential homologue based on percentage identity of amino acid sequence was identified. The best hit was then submitted as a query to probe the *S. cerevisiae strain* S288c proteome by BLASTp (WU-BLAST2) seach. If the original query was returned as a hit in this 'reverse' search then its P value was recorded. Based on these analyses the most likely homologues of each ATG and protein complementary to autophagy probed are shaded in red in Figure 3.1. Homologues shaded blue are considered to be unlikely to represent true homologues of their query proteins.

From this initial analysis, it appeared that a number of ATG proteins appeared to be missing or highly divergent in *P. falciparum*. For example, the genes considered most likely to encode homologues of ATG1, ATG4 and ATG15, are predicted to encode proteins that show only 9.3, 5.9 and 4.9 % identity to the yeast proteins, respectively. This might indicate that the autophagic machinery encoded by *P. falciparum* represents a reduced core set of components (Duszenko *et al.*, 2011). Conversely, a number of genes were identified that are predicted to encode potential homologues to ATG proteins and proteins complementary to autophagy with much greater confidence. Genes considered most likely to encode homologues of ATG3, ATG8 and ATG12, are predicted to encode proteins that show 28.0, 38.1 and 16.0 % identity to yeast proteins, respectively. These proteins in yeast are involved in the ATG8 conjugation pathway (Kabeya *et al.*, 2004), potentially indicating that this pathway, highly conserved amongst eukaryotes, is also conserved in *P. falciparum*.

In order to explore members of the ATG8 conjugation pathway further, gene-specific primers were designed to amplify the genes likely to encode potential ATG3, 4, 5, 7, 8, 10 and 12 homologues. PCR analyses using these primers amplified products of the expected sizes when using gDNA isolated from 3D7 *P. falciparum* as a template. However, when using either a cDNA library or cDNA generated from RNA collected from asynchronous 3D7 parasites as a template, only the ORFs of *atg*3, 8 and 12 were amplified. This suggested that either the gene annotations for the remaining genes were incorrect, or that they were not transcribed during the intraerythrocytic development of *P. falciparum*. The *atg* gene product with the highest degree of confidence was that of PF10_0193, predicted to represent a homologue of ATG8. Therefore the characterisation of this gene and its protein product became the focus of this study.

Role	UniProtKB/Swiss-Prot accesion #	Protein	Gene I.D.	Gene Description	BLASTp P value	Wu BLAST E value	% identity	% similarity	Cloned from gDNA	Cloned from cDNA
Core	P40344	ATG3	PF3D7_0905700.2	autophagy-related protein 3, putative	4.20E-42	1.3E-39	28.0	40.5	Y	Y
	P53867	ATG4	PF3D7_1417300	conserved Plasmodium protein	5.00E-09	2.4E-7	5.9	10.6	Y	N
	NP_015176	ATG5	PF3D7_1126400	large ribosomal subunit processing factor, putative	0.56	NF	8.2	15.7	Y	N
	P38862	ATG7	PF3D7_1126100	ThiF family protein	4.00E-51	2.9E-37	12.4	19.3	Y	N
	P38182	ATG8	PF3D7_1019900	autophagy-related protein 8, putative	3.10E-24	3.8E-24	38.1	57.9	Y	Y
	Q07879	ATG10	PF3D7_1322900	conserved Plasmodium protein	NA	NA	7.2	15.6	Y	N
	P38316	ATG12	PF3D7_1470000	autophagy-related protein 12, putative	3.50E-09	0.018	16.0	23.5	Y	Y
Core	P53104	ATG1	PF3D7_1450000	serine/threonine protein kinase, putative	3.70E-25	4.5E-25	9.3	14.9		
	P53855	ATG2	PF3D7_0321700	microtubule and actin binding protein, putative	0.047	NF	10.4	19		
	Q02948	ATG6	PF3D7_0822400	conserved Plasmodium protein	2.30E-05	0.0024	12.5	21.2		
	Q12142	ATG9	PF3D7_0502000	conserved Plasmodium protein	0.0028	NF	11.7	20.9		
	Q06628	ATG13	PF3D7_0707700	ubiquitin-protein ligase e3, putative	0.018	NF	11.3	18.6		
	P38270	ATG14	PF3D7_0214700	conserved Plasmodium protein	0.00013	0.00016	12.8	22.7		
	P25641	ATG15	PF3D7_1351700	alveolin, putative	0.9998	NF	4.9	10.2		
	Q03818	ATG16	PF3D7_1451500	conserved Plasmodium protein	0.0017	NF	18.8	27.9		
	P43601	ATG18	PF3D7_1012900	conserved Plasmodium protein	1.90E-17	1.4E-17	22.6	33.5		
	P25568	ATG22	PF3D7_0206200	metabolite/drug transporter, putative	0.012	0.0082	14.6	29.8		
Shared Specific	Q12527	ATG11	PF3D7_0216700.1	conserved Plasmodium protein	3.80E-11	8.1E-6	11.8	20.7		
	Q06410	ATG17	PF3D7_0714100	conserved Plasmodium protein	1.60E-06	0.043	11.9	18		
	Q07528	ATG20	PF3D7_1354900	conserved Plasmodium protein	3.80E-06	0.2	13.1	20.2		
	P47057	ATG24	PF3D7_1419600	conserved Plasmodium protein	0.0001	NF	14.2	26.4		
	Q12092	ATG29	PF3D7_0608600	conserved Plasmodium protein	0.15	NF	12.3	20		
	Q12421	ATG31	PF3D7_0722500	cell cycle control protein cwf15, putative	0.064	NF	10.3	17.5		

Role	UniProtKB/Swiss-Prot accesion #	Protein	Gene I.D.	Gene Description	BLASTp P value	Wu BLAST E value	% identity	% similarity	Cloned from gDNA	Cloned from cDNA
Cvt	P35193	ATG19	PF3D7_1236000	conserved Plasmodium protein	0.0029	NF	17.7	27.4		
	Q02887	ATG21	PF3D7_1012900	conserved Plasmodium protein	3.90E-12	3.8E-12	16.8	26.2		
	Q06671	ATG23	PF3D7_0204300	conserved Plasmodium protein	3.80E-07	NF	11.1	18.1		
	P46989	ATG27	PF3D7_0424800	Plasmodium exported protein (PHISTb)	NF	NF	11.7	21.6		
Mitophagy	P40458	ATG32	PF3D7_0532100	early transcribed membrane protein 5	NF	NF	5.7	9.6		
	Q06485	ATG33	PF3D7_1303000	conserved Plasmodium protein	0.55	0.63	10.2	16.8		
Pexophagy	Q6JUT9 (*O. angusta*)	ATG25	PF3D7_1023600	conserved Plasmodium protein	4.90E-06	NA	11.7	22.1		
	Q06321	ATG26	PF3D7_0521900	conserved Plasmodium protein	0.19	NF	9.1	16.7		
	Q5IF00 (*K. pastoris*)	ATG28	PF3D7_1126700	conserved Plasmodium protein	7.60E-06	NA	12.5	21.2		
	AAQ63446 (*K. pastoris*)	ATG30	PF3D7_1016000	conserved Plasmodium protein	0.005	NA	15.3	24.9		
Complementary	P07267	Pep4	PF3D7_1407800	plasmepsin IV	3.10E-47	3.8E-47	24.8	36.5		
	P28795	Pex3	PF3D7_1119700	conserved Plasmodium protein	0.34	NF	11.3	22.2		
	P53112	Pex14	PF3D7_0903600.1	conserved Plasmodium protein	0.00029	NF	7.1	12.9		
	P09232	Prb1	PF3D7_0507500	subtilisin-like protease 1	1.60E-05	0.0038	15.6	24.7		
	P32939	Rab7	PF3D7_0903200	Rab GTPase 7	3.10E-63	3.8E-63	57.7	67.8		
	P35169	Tor1	PF3D7_0515300	phosphatidylinositol 3-kinase	0.00028	6.1E-5	9.7	19.5		
	P32600	Tor2	PF3D7_0509800	phosphatidylinositol 4-kinase	0.0011	0.019	8.9	15.8		
	P39968	Vac8	PF3D7_0812400	karyopherin alpha	3.00E-14	1.8E-12	18.5	31.2		
	P52917	Vps4	PF3D7_1457500	ATPase Vps4, putative	1.20E-94	2.1E-89	41.8	57.4		
	P22219	Vps15	PF3D7_0823000	protein kinase , putative	9.30E-15	3.9E-6				
	P36017	Vps21	PF3D7_0106800	Rab GTPase 5c	3.10E-49	3.7E-49	44.3	53.5		
	P22543	Vps34	PF3D7_0515300	phosphatidylinositol 3-kinase	1.90E-84	1.6E-81	9.3	15.1		
	Q9BQS8 (*H. sapiens*)	FYCO1	PF3D7_1036400	liver stage antigen 1	2.10E-41	NA	14.4	21.4		

Figure 3.1: Identification of genes potentially encoding homologues of ATGs and proteins associated to autophagy in the *P. falciparum* 3D7 genome.

The protein sequences of ATGs and proteins associated or complementary to autophagy in *S. cerevisiae* (unless stated otherwise) were used as queries in BLASTp searches of the predicted *P. falciparum* 3D7 proteome. An initial screen of core ATGs (performed by Dr. R. Williams) is presented first. Hits with the lowest P values were aligned against their queries using AlignX (Life Technologies). In instances where the % identity between the whole amino acid sequence of a hit was less than 10 % of its query, hits of higher P values were examined. Hits considered the strongest following alignment to their queries were then used as queries in BLASTp (Wu-BLAST2 (Saccharomyces Genome Database)) and the E values of positive identifications were recorded. Genes shaded in red are considered likely to encode true homologues.Queries are designated as core autophagy components, components of specific autophagy or proteins complementary to the process of autophagy but named following discovery of their involvement in other processes (Inoue and Klionsky, 2010). NF (Not Found), NA (Not Applicable).

3.2.2 Alignment of a putative *Pf*ATG8 homologue with known ATG8 homologues

The protein sequence of the potential *Pf*ATG8 homologue identified in bioinformatic screening of the 3D7 *P. falciparum* genome was analysed in comparison to the protein sequences of characterised ATG8 homologues in other organisms and other putative *Plasmodium* ATG8 homologues using pair wise alignment available online via (http://www.ebi.ac.uk/Tools/psa/emboss_needle/ [Last accessed 14/09/2012]) (Figure 3.2(A and B)). As expected, having used *Sc*ATG8 as a query, the similarity between *Pf*ATG8 and *Sc*ATG8 was high (64.3 %) as was the amino acid identity (38.9 %). The degree of similarity was also high with human ATG8 homologues, particularly with members of the GABARAP family such as GATE-16 (62.5 %). The degree of conservation of putative ATG8 protein sequences within *Plasmodium spp*. was also very high (97.6 %). The similarity between *Pf*ATG8 and ATG8 homologues in other Apicomplexans and other parasitic protists varied but was generally high. This suggests that ATG8 is highly conserved amongst eukaryotes, with *Plasmodium spp*. being no exception. Interestingly the degree of similarity between *Pf*ATG8 and *Cryptosporidium hominis* was considerably lower than that with *Cryptosporidium muris*, possibly indicating a divergence of the function or role of ATG8 in *Cryptosporidium hominis* or that the homologue identified in this organism has been incorrectly annotated. The protein sequences of *Sc*ATG8 and the putative *Pf*ATG8 homologue were aligned using ClustalW2 (EMBL-EBI) available online at (http://www.ebi.ac.uk/Tools/msa/clustalw2/ [Last accessed 14/09/2012]). Key residues in *Sc*ATG8 responsible for interaction with ATG4

appeared to be highly conserved in *Pf*ATG8 (Figure 3.2(C)) (Amar *et al.*, 2006). Interestingly, the C-terminus of *Pf*ATG8 features a conserved glycine residue, responsible for lipidation to PE, which is not followed by any other residues. This exposed C-terminal glycine is also a feature of ATG8 homologues in *Trypanosoma brucei* (Tb927.7.5900) and *Arabidopsis thaliana* (Q8S925). In *T. brucei*, *Tb*ATG8a and its exposed C-terminal glycine residue have been linked with a high rate of basal autophagy, while a second, more canonical homologue *Tb*ATG8b is believed to play a role in starvation or stress-induced autophagy (Koopmann *et al.*, 2009). Also of note was the observation of a 9 amino acid motif (YGSNMKLFR) that does not align with any ATG8 homologue tested. This motif is conserved within all putative *Plasmodium* ATG8 homologues and is therefore considered to be *Plasmodium*-specific.

A

	*Pf*ATG8	
	% identity	% similarity
*Sc*ATG8	38.9	64.3
MAPLC3a	33.6	48.9
MAPLC3b	30.5	45.4
GABARAPL1	38.1	58.7
GATE-16	39.8	62.5
*Pb*ATG8	87.9	97.6
*Pv*ATG8	88.7	97.6
*Pk*ATG8	88.7	97.6
*Py*ATG8	87.9	97.6
*Pc*ATG8	89.5	97.6

B

	*Pf*ATG8	
	% identity	% similarity
*Ch*ATG8	32.1	42.5
*Cm*ATG8	58.6	73.4
*Tg*ATG8	66.1	83.1
*Nc*ATG8	66.1	83.1
*Ta*ATG8	42.5	60.4
*Tb*ATG8a	34.4	56.8
*Tb*ATG8b	33.1	58.5
*Lm*ATG8	35.8	52.2
*Lm*ATG8a.1	21.1	39.5
*Lm*ATG8b.1	23	39.3
*Lm*ATG8c.1	17.8	34.2

C

```
ScATG8    1-MKSTFKSEYPFEKRKAESERIADRFKNRIPVICEKAEKSDIPEI-44
PfATG8    1-MPS-LKDEVSFENRVAETHKIRSKYPNRIPVVCERANRSNLPII-43
            * * :*.* .**:* **:.:* .:: *****:**:*::*::* *

ScATG8   45-DKRKYLVPADLTVGQFVYVIRKRIMLPP---------EKAIFIF-78
PfATG8   44-EKKKFLVPMNMLVGEFKFILHQHINQSAYGSNMKLFRERTIYLF-87
            :*:*:*** :: **:* ::::::*  ..          *::*::*

ScATG8   79-VNDTLPPTAALMSAIYQEHKDKDGFLYVTYSGENTFGR-117
PfATG8   88-VNNIVPKTGLLMQDLYEMYKDEDGYLYMEYSCESCLG-124
            **: :* *. **. :*: :**:**:**: ** *. :*
```

Figure 3.2: Analysis of a putative *Pf*ATG8 by alignment to ATG8 homologues from other organisms.

(A and B) The amino acid sequence of *Pf*ATG8 was compared to those of other organisms by pair-wise alignment using EMBOSS Needle (EMBL-EBI). Percentage identity and similarity are shown for yeast, mammalian and putative *Plasmodium spp*. homologues (A) and Apicomplexan and other parasitic protozoa (B). Accession numbers used are as follows: *Pf*ATG8 (PF10_0193) *Plasmodium falciparum*; *Sc*ATG8 (P38182) *Saccharomyces cerevisiae*; MAPLC3a (NP_115903.1) *Homo sapiens*; MAPLC3b (NP_852610.1) *H. sapiens*; GABARAPL1 (NP_113600.1) *H. sapiens*; GATE-16 (NP_009216.1) *H. sapiens*; *Pb*ATG8 (PBANKA_050410) *P. berghei*; *Pv*ATG8 (PVX_001860) *P. vivax*; *Pk*ATG8 (PKH_060390) *P. knowlesi*; *Py*ATG8 (PY00606) *P. yoelii*; *Pc*ATG8 (PCHAS_050420) *P. chabaudi chabaudi*; *Ch*ATG8 (Chro.70444) *Cryptosporidium hominis*; *Cm*ATG8 (CMU_014110) *C. muris*; *Tg*ATG8 (TGME49_054120) *Toxoplasma gondii*; *Nc*ATG8 (NC_LIV_041240) *Neospora caninum*; *Ta*ATG8 (TA12615) *Theileria annulata*; *Tb*ATG8a (Tb927.7.5900) *Trypanosoma brucei*;*Tb*ATG8b (Tb927.7.5910) *T. brucei*; *Lm*ATG8 (LmjF.19.1630) *Leishmania major*; *Lm*ATG8a.1 (LmjF.19.0840) *L. major*; *Lm*ATG8b.1 (LmjF.19.0820) *L. major* and *Lm*ATG8c.1 (LmjF.09.0150) *L. major*.

(C The alignment between the *Sc*ATG8 query and *Pf*ATG8 hit sequences generated in ClustalW2 (EMBL-EBI) is presented graphically. Residues that constitute the first hydrophobic pocket are shown in red; the second hydrophobic pocket in blue; residues crucial for ATG4 binding in green; and the glycine residue essential for binding of ATG7, ATG3 and phosphatidylethanolamine in orange (* indicates conservation; : indicates high similarity and . indicates similarity).

3.2.3 Modelling of the tertiary structure of a putative *Pf*ATG8

The crystal structure of *Sc*ATG8 and a number of ATG8 homologues from other organisms, including LC3 of humans, have been solved (Kumeta *et al.*, 2010, Sugawara *et al.*, 2004). As it was apparent that a high level of primary sequence homology exists between *Pf*ATG8 and other ATG8 homologues, modelling of the tertiary structure of *Pf*ATG8 was performed in order to add insight into the structural properties of *Pf*ATG8. The amino acid sequence of *Pf*ATG8 was submitted along with those of yeast and human homologues to I-TASSER, an online server delivering qualitative tertiary structure modelling (Zhang, 2008). A total of 3 models were generated for *Pf*ATG8, with the single model with the greatest confidence (C) score of 1.01 being considered the most accurate. C-scores fall in the range of -5 to 2, with a higher value indicating a greater significance of alignment. A score of 1 therefore indicates a model that is highly likely to represent an accurate tertiary structure (Figure 3.3(A)). Models with the highest C-score for each yeast and human ATG8 homologue were similarly selected.

In order to test the accuracy of the models generated, the models generated for each yeast and human ATG8 homologue were aligned to their relevant solved structure using TM-Align, an online server delivering quantification of similarity between protein structures (Zhang and Skolnick, 2005). This algorithm returns a TM-score. Similar to more conventional root-mean-square-deviation scores, this value indicates the degree of similarity between 2 structures. A value greater than 0.5 is considered to indicate a high degree of similarity. As expected, TM-scores for alignments between the solved structures of ATG8 homologues and models generated from primary sequence were all high, typically ~ 0.95. A score of 1, indicating perfect alignment was not observed between any pair potentially due to the inherent mobility of the N-terminus (Schwarten *et al.*, 2010) and the difficulties associated with accurately resolving the N- and C-termini of crystallised proteins due to the unreliable diffraction patterns resulting from these freely flexible amino acids (http://www.rcsb.org/pdb/101/static101.do?p=education_discussion/Looking-at-Structures/missing.html [Last accessed 23/08/2012]).

The degree of similarity between the *Pf*ATG8 model and those of other homologues of ATG8 was analysed. The models generated from primary amino acid sequence rather than the solved structures were chosen for alignment for consistency as in some cases multiple, varying solved structures of a single ATG8 homologue (e.g. crystal and NMR structures) exist. TM-scores ranging from 0.86 to 0.95, showed that the model of *Pf*ATG8 was very similar in structure to those of other ATG8 homologues (Figure 3.3(B and C)). Interestingly, the highest similarities were with *Sc*ATG8 and GABARAP family homologues, with slightly lower similarities observed with LC3 family homologues. As *P. falciparum* only appears to encode a single ATG8 homologue, it would be likely that it would share a high degree of similarity to ATG8 homologues of organisms which also possess single homologues, such as *S. cerevisiae*. A higher degree of similarity with the GABARP family of human homologues, in comparison to the LC3 family may indicate that *Pf*ATG8 has functional properties more akin to the GABARAP family proteins GABARAPL1 and GATE-16 and possibly that this family of ATG8 homologues is more closely related to *Sc*ATG8 than the members of the LC3 family, in fitting with previous findings (Alberti *et al.*, 2010, Slavikova *et al.*, 2005). As expected, the 9 amino acid region, observed only in the potential ATG8 homologues in *Plasmodium spp*. did not align with any region of other ATG8 homologue models or solved structures. These residues appeared to form an extended loop between the 3rd alpha helix and 3rd beta sheet. Experimentally solving the structure of *Pf*ATG8 would be needed to determine if the position of these residues is accurately predicted, as they may have been presented in an unstructured loop due to the lack of similar sequences within the reference structures available. Whether these residues contribute a functional capacity of *Pf*ATG8 not possessed by other ATG8 homologues is unclear. Searching for known motifs in *Pf*ATG8 using an online protein motif identifier (http://motifsearch.com/ [Last accessed 14/09/2012]) did not reveal any likely attributes for this region of the protein.

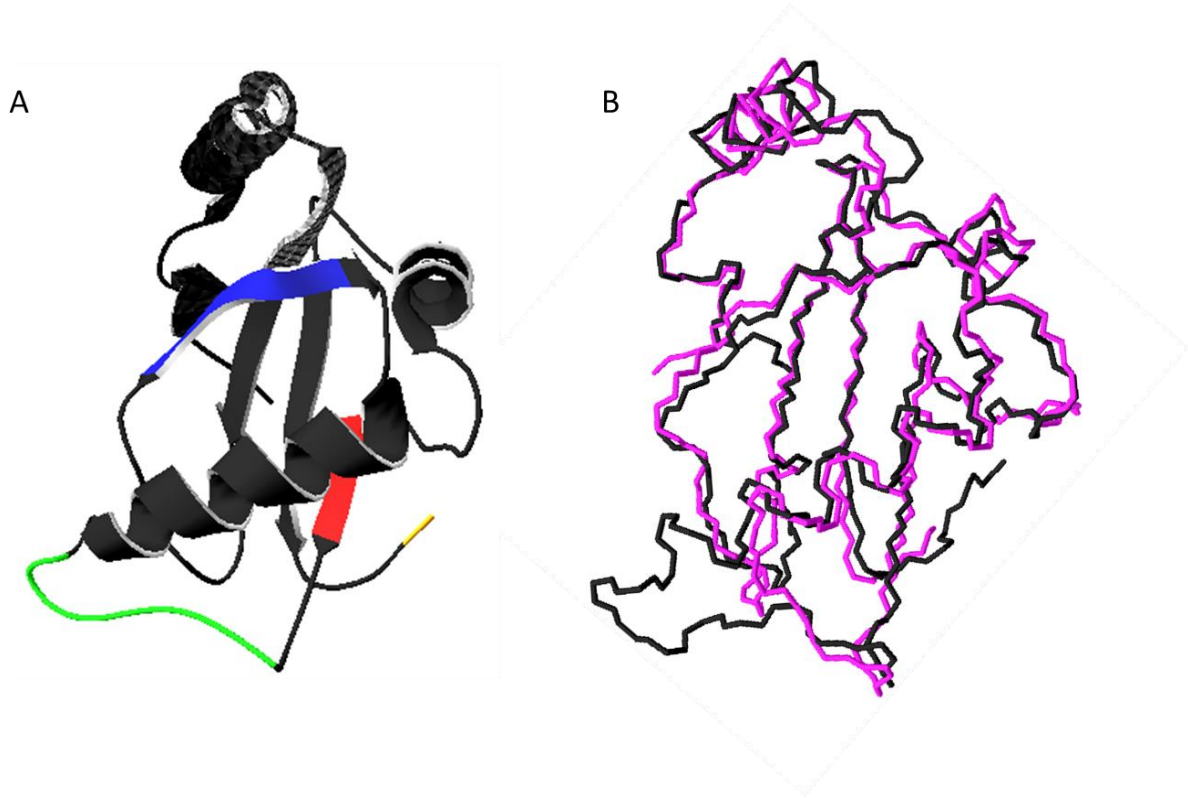

C

	PfATG8
	TM-score
ScATG8	0.943
MAPLC3a	0.901
MAPLC3b	0.855
GABARAPL1	0.947
GATE-16	0.951

Figure 3.3: Modelling of the predicted tertiary structure of a putative *Pf*ATG8.

(A) The predicted amino acid sequence of *Pf*ATG8 was submitted to I-TASSER. A predicted tertiary structure with a high confidence score of 1.01 is shown. Residues predicted to constitute the *Pf*ATG4 and *Pf*ATG3 interacting motifs are shown in blue and red, respectively. Residues forming an extended loop specific to *Plasmodium spp*. are shown in green. The C-terminal glycine residue predicted to facilitate membrane association via phospholipid conjugation is shown in orange.

(B) The model of *Pf*ATG8 tertiary structure (black) was aligned with the model for *Sc*ATG8 (pink), using TM-Align.

(C) The model of *Pf*ATG8 tertiary structure was aligned with the models for *Sc*ATG8, MAPLC3a, MAPLC3b, GABARAPL1 and GATE-16 using TM-align and the resulting TM-scores are shown.

3.2.4 Yeast complementation with a putative *Pf*ATG8

All evidence pointed towards the likelihood that an ATG8 homologue was encoded in the genome of *P. falciparum*. In order to determine whether this putative *Pf*ATG8 homologue was comparable functionally to *Sc*ATG8, a

complementation experiment was performed in a yeast line lacking *Sc*ATG8. In the yeast *S. cerevisiae* a modified autophagy pathway called the cytoplasm to vacuole targeting (Cvt) pathway has been described (Baba *et al.*, 1997). Rather than engulfing cytosolic cargo in a non-specific manner, with the end result of cargo degradation, the Cvt pathway involves the specific recruitment of the precursor form of the hydrolase aminopeptidase 1 (pAP1) into forming autophagosomes. Delivery of the autophagosome contents to the vacuole results in the processing of the hydrolase into its mature form (mAP1). This process relies on not only a unique subset of selective autophagy proteins but crucially also relies on the core subset of autophagy proteins including ATG8 (Figure 3.4). *Sc*ATG8 knockout lines grow normally under nutrient rich conditions but have reduced survival under conditions of nutrient starvation. One key phenotype of *Sc*ATG8 knockout lines is that while pAP1 can be detected, mAP1 is not detectable (Scott *et al.*, 1996). Transformation of *Sc*ATG8 and other ATG knockout lines with constructs designed to drive expression of ATG8 and other ATG homologues has been successfully used to determine their functionality by the restoration of a Cvt-positive phenotype witnessed by the presence of mAP1 (Alvarez *et al.*, 2008, Marino *et al.*, 2003, Williams *et al.*, 2009).

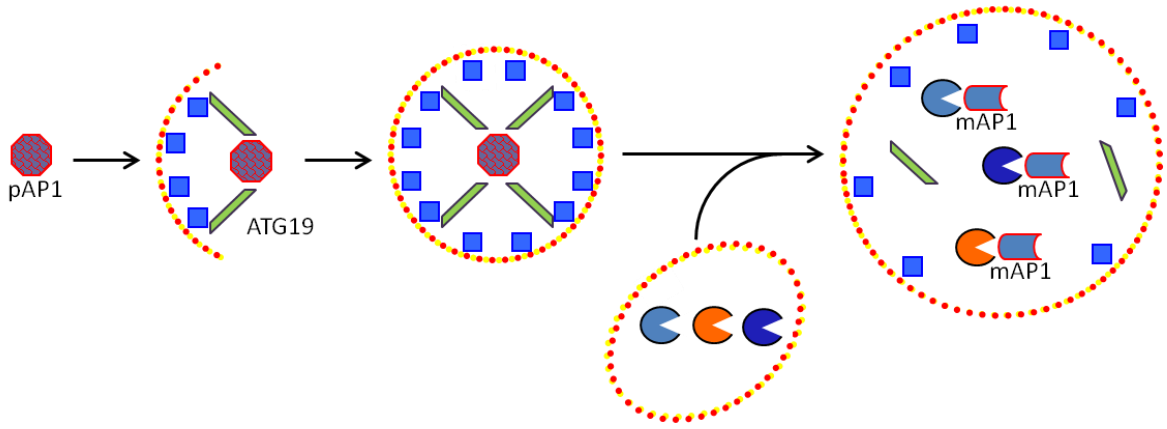

Figure 3.4: Aminopeptidase 1 maturation in *S. cerevisiae*.

The premature form of aminopeptidase 1 (pAP1) (purple) is sequestered into autophagosomes via specific recruitment by the cytosol-to-vacuole (Cvt) pathway protein ATG19 (green). Following fusion with the food vacuole, pAP1 is hydrolytically processed into is active mature form, mAP1. Maturation of aminopeptidase 1 is therefore relient on ATG8 (blue) and autophagosome formation and trafficking.

The yeast expression vector pCM186 is used as a centromeric plasmid from which tetracycline-repressible expression of a protein of interest is driven (Gari *et al.*, 1997). Unlike in vectors commonly used to transform bacterial cells, yeast cells

successfully transformed with pCM186-based constructs are selected by their ability to grow in nutrient-deprived media rather than under antibiotic selective pressure. The pCM186 vector backbone contains an expression cassette (URA3) which drives expression of orotidine 5-phosphate decarboxylase. This enzyme is involved in the *de novo* synthesis of pyrimidine ribonucleotides and negates the requirement for supplementation of growth medium with exogenous uracil (http://www.yeastgenome.org/cgi-bin/locus.fpl?locus=ura3#S000081430 [Last accessed 14/09/2012]). Therefore, successful transformants of yeast lines lacking endogenous URA3 can be selected for by growth in medium lacking uracil (SC medium). The ORF of *Pfatg*8 was cloned into pCM186 to generate the construct *Pf*ATG8-pCM186. This was transformed into the *Sc*ATG8 knockout line YBL078c (EuroScarf). In a separate transformation, the YBL078c line was transformed with *Lm*ATG12-pCM186, a construct sharing the same backbone but with the ORF of *Lmatg*12 inserted into the same position as *Pfatg*8. This has been previously shown not to restore a Cvt-positive phenotype in a *Sc*ATG8 knockout (Williams *et al.*, 2009) and was used as a negative control. Successful transformants were selected and then grown in selective medium or medium lacking all amino acids in order to induce AP1 maturation. As a positive control to identify pAP1 and mAP1 by western blot, a wild type line (Y00000) was similarly cultured. The presence of each form of AP1 was detected in protein extracts by western blotting with antisera directed against AP1 (Klionsky *et al.*, 1992). Both precursor and mature forms of AP1 were observed in wild type cell extracts obtained from cells grown under normal conditions, showing that the Cvt pathway was active (Figure 3.5). Only mAP1 was observed in nutrient starved wild type cells. This indicates that the starvation procedure was sufficient to induce an upregulation of AP1 maturation. While only the precursor form of AP1 was observed in protein extracted from cells transformed with *Pf*ATG8-pCM186 grown in SC medium, the mature form was also detected following starvation. This indicates that the Cvt pathway is active, albeit to a lesser extent than in wild type cells. In protein extracted from the negative control, only the precursor form of AP1 was detected, even following starvation. The presence of mAP1 in starved cells transformed with *Pf*ATG8-pCM186 represents a specific, although only partial restoration of a Cvt-positive phenotype. This shows that *Pf*ATG8 is a functional homologue of *Sc*ATG8 and

that it is likely to interact with other autophagy proteins in *S. cerevisiae*, such as *Sc*ATG3 and *Sc*ATG7, in the same manner as *Sc*ATG8.

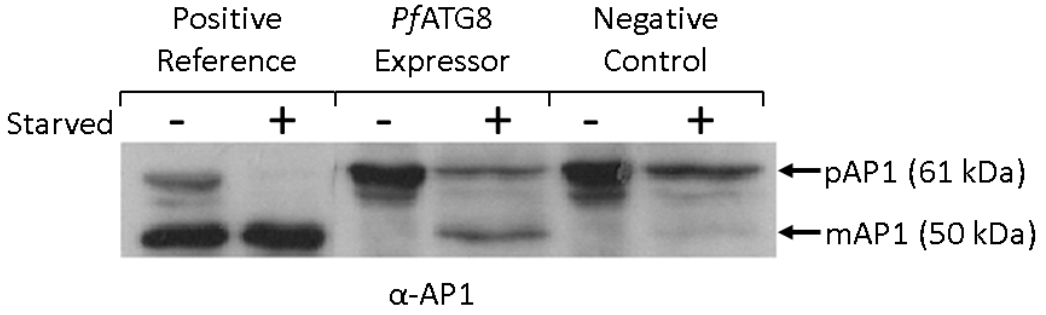

Figure 3.5: Complementation of *Sc*ATG8 with *Pf*ATG8 in *S. cerevisiae*.

An autophagy deficient line of *S. cerevisiae*, YBL0778c (EuroScarf) was transformed with plasmids driving expression of *Pf*ATG8 or *Lm*ATG12 (negative control). Transformants were grown to OD_{600} = 1.0 before being divided into "non-starved" cultures without induction of autophagy and "starved" cultures with induction of autophagy. Wild type *S. cerevisiae* Y00000 (EuroScarf) was cultured in YPD medium to OD_{600} = 1.0 before being divided and harvested as above (positive reference). Proteins were separated by SDS-PAGE (7.5%) and the precursor and mature forms of aminopeptidase 1 (pAP1 and mAP1, respectively) were detected by western blotting using rabbit anti-AP1 antiserum (1:1,000) and anti-rabbit HRP-conjugated polyclonal goat antibodies (1:10,000).

3.2.5 Recombinant expression of His-*Pf*ATG8

A functional homologue of ATG8 appeared to be encoded in the genome of *P. falciparum*. In order to study the *Pf*ATG8 homologue in the parasite itself, recombinant *Pf*ATG8 protein was expressed in order to generate antibodies specific to *Pf*ATG8. The ORF of *Pfatg*8, minus the start codon was amplified from cDNA and inserted into the pET28a(+) plasmid by directional cloning. This enables the expression of an N-terminally His-tagged version of *Pf*ATG8 in *E. coli* from a plasmid inducible by IPTG. The *E. coli* line BLR (DE3) was selected for expression experiments as it features a copy of T7 RNA polymerase and features an additional pLysS construct, which aid in the expression and extraction of recombinant proteins (Studier *et al.*, 1990, Zhang and Studier, 1997). Initially a small scale expression trial was performed in order to determine optimal conditions for expression of His-*Pf*ATG8 retrievable from the soluble fraction of protein extracts. At temperatures of 15, 20 and 25 °C, from an overnight culture, a large amount of His-*Pf*ATG8 (~ 16 kDa) was detected in the soluble fraction by western blotting of protein extracts with anti-His antibodies (Figure

3.6(A)). At 37 °C, less His-*Pf*ATG8 was detected in the soluble fraction. Due to the small size of His-*Pf*ATG8 it was difficult to identify any potential degradation products resulting from breakdown of His-*Pf*ATG8 by proteolysis in *E. coli*. Several reactive bands larger than His-*Pf*ATG8 were observed, suggesting that either His-*Pf*ATG8 forms stable covalent complexes or proteins cross-reactive with anti-His antibodies were present. In a compromise between yield and purity, expression for 16 h at 20 °C was chosen for subsequent larger scale protein expression. Typically 1 - 2 l of bacterial culture were induced per experiment. Two purification methodologies were performed in order to reduce the presence of any contaminating proteins. Both relied on metal chelating affinity purification of His-tagged *Pf*ATG8 using nickel (Ni^{2+}) charged resin columns (Crowe *et al.*, 1994). An immobilized metal affinity chromatography (IMAC) column packed with iminodiacetic acid and charged with Ni^{2+} ions was used in a semi-automated protocol using a Biologic DuoFlow System (Bio-Rad). This enabled a constant concentration gradient of imidazole to be used to elute proteins bound to the resin. A second, simplified method was also used where Ni-NTA resin (Qiagen) was packed into disposable columns and bound proteins were eluted with a step wise imidazole concentration gradient. The 'IMAC' and 'bench-top' purification methodologies were compared for the purity of His-*Pf*ATG8 eluted (Figure 3.6(B)) and the total protein concentration of eluted fractions was analysed by Bradford assay. The purification of His-*Pf*ATG8 appeared to be more complete when using IMAC methodology, however, eluted protein was more dilute then when using bench-top methodology. Typical protein yields between the two methodologies were similar and ranged between 2 and 5 mg per litre of inoculated culture. Total protein concentrations in elutions from bench-top purification procedures were typically 2.5 mg/ml while elutions from IMAC purification procedures were typically 1 mg/ml, as a greater elution volume was used.

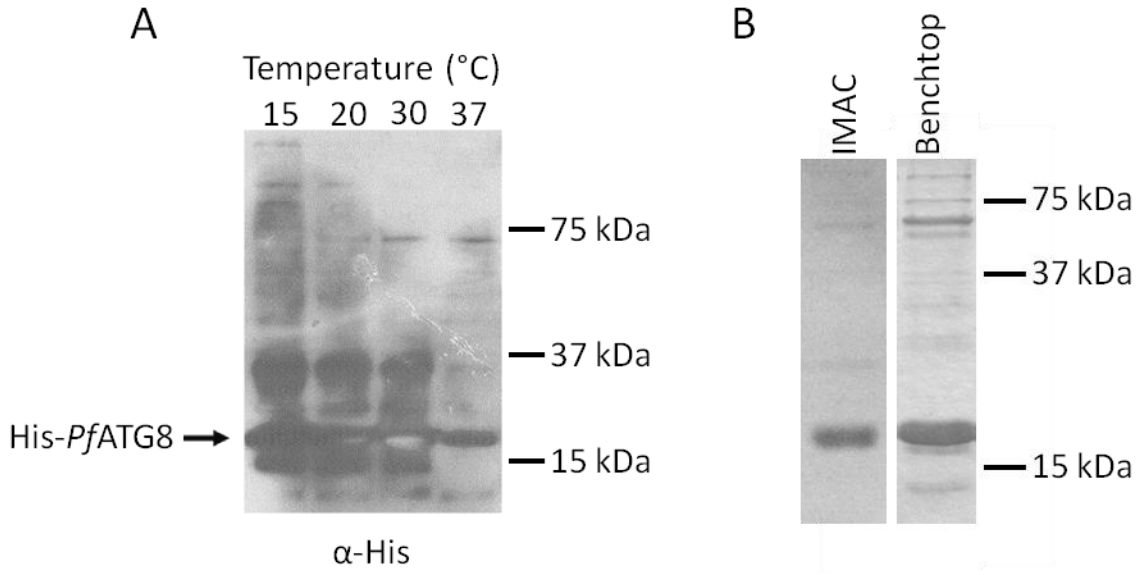

Figure 3.6: Optimisation of His-*Pf*ATG8 expression and purification.

(A) Western blot analysis of His-*Pf*ATG8 expression in *E. coli*. BLR (DE3) cells were transformed with His-*Pf*ATG8-pET28a(+) and expression of His-*Pf*ATG8 was induced with 1 mM IPTG. Soluble protein was extracted using BugBuster reagent (Merck) following overnight culture at 15, 20 , 30 and 37 °C and expression of His-*Pf*ATG8 was analysed by western blotting with mouse monoclonal anti-His (1:10,000) and anti-mouse HRP-conjugated polyclonal (1:10,000) antibodies.

(B) Analysis of nickel affinity purification of His-*Pf*ATG8. Protein extracted from BLR (DE3) cells expressing His-*Pf*ATG8 for 16 h at 20 °C was applied to nickel affinity purification resin either using semi-automated IMAC or manual bench-top methods. His-*Pf*ATG8 was eluted from columns with up to 500 mM imidazole. Proteins were separated by 15 % SDS-PAGE and stained with Coomassie to allow visualisation of His-*Pf*ATG8 and any remaining contaminants.

3.2.6 Generation of antisera against His-*Pf*ATG8

In total, 500 µg of purified His-*Pf*ATG8 was required for inoculation into a rabbit for an 87 day antiserum generation programme. In total, 3 independent antiserum generation programmes were performed by Eurogentec (Belgium), each making use of 2 rabbits. To reduce the amount of contaminating proteins, affinity purified His-*Pf*ATG8 was separated by 15 % SDS-PAGE and gel slices were excised from the Coomassie (Gelcode Blue Safe) stained gel. Gel slices were taken which contained His-*Pf*ATG8, leaving the contaminating proteins behind. Figure 3.7 shows a digital image of the Coomassie-stained polyacrylamide gel containing His-*Pf*ATG8 as the major protein present used in each of the 3 antisera programmes. Antiserum from each rabbit in each programme was tested against recombinant protein and protein extracted from wild type *P. falciparum* by western blotting. The analysis of 1 of each rabbit is shown and in each case antisera collected from each rabbit were found to be similar.

Antiserum generated from the first His-*Pf*ATG8 purification (A) were found to react with His-*Pf*ATG8 in recombinant protein extracts and a protein corresponding in size to *Pf*ATG8 in parasite protein extracts. However, additional proteins were also detected in both recombinant and parasite protein extracts. This antiserum was subjected to purification (see 3.2.7) in an attempt to isolate antibodies specific for *Pf*ATG8. Antiserum generated from purification B were found to specifically detect His-*Pf*ATG8 and *Pf*ATG8 and so was used for the analysis of endogenous *Pf*ATG8 by western blotting and IFA analysis. Antiserum generated from purification C was tested against recombinant and parasite protein by western blotting but was not used in further experiments because it was seen to only poorly detect *Pf*ATG8 in parasite protein extracts.

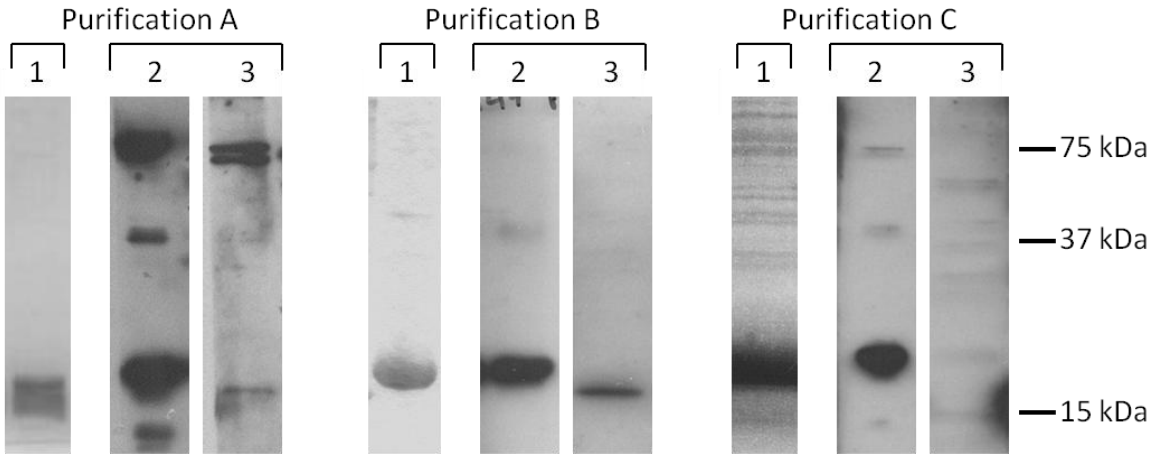

Figure 3.7: Generation and testing of antisera raised against purified His-*Pf*ATG8.

Gel slices containing His-*Pf*ATG8 were cut from Coomassie-stained 15% SDS-PAGE gels for inoculation of rabbits to generate anti-His-*Pf*ATG8 antisera on three separate occasions (A, B and C). Lane 1 shows the Coomassie (Gelcode Blue Safe) stained gel and indicates the purity of the His-*Pf*ATG8 sample used for inoculation. Lane 2 shows the detection by western blotting of proteins in a purified recombinant His-*Pf*ATG8 protein extract (similar to that shown in lane 1). The predicted size of His-*Pf*ATG8 is 16 kDa. Lane 3 shows the detection by western blotting of proteins in total protein extracts from asynchronous D10 *P. falciparum*. The predicted size of *Pf*ATG8 is 14.6 kDa. In each case antisera were diluted to 1:2,000 and were reported with secondary anti-rabbit HRP-conjugated goat polyclonal antibodies (1:10,000).

3.2.7 Purification of antisera against His-*Pf*ATG8

Antiserum generated from purification A was seen to detect His-*Pf*ATG8 and *Pf*ATG8 by western blotting of recombinant or parasite protein extracts, respectively. However, additional protein bands were also detected in each extract (Figure 3.8(A – UP1)).

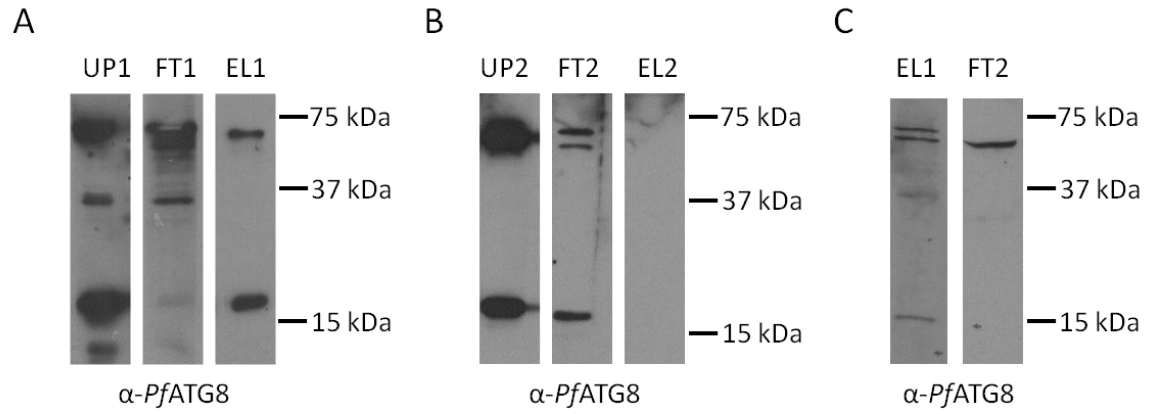

Figure 3.8: Western blot analysis of the attempts to purify anti-His-*Pf*ATG8 antisera.

(A) α-*Pf*ATG8 antisera was purified against recombinant His-*Pf*ATG8 bound to AminoLink resin. Unpurified (UP1) (1:2,000), flow through (FT1) (1:500) and eluted antisera (EL1) (1:200) were tested against protein extracted from BLR (DE3) cells expressing His-*Pf*ATG8 separated by 15 % SDS-PAGE. Reactive proteins were detected in each case with anti-rabbit HRP-conjugated goat polyclonal antibodies (1:10,000).

(B) Eluted antisera purified against recombinant His-*Pf*ATG8 was further purified against His-*Pf*LipLA1 bound to AminoLink resin. Unpurified (UP2) (1:100), flow through (FT2) (1:10) and eluted antisera (EL2) (1:10) were tested as detailed above.

(C) Purification fractions specific for α-*Pf*ATG8 antibodies (EL1 and FT2) were tested against 60 µg protein extracted from 3D7 parasites, separated by 15 % SDS-PAGE. Reactive proteins were detected in each case with anti-rabbit HRP-conjugated goat polyclonal antibodies (1:10,000).

Proteins of ~ 30, 65 and 70 kDa in recombinant protein extracts were cross-reactive with unpurified (UP1) antiserum, while proteins of ~ 65 and 70 kDa in parasite protein extracts were also cross-reactive (see Figure 3.7). It was possible that the cross-reactive proteins represented conjugation products of *Pf*ATG8, either with heterologous proteins or between other *Pf*ATG8 proteins. Attempts to purify the antiserum were performed in order to determine whether the cross-reactive bands represented unrelated contaminants or possible *Pf*ATG8 conjugation products. AminoLink resin (Thermo Scientific) was used to sequester His-*Pf*ATG8 (Allan *et al.*, 2000), recombinantly expressed and purified in the same manner as had been for the preparation of antisera generation. Antiserum raised against purification A was then passed over the immobilized protein and the flow through and eluted fractions were collected. It appeared that a proportion of antibodies reactive against proteins of ~ 30, 65 and 70 kDa had not bound to sequestered His-*Pf*ATG8 and were therefore present in the flow through fraction (Figure 3.8(A – FT1)). Only weak detection of His-*Pf*ATG8 was observed showing that saturation of the AminoLink resin had not been reached. Detection of His-*Pf*ATG8 was observed when using the eluted fraction, as was a

protein of ~ 70 kDa (Figure 3.8(A – EL1)). This suggested that the cross-reactive proteins of ~ 30 and 65 kDa indeed represented unrelated contaminants, as the species of antibodies which had detected them had not bound to the sequestered His-*Pf*ATG8 protein. The protein of ~ 70 kDa on the other hand, potentially represented a *Pf*ATG8 conjugation product, as the species of antibodies which detects this protein, along with those which detected His-*Pf*ATG8 had bound to the sequestered His-*Pf*ATG8 protein.

In order to test this further an additional round of purification was performed. Contaminating proteins of ~ 65 and 70 kDa have been observed in purifications of recombinantly expressed *Plasmodium* and *Leishmania* proteins by members of this lab (Bissett, 2009, Patzewitz, 2009). These are predicted to be *E. coli* chaperonins, which are difficult to remove from recombinant protein preparations such as that for His-tagged lipoate protein ligase A1 (His-*Pf*LiplA1), a cofactor essential to the function of alpha-keto acid dehydrogenase complexes (Gunther *et al.*, 2005). His-*Pf*LiplA1 was therefore expressed and purified by the bench-top method as described earlier. The (semi-)purified protein preparation, containing contaminant proteins of ~ 70 kDa, was applied to fresh AminoLink resin. The eluted antiserum fraction from the previous round of purification was then passed over the sequestered protein with the aim to remove any species of antibodies reactive against contaminant proteins. Therefore, purified antibodies against His-*Pf*ATG8 were expected to be present in the flow through, while any antibodies cross-reactive to epitopes present in both His-*Pf*ATG8 and His-*Pf*LiplA1 protein preparations would bind to the sequestered protein and would only be released in the elution. As expected, a population of antibodies reactive to His-*Pf*ATG8 were present in the flow through fraction (Figure 3.8(B – FT2)). However, antibodies reactive to proteins both of ~ 65 and 70 kDa were also present. No reactive bands were seen when the elution of the second round of purification was tested, suggesting that cross-reactive antibodies had not been separated following binding to the sequestered His-*Pf*LiplA1 protein preparation (Figure 3.8(B – EL2)).

The purification fractions known to contain antibodies reactive with His-*Pf*ATG8 were then tested on protein extracted from wild type 3D7 parasites (Figure 3.8(C)). Endogenous *Pf*ATG8 was detected with the EL1 fraction but not with

FT2. Proteins of ~ 65 and 70 kDa were also detected by the EL1 fraction and a protein of ~ 65 kDa was detected by the FT2 fraction.

While efforts to purify the antiserum raised against His-*Pf*ATG8 appeared to have removed antibodies cross-reactive to a 30 kDa protein in recombinant protein preparations, a population of antibodies reactive only to His-*Pf*ATG8 was not achieved. This may have suggested that the proteins of ~ 65 and 70 kDa represented *Pf*ATG8 conjugates. However, it would not be expected to see *Pf*ATG8 intermediates (with *Pf*ATG3 or *Pf*ATG7) when separated by denaturing SDS-PAGE as the bonds between these proteins are labile thioester bonds (Nakatogawa and Ohsumi, 2012). The identity of these potential conjugates remained unclear. In order to test whether these proteins were detected using an independently generated batch of antisera, His-*Pf*ATG8 protein from purification B was used in a second antiserum generation programme (see Figure 3.7). These antisera were not subjected to purification as they appeared to specifically detect His-*Pf*ATG8 or *Pf*ATG8 in recombinant or parasite protein extracts, respectively. Proteins of ~ 65 and 70 kDa were not detected by these antisera. These antisera were therefore used in subsequent experiments unless stated otherwise.

3.2.8 Analysis of *Pf*ATG8 expression in *P. falciparum* blood stage parasites

Data on *Pfatg8* transcript levels available from PlasmoDB showed a peak in transcript level during the later stages of intraerythrocytic development. No data, however, had been published detailing *Pf*ATG8 protein expression. As it is known that there can often be a discrepancy between transcript level and protein expression level (Le Roch *et al.*, 2004), antisera generated from His-*Pf*ATG8 purification B was used to analyse *Pf*ATG8 expression across the intraerythrocytic development of 3D7 wild type parasites. Parasites were tightly synchronised using two treatments with 5 % sorbitol 6 h apart and were harvested when at ring, trophozoite, early schizont and late schizont stages, confirmed by analysis of Giemsa-stained thin smears at each time point. Protein extracted from each stage was separated and analysed by western blotting with anti-*Pf*ATG8 (Figure 3.9). Blots were stripped and reprobed with antisera raised against *P. falciparum* BCDH to act as a loading control (see 2.8.5). This enabled

the quantification of band intensities representing endogenous *Pf*ATG8 at each time point by analysing the blot densitometrically using ImageJ software. It was observed that expression of *Pf*ATG8 varied across intraerythrocytic development, with a clear increase during the later stages of development. *Pf*ATG8 abundnace was ~ 10 fold higher in late schizonts than in ring stage parasites. This data supported that of transcript levels, suggesting that in the case of *Pf*ATG8, the increase in transcript level coincides with an increase in protein abundance.

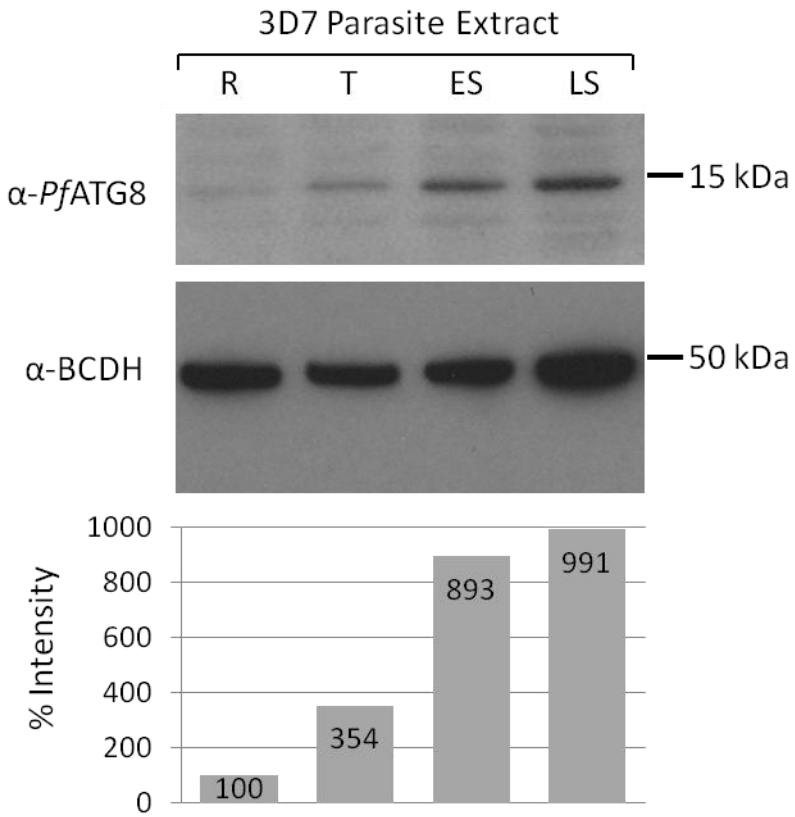

Figure 3.9: Western blot analysis of *Pf*ATG8 expression in 3D7 parasites.

Twenty µg of protein isolated from synchronised 3D7 *P. falciparum* (ring (R), trophozoite (T), early schizont (ES) and late schizont (LS) stages) were separated by 15 % SDS-PAGE and *Pf*ATG8 was detected by western blotting using rabbit anti-*Pf*ATG8 antisera (1:5,000) and anti-rabbit HRP-conjugated goat polyclonal antibodies (1:10,000). The western blot was stripped and reprobed with rabbit anti-BCDH antisera (1:1,000) as a loading control. The bottom panel displays the intensity of *Pf*ATG8, calculated densitometrically using ImageJ, for each life cycle stage as a percentage of the amount of *Pf*ATG8 in the ring stage parasites, normalised to the loading control.

3.2.9 Analysis of *Pf*ATG8 lipidation

It has been shown in other organisms that ATG8 homologues become lipidated to phosphatidylethanolamine (PE) (Besteiro *et al.*, 2011, Besteiro *et al.*, 2006, Mizushima and Yoshimori, 2007). This lipidation is responsible for the association

of ATG8 to the membranes of autophagosomes via conjugation to PE embedded in such membranes (Kabeya *et al.*, 2000). Fortunately, the lipidated and non-lipidated forms of ATG8 homologues can often be distinguished by SDS-PAGE due to the increased hydrophobicity of the lipidated form of ATG8 causing it to become more mobile (Kabeya *et al.*, 2000). As a result, the lipidated form (ATG8-II) can often be seen below the non-lipidated form (ATG8-I) in western blots, even though the lipidated form is actually of greater mass. It appeared from western blotting that *Pf*ATG8 was only present as a single form during the analysis of expression throughout intraerythrocytic development. However, it has been shown that unlike human ATG8 homologues, the two forms of *Sc*ATG8 and other yeast ATG8 homologues can only be distinguished when 6 M urea SDS-PAGE is performed (Kirisako *et al.*, 2000).

In order to determine if separation of two forms of *Pf*ATG8 could be achieved, protein extracts from wild type D10 parasites were separated by 6 M urea SDS-PAGE either with or without prior incubation with phospholipase D. Phospholipase D belongs to a family of enzymes which generate phosphatidic acid following the cleavage of the soluble head group from various phospholipids (McDermott *et al.*, 2004). While it is primarily indicated in catalysing the cleavage of phosphatidylcholine, it is also used to analyse the conjugation of ATG8 to phosphatidylethanolamine, as the protein component (ATG8) will also be separated along with the head group from the phosphatidic acid moiety (Tanida *et al.*, 2004). Following separation by 6 M urea SDS-PAGE, *Pf*ATG8 was detected in D10 extracts by western blotting with antisera raised against His-*Pf*ATG8 purification B. While separation by 6 M urea SDS-PAGE did appear to influence the mobility of *Pf*ATG8 through the gel, separation of a second form of *Pf*ATG8 in either phospholipase D-treated or untreated samples was not apparent (Figure 3.10). However, it was noted that the intensity of bands corresponding to *Pf*ATG8 appeared to diminish proportionally with the amount of phospholipase D added.

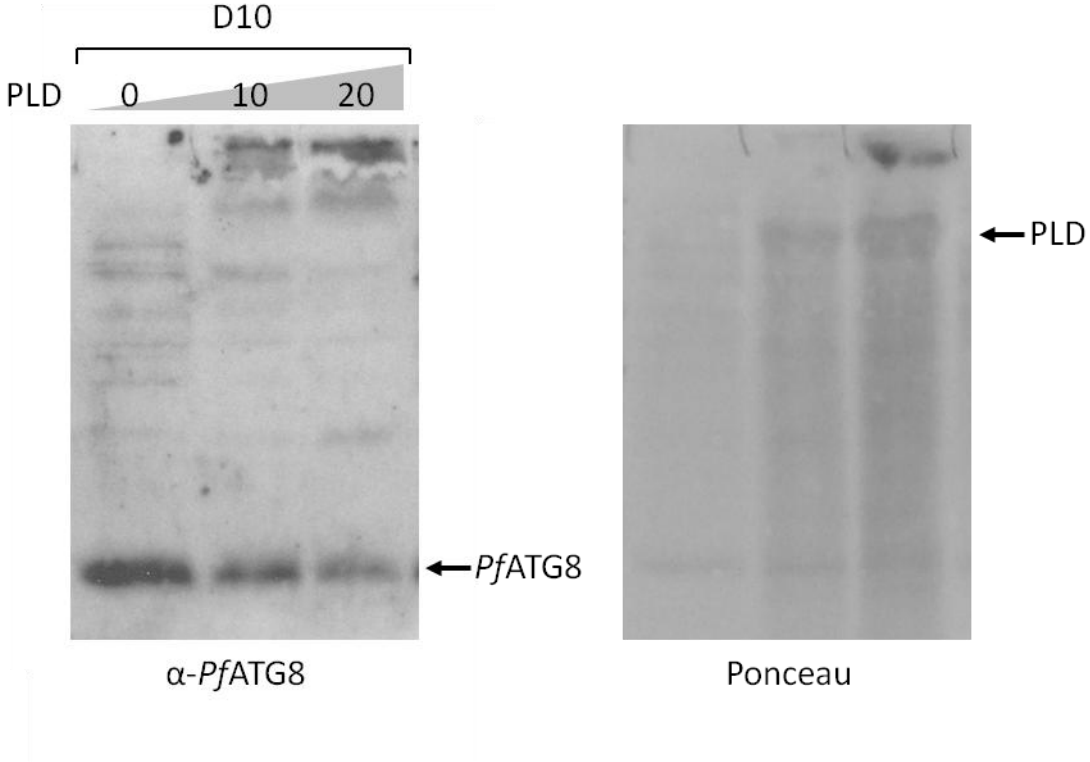

Figure 3.10: Analysis of *Pf*ATG8 lipidation.

Twenty µg protein extracted from D10 parasites was incubated with 0, 10 or 20 units of phospholipase D (*Streptomyces chromofuscus*) (PLD) for 1 h at 30 °C prior to separation by 6 M urea 15 % SDS-PAGE. (left) *Pf*ATG8 was detected by western blotting using rabbit anti-*Pf*ATG8 antisera (1:5,000) and anti-rabbit HRP-conjugated goat polyclonal antibodies (1:10,000). (right) Ponceau S-stained membrane indicating loading of protein to each lane.

3.2.10 Generation of transgenic parasite lines

It appeared that *Pf*ATG8 was differentially expressed during intraerythrocytic development but it had proved difficult to determine whether the endogenous protein was post-translationally modified. In order to circumvent the reliance on antisera specific for the endogenous protein an additional method was required to further the characterisation of *Pf*ATG8. A commonly used method to facilitate characterisation of parasite proteins involves the generation of transgenic parasite lines which express an epitope-tagged fusion protein which can then be specifically and sensitively detected by using epitope-specific monoclonal antibodies.

A variety of tags can be used in the generation of fusion proteins and careful choices need to be made in order to satisfy different requirements. Introducing a fluorescent tag would allow the visualisation of *Pf*ATG8 in live cells by fluorescence light microscopy. Fluorescent tags have also previously been

exploited as a target for immunofluorescence and immunoelectron microscopy with anti-tag antibodies when antibodies against ATG8 itself are absent or lack specificity (Reggiori *et al.*, 2004b). However, the addition of a large fluorescent tag (GFP-based tags are ~ 29 kDa) can, in some instances, affect the localisation and stability of the protein of interest (Hanson and Kohler, 2001). Using much smaller epitope tags, such as myc, 3 x haemagglutinin (HA) or 6-His tags could provide a more reliable tool for localisation by immunomicroscopy (Lee *et al.*, 2008, Roehl *et al.*, 1996) but would not facilitate direct visualisation of the fusion protein in live cells. Positioning of the tag is of key relevance to the goals of a particular experiment. N-terminal tags are used to label ATG8 from its translation to the point at which ATG8, sequestered within an autophagosome as cargo, is degraded following fusion with a lytic compartment. N-terminal tagging of ATG8 has been used extensively in the study of autophagy in organisms ranging from yeast to human (Cheong and Klionsky, 2008). On the other hand, C-terminal tags are used to analyse the activity of the ATG4 cysteine peptidase on the C-terminus of ATG8 (Cao and Klionsky, 2008). In most organisms, the glycine residue responsible for lipid conjugation is followed by 1 or more amino acid residues in the newly translated form of ATG8 (pATG8). The glycine residue is quickly exposed by the peptidase action of ATG4 to produce the lipidation-competent form ATG8-I (Tra *et al.*, 2011). ATG4 also plays a role in cleavage of the lipidated form of ATG8 (ATG8-II) to release ATG8-I from the outer face of autophagosomes (Tanida *et al.*, 2004), although the control of this process remains poorly understood (Nair *et al.*, 2012). Hence if a tag is situated 3' of the glycine residue it will be cleaved from ATG8 when the lipidation-competent form (ATG8-I) is generated. This can provide valuable evidence for the specificities of ATG4 peptidases against multiple ATG8 homologues (Li *et al.*, 2011a, Williams *et al.*, 2009).

In order to provide a platform for later detection of fusion protein localisation in live parasites by fluorescent light microscopy (see Chapter 5), fluorescent protein tags were chosen to aid the characterisation of the *Pf*ATG8 protein. An N-terminally-tagged copy of the gene was generated and introduced into 3D7 and D10 lines. The Multisite Gateway system was employed to generate constructs for transfection (Figure 3.11). Firstly a set of entry clones were generated by the BP reaction between pDONR intermediate vectors and PCR

fragments amplified to contain relevant *att* sites to facilitate homologous recombination.

A full length *Pfatg*8 and a *Pfatg*8 mutant form were cloned into pDONR P2R-P3. The former, (A8) was the *Pfatg*8 ORF with its start codon removed. The later, (A8ΔG) was the *Pfatg*8 ORF with both its start codon and 3' GGA codon, encoding the C-terminal glycine residue removed. Therefore the translated protein product of the A8ΔG ORF would not possess a C-terminal glycine residue. This was intended to provide a tool with which to explore the potential lipidation of *Pf*ATG8. Two different tags were cloned into pDONR 221 to provide scope for future colocalisation experiments. mCherry (mC) is derived from a monomeric red fluorescent protein (mRFP) from *Discosoma sp*. and is commonly used in fusion proteins primarily due to its impressive photostability (Shaner *et al.*, 2004, Shaner *et al.*, 2005). It absorbs at 587 nm and emits at 610 nm and has been used in *P. falciparum* before (Putrianti *et al.*, 2010). Enhanced yellow fluorescent protein (eY) is a dimeric fluorescent protein based on green fluorescent protein (GFP), derived from *Aequorea victoria* (Shaner *et al.*, 2005). It absorbs at 514 nm and emits at 527 nm and has also been used in *P. falciparum* before (Armstrong and Goldberg, 2007). Two different promoter regions were cloned into pDONR P4-P1R to differentially drive expression of the different fusion proteins. As demonstrated in Chapter 3.2.8, expression of *Pf*ATG8 from its endogenous genomic locus peaks during the schizont stages of intraerythrocytic parasite development. In order to generate transgenic parasite lines in which the expression of the fusion protein closely resembled that of endogenous *Pf*ATG8, the endogenous *Pfatg*8 promoter region was used as a promoter to drive expression of fusion proteins. Specific primers were used to amplify the 810 bp sequence upstream of the *Pfatg*8 ORF and this sequence was regarded as the endogenous promoter region (EP). A second promoter region was used that was intended to drive constitutive expression of tagged-*Pf*ATG8 in blood stage parasites. The promoter region of *Pfhsp*86 (PF07_0030) has previously been shown to drive constitutive expression of fusion proteins in *P. falciparum* (Miao *et al.*, 2010). This promoter region (86) was predicted to drive expression of tagged-*Pf*ATG8 equally in all intraerythrocytic parasite stages, allowing visualisation of the fusion protein in stages where expression driven by the endogenous promoter might be low. This group of 6 intermediate clones was

then used to generate expression constructs for transfection following homologous recombination with two different pDEST vectors, pCHDR-3/4 and pHBlR-3/4 via the LR reaction. The use of two different destination vectors would facilitate later co-transfections.

The expression constructs EP-mC-A8, EP-mC-A8ΔG, 86-mC-A8, EP-eY-A8, EP-eY-A8ΔG and 86-eY-A8, 86-eY-A8ΔG (see Table 2.1 and Figure 3.11) were transfected into both 3D7 and D10 *P. falciparum* on two separate occasions. Parasites resistant to the appropriate selective drug were typically visible in Giemsa-stained thin smears after 6 - 8 weeks. The expression of the fluorescently tagged proteins was examined by western blotting.

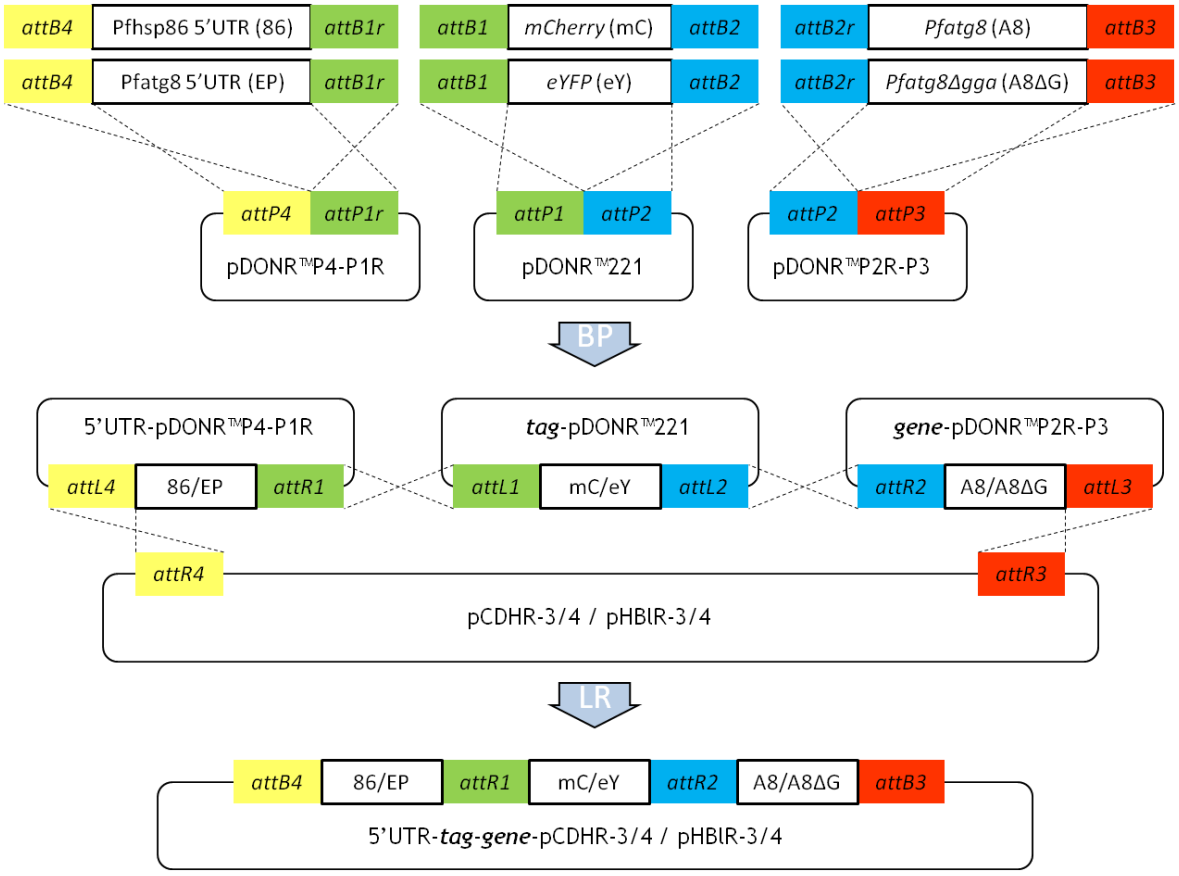

Figure 3.11: Schematic representation of Gateway cloning.

Three sequence elements are amplified by PCR with primers designed to introduce *attB* flanking regions to each end of the PCR product. These regions promote integration of PCR products into intermediate (pDONR) vectors via homologous recombination with *attP* regions (BP reaction). Intermediate clones containing different PCR products are mixed and via homologous recombination with *attR* regions, ordered integration into a final vector is performed via the LR reaction.

In this study, promoter elements (86/EP) were introduced into pDONR P4-P1R, (mC/eY) tags into pDONR 221 and (A8/A8ΔG) gene ORFs into pDONR P2R-P3. This cloning design was employed in order to N-terminally tag gene ORFs. Constructs generated for transfection were EP-mC-A8, EP-mC-A8ΔG, 86-mC-A8, EP-eY-A8, EP-eY-A8ΔG and 86-eY-A8, 86-eY-A8ΔG.

3.2.11 Analysis of mCherry-*Pf*ATG8 and mCherry-*Pf*ATG8ΔG expression

D10 parasites transfected with EP-mC-A8 or EP-mC-A8ΔG and selected with WR99210 were isolated from erythrocytes by incubation in 0.2 % saponin and parasite protein was extracted. Protein extracts were analysed for expression of mCherry-*Pf*ATG8 or mCherry-*Pf*ATG8ΔG by western blotting with anti-mCherry monoclonal antibodies (Figure 3.12). A single band of the estimated molecular mass of mCherry-*Pf*ATG8 (44 kDa) was observed in protein extracted from parasites transfected with EP-mC-A8ΔG, while this and a second, smaller band (42 kDa) was observed in protein from parasites transfected with EP-mC-A8. No band of the estimated molecular mass of free mCherry protein (29 kDa) was observed in either extract suggesting that both mCherry-*Pf*ATG8 and mCherry-*Pf*ATG8ΔG fusion proteins are stably expressed in each parasite line. No bands were detected by anti-mCherry antibodies in protein extracted from D10 wild type parasites showing that the bands detected in EP-mC-A8ΔG and EP-mC-A8 extracts were specific to the transgenic expression of the fusion proteins.

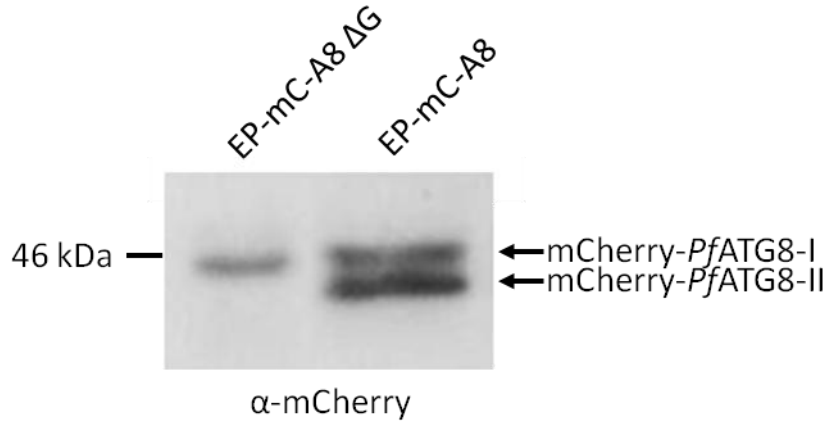

Figure 3.12: Analysis of mCherry-*Pf*ATG8 and mCherry-*Pf*ATG8ΔG expression.

Twenty µg of protein isolated from parasites transfected with EP-mC-A8ΔG or EP-mC-A8 was separated by 7.5 % SDS-PAGE and analysed by western blotting with mouse anti-mCherry monoclonal (1:1,000) and rat anti-mouse HRP-conjugated (1:10,000) polyclonal antibodies.

3.2.12 Analysis of mCherry-*Pf*ATG8 modification

The presence of a second, smaller band of mCherry-*Pf*ATG8 that was not detected in extracts from parasites expressing mCherry-*Pf*ATG8ΔG suggested protein processing or degradation specific to full length *Pf*ATG8. As it is well

known that ATG8 is processed into a phosphatidylethanolamine-conjugated form (ATG8-II) in other organisms (Mizushima and Yoshimori, 2007), protein extracted from parasites expressing mCherry-*Pf*ATG8 was analysed further by using phospholipase D. Protein extracted from parasites transfected with EP-mC-A8 was incubated with phospholipase D from *Streptomyces chromofuscus* and mCherry-*Pf*ATG8 was detected by western blotting. When compared to an untreated control of the same extract, the relative proportions of the two anti-mCherry reactive bands was altered by phospholipase D treatment (Figure 3.13). Analysis of band intensities by densitometry (ImageJ) revealed that the ratio of intensity of the lower band in relation to the upper band dropped from 1.5 in the untreated extract to 0.7 in the treated extract, indicating that the lower band was greatly reduced by phospholipase D treatment. This suggested that the band running at 42 kDa seen in extracts from parasites expressing mCherry-*Pf*ATG8 represents a lipidated form of the fusion protein, which is cleaved by phospholipase D. This is most likely to be a phosphatidylethanolamine-conjugated form as seen in other organisms but, due to the lack of specificity of phospholipase D, without further characterisation this can not certain. The observation that this lipid modified form is not present in extracts from parasites that express mCherry-*Pf*ATG8ΔG suggests that the C-terminal glycine residue of *Pf*ATG8 is necessary for the modification. This further supports the notion that the modified form of mCherry-*Pf*ATG8 is lipid modified, as has been demonstrated in other organisms (Kabeya *et al.*, 2004). For ease of explanation, the two forms of mCherry-*Pf*ATG8 will subsequently be referred to as lipidated (mCherry-*Pf*ATG8-II) and non-lipidated (mCherry-*Pf*ATG8-I).

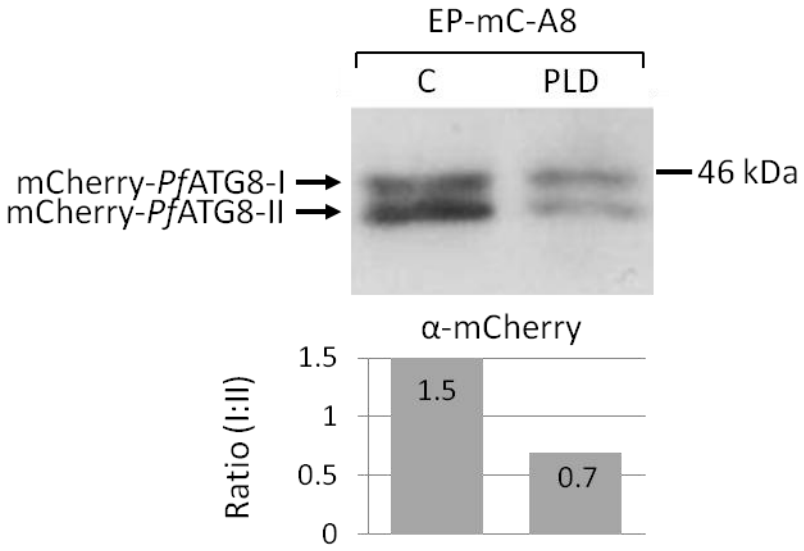

Figure 3.13: Analysis of mCherry-*Pf*ATG8 modification.

Twenty µg protein extracted from parasites transfected with EP-mC-A8 was incubated with 20 units of phospholipase D (*S. chromofuscus*) or an equivalent volume of ddH_2O at 30 °C for 1 h before being separated by 7.5 % SDS-PAGE. mCherry-*Pf*ATG8 was analysed by western blotting with mouse anti-mCherry monoclonal (1:1,000) and rat anti-mouse HRP-conjugated (1:10,000) polyclonal antibodies. The relative intensities of upper and lower bands in a sample were calculated densitometrically using ImageJ and are presented graphically. Numbers indicate the ratio of non-lipidated mCherry-*Pf*ATG8 (upper band) to lipidated mCherry-*Pf*ATG8 (lower band).

3.2.13 Analysis of mCherry-*Pf*ATG8 expression throughout intraerythrocytic development

In order to determine whether the expression of mCherry-*Pf*ATG8 was under temporal control, similarly to the expression of endogenous *Pf*ATG8 in different intraerythrocytic life cycle stages, a time course expression profile was examined in parasites transfected with either EP-mC-A8 or 86-mC-A8. Parasites transfected with EP-mC-A8 or 86-mC-A8 were synchronised twice, 6 h apart to ensure close synchronicity. Protein was extracted from synchronised parasites at defined time points after isolation of parasites from erythrocytes. Visualisation of parasites in Giemsa-stained thin smears allowed the classification of distinct life cycle stages for each time point - ring (R), trophozoite (T), early schizont (ES) and late schizont (LS). mCherry-*Pf*ATG8 was analysed in protein extracts by western blotting and the relative intensities of anti-mCherry reactive bands were compared by densitometry. The left half of Figure 3.14 shows the analysis of mCherry-*Pf*ATG8 expression in parasites transfected with EP-mC-A8. For comparison, the right half of Figure 3.14 shows mCherry-*Pf*ATG8 expression in parasites transfected with 86-mC-A8. As this analysis included a comparison of

mCherry-*Pf*ATG8 expression between lanes, as well as an analysis of the relative proportions of lipidated and non-lipidated mCherry-*Pf*ATG8, antibodies against BCDH were used as a loading control.

Expression of endogenous *Pf*ATG8 was shown to peak during schizont stages in 3D7 parasites. Expression of mCherry-*Pf*ATG8 appeared to peak during trophozoite stages when driven by either the endogenous *Pfatg*8 or *Pfhsp*86 promoter regions. While total expression levels were lower when driven by the endogenous *Pfatg*8 promoter region, when compared to the constitutive *Pfhsp*86 promoter (middle panel), an increase in the proportion of lipidated mCherry-*Pf*ATG8 was observed in the schizont stages (lower panel). This suggested that despite a slight difference in the expression profile of the fusion protein, in relation to endogenous *Pf*ATG8, parasites expressing mCherry-*Pf*ATG8 under control of the endogenous promoter region exhibited a temporal control over protein processing, with a profile similar to that of the expression of endogenous *Pf*ATG8. The total expression level of mCherry-*Pf*ATG8 was higher at each time point when driven by the constitutive *Pfhsp*86 promoter. However, the lipidation state of mCherry-*Pf*ATG8 in these parasites did not appear to vary in the different life cycle stages (lower panel). This suggested that the loss of temporal control of mCherry-*Pf*ATG8 expression, as a result of the use of a constitutive promoter, had an effect on the control of the lipidation of the fusion protein.

In light of the apparent differences in expression and protein processing when driven by each promoter region, further analysis was concentrated on parasites transfected with EP-mC-A8 or EP-mC-A8ΔG, unless stated otherwise, as this was believed to best resemble the expression of endogenous *Pf*ATG8.

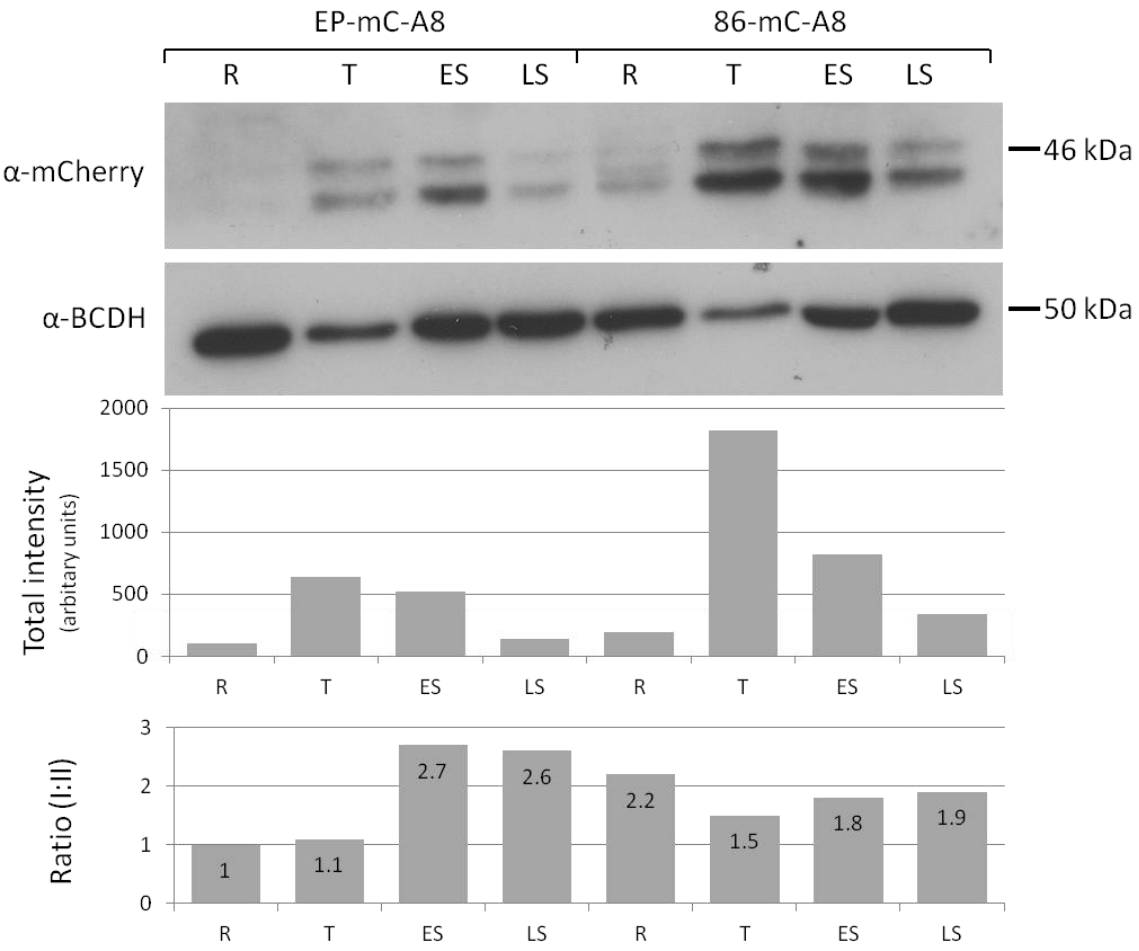

Figure 3.14: Analysis of mCherry-*Pf*ATG8 expression throughout intraerythrocytic development.

Parasites transfected with EP-mC-A8 (left) or 86-mC-A8 (right) were synchronised and protein extracted at defined life cycle stages: ring (R); trophozoite (T); early schizont (ES) and late schizont (LS). Twenty µg protein extract was separated by 7.5 % SDS-PAGE and analysed by western blotting with mouse anti-mCherry monoclonal (1:1,000) and rat anti-mouse HRP-conjugated (1:10,000) polyclonal antibodies. The western blot was stripped and reprobed with rabbit anti-BCDH antisera (1:1,000) as a loading control. The total intensity (upper graph) and relative intensities of upper and lower anti-mCherry reactive bands (lower graph) in each lane were calculated densitometrically using ImageJ and normalised to loading controls. Numbers indicate the ratio of non-lipidated mCherry-*Pf*ATG8 (upper band) to lipidated mCherry-*Pf*ATG8 (lower band).

3.3 Discussion

3.3.1 Discovery of an ATG8 homologue in *P. falciparum*

This chapter has detailed the identification of a putative ATG8 homologue in *P. falciparum* and the subsequent characterisation of this protein. Initial bioinformatic screening of the predicted *P. falciparum* 3D7 proteome revealed the presence of a number of potential homologues to ATG proteins along with proteins complementary to autophagy. While some of the strongest putative

homologues were members of the ATG8 and ATG12 conjugation pathways, many other putative homologues showed only low levels of similarity in amino acid sequence to their queries. It was often observed that the hits found in *P. falciparum* were substantially larger proteins than their queries, with only small regions within the amino acid sequence that aligned with the query sequence. This is characteristic of many *Plasmodium* proteins in previous screens (Pizzi and Frontali, 2001). This raises the question as to whether or not these proteins are likely to represent homologues to the autophagy proteins of the yeast *S. cerevisiae*. The level of identity between certain human ATG homologues and their yeast counterparts is equally as low as some of the potential homologues identified here. For example, the mammalian homologue of ATG14 shows only 13 % sequence identity to yeast ATG14 and could only be identified following position-specific iterative BLAST searches (Itakura *et al.*, 2008). Therefore, some apparently weak putative homologues identified in this screen should not be immediately discounted on the basis of low similarity in amino acid sequence to their yeast counterparts. More detailed analysis of conserved motifs and residues known to confer functional attributes will be needed to help determine if these hits represent potential homologues in *P. falciparum*. While this level of analysis for each potential homologue identified was beyond the scope of this study, it was noted for example, that the potential ATG3 homologue appeared to possess a conserved catalytic cysteine residue known to participate in protein function (Yamada *et al.*, 2007).

In support of this initial screen was the fact that a number of hits designated as potential ATG homologues during this study have since been re-annotated as such on PlasmoDB. Also, additional assignation of gene ontology terms and similarities to proteins in the Protein Data Bank (http://www.rcsb.org/pdb) support the identification of potential ATG homologues reported here. A thorough screen looking for ATG homologues in a number of protists has also since been published (Rigden *et al.*, 2009). The genes identified and presented here are the same as those identified and reported in their screen of the *P. falciparum* genome. Together, these factors suggest that the bioinformatic screen performed in this study was robust and helped in the identification of a number of putative homologues to autophagy proteins, especially those involved in the conjugation pathways of ATG8 and ATG12.

The presence of likely homologues to proteins involved in the ATG8 and ATG12 conjugation pathways supported the notion that a core, minimal set of autophagy genes are maintained in all eukaryotes (Mizushima *et al.*, 2002). In some species, such as *Giardia lamblia* and *Encephalitozoon cuniculi*, loss of subsets of autophagy genes appears to have occurred (Rigden *et al.*, 2009). This is likely due to the occupation of specific niches, which reduces the reliance on certain aspects of autophagy. Whether *P. falciparum* could also be an example of such a diverged organism is an interesting question. As previously discussed, this parasite has a number of adaptations and specialisations enabling the fulfilment of its life cycle in different tissues and environments within two different hosts. How this has impacted on the requirement of an autophagic process was a key focus of this study. Of the putative homologues of members of the ATG8 and ATG12 conjugation pathways, the DNA sequences of *Pfatg*3, *Pfatg*8 and *Pfatg*12 could be amplified from both gDNA and cDNA using gene specific primers. The fact that these genes appear to be transcribed in the intraerythrocytic stages of parasites suggested that, at least in part, the components needed for an autophagic process might be present in *P. falciparum*. The genes predicted to encode putative ATG4, ATG5, ATG7 and ATG10 homologues could only be amplified form gDNA, suggesting that these homologues may only be present as low abundance transcripts or that the gene annotations of transcript start and finish sites are incorrect. Further work will be needed to determine whether homologous proteins to these members of the ATG8 and ATG12 conjugation pathways are expressed in *P. falciparum* intraerythrocytic stages.

The genomic and transcript sequences of the potential ATG3 homologue amplified from gDNA and cDNA were also sequenced in full with 1 or 2 times coverage, respectively. It was found that there were a number of small differences from the sequence published on PlasmoDB. Most of these were within intronic regions but the boundary between exon 5 and intron 5 was found to have been miss-annotated. This alternative sequence would result in a predicted protein product containing an additional VQNVQN repeat. This gene was later re-annotated as a result of being found to be subjected to differential splicing to yield different protein isoforms (Sorber *et al.*, 2011). One of the re-annotated coding sequences PF3D7_0905700.1 was identical to the sequence

amplified from cDNA in this study. This highlights the complexity inherent in the steps between genomic sequence, transcript and protein expression in *P. falciparum* (Le Roch *et al.*, 2004). It is possible that other putative homologues identified in this bioinformatic screen are also subjected to alternative splicing events or that their gene annotations are simply incorrect. This could result in what appear to be poor putative homologues with low levels of overall similarity to queries, actually much more closely resembling their queries.

In this study a putative homologue for ATG8 was identified in the predicted proteome of *P. falciparum*. ATG8 is fundamental to autophagy in other organisms and it often used as a marker for autophagosomes (Kabeya *et al.*, 2004, Koopmann *et al.*, 2009, Nakatogawa *et al.*, 2007). It remained to be determined whether this putative ATG8 homologue was functionally similar to *Sc*ATG8 and whether the protein itself was expressed in *P. falciparum* intraerythrocytic stages. Presented here is evidence that not only is the *Pf*ATG8 protein expressed in *P. falciparum* intraerythrocytic stages but that it can functionally compensate for *Sc*ATG8. Yeast complementation showed that unlike *Lm*ATG12, *Pf*ATG8 can complement for the loss of *Sc*ATG8, partially restoring the autophagy-positive phenotype of aminopeptidase 1 maturation. Less mAP1 was detected in the complemented line than in wild type cells. This is possibly due to lower expression of *Pf*ATG8 in the complemented line in comparison to *Sc*ATG8 expression in wild type cells, as *Pf*ATG8 expression could not be detected with antisera raised against His-*Pf*ATG8 purification B in protein extracted from the complemented line. Another contributing factor could be a limited interaction capacity between *Pf*ATG8 and the members of the conjugation pathway of the yeast *Sc*ATG8 (Williams *et al.*, 2009). For example, if *Pf*ATG8 was transferred from *Sc*ATG7 to *Sc*ATG3 with a lower efficiency than *Sc*ATG8, then it might be anticipated that the autophagic capacity of the complemented line would be lower than wild type yeast cells. A different mechanism of interaction between the ATG8 and ATG3 homologues of *P. berghei* has been alluded to (Duszenko *et al.*, 2011), so much so that *Pb*ATG8 can not complement *Sc*ATG8. It is certainly possible that *Pf*ATG8 exhibits a reduced interaction with *Sc*ATG3 in comparison to that of *Sc*ATG8. Despite this, data presented here does show that *Pf*ATG8 is able to complement *Sc*ATG8.

*Pf*ATG8 was then seen to be differentially expressed during intraerythrocytic development, with a 10 fold increase in protein abundance evident in schizont stage parasites when compared to ring stages. The fact that this coincides with an increase in transcript level suggests that this is due to an upregulation in gene expression but may also be partly dependent on decreased turnover and increased stability of the protein during these stages (Foth *et al.*, 2011). Interstingly, the reported transcript levels for the putative *Pf*ATG4 homologue identified during bioinformatic screening exhibited a similar transcriptional pattern, albeit slightly less pronounced. This might provide further indication that this protein may represent a true homologue of ATG4 in *P. falciparum*. It was noted that the available transcript profiles of other putative ATG homologues, including those of ATG3 and ATG12, indicated that transcript levels for these genes were generally constitutive during intraerythrocytic development. This potentially suggests that the regulation of *Pf*ATG8 may be, in part, controlled by the level of transcription and translation of its interacting partners.

An attempt was made to determine whether endogenous *Pf*ATG8 was present as both lipidated and non-lipidated forms, as has been seen with ATG8 homologues in other organisms (Tanida *et al.*, 2004). Incubation of protein extracted from wild type parasites with phospholipase D before separation by 6 M urea SDS-PAGE did not result in the separation of two distinct protein species representing non-lipidated *Pf*ATG8-I and lipidated *Pf*ATG8-II. However, it did appear to result in a decrease in the amount of the single reactive protein. Unfortunately a valid loading control was not obtained for this blot, so it can not be determined whether this decrease represented a specific effect of phospholipase D incubation or was a result of less total protein being loaded or a non-specific peptidase contaminant of the phospholipase D added. Based on the Ponceau S-stained membrane of this gel, it appeared that if anything, slightly more total protein was actually loaded into the lanes of protein treated with phospholipase D.

Potentially, this finding suggested that incubation with phospholipase D decreased the amount of the lipidated species of *Pf*ATG8 (*Pf*ATG8-II), however the resultant non-lipidated *Pf*ATG8 (*Pf*ATG8-I) was not detected. This may have been due to the differing reactivity of the antiserum raised against His-*Pf*ATG8

to the lipidated and non-lipidated forms of *Pf*ATG8. It has been shown that antibodies raised against ATG8 homologues in other organisms preferentially recognise the lipidated form of ATG8 (Ichimura *et al.*, 2004, Woods, 2009), potentially due to a conformational change in the N-terminus of the protein, which exposes an immunogenic epitope (Mizushima and Klionsky, 2007). If this was also true for the antisera raised against His-*Pf*ATG8, then the presence of non-lipidated *Pf*ATG8-I may have been missed in these experiments. If these antisera can only detect lipidated *Pf*ATG8-II, then that would suggest that the single band detected following separation by either by 'normal' or 6 M urea SDS-PAGE actually represents lipidated *Pf*ATG8-II. Considering the fact that *Pf*ATG8 appears to be expressed in a lipidation-competent form i.e. with an exposed C-terminal glycine residue, it might be that *Pf*ATG8-I is converted to *Pf*ATG8-II quickly after expression and therefore *Pf*ATG8-I levels are low. The presence of a PE-conjugated form of the ATG8 homolgue in *T. gondii* has recently been confirmed by fluorographic analysis of ^{3}H-ethanolamine uptake (Besteiro *et al.*, 2011). A similar experiment could be used to determine whether the single form of endogenous *Pf*ATG8 is lipidated or not.

3.3.2 Establishment of tools to study *Pf*ATG8

As it was unclear whether endogenous *Pf*ATG8 was subjected to post-translational modification using *Pf*ATG8-specific antisera, additional tools were needed to further the characterisation of the *Pf*ATG8 protein. It was therefore decided to generate transgenic *P. falciparum* lines in which fluorescently tagged *Pf*ATG8 or *Pf*ATG8ΔG were expressed, with an intention of later performing live cell fluorescence microscopy.

Separation of proteins extracted from parasites expressing mChery-*Pf*ATG8 by 'normal' SDS-PAGE was sufficient to resolve two different forms of the protein, as detected using monoclonal antibodies specific for the mCherry tag, similarly to what has been reported for other ATG8 homologues (Ichimura *et al.*, 2004, Kabeya *et al.*, 2004, Williams *et al.*, 2009). It is possible that the increased size of the fusion protein in comparison to the endogenous *Pf*ATG8 protein facilitated more pronounced separation of the two protein forms by SDS-PAGE. This factor, in combination with the issues surrounding use of ATG8-specific antisera discussed above, meant that the analysis of fusion proteins using mCherry-

specific antibodies was greatly informative and added to what was discovered about the endogenous *Pf*ATG8 protein. Of note was that probing protein extracted from parasites expressing mCherry-*Pf*ATG8 with *Pf*ATG8-specific antisera only very weakly detected a protein band representing mCherry-*Pf*ATG8. It could not be determined whether the weak band detected represented the upper or lower separating forms of the fusion protein.

Treatment of protein extracts isolated from parasites expressing mCherry-*Pf*ATG8 with phospholipase D resulted in a decrease in the ratio of the more mobile band in relation to the less mobile band. The fact that the truncated mCherry-*Pf*ATG8ΔG fusion protein was only observed to separate as the less mobile form, suggested that without the C-terminal glycine, modification can not occur. These data strongly suggested that the two forms of mCherry-*Pf*ATG8 represented lipidated and non-lipidated protein.

It was earlier shown that endogenous *Pf*ATG8 is differentially expressed during intraerythrocytic development, displaying a ~ 10 fold increase in schizonts in comparison to rings. Analysis of the expression profile of mCherry-*Pf*ATG8 revealed that while this fusion protein reached a peak in expression earlier, in trophozoite stages, it appeared to be differentially processed, in a similar profile to the expression of endogenous *Pf*ATG8. The increase in the relative amount of the lipidated fusion protein when expressed under control of the endogenous *Pfatg*8 promoter was seen to coincide with peak expression of the endogenous *Pf*ATG8 protein. It would therefore appear that as well as the temporal control over the expression of *Pf*ATG8, other factors influence its lipidation; otherwise more mCherry-*Pf*ATG8 would be converted to the lipidated form in trophozoites. It is known that components of the ATG12 and ATG8 conjugation pathway are needed for lipidation of ATG8, even when upstream signals of autophagy are absent (Kageyama *et al.*, 2011). It is therefore likely that the abundance of these conjugation partners may limit the lipidation of mCherry-*Pf*ATG8. Even if the expression of mCherry-*Pf*ATG8 is 'inappropriately' high in trophozoite stages, without the presence of ATG3 or other conjugation partners, it can be understood why the conversion to the lipidated form is limited. While the scope of this study was limited to the characterisation of the homologue of ATG8, bioinformatic screening of the 3D7 parasite genome revealed the presence of a number of genes encoding other likely ATG

homologues. To fully understand *Pf*ATG8 it will be necessary to also characterise other components of the ATG12 and ATG8 conjugation pathways.

From the bioinformatic analysis of the *P. falciparum* genome a great deal was learnt about the potential for the parasite to encode components of the autophagic machinery as demonstrated in other organisms. The *in silico*, functional and biochemical characterisation of a homologue of the fundamental autophagy protein ATG8 demonstrated that in *P. falciparum* intraerythrocytic stages a functional *Pf*ATG8 homologue is expressed and appears to be post-translationally modified. While analysis of this modification could be improved upon further, data collected is consistent with the hypothesis that *Pf*ATG8 becomes lipidated, similarly to the ATG8 homologues of other organisms. Hence, evidence collected so far indicated the conservation of a functional *Pf*ATG8 homologue in *P. falciparum* intraerythrocytic stages, suggesting that it can contribute to an autophagic process in these parasites. As ATG8 homologues are necessary for autophagy in other organisms, the characterisation of *Pf*ATG8 was continued by attempts to generate parasite lines lacking *Pfatg*8.

4 Genetic ablation of *Pfatg8*

4.1 Introduction

ATG8 in *Saccharomyces cerevisiae* is not essential for growth under normal culture conditions but is essential for the process of autophagy (Ichimura *et al.*, 2000). Indeed, it is the ability to genetically knockout *atg*8 from this organism that allows for yeast complementation experiments to be performed (Williams *et al.*, 2009). However, *S. cerevisiae* lines lacking ATG8 do show a severe growth defect when placed under conditions of limited nutrient availability (Kirisako *et al.*, 1999). In higher eukaryotes with single ATG8 homologues, similar effects are observed following genetic ablation or knockdown of ATG8 levels. For example, RNAi inactivation of the *C. elegans* homologue of *atg*8, *lgg*-1 has been shown to result in a loss of complete conversion to the dauer stage of the worm (Melendez *et al.*, 2003). In higher eukaryotes with multiple copies or families of *atg*8, such as mammals, determining the essentiality of individual *atg*8 genes has proven difficult, largely due to the high degree of sequence similarity between genes and the functional redundancy between gene products (Kabeya *et al.*, 2004). It is now becoming clear that expansion of *atg*8 families has allowed for specialisation and differential involvement of ATG8 homologues during autophagy (Weidberg *et al.*, 2010, Williams *et al.*, 2009). In order to assess whether *Pf*ATG8 is essential to parasite survival under normal culture conditions, genetic knockout of the endogenous *Pfatg*8 was attempted.

Several methodologies exist for genetic deletion or disruption of target genes in *Plasmodium* (reviewed in (Goldberg *et al.*, 2011)). One such method used in this lab (Gunther *et al.*, 2009, Patzewitz *et al.*, 2012) involves the removal of a target gene from its chromosomal locus by replacement with a selectable marker. This process relies on homologous recombination between genomic and plasmid elements. Two plasmid elements, homologous to the gene locus under investigation, flank a region of non-homologous sequence, typically a selectable marker cassette, which replaces the genomic sequence between the homologous elements during a double cross over event (de Koning-Ward *et al.*, 2000). Due to the haploid genome of *P. falciparum* blood stages, genetic knockout or modification of a gene locus can be achieved by a single crossover event, and can be selected for with a single selectable marker (Su *et al.*, 2007).

The pCC-4 construct used in this study possesses two multiple cloning sites into which regions homologous to regions within or flanking the locus of a gene of interest can be cloned (Figure 4.1) (Maier *et al.*, 2006). Between these two sites is a blasticidin resistance cassette (*BSD*). During a double cross over event the gene locus under investigation will be replaced by *BSD* resulting in parasites that are resistant to blasticidin-S-HCl (BLA). Maintenance of episomal plasmid or integration into the genome via single cross over can be selected against, due to the presence of an additional selectable marker, referred to as a negative selectable marker (Duraisingh *et al.*, 2002). The backbone of the pCC-4 construct contains a modified cytosine deaminase (*CD*) cassette, from which a bi-functional chimera of cytosine deaminase and uracil phosphoribosyl transferase is expressed (Maier *et al.*, 2006). Through the activities of these enzymes, 5-fluorocytosine (5-FC) is converted into 5-Fluorouracil (5-FU), which is toxic to parasites via inhibition of RNA synthesis and thymidylate synthase. Therefore, when culture medium is supplemented with 1 μM 5-FC, parasites expressing the chimeric enzyme will be killed (Maier *et al.*, 2006). When a double cross over event occurs, the backbone of the plasmid is lost meaning that parasites in which the gene locus under investigation has been replaced will be unaffected by the addition of 5-FC.

The frequency of double crossover events in *P. falciparum* is low (Duraisingh *et al.*, 2002). To increase the likelihood of generating parasites in which a double cross over event has occurred, prior to supplementation of culture medium with 5-FC, repeated cycles of positive selective drug pressure are performed (Maier *et al.*, 2006). When parasites are detected following transfection, which are resistant to the selective drug used, cultures are divided into two, the first being supplemented with 5-FC and the second being taken off selective pressure. During this period of unhindered growth, loss of episomal plasmid is common due to the lack of selective pressure (O'Donnell *et al.*, 2002). This means that the population of parasites maintaining episomal plasmid decreases. Parasites in which an integration event has already occurred will be largely unaffected by the lack of selective pressure. Once the selective drug is reapplied, parasites that had lost episomal plasmid will be killed, whereas those in which an integration event had already occurred will have maintained resistance and will potentially outgrow any remaining parasites with episomal plasmid, provided the

integration event is not of any fitness cost to the parasite. This cycling process is performed in order to accelerate selection of integrated parasites and has been successfully used to knockout non-essential genes such as those encoding erythrocyte binding-like proteins in intraerythrocytic *P. falciparum* parasites (Lopaticki *et al.*, 2011).

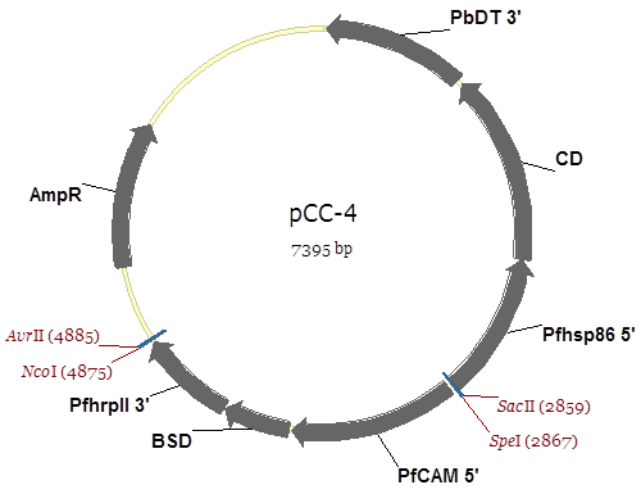

Figure 4.1: Plasmid map of pCC-4

Key features are highlighted in grey. *Sac*II and *Spe*I sites indicate the insertion site for the 5' homologous flank. *Nco*I and *Avr*II sites indicate the insertion site for the 3' homologous flank. Flanks ~ 500 bp in length are typically used to facilitate homologous recombination (Patzewitz *et al.*, 2012). The *BSD* cassette, with *Pf*CAM 5' and *Pf*hrpII 3' regulatory elements is shown between the two flank insertion sites. The *CD* cassette with *Pf*hsp86 5' and *Pb*DT 3' regulatory elements forms part of the plasmid backbone along with the ampicillin resistance marker (AmpR) for selection in *E. coli*.

4.2 Results

4.2.1 *Pfatg8* knockout in wild type parasites

To determine whether *Pfatg8* is an essential gene in the intraerythrocytic stages of *P. falciparum*, the pCC-4 construct was employed in knockout attempts by gene replacement. Due to the small size of the *Pfatg8* ORF (375 bp), homologous flanks that would facilitate homologous recombination between plasmid and the gene locus had to come from non-coding regions upstream and downstream of the *Pfatg8* ORF. The genome of *P. falciparum* is highly enriched for adenosine and thymidine, especially in non-coding regions (Gardner *et al.*, 2002). Regions were therefore carefully selected so that the complexity of sequence was

deemed sufficient to promote specific annealing of primers used in their amplification. As represented in Figure 4.2, 610 bp and 637 bp regions were selected from the non-coding regions upstream and downstream of the *Pfatg8* ORF, respectively. These regions do not encroach into the coding regions of neighbouring genes and so were predicted not to affect any other gene loci following integration of the *BSD* cassette into the *Pfatg8* locus by double homologous recombination. These sequences, referred to as 5' and 3' flanks, were amplified from *P. falciparum* D10 gDNA and were cloned into the pCC-4 plasmid as described in Chapter 2.7.7 and 2.7.11 to generate the construct *Pfatg8*-pCC-4.

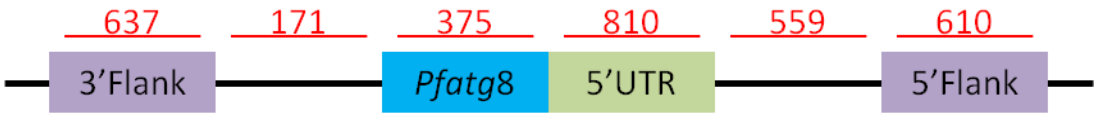

Figure 4.2: Schematic representation of the *Pfatg8* (PF10_0193) genomic locus.

The *Pfatg8* ORF (PF10_0193) is encoded by a single exon on the anti-sense strand of chromosome 10. The 5' UTR, as was cloned into Gateway expression constructs, runs for 810 bp upstream of the start codon of *Pfatg8*. A 610 bp region ending 1,369 bp upstream of the start codon was amplified as the 5' flank. A 637 bp region starting 171 bp downstream of the stop codon of *Pfatg8* was amplified as the 3' flank.

The construct *Pfatg8*-pCC-4 was used to transfect 3D7 and D10 wild type *P. falciparum* on two independent occasions. Parasites resistant to BLA were detected in Giemsa-stained thin smears, after 6 – 8 weeks in 3 of the 4 transfections. Cultures were then cycled according to Figure 4.3. Stabilates were made and DNA isolated when parasites resistant to either BLA or BLA and 5-FC were detected.

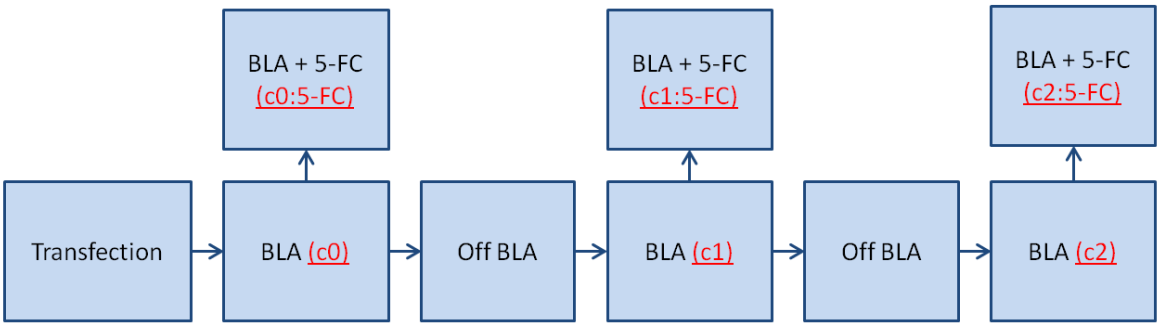

Parental line	Construct	Stabilate					
		(c0)	(c0:5-FC)	(c1)	(c1:5-FC)	(c2)	(c2:5-FC)
D10	*Pfatg8*-pCC-4					D10a c2	D10a c2:5-FC
D10	*Pfatg8*-pCC-4						
3D7	*Pfatg8*-pCC-4						
3D7	*Pfatg8*-pCC-4						
EP-mC-A8 (D10)	*Pfatg8*-pCC-4	D10c c0	D10c c0:5-FC				
EP-mC-A8 (D10)	*Pfatg8*-pCC-4						
D10	*mCherry-Pfatg8*-pCC-4						
D10	*mCherry-Pfatg8*-pCC-4						
3D7	*mCherry-Pfatg8*-pCC-4						
3D7	*mCherry-Pfatg8*-pCC-4						

Figure 4.3: Schematic representation of knockout strategy

(upper) Following transfection and initial selection with blasticidin (BLA), parasites were stabilated and DNA was isolated. Cultures were then divided into two independent lines. One culture was supplemented with 1 µM 5-FC. If parasites resistant to both BLA and 5-FC were detected up to 3 weeks later, they were stabilated and DNA was isolated. The other culture was taken off BLA selective pressure for 3 weeks. BLA resistant parasites were then reselected and the next cycle initiated. Up to three cycles (c0, c1, and c2) were performed.

(lower) The constructs *Pfatg8*-pCC-4 or *mCherry-Pfatg8*-pCC-4 (see 4.2.3) were transfected into the indicated parasite lines. Green boxes indicate when parasites resistant to either BLA or BLA and 5-FC were generated. Red boxes indicate when drug resistant parasites were not detected. Boxes with heavy outlines indicate parasite lines analysed by Southern blotting and presented here with their appropriate nomenclature.

To determine the genotype of transfected parasites, DNA from each cycle was subjected to analyses by PCR and Southern blotting and was compared to gDNA collected from their relevant D10 or 3D7 parental lines. Primer pairs were selected that would generate PCR products of distinct lengths, characteristic of the various integration events predicted to occur (see 2.7.6.6). The predicted sizes of PCR products formed when primer pairs align as a result of each integration event are detailed in blue in Figure 4.4. For analysis by Southern blotting, DNA was first digested with *Spe*I, which was predicted to cut either side of the *Pfatg8* locus and once within the *Pfatg8*-pCC-4 construct. A set of 4 DNA probes were generated for use in Southern blotting:-

- *Pfatg8*-specific – this probe is specific to the genomic *Pfatg8* ORF and is predicted to detect only a fragment representing the endogenous *Pfatg8* locus.

- 3' flank – this probe is predicted to detect fragments derived from both the endogenous *Pfatg8* locus and the plasmid.

- *CD* – this probe is specific to the *CD* cassette in the backbone of the plasmid.

- *BSD* – this probe is also specific to the *BSD* cassette between the 2 flanks in the plasmid.

The size of the fragments detected by each of these probes in each predicted scenario of integration events are shown in red in Figure 4.4. For the sake of brevity, the analysis of parasite cultures D10a c2 and D10a c2:5-FC is shown here. Analysis of parasites from earlier cycles showed similar results.

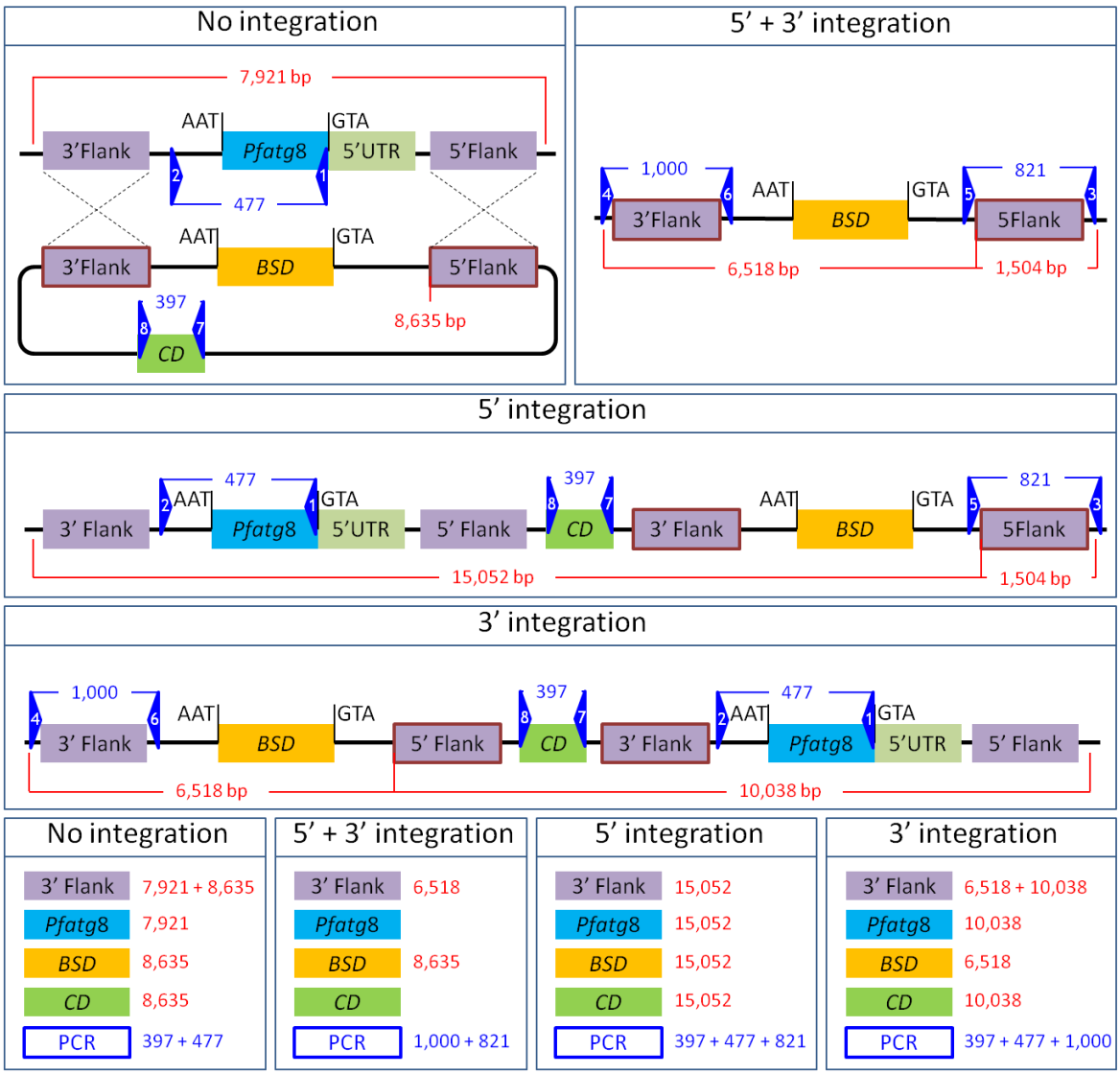

Figure 4.4: Graphical representation of predicted integration events.

(No integration) The ORF of *Pfatg8* (PF10_0193) lies on the complementary strand of chromosome 10. Digestion of DNA with *Spe*I is predicted to yield a fragment 7,921 bp in length which contains the *Pfatg8* ORF, 5'UTR and 5' and 3' homologous flanks. The construct *Pfatg8*-pCC-4 features a *BSD* cassette between 5' and 3' homologous flanks and contains a single *Spe*I site. PCR primers (1) and (2) would produce a 477 bp product representing the endogenous *Pfatg8* locus. PCR primers (7) and (8) would produce a 397 bp product representing the *Pfatg8*-pCC-4 plasmid backbone.

(5' + 3' integration) A double cross event over between the corresponding 5' and 3' homologous flanks of *Pfatg8*-pCC-4 and the genomic *Pfatg8* locus is predicted to result in the replacement of the *Pfatg8* ORF and 5'UTR with the *BSD* cassette. PCR primers (3) and (5) would produce an 821 bp product representing 5' integration. PCR primers (4) and (6) would yield a 1,000 bp product representing 3' integration.

(5' integration) Single cross over at the 5' homologous flank is predicted to result in the integration of the *Pfatg8*-pCC-4 construct upstream of the *Pfatg8* ORF. PCR primers (1) and (2), (3) and (5) and (7) and (8) would be expected to produce their products.

(3' integration) Single cross over at the 3' homologous flank is predicted to result in the integration of the *Pfatg8*-pCC-4 construct downstream of the *Pfatg8* ORF. PCR primers (1) and (2), (4) and (6) and (7) and (8) would be expected to produce their products.

Predicted fragment sizes detected by each probe used in analysis by Southern blotting are shown in red and predicted PCR product sizes are shown in blue.

DNA isolated from D10a c2 was first analysed by PCR (Figure 4.5). Primer pairs amplified products of the expected sizes representing the endogenous *Pfatg8* locus, the *CD* cassette and 5' integration. A product was seen with the primer pair intended to show 3' integration but this was of a smaller size than expected. Control reactions showed, where possible, that primers correctly annealed.

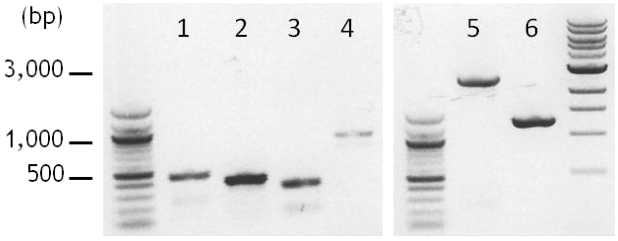

Product (primers)	Expected	Actual (~)
1 - *Pfatg8* locus (1+2)	477	480
2 - *CD* cassette (7+8)	397	400
3 - 3' integration (4+6)	1,000	300
4 - 5' integration (3+5)	821	850
5 - 5' control (2+3)	2,800	2,800
6 - 3' control (1+4)	1,300	1,300

Figure 4.5: PCR analysis of DNA isolated from D10a c2.

DNA isolated from D10a c2 was used as a template for PCR reactions using primers designed to form pairs indicative of the predicted genomic events during knockout of the *Pfatg8* ORF. PCR products were generated with primer pairs indicating that the intact endogenous *Pfatg8* locus, the *CD* cassette and the resultant locus of 5' integration were present. Ladders used are 100 bp (left) and 1 kb (right) both (N.E.B.).

The presence of a PCR product amplified using primers only predicted to form a pair once integration had occurred, suggested that, in at least a proportion of parasites in D10a c2, an integration event might have occurred. In order to test this further, the same DNA was analysed by Southern blotting, along with gDNA from the D10 parental line and DNA from D10a c2:5-FC i.e. parasites from the same cycle but those that were additionally resistant to 5-FC. Figure 4.6(A) shows the Southern blot analysis of the D10 parental line of D10a c2 and D10a c2:5-FC. A single fragment representing the endogenous *Pfatg8* locus (7,921 bp) was detected by the 3' flank and *Pfatg8*-specific probes, while no other fragments were visible with either these or the *BSD* or *CD* probes. This showed that the probes used were specific and that digestion by *Spe*I had produced the expected fragment size for the endogenous locus.

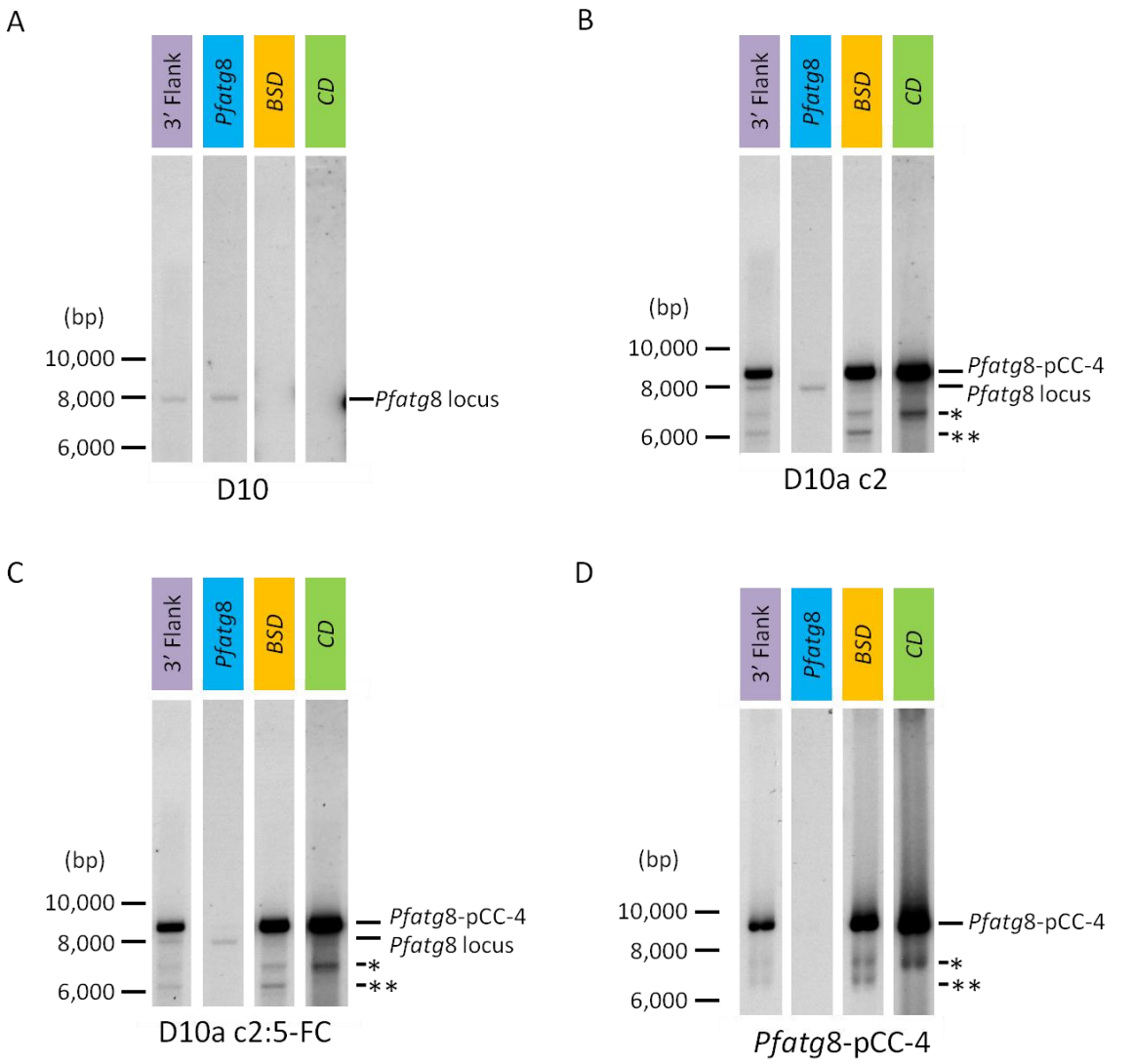

Figure 4.6: Southern blot analysis of wild type D10 parasites, parasites transfected with *Pfatg*8-pCC-4 and the *Pfatg*8-pCC-4 construct itself.

(A) 1.5 µg gDNA from D10 wild type parasites was digested overnight with *Spe*I, separated by electrophoresis in 0.7 % agarose and analysed by Southern blotting with 3' flank, *Pfatg*8-specific, *BSD* and *CD* probes. Size standards are indicated in bp to the left of each blot. Likely fragment identities are indicated to the right and the probe used is detailed above each lane.

(B) 1.5 µg DNA from D10 parasites transfected with *Pfatg*8-pCC-4 and selected with blasticidin was digested and analysed as above. A fragment representing the genomic *Pfatg*8 locus is detected by 3' flank and *Pfatg*8-specific probes. Additional fragments detected by 3' flank, *BSD* and *CD* probes (*), or 3' flank and *BSD* probes (**) are indicated.

(C) 1.5 µg DNA from D10 parasites transfected with *Pfatg*8-pCC-4 and selected with blasticidin and 5-FC was digested and analysed as above. An identical banding pattern is observed as in (B).

(D) 5 ng of *Pfatg*8-pCC-4 was digested overnight with *Spe*I and analysed as above. Bands with likely identities to those shown above are indicated.

Figure 4.6(B) shows the analysis of D10a c2. The *Pfatg*8-specific probe detected a fragment representing the endogenous locus (7,921 bp). The 3' flank probe detected fragments representing the endogenous locus and linearised plasmid

(8,635 bp). A fragment representing linearised plasmid was also detected by the *BSD* and *CD* probes. Interestingly, in addition to fragments representing the endogenous locus and linearised plasmid, a fragment was detected close in size to a predicted product of integration (6,518 bp) by the 3' flank and *BSD* probes. An additional fragment of ~ 7,000 bp was also detected by the 3' flank, *BSD* and *CD* probes. This appeared to be congruous with the analysis by PCR in suggesting that while the endogenous *Pfatg8* was detected, an integration event may have occurred in a sub-population of parasites in D10a c2.

Figure 4.6(C) shows the Southern blot analysis of D10a c2:5-FC. An identical banding pattern to that of D10a c2 with all 4 probes was observed. The presence of fragments representing linearised plasmid suggested that addition of 5-FC to the culture medium had not provoked death of parasites maintaining episomal plasmid as expected. This has previously been reported by members of this lab (Patzewitz, 2009).

These analyses pointed towards the possibility of an integration event between *Pfatg8*-pCC-4 and the D10 genome. However, in the absence of selection against parasites maintaining episomal plasmid it was difficult to determine whether a double crossover event had occurred i.e. one that would cause a replacement of the *Pfatg8* locus with the *BSD* cassette. Fragments of ~ 7,000 and 6,500 bp were not detected by any of the 4 probes in gDNA from the D10 parental line, showing that the fragments detected were specific to transfected lines. To show that these fragments were the result of integration between the *Pfatg8*-pCC-4 construct and the D10 genome and were not merely representative of episomal plasmid, 5 ng plasmid DNA from the maxiprep used for transfection was also digested with *Spe*I and analysed by Southern blotting (Figure 4.6(D)). As expected the *Pfatg8* specific probe did not react with any fragment following linearization of *Pfatg8*-pCC-4. While the 3' flank, *BSD* and *CD* probes detected a fragment representing linearised plasmid (8,635 bp) they also detected fragments of ~ 7,000 and 6,500 bp in an identical pattern to those seen in D10a c2 and c2:5-FC. These fragments were therefore determined to represent unexpected digestion products of the *Pfatg8*-pCC-4 construct following incubation with *Spe*I. This suggested that the fragments thought to represent potential integration events in the analysis of D10a c2 and D10a c2:5-FC were in

fact likely to represent unexpected digestion products of episomally maintained plasmid, potentially the result of *Spe*I star activity (Wei *et al.*, 2008).

Attempts to knockout the *Pfatg8* ORF by gene replacement in wild type *P. falciparum* had appeared to be unsuccessful. This suggested that either the *Pfatg8* gene is essential to parasite viability during the erythrocytic stages, or that the locus can not be targeted for genetic manipulation. In order to test these two possibilities, further transfection strategies were explored.

4.2.2 *Pfatg8* knockout in mCherry-*Pf*ATG8 expressing parasites

The possibility that the *Pfatg8* locus could not be replaced in wild type parasites due to the essentiality of this gene was tested by attempts to perform the same knockout in parasites expressing an additional copy of *Pf*ATG8. A parasite line previously transfected with EP-mC-A8 and known to be expressing mCherry-*Pf*ATG8 was therefore transfected with *Pfatg8*-pCC-4. This was predicted to alleviate any reliance on the endogenous *Pfatg8* ORF that may have prevented gene knockout in wild type parasites, by providing a platform for *Pf*ATG8 expression from an episomal plasmid. D10 parasites originally transfected with EP-mC-A8 and selected with WR99210, were transfected with *Pfatg8*-pCC-4 on two independent occasions and parasites resistant to both WR99210 and BLA were detected in Giemsa-stained thin smears up to 8 weeks later in 1 of the 2 transfections (D10c) (Figure 4.3). DNA was isolated from these parasites and as before, cycling on and off BLA and additional selection with 5-FC was performed. At all times parasites were maintained under WR99210 selection. Parasites viable in the presence of 5-FC were attained from the first cycle (D10c c0:5-FC) but were not attained following cycling off BLA.

DNA from D10c c0 and D10c c0:5-FC was analysed by Southern blotting. Figure 4.7(A) shows the analysis of D10c c0 using the 4 previously described probes. A fragment representing the endogenous locus (7,291 bp) was detected by both the 3' flank and *Pfatg8*-specific probes and not by the plasmid-specific *BSD* and *CD* probes. Surprisingly, a fragment representing linearised plasmid (8,635 bp) was not detected by the 3' flank, *BSD* or *CD* probes. Instead, a much larger fragment was detected by all 4 probes. Although this fragment separates above the maximum reference band in the ladder used, its size can be approximated to

~ 15,000 bp. As 5' integration is predicted to produce a fragment of 15,052 bp and this fragment would be detected by all 4 probes, it was thought that this fragment might represent a subpopulation of parasites in which a 5' integration event had occurred. As either a 5' or 3' integration has been observed to precede a double cross over event (Duraisingh *et al.*, 2002), it was predicted that additional selection with 5-FC might promote a second cross over at the 3' flank, producing parasites in which the *Pfatg8* locus had been replaced.

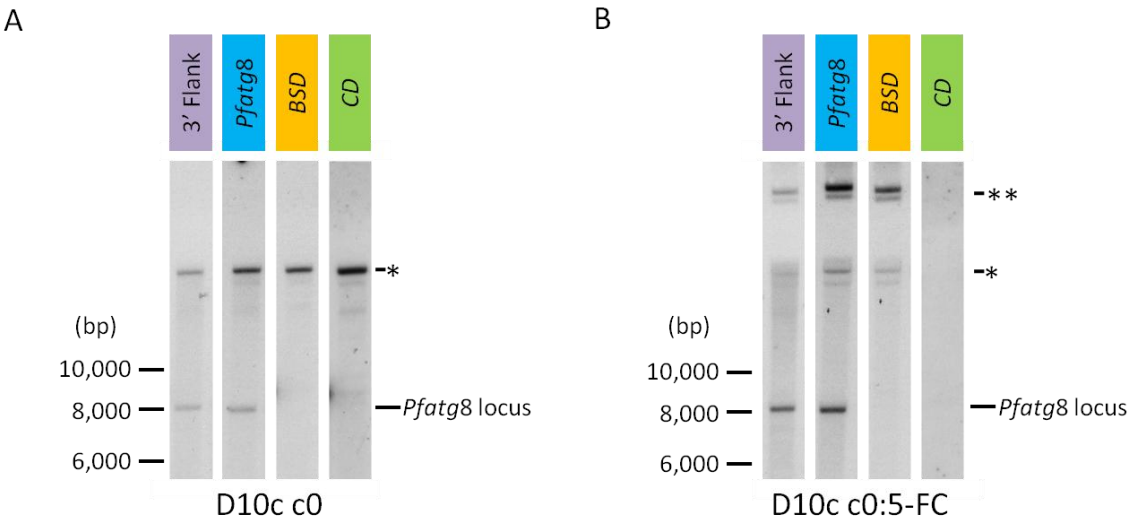

Figure 4.7: Southern blot analysis of the genomic *Pfatg8* locus in D10c c0 and D10c c0:5-FC.

(A) 1.5 µg DNA from D10 parasites transfected with EP-mC-A8 and *Pfatg8*-pCC-4 and selected with WR99210 and BLA was digested overnight with *Spe*I, separated by electrophoresis in 0.7 % agarose and analysed by Southern blotting with 3' flank, *Pfatg8*-specific, *BSD* and *CD* probes. Size standards are indicated in bp to the left of each blot. Likely fragment identities are indicated to the right and the probe used is detailed above each lane. Additional fragments detected by 3' flank, *Pfatg8*-specific, *BSD* and *CD* probes (*) are indicated.

(B) 1.5 µg DNA from D10 parasites transfected with EP-mC-A8 and *Pfatg8*-pCC-4 and selected with WR99210, BLA and 5-FC was digested and analysed as above. Additional fragments detected by 3' flank, *Pfatg8*-specific and *BSD* probes (**) are indicated.

Figure 4.7(B) shows the analysis of D10c c0:5-FC. It was apparent that opposed to the lack of negative selection observed with transfection D10a, selection of D10c c0 in the presence of 5-FC had resulted in a different banding pattern to that observed without 5-FC selection. Similarly to D10c c0, the 3' flank and *Pfatg8*-specific probes detected a fragment representing the endogenous locus (7,291 bp). However, no fragments were detected by the *CD* probe. This suggested that the presence of 5-FC had resulted in the loss of the *CD* cassette, showing that an integration event by double cross over had occurred leading to loss of the plasmid backbone. A fragment of ~ 15,000 bp corresponding to that

observed in D10c c0 was faintly detected by the 3' flank, *Pfatg*8-specific and *BSD* probes. In addition, the same 3 probes also detected two similarly sized fragments of even larger size. A fragment of 6,518 bp representing replacement of the *Pfatg*8 ORF with the *BSD* cassette was not detected by the 3' flank or *BSD* probes. This, along with the detection of a fragment representing the unaltered *Pfatg*8 locus suggested that the integration observed might have been into an off target locus or loci. However, due to the possibility of a population of parasites in which the *Pfatg*8 ORF had been replaced, the D10c c0:5-FC line was selected for cloning via limiting dilution (Kirkman *et al.*, 1996). This was performed in order to isolate a clonal parasite line in which the *Pfatg*8 ORF may have been replaced with the *BSD* cassette. A total of 17 clones were obtained and analysis of the *Pfatg*8 locus in 12 clones was initially performed by PCR using DNA produced from small scale isolation (Figure 4.8).

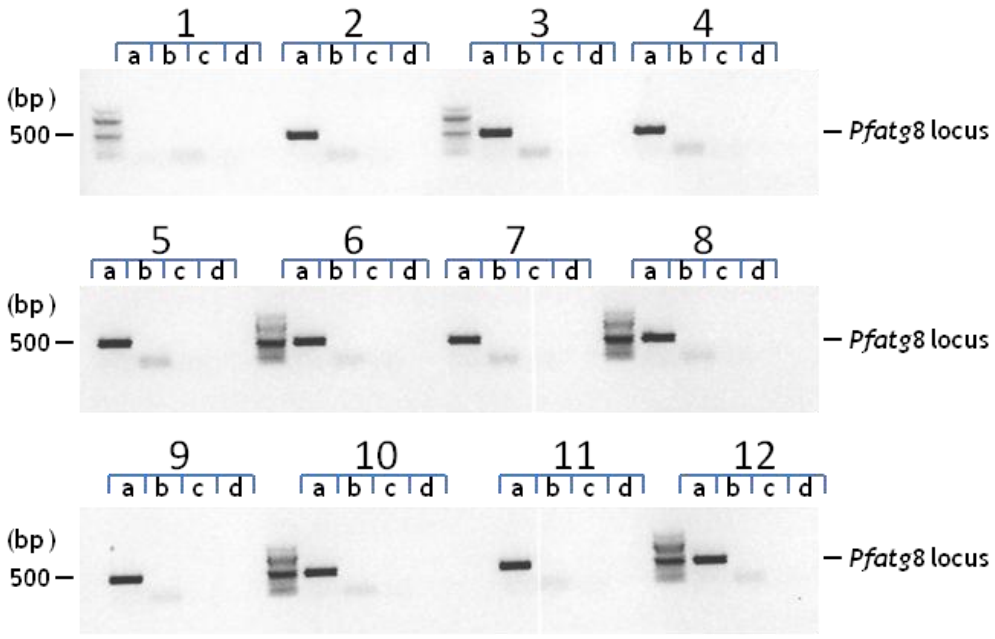

Product (primers)	Expected
a - *Pfatg8* locus (1+2)	477
b - *CD* cassette (7+8)	397
c - 3' integration (4+6)	1,000
d - 5' integration (3+5)	821

Figure 4.8: PCR analysis of clones of D10c c0:5-FC generated by limiting dilution.

Clonal lines were isolated from D10c c0:5-FC by limiting dilution. DNA isolated from 12 clones was used as a template for PCR reactions using primers designed to form pairs indicative of the predicted genomic events during knockout of the *Pfatg*8 ORF. PCR products representing the endogenous *Pfatg*8 locus were amplified from isolates 2-12 with primers (1) and (2). PCR products representing the *CD* cassette (7+8), 5' integration (3+5) or 3' integration (4+6) were not detected in any isolate. A 100 bp ladder was used to determine PCR product sizes (N.E.B.).

Eleven of the clones appeared to possess an unaltered endogenous *Pfatg*8 locus, as demonstrated by the presence of a 477 bp product amplified with the primer pair covering the *Pfatg*8 ORF in its genomic locus. In one clone (1), D10c c0:5-FC CLONE, this band was not present, suggesting that the endogenous *Pfatg*8 locus might have been altered. PCR products were not amplified using primer pairs covering the *CD* cassette in any clone, supporting the observation by Southern blotting that the *CD* cassette had been lost as a result of 5-FC selection. Also, in no clone were products amplified that were predicted to represent 5' or 3' integration events. This may have been expected in the 11 clones in which the *Pfatg*8 locus appeared to be unaltered but would have been predicted to be detected in D10c c0:5-FC CLONE. Therefore, to determine whether the *Pfatg*8

ORF had been replaced by the *BSD* cassette in D10c c0:5-FC CLONE, a larger scale DNA isolation was subjected to analysis by Southern blotting using the 3' flank and *Pfatg8*-specific probes (Figure 4.9(A)).

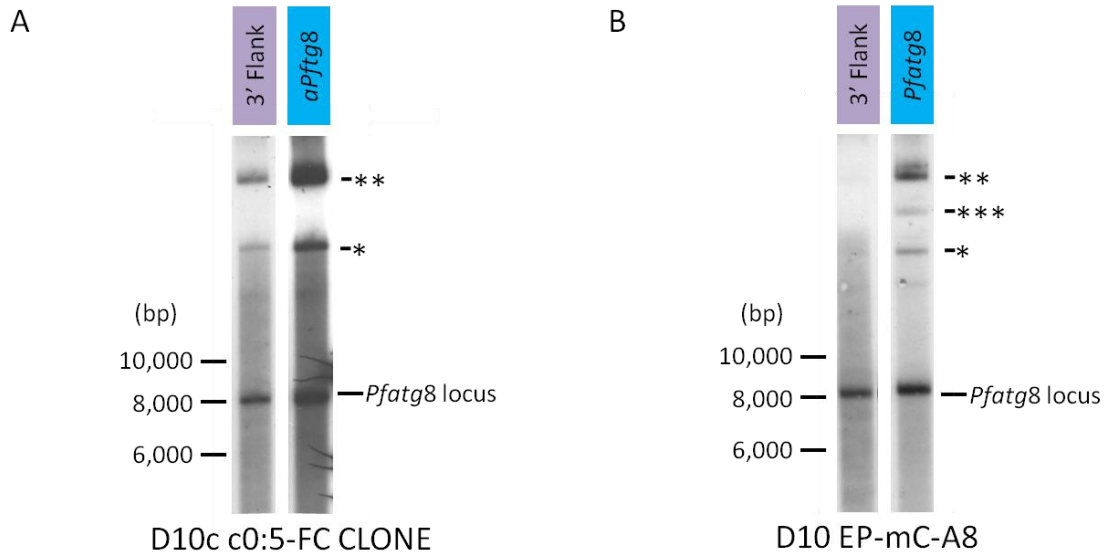

Figure 4.9: Southern blot analysis of the genomic *Pfatg8* locus in D10c c0:5-FC CLONE and its parental mCherry-*Pf*ATG8 expressing line, EP-mC-A8.

(A) 1.5 µg DNA from a clonal population of D10 parasites transfected with EP-mC-A8 and *Pfatg8*-pCC-4 and selected with WR99210 and BLA and 5-FC was digested overnight with *Spe*I and was analysed by Southern blotting with 3' flank and *Pfatg8*-specific probes. Size standards are indicated in bp to the left of each blot. Likely fragment identities are indicated to the right and the probe used is detailed above each lane. Additional fragments detected by 3' flank and *Pfatg8*-specific probes (*) and (**) are indicated.

A fragment representing the genomic *Pfatg8* locus is detected by both probes, as are two fragments corresponding to those seen in the non clonal line D10c c0:5-FC (*) and (**).

(B) 1.5 µg DNA from D10 parasites transfected with EP-mC-A8 and selected with WR99210 was digested and analysed as above. Additional fragments detected by the *Pfatg8*-specific probe (*), (**) and (***) are indicated.

The 7,291 bp fragment representing the endogenous *Pfatg8* locus was detected by both probes, along with much larger fragments, likely to be those also detected in the progenitor line, D10c c0:5-FC. In contrast to the PCR analysis of this clone, it appeared that the *Pfatg8* ORF was still present and that while integration of the *Pfatg8*-pCC-4 construct had occurred, it had not affected the target locus.

It appeared that the fragments of ~ 15,000 bp and larger represented integration events into an off target locus or loci. As had been seen in the analysis of D10a, the presence of the episomal plasmid can sometimes lead to unexpected banding patterns when analysed by Southern blotting. In order to add evidence

that these fragments were the result of integration events between *Pfatg*8-pCC-4 and the D10 genome, DNA isolated from the parental line of D10c, EP-mC-A8, was also analysed by Southern blotting Figure 4.9(B). These parasites were known to be expressing mCherry-*Pf*ATG8 and were predicted to maintain EP-mC-A8 as an episomal plasmid due to the presence of the Rep20 element (O'Donnell *et al.*, 2002). The EP-mC-A8 construct does not contain any *Spe*I sites and therefore was expected to run as undigested plasmid following *Spe*I digest of isolated DNA.

As expected, a fragment representing the endogenous *Pfatg*8 locus was detected with the 3' flank and *Pfatg*8-specific probes, as this construct is not predicted to recombine with the *Pfatg*8 locus. This shows that similarly to wild type D10, the *Pfatg*8 ORF was unaltered. Interestingly, the *Pfatg*8-specific probe also detected multiple larger fragments. These fragments corresponded with those seen in Southern blotting analysis of D10c c0, D10c c0:5-FC and D10c c0:5-FC CLONE. The presence of these fragments suggests that the EP-mC-A8 construct may in fact integrate into the D10 genome at a locus or loci distinct from the *Pfatg*8 locus, independently of the presence of the *Pfatg*8-pCC-4 construct.

4.2.3 *Pfatg*8 tagging and targeting control

Attempts to replace the *Pfatg*8 ORF with the *BSD* cassette of *Pfatg*8-pCC-4 either in wild type parasites or those expressing mCherry-*Pf*ATG8 (along with endogenous *Pf*ATG8) had proven unsuccessful. This raised the question as to whether the *Pfatg*8 locus was amenable to genetic manipulation (Patzewitz *et al.*, 2012). A commonly used strategy to determine whether a gene locus of interest can be targeted in *P. falciparum* is to employ a construct designed to integrate into the gene locus via a single cross over event (Patzewitz *et al.*, 2012, Russo *et al.*, 2009). Introduction of the full plasmid sequence into the locus of interest can disrupt the gene ORF if a truncated homologous region is used, or if a full length homologous region is used then the gene ORF will remain intact (de Koning-Ward *et al.*, 2000). However, in this study a different method using the pCC-4 construct and therefore relying on double homologous recombination was utilised instead. This was chosen as it provided a method to both confirm that the *Pfatg*8 locus was able to be targeted by pCC-4-based constructs and also to replace the endogenous *Pfatg*8 ORF with an N-terminally

tagged *Pfatg*8 gene. It was anticipated that by effectively N-terminally tagging the endogenous *Pfatg*8 gene, an additional tool to study *Pf*ATG8 in live parasites would result.

To do this, the *Pfatg*8-pCC-4 construct was modified so that both the BSD cassette and a cassette driving expression of mCherry-*Pf*ATG8 would replace the endogenous *Pfatg*8 ORF. The construct *mCherry-Pfatg8*-pCC-4 was generated by replacing the 5' homologous flank of *Pfatg*8-pCC-4 with the mCherry-*Pf*ATG8 expression cassette from the construct EP-mC-A8. This contains the *Pfatg*8 ORF in frame with the upstream mCherry sequence and endogenous *Pfatg*8 5' UTR and is followed by the *Pb*DT 3' UTR. This created a construct containing an effective 5' flank of 810 bp, corresponding to the endogenous *Pfatg*8 promoter region and a 3' flank identical to that of *Pfatg*8-pCC-4. The predicted integration events between mCherry-*Pfatg*8-pCC-4 and the *Pfatg*8 locus are shown in Figure 4.10 and the predicted fragment sizes following digestion with *Spe*I are again indicated in red.

The *mCherry-Pfatg*8-pCC-4 construct was transfected into D10 and 3D7 parasites twice on two independent occasions. Unfortunately no BLA resistant parasites were detected in Giemsa-stained thin smears up to 10 weeks after transfection (see Figure 4.3).

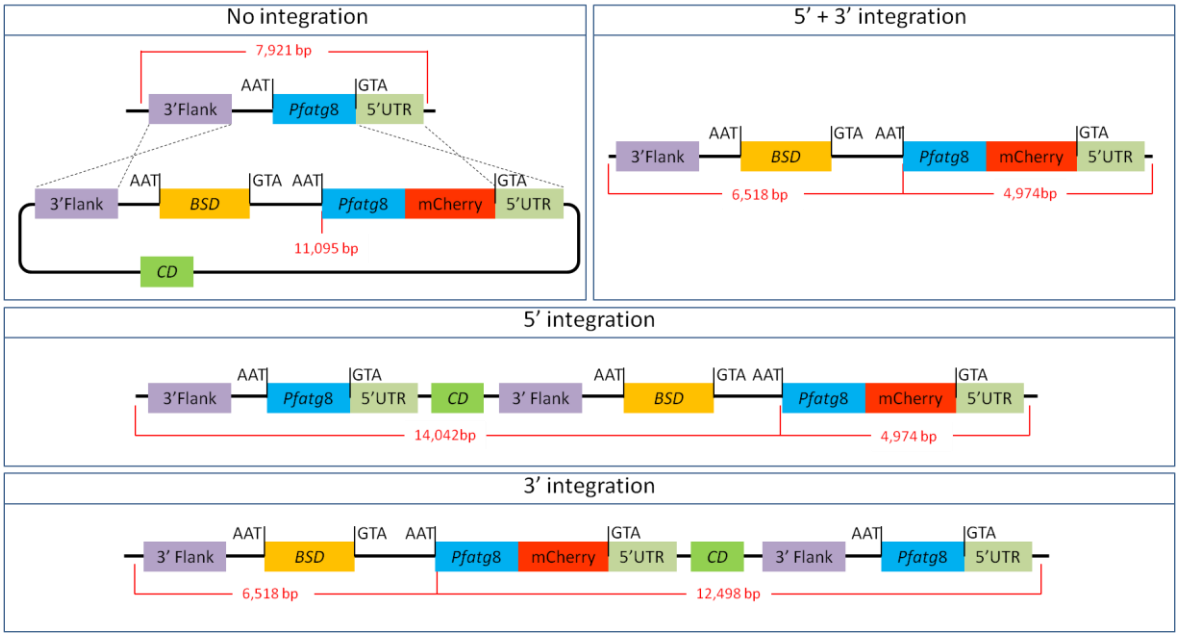

Figure 4.10: Schematic representation of potential integration events between *mCherry-Pfatg*8-pCC-4 and the endogenous *Pfatg*8 locus.

(No integration) The *mCherry-Pfatg*8-pCC-4 construct has the same 3' flank as *Pfatg*8-pCC-4 but the 5' flank has been replaced by an mCherry-*Pf*ATG8 expression cassette. The promoter region within the 5' UTR is predicted to act as the 5' flank to facilitate homologous recombination.

(5' and 3' integration) A double crossover event is predicted to result in the replacement of the endogenous *Pfatg*8 ORF with the plasmid derived *mCherry-Pfatg*8 and *BSD* cassettes.

(5' integration) A single cross over event between the shared 5' UTR elements would result in the integration of the *mCherry-Pfatg*8-pCC-4 plasmid upstream of the endogenous *Pfatg*8 ORF.

(3' integration) A single crossover event between the shared 3' flanks would result in the integration of the *mCherry-Pfatg*8-pCC-4 plasmid downstream of the *Pfatg*8 ORF.

4.3 Discussion

4.3.1 Interpretation of results

This chapter has detailed the efforts made to deduce whether the *Pfatg*8 gene is essential for the blood stages of *P. falciparum*. Attempts to generate *Pfatg*8 knockouts either in a wild type parental line or in a line expressing mCherry-*Pf*ATG8 were unsuccessful. This indicates that either *Pfatg*8 is essential to the viability of erythrocytic parasites, or that the *Pfatg*8 locus is not amenable to manipulation using pCC-4-based constructs.

The presence of a DNA fragment representing linearised *Pfatg*8-pCC-4 plasmid in D10 parasites transfected with *Pfatg*8-pCC-4 and selected with both BLA and 5-FC indicates that negative selection had been unsuccessful in these parasite

lines. In the absence of negative selection, it is unlikely that a double cross over integration event will occur (Maier *et al.*, 2006). A lack of negative selection suggests that either these parasites were not converting 5-FC to 5-FU or that the 5-FU produced did not cause cell death. This could occur through multiple mechanisms. The fact that the same batch of 5-FC was successfully used to select against parasites maintaining the *CD* cassette in D10c c0:5-FC shows that the 5-FC used was efficacious. Resistance to 5-FC has been shown to be rapidly achieved by fungal agents - the usual indication of 5-FC is in antifungal therapy (Quinto-Alemany *et al.*, 2012). This could occur through changes to transporters responsible for the uptake of 5-FC, transcriptional repression of the *CD* cassette or changes to the translation, post-translational modification or turnover of CD (Chapeland-Leclerc *et al.*, 2005, Papon *et al.*, 2007). Mechanisms to combat the effects of 5-FU could also provide a level of resistance to negative selection. 5-FU acts as a thymidylate synthase inhibitor in the pyrimidine biosynthetic pathway. Modification of this pathway may out-compete 5-FU by the upregulation of pyrimidine biosynthesis (Sanglard, 2002, Vermes *et al.*, 2000). The mechanism of 5-FC resistance in *P. falciparum* has not been identified.

Knockout of the endogenous *Pfatg8* locus using the *Pfatg8*-pCC-4 construct was also attempted in a parental line previously transfected with EP-mC-A8. In the analysis of these lines no DNA fragment representing linearised *Pfatg8*-pCC-4 was detected, as had been the case in wild type parasites transfected with the same construct. However, there was a larger fragment not seen in the analysis of the aforementioned parasite lines. This suggested that either the *Pfatg8*-pCC-4 plasmid had readily integrated, or that a recombination event had occurred between the *Pfatg8*-pCC-4 and EP-mC-A8 plasmids, resulting in a larger product following linearization by *Spe*I. It has been shown that plasmids with homologous regions rapidly recombine following transfection into *P. falciparum* intraerythrocytic stages (Kadekoppala *et al.*, 2001, Krnajski *et al.*, 2002). Care was taken in the selection of plasmid pairings but the limited repertoire of transcriptional regulatory elements available meant that some elements were common to both plasmids in co-transfected lines. The cassettes conferring drug resistance to blasticidin or WR99210 in the constructs *Pfatg8*-pCC-4 and EP-mC-A8, respectively, share the same *Pf*CAM 5' and *Pf*hrpII 3' regulatory elements. The length of homologous sequence between the two constructs may have been

sufficiently long to facilitate recombination between the plasmids transfected into *P. falciparum* parasites (Kadekoppala *et al.*, 2001). The 3' regulatory element of the mCherry-*Pfatg*8 cassette in EP-mC-A8, *Pb*DT 3', is also used in *Pfatg*8-pCC-4 as the 3' regulatory element of the *CD* cassette (Maier *et al.*, 2006, van Dooren *et al.*, 2005). Parasites transfected with EP-mC-A8 rather than 86-mC-A8 were chosen for co-transfection with *Pfatg*8-pCC-4 as the *Pfhsp*86 5' UTR is also common to both 86-mC-A8 and *Pfatg*8-pCC-4. This was intended to limit the possibility of recombination between the two plasmids that might interfere with integration of *Pfatg*8-pCC-4 into the *Pfatg*8 locus. Recombination between the two plasmids could create a larger product following linearization with *Spe*I, having 'inherited' only one *Spe*I site from the *Pfatg*8-pCC-4 construct. The predicted resultant construct size of 16 kb could explain the absence of a fragment representing linearised *Pfatg*8-pCC-4 in D10c c0 with a larger fragment detected in its place. The complexity of outcomes of recombination between the two plasmids and any subsequent integration into the *Pfatg*8 locus or any off-target locus or loci would make analysis by Southern blotting alone very difficult and would therefore require additional analysis by pulsed field gel electrophoresis and other methods to determine if intergration had occured (Krnajski *et al.*, 2002).

Considering the analysis of the genome of parasites transfected with only EP-mC-A8, recombination between the two constructs may also have been further complicated by prior integration of the EP-mC-A8 construct into an unknown locus. EP-mC-A8 does not contain any *Spe*I sites and should therefore be detected as non-linearised plasmid by Southern blotting with the *Pfatg*8-specific probe. However, it was evident that multiple DNA fragments were detected using the *Pfatg*8-specific probe. This suggested that integration of the EP-mC-A8 construct into the parasite genome had already occurred prior to transfection with the *Pfatg*8-pCC-4 construct. This integration would likely be by a single cross over recombination event, as recombination by double cross over would result in loss of WR99210 resistance and would be unlikely in the absence of negative selection. Therefore it is likely that the banding pattern observed in Southern blot analysis of the EP-mC-A8 parasite line represents either random integration of the construct into the parasite genome or possibly integration into

the *Pfatg8* locus itself. Again, considering that the EP-mC-A8 line is not clonal, a mixture of populations with different integration events may have been present.

Integration of the EP-mC-A8 construct into the *Pfatg8* genomic locus before introduction of the *Pfatg8*-pCC-4 construct could have resulted in unexpected integration events between the *Pfatg8*-pCC-4 plasmid and the modified genomic locus. Integration of the EP-mC-A8 construct into an unrelated locus could also create an 'artificial locus' containing sequences homologous to those within *Pfatg8*-pCC-4. Again, the complexity and number of outcomes resulting from these possible integration events would lead to the determination of the status of the genomic locus by Southern blotting and PCR analysis being extremely difficult.

Whatever recombination or integration events had occurred in the D10c line, transfected with both EP-mC-A8 and *Pfatg8*-pCC-4, the addition of 5-FC to culture medium did have an effect on the banding pattern observed during analysis by Southern blotting. The *CD* cassette had been lost, shown by the absence of any DNA fragment detected by the *CD* probe. Additional fragments were detected with the 3' flank, *Pfatg8*-specific and *BSD* probes that were not detected before 5-FC selection. This suggested that addition of 5-FC had indeed caused the loss of the *CD* cassette and integration of the *Pfatg8*-pCC-4 construct by a double cross over event had occurred. Pulsed field gel electrophoresis could be used to determine the likely location(s) of integration events (Gunther *et al.*, 2009, Krnajski *et al.*, 2002).

Cloning of the D10c c0:5-FC parasite line by limiting dilution showed that while an integration event had occurred, the endogenous *Pfatg8* locus remained unaltered. The absence of a PCR product amplified by primer pairs covering the endogenous *Pfatg8* locus was surprising, given the presence of a fragment representing the endogenous *Pfatg8* locus in Southern blot analysis. Further PCR analysis was performed and results supported the initial findings. The endogenous *Pfatg8* locus was detected using the relevant primer pair in DNA collected from wild type parasites, along with the other 11 clones, showing that the primers (1) and (2) were able to anneal as expected. However, the DNA isolates used for PCR and Southern blot analysis were collected independently and PCRs were not repeated on DNA isolated from parasites for analysis by

Southern blotting. It is possible that the yield of DNA isolated from D10c c0:5-FC CLONE for PCR analysis was overestimated in relation to isolates from the other clones, leading to undetectable amplification of the product representing the intact endogenous *Pfatg8* locus. During further analysis by PCR, a product covering the 3' flank, generic to both the unaltered locus and the locus resultant from integration was detected, while no product covering the 5' flank was detected. This potentially indicated that a poor yield or quality of this DNA isolate was responsible for poor amplification of PCR products. During Southern blotting, the amount of DNA loaded is verified visually, meaning that even amounts of DNA between isolates can be judged. Given this assurance and the fact that Southern blotting is widely regarded as a more qualitative analysis method than PCR (Schiffman *et al.*, 1991), evidence gathered from Southern blotting was deemed more reliable than that from PCR analysis.

Verification of the methodology used to attempt knockout of *Pfatg8* proved unsuccessful. Targeting the *Pfatg8* locus with a pCC-4-based construct designed not to remove the *Pfatg8* ORF but rather to introduce a *mCherry-Pfatg8* ORF in its place was intended to have shown that the *Pfatg8* locus is amenable to manipulation. Without this evidence it is impossible to say that the inability to knockout *Pfatg8* is due to the essentiality of the *Pf*ATG8 protein (Patzewitz *et al.*, 2012). Parasites resistant to BLA were not detected following transfection with the *mCherry-Pfatg8*-pCC-4 construct. The *mCherry-Pfatg8*-pCC-4 construct is large (> 10 kb) and contains both *Plasmodium*-specific A/T rich and non-*Plasmodium* sequences. These factors have been suggested to result in problems with plasmid stability in *E. coli* (Tonkin *et al.*, 2004). While the areas covering the inserted sequences of all plasmids used for transfection into *P. falciparum* were sequenced, this would not detect issues surrounding plasmid stability such as structural and isoforms variances (Silva *et al.*, 2012), which may have limited transfection efficiency in *P. falciparum*.

The *mCherry-Pfatg8*-pCC-4 construct was designed in an attempt to kill two birds with one stone. A simpler method for genomic locus targeting relies on single cross over integration (Patzewitz *et al.*, 2012). Introducing an upstream sequence encoding an mCherry-tag to the endogenous *Pfatg8* ORF seemed impossible using a construct designed to integrate by single cross over. This was desired as a mechanism for monitoring endogenously expressed *Pf*ATG8 in live

parasites. Therefore the decision was made to attempt to combine the analysis of *Pfatg*8 locus susceptibility to genetic manipulation with an attempt to effectually introduce a tag to the endogenous *Pfatg*8 ORF.

The *mCherry-Pfatg*8-pCC-4 construct was made by replacing the 5' homologous flank of *Pfatg*8-pCC-4 with the expression cassette from the EP-mC-A8 construct. The length of regions homologous to genomic sequence was therefore increased from 610 bp in the 5' flank of *Pfatg*8-pCC-4, to 810 bp in the endogenous promoter region of *mCherry-Pfatg*8-pCC-4. Whether the increased length of homology could improve the efficiency of recombination has yet to be determined. Also, the possibility of recombination between the endogenous *Pfatg*8 ORF and the *Pfatg*8 coding sequence within the plasmid has not been explored. Homologous flanks of typically 500 bp are commonly used in this lab to facilitate integration into gene loci (Patzewitz *et al.*, 2012). Whether the 372 bp sequence encoding the *Pfatg*8 ORF shared between the genome and plasmid would be sufficient to facilitate homologous recombination could be assessed by Southern blotting. Unfortunately, if this was to occur, then recombination between the plasmid and the *Pfatg*8 locus would not be guaranteed to replace the endogenous *Pfatg*8 ORF with the full mCherry-*Pf*ATG8 expression cassette. This could possibly be avoided by generating the *Pfatg*8 coding portion of the mCherry-*Pf*ATG8 expression cassette synthetically i.e. adjusting the nucleic acid sequence without affecting the translated sequence (Yeoh *et al.*, 2007).

Replacement of the endogenous *Pfatg*8 ORF with an mCherry-tagged *Pfatg*8 ORF would have facilitated visualisation of the tagged fusion protein by live cell fluorescent microscopy. However, using a small epitope tag (e.g. myc) might result in a smaller plasmid more stable in *E. coli* and with a smaller region intended to integrate into the genome, potentially improving integration efficiency. The localisation of the epitope-tagged *Pf*ATG8 fusion protein could then be detected by IFA with antibodies specific for the tag (Sun *et al.*, 2008).

4.3.2 Future considerations

Due to the apparent inability to achieve genetic ablation of *Pfatg*8 using the pCC-4 construct, additional methods may be needed to determine whether *Pf*ATG8 is essential to parasite viability. While many methods have been

employed they are often hampered by the same issues surrounding low transfection efficiencies and low integration efficiencies (Crabb *et al.*, 2004). Similarly to the negative selection strategy based around the bi-functional cytosine deaminase chimeric enzyme, a method based around thymidine kinase has also been employed to kill parasites maintaining episomal plasmid (Duraisingh *et al.*, 2002). This enzyme (from *Herpes simplex* virus) is encoded in the backbone of pHTK-based vectors and converts the pro-drug ganciclovir into toxic metabolites, which inhibit DNA synthesis by competing for deoxyguanosine triphosphate (Matthews and Boehme, 1988). This method has been employed in the analysis of a number of genes in *P. falciparum* (Duraisingh *et al.*, 2003, Haase *et al.*, 2008). Considering the apparent inconsistency in selection observed when wild type parasites transfected with *Pfatg*8-pCC-4 were treated with 5-FC, use of this similar system with a different selectable marker might prove more reliable in regards to application of negative selection.

Attempts to show that the endogenous *Pfatg*8 locus can be targeted by pCC-4-based constructs by using *mCherry-Pfatg*8-pCC-4 were unsuccessful. Additional methods exist for confirming a genomic locus can be targeted by homologous recombination. Constructs based on pHH-1 (Reed *et al.*, 2000) have routinely been used to confirm locus targeting (Patzewitz *et al.*, 2012), and also genetic manipulation of target genes (Gunther *et al.*, 2007, Storm *et al.*, 2011). Unlike pCC-4-based constructs, pHH-1 is designed to contain a single homologous region to promote integration of the entire plasmid by via a single cross over event. Use of a homologous area corresponding to a region within the ORF of a gene of interest can be used to effectively knock out a gene by insertion of the entire plasmid sequence into the ORF, disrupting the gene through frame shift, insertion of premature stop codons or other means (Crabb, 2002, Gunther *et al.*, 2007, Storm *et al.*, 2011). However, single cross over integration can also be used to show targeting of a gene locus without deleteriously disrupting the ORF of the gene of interest (Patzewitz *et al.*, 2012). Use of a homologous region encoding a sequence identical to the gene ORF results in the maintenance of a full gene ORF following integration of the plasmid. The gene of interest is maintained but has a 3' UTR derived from the plasmid, as its own 3' UTR is forced downstream behind the integrated plasmid. Knockout attempts were not performed with a pHH-1-based construct for two reasons. Firstly, due to the fact

that without negative selection to remove episomally maintained plasmids, it can often take a longer period of cycling off and on selective pressure to generate cultures with integrated plasmid. Secondly, the small size of the *Pfatg*8 ORF would also provide an obstacle for generating a construct with a homologous region sufficiently long to support efficient homologous recombination. Typically around 800 bp of sequence homologous to the gene ORF would be used, to ensure efficient targeting (Patzewitz *et al.*, 2012). The fact that the *Pfatg*8 ORF is only 375 bp in length likely means that portions of either the 5' UTR or 3' UTR regions would also be needed to facilitate recombination. Potential approaches that could be used are represented graphically in Figure 4.11. In either instance, an efficient disruption of the *Pfatg*8 ORF could not be assured. If a sequence covering a portion of the 5' UTR and a portion of the *Pfatg*8 ORF were used (A), depending on how much 5' UTR was needed to facilitate recombination, a functional *Pfatg*8 ORF might remain following integration. If a sequence covering a portion of the *Pfatg*8 ORF and a portion of the 3' UTR were used (B), careful primer design or site directed mutagenesis could be used to produce a *Pfatg*8 ORF without a stop codon. However, due to the likelihood of the 3' UTR encoding a stop codon in frame with the *Pfatg*8 ORF, it is possible that an 'artificially elongated' *Pf*ATG8 might be expressed. Due to these issues, attempts to knockout the *Pfatg*8 ORF were focussed on the use of the pCC-4 construct.

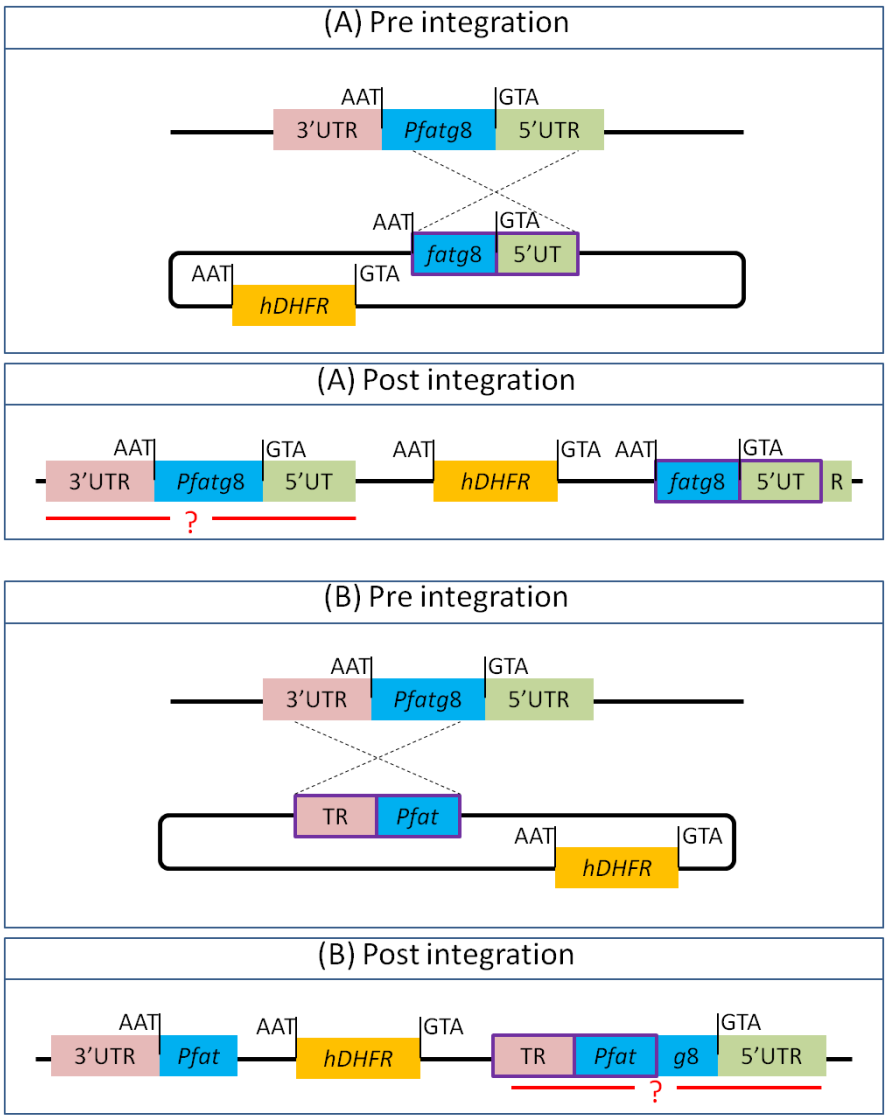

Figure 4.11: Schematic representation of potential gene disruption strategies using constructs based on pHH-1.

(A) A construct containing a homologous region covering portions of the 5' UTR and *Pfatg*8 ORF could integrate by single cross over. However, this might leave a functional *Pfatg*8 ORF (-?-).

(B) A construct containing a homologous region covering portions of the *Pfatg*8 ORF and 3' UTR could integrate by single cross over. However, even if the *Pfatg*8 ORF stop codon was excluded from the plasmid sequence, expression of *Pf*ATG8 plus additional residues encoded by the 3' UTR might occur (-?-).

However, the small size of the *Pfatg*8 ORF does not prevent the use of pHH-1-based constructs to be used to confirm locus targeting. Modifications of methods A or B, detailed above, could be used to provide evidence that the *Pfatg*8 gene locus is susceptible to modification by homologous recombination, even though the regions used would be different to those used in *Pfatg*8-pCC-4. Integration following a single cross over event could be analysed by PCR analysis and Southern blotting, similarly to the methodologies performed here.

The possibility remains that *Pf*ATG8 is essential for the viability of blood stage parasites. Indeed, it has been suggested that knockout of the *atg*8 gene homologue found in *P. berghei* has a lethal phenotype (Duszenko *et al.*, 2011) but no experimental data has so far been published. Where genetic knockout of a target gene is precluded by its essentiality, knockdown of transcript and protein levels can be used to mimic genetic knockout. RNA interference (RNAi) technology is commonly exploited to study the effects of down regulation of essential genes in parasites and other organisms (Manzano-Roman *et al.*, 2012). Unfortunately, *Plasmodium spp.* have been found to lack the necessary enzymes required to produce an RNAi induced down regulation of gene expression (Baum *et al.*, 2009). Goldberg and co-workers have developed a protein destabilisation mechanism for use in *P. falciparum*, based on ligand-regulatable FKBP tagging (Armstrong and Goldberg, 2007). This mechanism uses episomal expression of an FKBP-tagged fusion protein in order to alleviate reliance on the endogenous gene allowing knockout by the aforementioned methods. The FKBP domain fused to the protein product of the gene of interest will direct it for degradation unless it is stabilised by interaction with a rapamycin analogue ligand called Shld1. Expression of the fusion protein in the presence of Shld1 allows for the genetic knockout of the endogenous gene but then also facilitates tunable regulation of protein stability through controlled removal of Shld1. Resultant phenotypes can then be assessed (provided the result of protein down regulation isn't lethal). The observation that degradation of the fusion protein is not complete, even in the absence of Shld1, allows for the phenotypic analysis of parasites in which a genetic knockout of the gene of interest would be lethal (Patzewitz, 2009). The relatedness of the knockdown phenotype to the actual effect of genetic ablation will be influenced by the level of knockdown and the ability of the parasite to compensate for reduced protein levels.

This methodology can also be used to mimic genetic knockout of a gene of interest by the regulatable over expression of an inactive form of its protein product (Patzewitz, 2009, Santos *et al.*, 2011). Expression of an FKBP-tagged inactive form of a protein in the presence of Shld1 can lead to the inhibition of the endogenous protein through, for example, competition for binding partners or stalling of conjugation pathways. The culture of parasites without Shld1 following transfection with the construct used to drive expression of the inactive

fusion protein allows establishment of transfected lines without the deleterious phenotype associated with expression of the inactive fusion protein as it would be quickly degraded. This approach could possibly be used in the exploration of the effect of *Pf*ATG8 knockdown. Expression of an FKBP-tagged *Pf*ATG8ΔG could possibly result in a phenotype mimicking the effect of genetic knockout through competition of *Pf*ATG8 for binding partners involved in its conjugation pathway. However it would need to be experimentally determined whether the over expression of a mutant form of *Pf*ATG8 caused a competitive inhibition of endogenous *Pf*ATG8. From the analysis of transgenic parasites expressing mCherry-*Pf*ATG8ΔG, it would appear that this is not sufficient to cause a detectable phenotype indicating inhibition of endogenous *Pf*ATG8 function.

Attempts to knockout *Pfatg8* in the presence of episomally expressed mCherry-*Pf*ATG8 appeared to be hampered by recombination between the EP-mC-A8 and *Pfatg8*-pCC-4 constructs. A secondary issue observed when using the EP-mC-A8 construct as a platform to alleviate reliance on endogenous *Pf*ATG8, was that it appeared to integrate into the parasite genome into an unknown locus or loci. The Gateway system was used to generate constructs for mCherry-*Pf*ATG8 expression due to the simplicity of the cloning steps required and because of experimental evidence for its effectiveness (Gunther *et al.*, 2007, van Dooren *et al.*, 2005). However additional methods exist for generating transgenic lines in which fluorescent fusion proteins are expressed. For example a method for genetic integration utilising the Mycobacteriophage Bxb1 integrase has recently been described (Adjalley *et al.*, 2010, Nkrumah *et al.*, 2006). The serine integrase of Bxb1 is able to catalyse directional recombination between the viral *att*P site and its target *att*B site without the need for bacterial host factors, divalent cations or DNA supercoiling (Ghosh *et al.*, 2003). The availability of 3D7 and Dd2 parasite lines possessing an *att*B site integrated into the non-essential cg6 locus, facilitates co-transfection of a construct driving expression of Bxb1 integrase (pINT) along with a construct harbouring an *att*P site and the gene element(s) of interest.

Use of the Bxb1 integrase system might prove a better method of providing an exogenous copy of *Pfatg8* to facilitate knockout attempts. An mCherry-*Pf*ATG8 expression cassette could be directionally cloned into the modified pBLUESCRIPT vector, pLN, used in combination with pINT (Adjalley *et al.*, 2010). Expression of

the Bxb1 integrase from pINT would result in the integration of the mCherry-*Pf*ATG8 construct into the cg6 locus. This controlled and targeted integration can be easily assessed, unlike the apparently random integration observed when using EP-mC-A8. This technique could therefore be used to not only generate a parasite line stably expressing mCherry-*Pf*ATG8 from a genomic, rather than an episomal locus but could also be used to help determine whether the endogenous copy of *Pfatg*8 can be knocked out using *Pfatg*8-pCC-4.

Other methods for genetic knockout employing a modification of, or straying away from the reliance on homologous recombination are also now being employed in *P. falciparum*. Zinc-finger nuclease (ZFN) technology is increasingly being used for high efficiency and high specificity genetic modifications (Carroll, 2011). This technology relies on the coupling of a zinc-finger DNA binding domain, specifically engineered to bind a DNA sequence of interest, with a DNA cleavage domain. Following recognition of target DNA sequences by the zinc finger domain, double strand breaks are created, which are repaired by the organisms endogenous DNA repair mechanisms. Typically, non-specific cleavage domains of restriction endonucleases such as FokI are used, which require dimerisation before performing DNA cleavage (Kim *et al.*, 1996). Therefore zinc-finger nucleases are designed to work in pairs, greatly increasing their specificity by ensuring cleavage only occurs when two heterologous subunits form the cleavage complex. Careful design of ZFNs ensures that cleavage complexes cannot be formed by two homologous subunits (Miller *et al.*, 2007). The double stranded break created by a cleavage complex can be repaired in one of two ways. The organism's endogenous DNA repair machinery might, in the absence of a homologous template to guide repair, rely on non-homologous end joining (Carroll, 2011). This process commonly results in mutation to the original sequence by introducing deletions or insertions resulting in frame shifts and in some cases effectual genetic ablation. This process of repair can therefore result in a gene knockout but this is not assured. However, by the exogenous provision of a sequence with regions homologous to the site of double stranded break, homologous recombination can be employed to repair the break. Design of the homologous sequence acting as a template for repair to contain a non-homologous region enables the insertion of a non-homologous sequence into the specific locus determined by zinc-finger design. This can be exploited to insert

regions containing premature stop codons or other elements that modify a gene of interest. While use of this process has yet to be published in *P. falciparum*, work is underway to establish a robust and highly specific mechanism for genetic ablation of target genes in *P. falciparum* (Personal communication with Prof. David Fidock). Their work suggests that a ZFN system can be employed to produce homogenous knockout populations of parasites within 2 weeks of transfection. This could certainly change the way that knockout experiments are performed in *P. falciparum* and it certainly has the possibility to be used to determine whether or not *Pfatg*8 is essential to intraerythrocytic *P. falciparum* parasites.

The transfection method used here involves electroporation of erythrocytes infected with ring stage parasites with a low voltage and high capacitance electric pulse (Crabb *et al.*, 2004). This method has been modified and improved since its first use and has been used extensively (Fidock and Wellems, 1997, Wu *et al.*, 1995). While it has proved reliable and efficient, an additional method relying on the spontaneous uptake of exogenous DNA by intraerythrocytic parasites has since been developed (Deitsch *et al.*, 2001). Preloading of erythrocytes with DNA for transfection has recently been shown to be 5-180 times more efficient than a method similar to that used here (Hasenkamp *et al.*, 2012). While transfection efficiency did not appear to be a limitation to generation of fusion protein expressing parasites, roughly 90 % success rate was observed, potentially a more efficient method could help improve upon the 40 % success rate observed for transfection with pCC-4-based constructs.

While significant advances have been made in our understanding of parasite biology since the first transient transfection reported in 1995 (Wu *et al.*, 1995), overcoming the obstacles to genetic manipulation of *P. falciparum* has proven difficult. However, a range of techniques can now be performed in *Plasmodium* and related parasites (Goldberg *et al.*, 2011). Steps towards automation of *P. falciparum* transfection and analysis are now being made (Caro *et al.*, 2012) and may well be coupled with high-throughput forward genetic approaches (Balu *et al.*, 2005, Fonager *et al.*, 2011). It seems possible that recent developments in our ability to genetically manipulate *P. falciparum* and other related parasites will mean that a new period of enlightenment in this, the post genomic era of research, is on the horizon.

5 Localisation and function of *Pf*ATG8

5.1 Introduction

Due to the association of ATG8 with autophagosomes from early in their formation through to degradation of cargo in the lytic compartment, introducing a tagged *atg*8 copy into model organisms has proven to be an invaluable tool in the study of autophagosomes and autophagy (Klionsky, 2011). In Chapter 3, antisera raised against recombinantly expressed His-*Pf*ATG8 were used to examine the expression of *Pf*ATG8 in wild type parasites. Transgenic parasite lines expressing mCherry-*Pf*ATG8 or mCherry-*Pf*ATG8ΔG were also generated which aided the analysis of the lipidation state of *Pf*ATG8. In order to build on these findings, the aim of work presented in this chapter was to examine the localisation of the endogenous *Pf*ATG8 protein and to use the transgenic lines as a tool to study *Pf*ATG8 localisation further. It was anticipated that *Pf*ATG8/mCherry-*Pf*ATG8 would localise to puncatate structures representing autophagosomes, similarly to what has been seen with ATG8 homologues in other organisms.

5.2 Results

5.2.1 Analysis of *Pf*ATG8 localisation in *P. falciparum* blood stage parasites

In order to determine the subcellular localisation of *Pf*ATG8 in the intraerythrocytic stages of *P. falciparum*, immunofluorescence assays (IFA) were performed using an Axioskop 2 mot plus microscope. *Pf*ATG8 was detected with antisera raised against His-*Pf*ATG8 purification B. Both 3D7 and D10 parasites were analysed although for the sake of brevity, only images collected of D10 parasites are shown (Figure 5.1). The localisation of *Pf*ATG8 was seen to be similar in both D10 and 3D7 *P. falciparum* lines, concentrating to defined areas within the parasite. *Pf*ATG8 appeared to localise to punctate structures along with larger, elongated structures, most prominent in the later stages of intraerythrocytic development. The localisation of *Pf*ATG8 to such structures supported the belief that similarly to mCherry-*Pf*ATG8, endogenous *Pf*ATG8 is also post-translationally modified and that this impacts on its localisation.

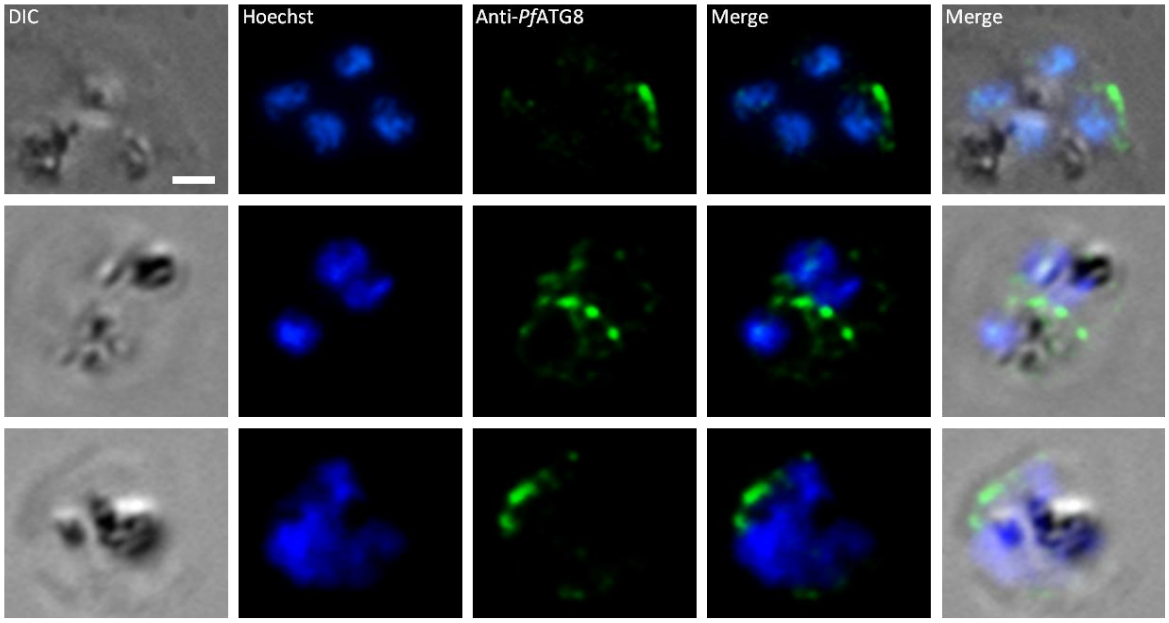

Figure 5.1: Analysis of *Pf*ATG8 localisation.

Wild type D10 *P. falciparum* were prepared for IFA with rabbit anti-*Pf*ATG8 antisera from His-*Pf*ATG8 purification B (1:1,000) and goat anti-rabbit Alexa Fluor 488-conjugated polyclonal antibodies (1:1,500). Representative images of trophozoites are shown. Scale bar = 2 µm.

5.2.2 Analysis of mCherry-*Pf*ATG8ΔG and mCherry-*Pf*ATG8 localisation

The analysis of mCherry-*Pf*ATG8 by western blotting had shown that the protein was post-translationally modified into a form reminiscent of lipidated protein. On the other hand, the truncated form of the fusion protein, mCherry-*Pf*ATG8ΔG, was detected as only a single form, corresponding with the unmodified full length protein. Extraction of parasite protein with lysis buffer containing 1 % Triton X-100 detergent had disrupted parasite membranes to the extent that both the unmodified and lipid-modified forms of mCherry-*Pf*ATG8 were observed in the 'soluble' fraction. To determine the location of fusion proteins in live parasites, parasites transfected with EP-mC-A8, EP-mC-A8ΔG, 86-mC-A8, EP-eY-A8, EP-eY-A8ΔG and 86-eY-A8 and 86-eY-A8ΔG were analysed by live cell fluorescence light microscopy. A clear difference in the localisation of full length fusion proteins (mCherry-*Pf*ATG8 and eYFP-*Pf*ATG8) and truncated fusion proteins (mCherry-*Pf*ATG8ΔG and eYFP-*Pf*ATG8ΔG) was observed. For clarity, images collected from parasites transfected with EP-mC-A8 or EP-mC-A8ΔG are presented here.

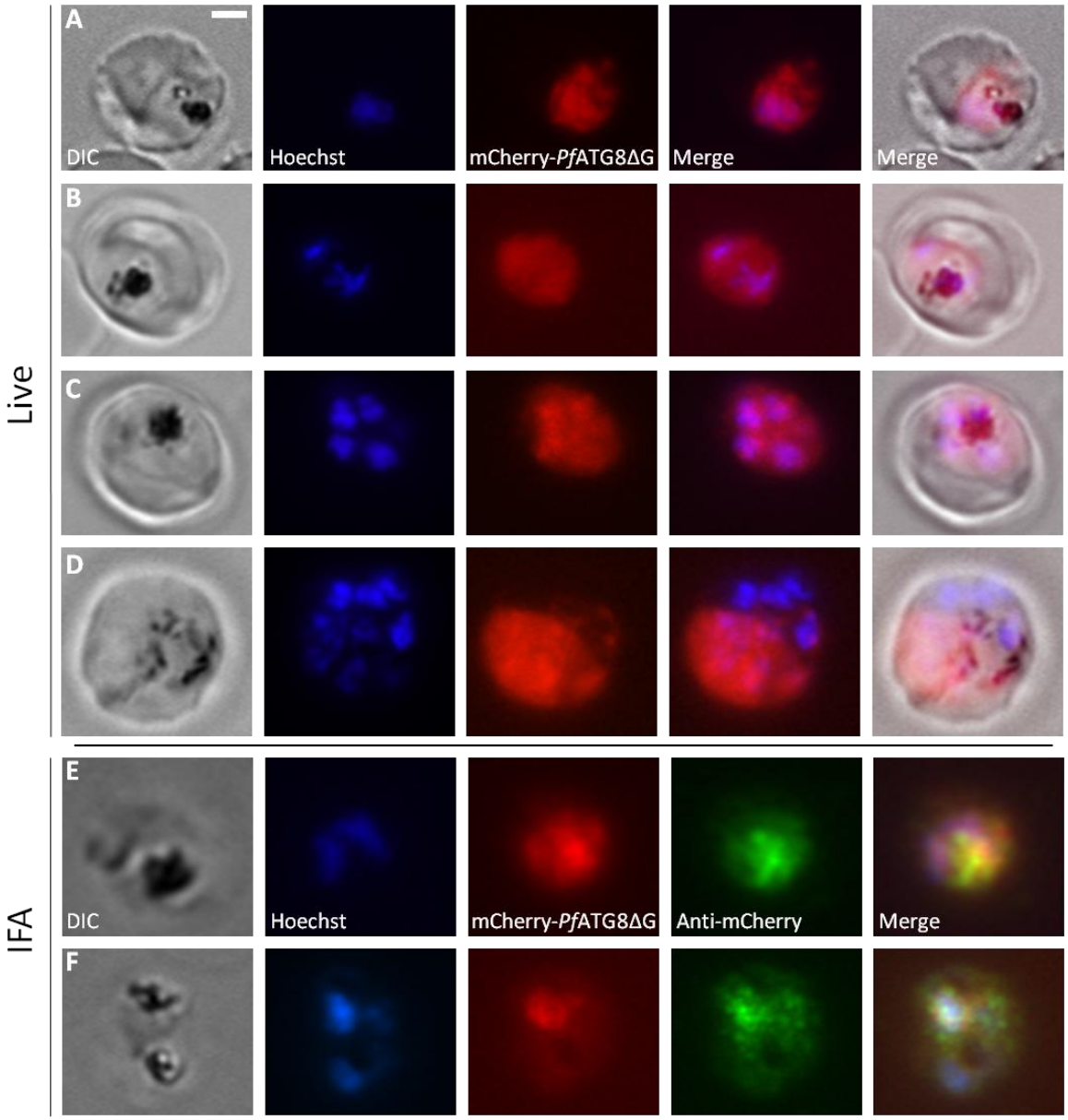

Figure 5.2: localisation of mCherry-*Pf*ATG8ΔG.

Parasites transfected with EP-mC-A8ΔG were analysed by live cell fluorescence light microscopy (A-D) and IFA with mouse anti-mCherry monoclonal (1:1,000) and goat anti-mouse Alexa Fluor 488-conjugated polyclonal antibodies (1:1,500) (E and F). Representative images of life cycle stages trophozoite (A, B, E and F), early schizont (C) and late schizont (D) are shown. Scale bar = 2 µm.

Parasites expressing mCherry-*Pf*ATG8ΔG and eYFP-*Pf*ATG8ΔG were analysed at different stages of intraerythrocytic development (mCherry-*Pf*ATG8ΔG shown in Figure 5.2). At all stages, in parasites in which a detectable amount of the fusion protein was expressed, mCherry-*Pf*ATG8ΔG and eYFP-*Pf*ATG8ΔG were found to be dispersed throughout the cytosol. As it appeared that the signal from mCherry fusion proteins was more easily detected than the signal from eYFP fusion proteins with less bleed through of signal from Hoechst 33258, further analysis was concentrated on parasites expressing mCherry-*Pf*ATG8ΔG. Parasites

expressing mCherry-*Pf*ATG8ΔG were prepared for IFA with anti-mCherry and anti-mouse Alexa Fluor 488-conjugated secondary antibodies. Antibody staining detected in the fluoresceine-isothiocyanate (FITC) channel was observed in the parasite cytosol and overlapped with the signal from mCherry fluorescence detected in the mChery channel. These findings supported and built upon the analysis of mCherry-*Pf*ATG8ΔG by western blotting by showing that without conversion of this protein into a lipidated form, a cytosolic localisation was characteristic.

In stark contrast to the localisation of the truncated fusion proteins, mCherry-*Pf*ATG8 and eYFP-*Pf*ATG8 were rarely observed to display a cytosolic dispersion. In the majority of parasites in which a detectable amount of the fusion protein was observed, both mCherry-*Pf*ATG8 and eYFP-*Pf*ATG8 were seen to localise to distinct subcellular structures with a characteristic pattern observed for each life cycle stage (mCherry-*Pf*ATG8 shown in Figure 5.3). Again, mCherry-*Pf*ATG8 was more easily detected than eYFP-*Pf*ATG8 with less bleed through of signal from Hoechst 33258. Further analysis was concentrated on parasites expressing mCherry-*Pf*ATG8.

Congruous with the expression profile of mCherry-*Pf*ATG8 as analysed by western blotting, in ring stage parasites, little mCherry-*Pf*ATG8 was detected. In parasites where a visible amount of the fusion protein was expressed, it appeared to be predominantly cytosolic but in some cells was also concentrated at a single focus. Not only did this support the observation that mCherry-*Pf*ATG8 was weakly expressed in ring stage parasites but also that only a low proportion of mCherry-*Pf*ATG8 was lipidated (1:1 ratio of non-lipidated to lipidated), again indicating that modification was responsible for localisation of the full length protein to subcellular structures. In trophozoite stage parasites, less cytosolic mCherry-*Pf*ATG8 was seen. Instead, it appeared that mCherry-*Pf*ATG8 labelled a tubular structure that varied in length and curvature between different cells of different ages. A longer structure was typically labelled in multi-nucleated trophozoites. In early schizont stages, mCherry-*Pf*ATG8 labelled longer, often more branched tubular structures. In late schizonts, mCherry-*Pf*ATG8 labelled elaborately branched tubular structures. This again supported the observations by western blot analysis that during the transition from ring to schizont stages, more mCherry-*Pf*ATG8 is converted to the lipidated form. In stages resembling

segmenter, where nuclear division appears complete, mCherry-*Pf*ATG8 was seen to label multiple small structures that appeared to be distributed into each forming daughter merozoite. The labelling of structures in these late stage parasites supported the observation of a high proportion of lipidated mCherry-*Pf*ATG8 in protein analysed by western blotting (1:2.7 ratio of non-lipidated to lipidated). Parasites expressing mCherry-*Pf*ATG8 were also prepared for IFA as detailed above. It was observed that anti-mCherry antibodies specifically detected the same structures labelled by mCherry-*Pf*ATG8.

Crucially, the appearance of the mCherry-*Pf*ATG8-labelled structures resembled those seen in IFA analysis of wild type parasites probed with rabbit anti-*Pf*ATG8 antisera and Alexa Fluor 488-conjugated secondary antibodies. This provided important evidence that the localisation of mChery-*Pf*ATG8 was representative of that of the endogenous protein. It was therefore deemed that mCherry-*Pf*ATG8 expressing parasites could be used as a substitute for wild type cells allowing much greater flexability in the analysis of *Pf*ATG8 localisation and function.

The increasing labelling of tubular structures by mCherry-*Pf*ATG8 during intraerythrocytic development, in combination with the increasing ratio of lipidated mCherry-*Pf*ATG8, as seen by western blot analysis, suggested that this localisation correlates with lipidation and therefore represents an association of mCherry-*Pf*ATG8 to a membrane-bound structure. Indeed, the fact that this structural localisation is entirely absent in parasites expressing the truncated mCherry-*Pf*ATG8ΔG, shows that the C-terminal glycine is essential for this localisation.

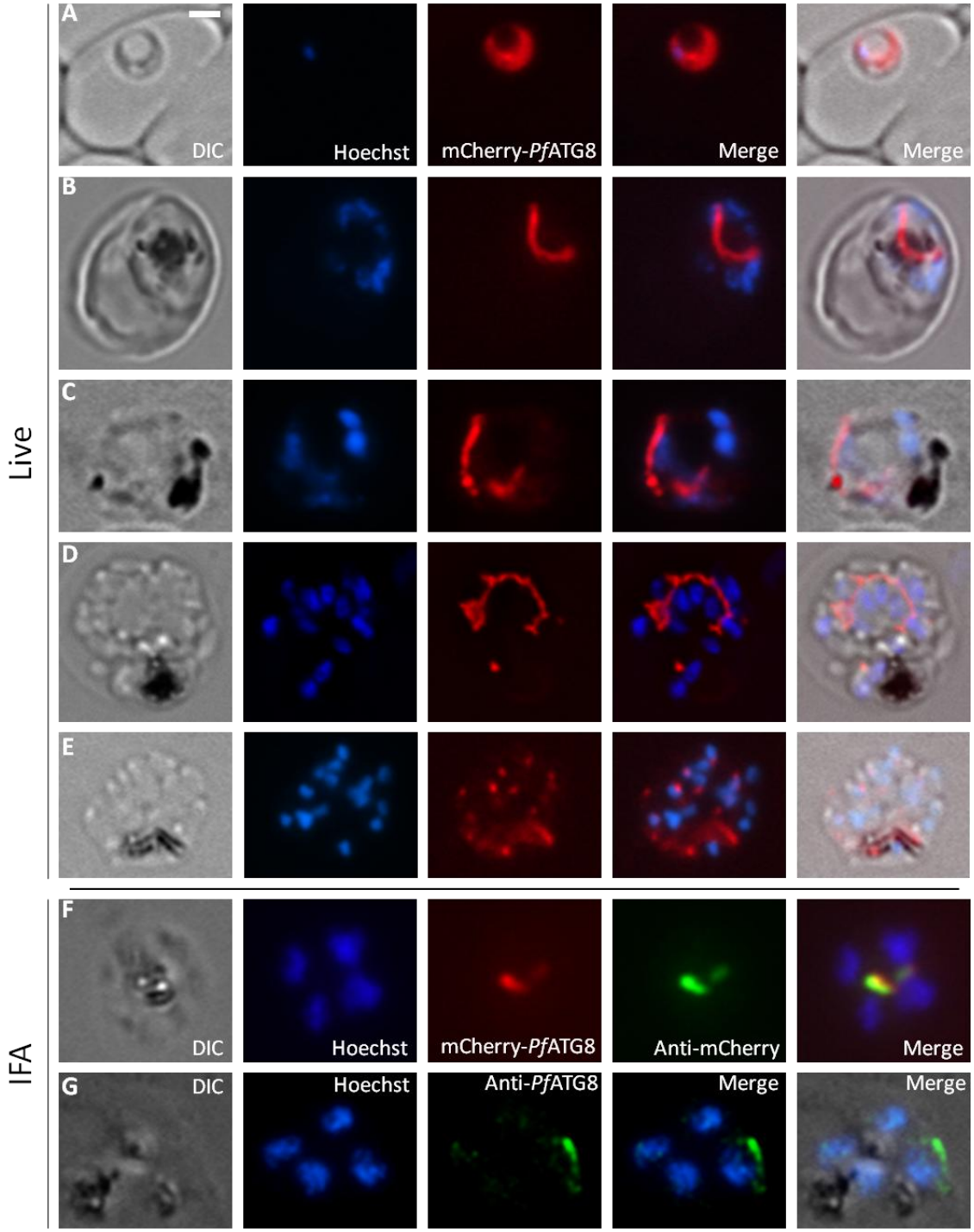

Figure 5.3: Localisation of mCherry-*Pf*ATG8.

Parasites transfected with EP-mC-A8 were analysed by live cell fluorescence light microscopy (A-E) and IFA with mouse anti-mCherry monoclonal (1:1,000) and goat anti-mouse Alexa Fluor 488-conjugated polyclonal antibodies (1:1,500) (F). Representative images of life cycle stages ring (A), trophozoite (B and F), early schizont (C), late schizont (D) and segmenter (E) are shown. A trophozoite parasite prepared for IFA with rabbit anti-*Pf*ATG8 antisera (1:1,000) and goat anti-rabbit Alexa Fluor 488-conjugated polyclonal antibodies (1:1,500) is shown for comparison (G). Scale bar = 2 µm.

Capturing images of merozoites proved difficult. They reinvade erythrocytes within seconds of rupture (Boyle *et al.*, 2010) and due to the mechanical pressure inflicted during live cell microscopy, it is difficult to ascertain whether

extracellular parasites are 'true' merozoites or the result of segmenter that that been ruptured prematurely. While others have shown that successful imaging of merozoites is possible (Angrisano *et al.*, 2012, Baum *et al.*, 2006), and various techniques have been successfully used to isolate and concentrate merozoites (Boyle *et al.*, 2010), these techniques were not performed as part of this study.

Of note is the observation that only a proportion of parasites were seen to express a visible amount of any of the fusion proteins and this proportion was seen to vary from ~ 45 % to as low as 15 % across all experiments performed. It was noted also, that when a cell line was in culture for an extended period of time, in excess of 4 weeks, the proportion of parasites expressing mCherry-*Pf*ATG8 reduced. For subsequent microscopy-based experiments, parasites in culture for no longer than 4 weeks following recovery from liquid nitrogen were used.

Along with the characteristic labelling of subcellular structures by mCherry-*Pf*ATG8, a small proportion of parasites with fluorescent signal in the digestive vacuole were also observed. The mCherry signal from this organelle was generally very low in relation to any signal from labelled structures. mCherry-*Pf*ATG8 degradation products were not observed in analysis by western blotting. The proportion of parasites exhibiting a vacuolar pattern also appeared to increase when parasites expressing mCherry-*Pf*ATG8 were at a low parasitaemia or imaged on sparsely loaded slides. These findings strongly suggested that the weak signal corresponding with the digestive vacuole in a small proportion of parasites represented an artefact, resultant from an over correction of auto-contrast. However, due to the possibility that mCherry fluorescence in the digestive vacuole was due to targeting of mCherry-*Pf*ATG8, these parasites were included in subsequent analysis.

In light of the array of localisation patterns of mCherry-*Pf*ATG8ΔG and mCherry-*Pf*ATG8 in parasites expressing these fusion proteins, and the varying proportion of parasites that show no visible levels of either protein, a robust scoring system was utilised in order to categorise each cell imaged (Figure 5.4).

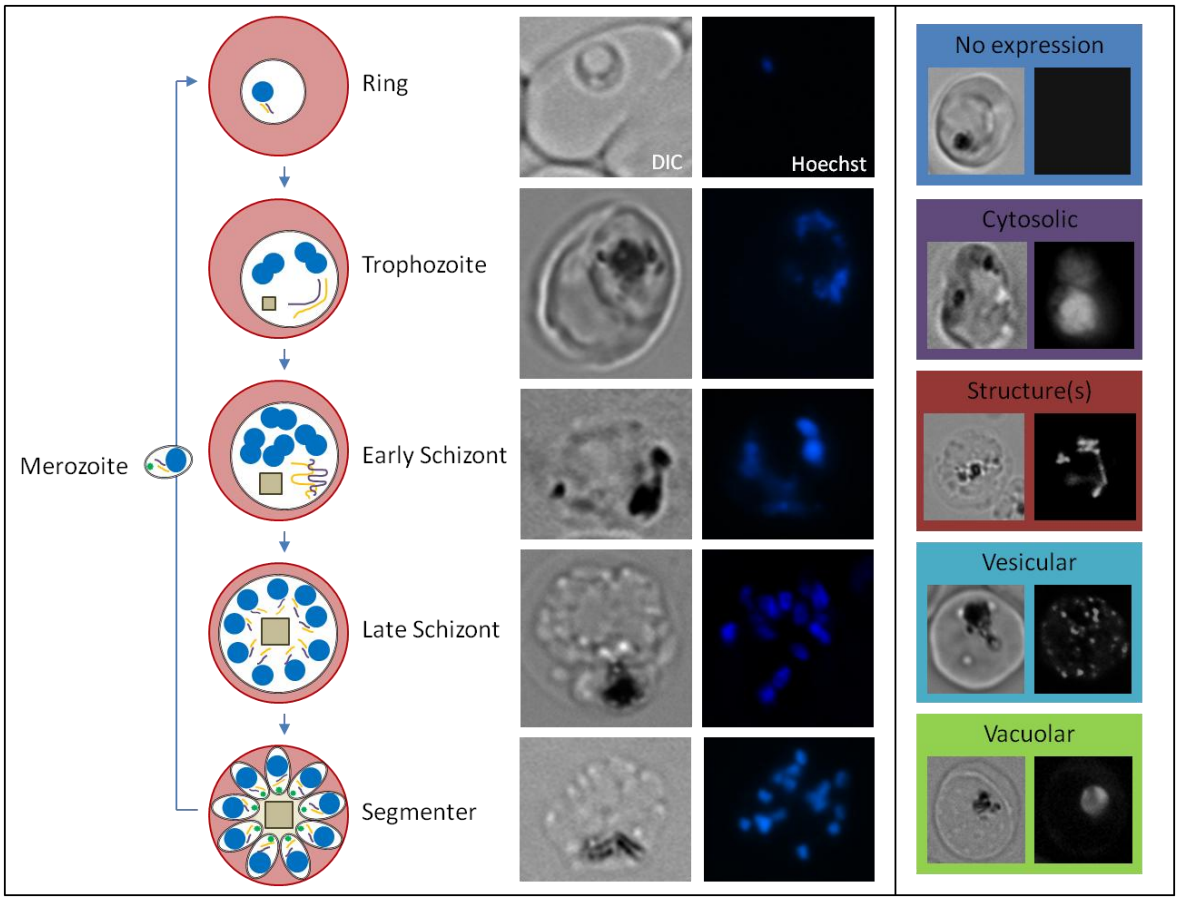

Figure 5.4: Classification of life cycle stage and scoring categories of mCherry-*Pf*ATG8 and mCherry-*Pf*ATG8ΔG expression.

(left) Intraerythrocytic parasites were classified as per their morphology under DIC illumination and the number and spatial distribution of nuclei.

(right) The distribution of fusion proteins in each parasite imaged was assigned to a scoring category in order to quantify any differences between parasite lines or following any treatment performed on parasite lines.

5.2.3 Effect of autophagy regulation on tagged-protein expression and localisation

The labelling of tubular structures by mCherry-*Pf*ATG8 was unexpected as it did not conform to the usual punctate labelling of autophagosomes by ATG8 in the cells of other organisms (Xie *et al.*, 2008). It was therefore necessary to determine whether these structures represented autophagosome-like structures or were in fact, structures unrelated to an autophagic process.

Labelling of tubular structures by GFP-*Lm*ATG8 has recently been reported in *Leishmania major* (Williams *et al.*, 2012). However, this fluorescence pattern is predicted to be a result of fusion between GFP-*Lm*ATG8-labelled punctate autophagosomes and the multi-vesicular tubular (MVT)-lysosome, similar to the

labelling of autophagolysosomes in mammalian cells (Dennemarker *et al.*, 2010). No punctate autophagosomes labelled by mCherry-*Pf*ATG8 were detected in parasites under normal growth conditions, suggesting that the labelling of these tubular structures was not the result of fusion between labelled punctate autophagosomes and a pre-existing lytic structure.

In the cells of many other organisms, even in the absence of conditions to trigger an autophagic response, a basal level of autophagy, characterised by punctate autophagosomes, is observed (Omatsu-Kanbe *et al.*, 2011). Basal autophagy is thought to be necessary for cell homeostasis by, among other roles, the removal of aberrantly folded proteins from the cytosol even under nutrient-rich conditions (Mizushima and Klionsky, 2007). Autophagy has also been strongly linked to cell aging (Vellai *et al.*, 2009), underlining its importance in cellular homeostasis and survival. By triggering autophagy through chemical or environmental manipulation, an increase in autophagosome formation and turnover can be analysed by ATG8 lipidation and localisation (Mizushima and Yoshimori, 2007). The apparent absence of mCherry-*Pf*ATG8-labelled punctate autophagosomes in parasites under normal culture conditions may indicate that a low (undetectable) level of basal autophagy is undertaken in these parasites. An array of compounds and environmental conditions are known to modulate the process of autophagy and the resultant localisation of ATG8 in other organisms. To help determine whether the structures labelled by mCherry-*Pf*ATG8 represented autophagic compartments, or to see if the localisation of mCherry-*Pf*ATG8 could be altered by triggering autophagy, experiments were performed in which manipulation of autophagy regulation was attempted.

5.2.3.1 Compound effectors of autophagy

In order to influence the regulation of a possible autophagic process in *P. falciparum* intraerythrocytic stages, the effect of the compounds wortmannin, rapamycin and bafilomycin A1 on parasite lines expressing mCherry-*Pf*ATG8 was analysed. These compound effectors of autophagy act on various stages of autophagosome formation and degradation and have apposing effects on ATG8 lipidation and localisation in other organisms, summarised in (Figure 5.5). For each drug treatment performed, changes in mCherry-*Pf*ATG8 expression and localisation analysed by live cell light microscopy would be used as a diagnostic

for any visible effect. Following treatment with wortmannin, the expression and lipidation of mCherry-*Pf*ATG8 was also analysed by western blotting of protein extracted from parasites following treatment. While the proportion of parasites exhibiting a visible expression of mCherry-*Pf*ATG8 was predicted to provide insight into mCherry-*Pf*ATG8 expression level, analysis by western blot was intended to supplement this analysis. As it has been shown in yeast that *Sc*ATG8 expression increases upon induction of autophagy this was intended to provide an indication that treatments intended to trigger autophagy were valid (Kirisako *et al.*, 1999).

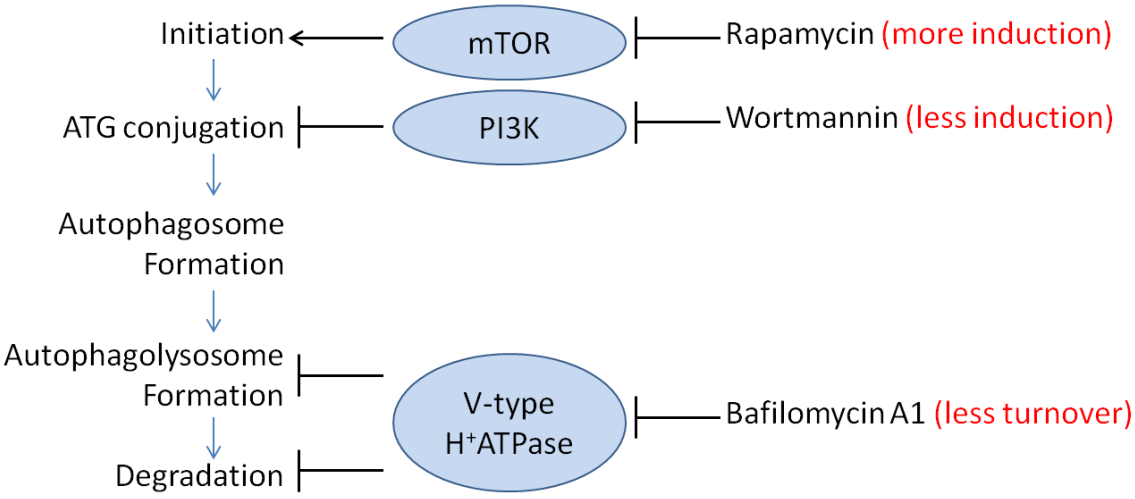

Figure 5.5: Compound modulators of autophagy.

Rapamycin inhibits TOR kinase, which in turn promotes the initiation of autophagy. Wortmannin inhibits PI3K, which in turn reduces the allocation of membrane to autophagosome generation. Bafilomycin A1 inhibits V-type H+ATPase, which in turn prevents both the fusion of autophagosomes with the lytic compartment and also lytic degradation of autophagolysosome contents.

Wortmannin is used as a potent, specific and irreversible inhibitor of phosphatidylinositol 3-kinase (PI3K) and has been used to study autophagy in a number of organisms (Ponpuak *et al.*, 2009). Through its inhibition of class III PI3K, which phosphorylates phosphatidylinositol, it prevents generation of phosphatidylinositol 3-phosphate (PI3P) on pre-autophagosome membranes. This, in turn, prevents the recruitment of ATGs to these autophagosome nucleation sites, resulting in an overall reduction in autophagosome formation and therefore turnover of intended cargo (Blommaart *et al.*, 1997). Wortmannin is however, known to have a number of off-target effects through interaction with protein kinases such as myosin light chain kinase (MLCK) (Nakanishi *et al.*, 1992) and mitogen-activated protein kinase (MAPK) (Ferby *et al.*, 1996)

dependent on treatment conditions, as well as a counter effect on autophagy regulation through inhibition of class I PI3K (Wu *et al.*, 2010).

A class III PI3K has been characterised in *P. falciparum* (Vaid *et al.*, 2010). Wortmannin has been used as a PI3K inhibitor in *P. falciparum* intraerythrocytic stages but evidence of its potency varies (Tawk *et al.*, 2010, Vaid *et al.*, 2010). Tawk and co-workers reported that wortmannin is unstable in culture medium (Yuan *et al.*, 2007). They showed that a single dose of 25 μM is not sufficient to cause a growth defect over 48 h. However, they did show that treatment of parasites enriched for late stages via Plasmion treatment (Lelievre *et al.*, 2005) with 100 nM wortmannin for 1.5 h was sufficient to cause a 58 % reduction in PI3P levels. Vaid and co-workers reported that as little as 3 μM wortmannin causes a 50 % growth inhibition over 144 h (6 days) with cultures being fed with wortmannin-dosed medium daily. They also showed that under shorter incubations the specific effects of wortmannin on PI3K can be seen. Incubation of late stage parasites with 10 μM wortmannin for ~ 5 h resulted in a 4 fold accumulation of haemoglobin in parasites. They showed along with other data that this results from an inhibition of endocytosis. Together these data suggest that wortmannin inhibits endocytosis in late stage parasites via the downregulation of PI3P synthesis by PI3K.

In light of the absence of a clear IC_{50} value for wortmannin, to determine an appropriate treatment for the parasite lines used in this study an IC_{50} experiment was performed with the D10 parental line of mCherry-*Pf*ATG8 and mCherry-*Pf*ATG8ΔG expressing parasites (Figure 5.6). An IC_{50} of 73.0 ± 14.6 μM (S.E.M.) over 72 h was considerably higher than that reported by Vaid and co-workers and that for other organisms (2-4 nM in mammalian cells (Powis *et al.*, 1994)). In consideration of the reported poor stability of this compound in culture medium, an IC_{50} experiment was also performed where drug-dosed medium was replaced each day. The resultant IC_{50} of 46.3 ± 22.4 μM (S.E.M.) was not statistically different to the first IC_{50} (unpaired t-test, P = 0.378), indicating that the stability of wortmannin in culture medium was not responsible for its lack of potency.

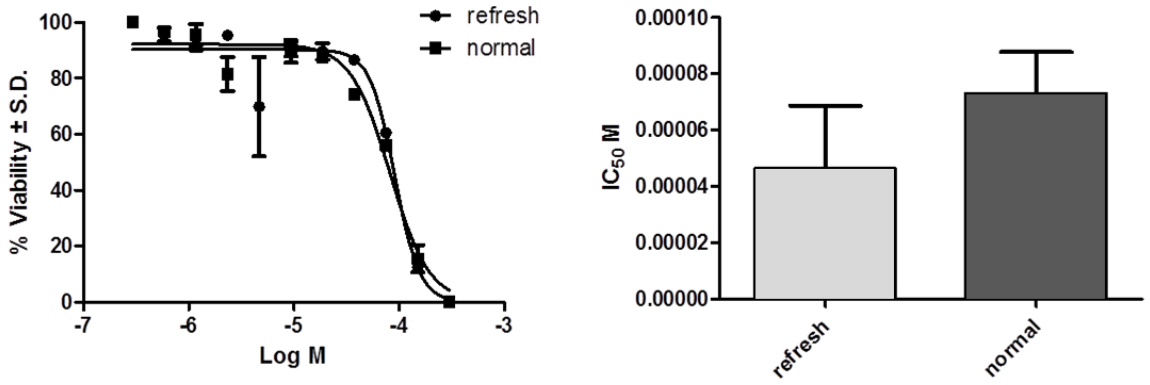

	Refresh	Normal
Bottom	0	0
Top	90.28	92.18
LogEC50	-4.014	-4.086
HillSlope	-3.667	-2.336
EC50	9.10E-05	8.20E-05

Unpaired t test	
P value	0.3738
Summary	n.s.
(P<0.5)?	no
One-/two-tailed P value	two-tailed
t, df	t=1.000, df=4

Figure 5.6: Determination of the IC_{50} value of wortmannin over 72 h.

(left) D10 parasites were treated with a serial dilution of wortmannin either once at the beginning of a 72 h experiment (normal), or daily (refresh). Parasite growth was measured after 48 h by analysing [^{3}H]-labelled hypoxanthine incorporation. Treatments were performed 3 times with 2 sets of technical replicates each time. A representative parasite viability curve is shown for an individual experiment. The IC_{50} for normal wortmannin treatment was 73.0 ± 14.6 µM (S.E.M.). The IC_{50} for wortmannin refreshed daily was 46.3 ± 22.4 µM (S.E.M.).

(right) The IC_{50} of wortmannin over 72 h was compared between a single dose (normal) and repeated dose (refresh). No significant difference was determined by unpaired t test (P = 0.3738).

A second PI3K inhibitor was also used by both Vaid and Tawk. LY294002 is structurally different from wortmannin, acting reversibly and less potently but it has been reported to be more stable in culture medium than wortmannin (Tawk et al., 2010). An IC_{50} experiment with a single dose of LY294002 was performed over 72 h with the D10 parental line of mCherry-*Pf*ATG8 expressing parasites. An IC_{50} of 42 ± 6.9 µM (S.E.M.) was approximately double than that reported by Tawk and Vaid. Due to the multitude of off target effects reported for this compound (Gharbi *et al.*, 2007), treatment of parasites with wortmannin was pursued as this appears to be the more commonly used compound.

Treatment with 10 µM wortmannin for 6 h was used to analyse the effect of PI3K inhibition on the expression, lipidation and localisation of mCherry-*Pf*ATG8. Asynchronous parasites expressing mCherry-*Pf*ATG8 were incubated under normal conditions i.e. at 37 °C under reduced oxygen, with culture medium dosed with 10 µM wortmannin or an equivalent volume of DMSO as a control on 3

separate occasions. Analysis of mCherry-*Pf*ATG8 by western blotting revealed no difference in either the ratio of non-lipidated to lipidated mCherry-*Pf*ATG8 (1:2.9 Control, 1:2.8 Wortmannin) or the overall expression of both forms between treated and control samples (Figure 5.7). The localisation of mCherry-*Pf*ATG8 was also assessed by preparing treated and untreated cells for live cell fluorescence light microscopy. There was no difference in either the proportion of parasites expressing a visible amount of mCherry-*Pf*ATG8 (~ 20 %) or the distribution of parasites into each scoring category. From these data it was concluded that under these conditions wortmannin has no effect on mCherry-*Pf*ATG8 expression, localisation and lipidation.

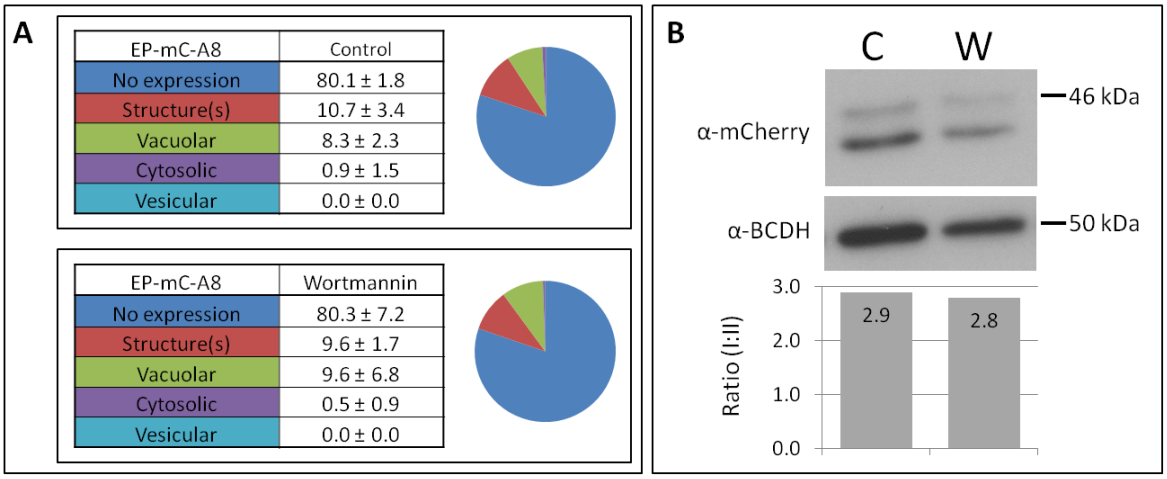

Figure 5.7: Effect of wortmannin on mCherry*Pf*ATG8 expression, localisation and lipidation.

Asynchronous parasites transfected with EP-mC-A8 were treated with 10 µM wortmannin or DMSO (Control) for 6 h under normal culture conditions. (A) Wortmannin and Control parasites were analysed by live cell fluorescent light microscopy. Treatments were performed three times with 375 (Wortmannin) and 323 (Control) cells being counted. Numbers indicate percentage of cells counted and scored into each category ± S.D. (B) 20 µg protein extracted from Wortmannin and Control parasites was separated by 7.5% SDS-PAGE and mCherry-*Pf*ATG8 was detected by western blotting with mouse anti-mCherry monoclonal (1:1,000) and rat anti-mouse HRP-conjugated polyclonal antibodies (1:10,000). The western blot was stripped and reprobed with rabbit anti-BCDH antisera (1:1,000) as a loading control. The relative intensities of upper and lower anti-mCherry reactive bands in each lane were calculated densitometrically using ImageJ, normalised to loading controls and are presented graphically. Numbers indicate the ratio of non-lipidated mCherry-*Pf*ATG8 (upper band) to lipidated mCherry-*Pf*ATG8 (lower band).

The use of wortmannin had been predicted to down regulate a potential autophagic process in intraerythrocytic parasites. If the labelling of structures with mCherry-*Pf*ATG8 in these parasites was the result of an autophagic process then it might have been presumed that such labelling would be decreased in the presence of wortmannin. In the absence of any effect of wortmannin on the expression, lipidation or localisation of mCherry-*Pf*ATG8, it was concluded that

the labelling of structures by mCherry-*Pf*ATG8 was not dependent on PI3K activity. Next, in order to determine if the localisation of mCherry-*Pf*ATG8 could be affected by triggering autophagy, parasites were treated with the compounds rapamycin and bafilomycin A1.

Rapamycin inhibits the Target of Rapamycin (TOR), a serine/threonine protein kinase. TOR (mTOR in humans and other mammals) forms complexes with a number of regulatory and effector proteins and acts as a point of convergence of a number of signalling pathways (Weichhart, 2012). In relevance to autophagy, mTOR has been shown to restrict the initiation of autophagy via, in part, its interaction with the ATG1 complex. Rapamycin, via interaction with FKBP12 inhibits mTOR and hence promotes initiation of autophagy, characterised by an increase in autophagosome formation (Chang *et al.*, 2009). While a gene predicted to encode a homologue of TOR has yet to be identified in *P. falciparum*, rapamycin has been found to have an IC_{50} of 2.6 μM over 48 h (Bell *et al.*, 1994).

Treatment with 4.5 μM rapamycin for 6 h was used to analyse the effect of rapamycin treatment on mCherry-*Pf*ATG8 localisation. Asynchronous parasites expressing mCherry-*Pf*ATG8 were incubated under normal conditions with culture medium dosed with 4.5 μM or an equivalent volume of DMSO as a control. The localisation of mCherry-*Pf*ATG8 was then assessed in treated or untreated parasites by live cell fluorescence light microscopy (Figure 5.8). There was no difference between treated or untreated parasites in either the proportion of parasites expressing a visible amount of mCherry-*Pf*ATG8 (~ 38 %) or the distribution of parasites into each scoring category. While analysis by microscopy was only performed once, a large number of parasites were imaged, resulting in a substantial data set. From this data it was concluded that under these conditions rapamycin has no effect on mCherry-*Pf*ATG8 localisation.

EP-mC-A8	Control
No expression	61.7
Structure(s)	21.7
Vacuolar	12.7
Cytosolic	4
Vesicular	0

EP-mC-A8	Rapamycin
No expression	64.3
Structure(s)	21
Vacuolar	8
Cytosolic	6.7
Vesicular	0

Figure 5.8: Effect of rapamycin on mCherry-*Pf*ATG8 expression and localisation.

Asynchronous parasites transfected with EP-mC-A8 were treated with 4.5 µM rapamycin or DMSO (Control) for 6 h under normal culture conditions and analysed by live cell fluorescence light microscopy. Treatments were performed once with 300 (Rapamycin) and 300 (Control) cells being counted. Numbers indicate percentage of cells counted and scored into each category.

Bafilomycin A1 is a reversible inhibitor of vacuolar (V)-type H+ATPase. Unlike wortmannin and rapamycin, bafilomycin A1 acts to regulate, not the initiation stages of autophagy but the later stages of autophagosome flux. Its inhibitory effect on autophagosome turnover is attributed to both reducing the proteolytic environment within endolysosomal compartments that rely on V-type H^+ATPase for acidification (particularly in short term treatments) and causing a block in the fusion of autophagosomes with these endolysosomal compartments (Klionsky *et al.*, 2008, Yamamoto *et al.*, 1998). Typically, an accumulation of ATG8-positive autophagosomes is observed in cells treated with bafilomycin A1. A V-type H^+ATPase pump has been identified in *P. falciparum* (Marchesini *et al.*, 2005) and bafilomycin A1 has been shown to have antimalarial properties, with an IC_{50} of 19.8 nM over 48 h (van Schalkwyk *et al.*, 2010).

Treatment with 100 nM bafilomycin A1 for 0.5 h was used to analyse the effect of V-type H^+ATPase inhibition on mCherry-*Pf*ATG8 localisation. Parasites expressing mCherry-*Pf*ATG8 were synchronised to ring stages by a single incubation in 5 % sorbitol. Approximately 16 h later, when cultures contained primarily trophozoite stages, parasites were incubated under normal conditions with culture medium dosed with 100 nM bafilomycin A1 or an equivalent volume of DMSO and the localisation of mCherry-*Pf*ATG8 was assessed by fluorescence light microscopy (Figure 5.9). There was no difference in either the proportion of parasites expressing a visible amount of mCherry-*Pf*ATG8 (~ 30 %) or the distribution of parasites into each scoring category. Again, while this analysis was only performed once, a strong data set was generated from which it was concluded that under these conditions bafilomycin A1 had no effect on mCherry-*Pf*ATG8 localisation.

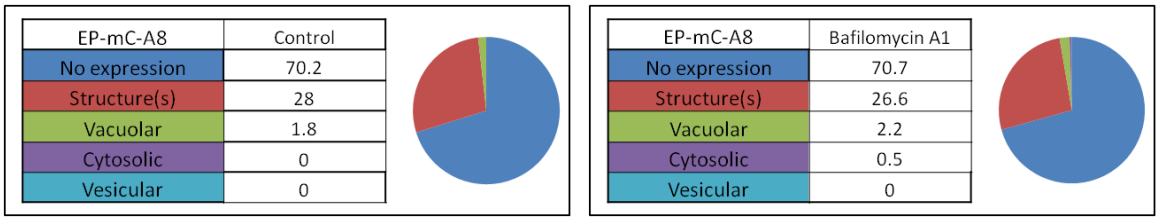

EP-mC-A8	Control
No expression	70.2
Structure(s)	28
Vacuolar	1.8
Cytosolic	0
Vesicular	0

EP-mC-A8	Bafilomycin A1
No expression	70.7
Structure(s)	26.6
Vacuolar	2.2
Cytosolic	0.5
Vesicular	0

Figure 5.9: Effect of bafilomycin A1 on mCherry-*Pf*ATG8 expression and localisation.

Late stage parasites transfected with EP-mC-A8 were treated with 100 nM bafilomycin A1 or DMSO (Control) for 0.5 h under normal culture conditions and analysed by live cell fluorescent light microscopy. Treatments were performed once with 410 (Bafilomycin A1) and 497 (Control) cells being counted. Numbers indicate percentage of cells counted and scored into each category.

Taken together, these experiments suggest that compounds known to regulate the process of autophagy and therefore the localisation of ATG8 in other organisms have no effect on mCherry-*Pf*ATG8 expression, lipidation or localisation in intraerythrocytic stages of *P. falciparum*.

Treatment with wortmannin had not caused a decrease in the labelling of sub-cellular structures by mCherry-*Pf*ATG8, suggesting that this process is not dependent on the activity of PI3K. Treatment with rapamycin or bafilomycin A1 had not caused an effect in the labelling of structures and had not resulted in the detection of canonical punctate autophagosomes by promoting their formation or preventing their degradation. These experiments had shown that the regulation of the process responsible for the labelling of subcellular structures by mCherry-*Pf*ATG8 appeared to be distinct from the expected autophagic regulation mechanisms. The primary indication of autophagy remains a response to nutrient starvation. While compound modulators of autophagy regulators have been used to manipulate ATG8 lipidation and localisation in other organisms, it is possible that divergency in the regulation mechanisms in *P. falciparum*, preclude the use of the same compounds used in other organisms. In order to determine whether mCherry-*Pf*ATG8 expression, lipidation and localisation are affected by nutrient starvation, experiments were performed which starved parasites of either amino acids, or both amino acids and glucose, bypassing the need to elucidate the downstream signalling and regulation pathways of these effects.

5.2.3.2 Environmental triggers of autophagy

As the primary environmental trigger for autophagy has long been regarded as amino acid starvation, experiments to explore the regulation of autophagy are often based on either limiting availability of amino acids or inhibiting their acquisition (Munafo and Colombo, 2001). To analyse the influence of amino acid starvation on mCherry-*Pf*ATG8 expression and localisation, parasites expressing mCherry-*Pf*ATG8 were subjected to an amino acid-limitation procedure. Parasites expressing mCherry-*Pf*ATG8 were synchronised to ring stages by a single incubation in 5 % sorbitol and returned to normal culture conditions. Around 16 h later, when cultures contained primarily trophozoite stages, parasites were transferred to amino acid-limited medium and cultured at 37 °C for 6 h. This culture medium is devoid of all amino acids with the exception of isoleucine, cysteine, methionine, glutamine and glutamic acid. Parasites were then dosed with 28 μM E64 or an equivalent volume of ethanol for a further 2 h. By limiting the availability of exogenous amino acids, this experiment was intended to force parasites to rely solely on amino acid acquisition from haemoglobin degradation and then block the degradation of haemoglobin by inhibiting cysteine peptidases with E64 (Liu *et al.*, 2006, Vaid *et al.*, 2010). mCherry-*Pf*ATG8 expression and lipidation state was analysed by western blotting (Figure 5.10). Little difference in either the ratio of non-lipidated to lipidated forms of mCherry-*Pf*ATG8 (1:3.3 Control, 1:2.6 E64) or the overall expression of both forms was seen between protein extracted from E64 treated or control parasites. The localisation of mCherry-*Pf*ATG8 was analysed by fluorescence light microscopy following E64 or control treatment (Figure 5.10). In an attempt to improve the efficiency of microscopic analysis, magnetic enrichment was performed to increase parasitaemia before imaging. No difference in either the proportion of parasites expressing a visible amount of mCherry-*Pf*ATG8 (~ 45 %) or the distribution of parasites into each scoring category was observed between E64 treated or control parasites. These data suggested that limiting the availability and acquisition of amino acids had no effect on mCherry-*Pf*ATG8 expression, lipidation and localisation.

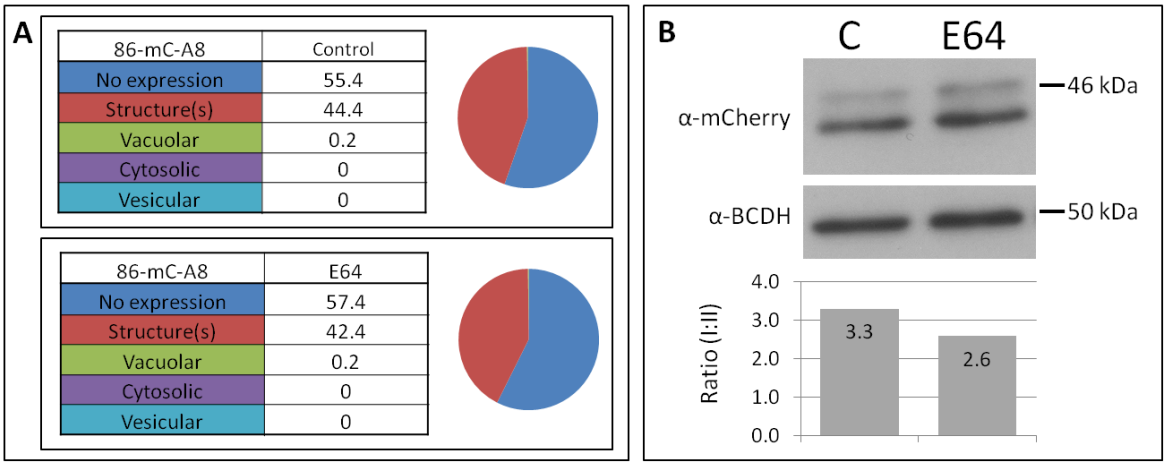

Figure 5.10: Effect of amino acid limitation and E64 treatment on mCherry-*Pf*ATG8 expression, localisation and lipidation.

Late stage parasites transfected with 86-mC-A8 were incubated in limited medium for 6 h under normal culture conditions before addition of 28 µM E64 or DMSO (Control) for a further 2 h incubation. (A) E64 and Control parasites were enriched by magnetic isolation and analysed by live cell fluorescent light microscopy. Treatments were performed once with 554 (E64) and 522 (Control) cells being counted. Numbers indicate percentage of cells counted and scored into each category. (B) 20 µg protein isolated from E64 and Control parasites was separated by 7.5 % SDS-PAGE and mCherry-*Pf*ATG8 was detected by western blotting with mouse anti-mCherry monoclonal (1:1,000) and rat anti-mouse HRP-conjugated polyclonal antibodies (1:10,000). The western blot was stripped and reprobed with rabbit anti-BCDH antisera (1:1,000) as a loading control. The relative intensities of upper and lower anti-mCherry reactive bands in each lane were calculated densitometrically using ImageJ, normalised to loading controls and are presented graphically. Numbers indicate the ratio of non-lipidated mCherry-*Pf*ATG8 (upper band) to lipidated mCherry-*Pf*ATG8 (lower band).

In order to test whether inhibition of aspartyl peptidases had an effect on mCherry-*Pf*ATG8 localisation in parasites adjusted to growth in amino acid-limited medium, the same experiment was repeated but with a 2 h incubation in 75 µM pepstatin A or DMSO as a control, rather than E64. Following magnetic enrichment, the localisation of mCherry-*Pf*ATG8 was analysed by live cell fluorescent light microscopy (Figure 5.11). Again, no difference in either the proportion of parasites expressing a visible amount of mCherry-*Pf*ATG8 (~ 20 %) or the distribution of parasites into each scoring category was observed between treated or control parasites. It should be noted that E64 and ethanol control treated parasites were those transfected with 86-mC-A8 rather than EP-mC-A8. This could account for the higher proportion of parasites exhibiting a visible level of mCherry-*Pf*ATG8 expression than that typical of parasites transfected with EP-mC-A8, as demonstrated by the relative expression profiles of each line shown in Figure 3.14. From these experiments it was concluded that amino acid starvation has no effect on mCherry-*Pf*ATG8 expression, lipidation or localisation.

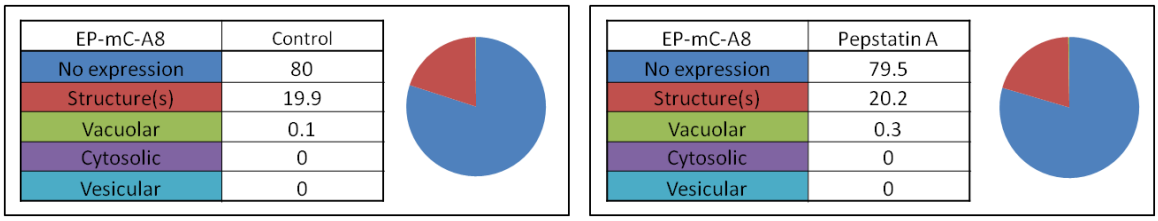

EP-mC-A8	Control
No expression	80
Structure(s)	19.9
Vacuolar	0.1
Cytosolic	0
Vesicular	0

EP-mC-A8	Pepstatin A
No expression	79.5
Structure(s)	20.2
Vacuolar	0.3
Cytosolic	0
Vesicular	0

Figure 5.11: Effect of amino acid limitation and pepstatin A treatment on mCherry-*Pf*ATG8 expression, localisation and lipidation.

Late stage parasites transfected with EP-mC-A8 were incubated in limited medium for 6 h under normal culture conditions before addition of 75 µM Pepstatin A or DMSO (Control) for a further 2 h incubation. Pepstatin A and Control parasites were enriched by magnetic isolation and analysed by live cell fluorescent light microscopy. Treatments were performed once with 396 (Pepstatin A), 679 (Pepstatin A control) cells being counted. Numbers indicate percentage of cells counted and scored into each category.

In order to analyse the effect of glucose starvation on mCherry-*Pf*ATG8 expression and localisation, parasites expressing mCherry-*Pf*ATG8 were synchronised to ring stages by a single incubation in 5 % sorbitol. Approximately 16 h later, while the culture contained primarily trophozoite stages, parasites were incubated at 37 °C under reduced oxygen, not in culture medium but in Earle's Balanced Salt Solution (EBSS) either supplemented with 11 mM glucose as a control (EBSS+G) or without glucose for 0.5 h. Parasite protein extracted from glucose starved and control parasites was analysed by western blotting (Figure 5.12). The ratio of non-lipidated to lipidated forms of mCherry-*Pf*ATG8 appeared to be unaffected by the removal of an extracellular source of glucose (1:2.1 Control, 1:2.3 EBSS) as was the overall expression level. Analysis of mCherry-*Pf*ATG8 localisation by fluorescence light microscopy following magnetic enrichment revealed no difference in either the proportion of parasites expressing a visible amount of mCherry-*Pf*ATG8 (~ 35 %) or the distribution of parasites into each scoring category. These data showed that removal of all amino acids and glucose from culture medium for 30 min did not cause an effect on mCherry-*Pf*ATG8 expression, lipidation or localisation.

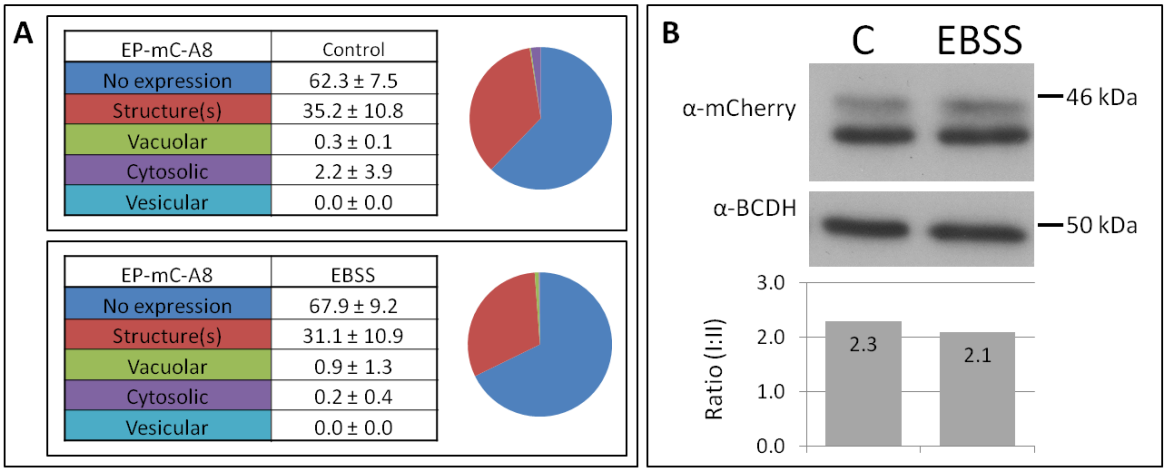

Figure 5.12: Effect of glucose starvation on mCherry-*Pf*ATG8 expression, localisation and lipidation.

Late stage parasites transfected with EP-mC-A8 were incubated in EBSS or EBSS supplemented with 11 µM glucose (Control) for 0.5 h under normal culture conditions. (A) EBSS and Control parasites were enriched by magnetic isolation and analysed by live cell fluorescent light microscopy. Treatments were performed three times with 1578 (EBSS), 1258 (Control) cells being counted. Numbers indicate percentage of cells counted and scored into each category ± S.D. (B) 20 µg protein isolated from EBSS and Control parasites was separated by 7.5 % SDS-PAGE and mCherry-*Pf*ATG8 was detected by western blotting with mouse anti-mCherry monoclonal (1:1,000) and rat anti-mouse HRP-conjugated polyclonal antibodies (1:10,000). The western blot was stripped and reprobed with rabbit anti-BCDH antisera (1:1,000) as a loading control. The relative intensities of upper and lower anti-mCherry reactive bands in each lane were calculated densitometrically using ImageJ, normalised to loading controls and are presented graphically. Numbers indicate the ratio of non-lipidated mCherry-*Pf*ATG8 (upper band) to lipidated mCherry-*Pf*ATG8 (lower band).

Parasites expressing mCherry-*Pf*ATG8ΔG were subjected to the same treatment and analysed by fluorescence light microscopy. Removal of glucose and all amino acids did not alter the proportion of parasites expressing a visible amount of mCherry-*Pf*ATG8ΔG (~ 15 %) or the distribution of parasites into each scoring category, with a cytosolic dispersion remaining the characteristic pattern (Figure 5.13). This showed that starvation of glucose did not induce a translocalisation of cytosolic mCherry-*Pf*ATG8ΔG to subcellular structures and supported the notion that in the absence of its C-terminal glycine residue, mCherry-*Pf*ATG8ΔG can not participate in the same process as full length mCherry-*Pf*ATG8.

EP-mC-A8ΔG	Control
No expression	86.5 ± 3.7
Structure(s)	0.0 ± 0.0
Vacuolar	0.2 ± 0.3
Cytosolic	12.8 ± 2.5
Vesicular	0.0 ± 0.0

EP-mC-A8ΔG	EBSS
No expression	85.0 ± 4.4
Structure(s)	0.1 ± 0.1
Vacuolar	0.1 ± 0.1
Cytosolic	14.9 ± 4.3
Vesicular	0.0 ± 0.0

Figure 5.13: Effect of glucose starvation on mCherry-*Pf*ATG8ΔG expression and localisation.

Late stage parasites transfected with EP-mC-A8ΔG were incubated in EBSS or EBSS supplemented with 11 μM glucose (Control) for 0.5 h under normal culture conditions. EBSS and Control parasites were enriched by magnetic isolation and analysed by live cell fluorescent light microscopy. Treatments were performed three times with 1662 (EBSS) and 4009 (Control) cells being counted. Numbers indicate percentage of cells counted and scored into each category ± S.D.

Together, these sets of experiments were designed to induce and manipulate the regulation of autophagy, in order to determine whether mCherry-*Pf*ATG8 was involved in an autophagic process. Data collected suggested that mCherry-*Pf*ATG8 was not involved in such a process. Under no conditions were canonical ATG8-positive punctate autophagosomes observed. This suggested that the subcellular structures labelled by mCherry-*Pf*ATG8 may well have been a novel autophagic structure. However, under no treatment conditions was the labelling of this structure by mCherry-*Pf*ATG8 seen to alter. This suggested that the labelling of this structure did not represent an autophagic process. As the labelling of this subcellular structure by mCherry-*Pf*ATG8 did not appear to represent the hallmarks of autophagy, it remained to be determined what the structure represented and why it was labelled by mCherry-*Pf*ATG8.

5.2.4 Characterisation of mCherry-*Pf*ATG8-labelled structures

The combination of an unusual localisation of mCherry-*Pf*ATG8 and the fact that commonly used compound and environmental modulators of autophagy appeared to have no effect on the expression or localisation of mCherry-*Pf*ATG8, suggested that this protein was not involved in an autophagic process. However, mCherry-*Pf*ATG8 was seen to label a subcellular structure, which exhibited a changing appearance in different stages of intraerythrocytic development. Labelling of this structure was entirely dependent on the C-terminal glycine of *Pf*ATG8, suggesting that this labelling correlates with its specific lipidation. In order to further characterise and place these structures in context of subcellular organisation, colocalisation studies were performed with co-expressed organelle markers, vital stains and antibodies in immunofluorescence assays.

5.2.4.1 Analysis of mCherry-*Pf*ATG8-labelled structures in relation to acidic compartments

Autophagosomes must become acidified before their contents can be degraded and recycled (Nakamura *et al.*, 1997). Acidification of autophagosomes occurs primarily via fusion with late endosomes, forming amphisomes or fusion with the lytic compartment, forming autophagolysosomes (Shintani and Klionsky, 2004). The precise chronology of these fusion steps is difficult to pin-point due to the tight integration of the endosomal and lysosomal systems and therefore these steps are often referred to as endolysosomal fusion (Hundeshagen *et al.*, 2011). Following these fusion events hydrolytic enzymes within the lytic compartment can degrade autophagosome contents. The contents of autophagosomes can also be degraded following acquisition of proton pumps and hydrolytic enzymes directly from the trans-Golgi network (Rajawat *et al.*, 2010).

Plasmodium spp. possess a large digestive vacuole, the site of haemoglobin degradation, but appear to lack canonical lysosomes. Therefore the likely endolysosomal target of autophagosomes, should a canonical autophagy process exist, would be the digestive vacuole. It also can not be discounted that autophagosomes could be acidified and degrade their contents without fusion with a lytic compartment by gaining digestive enzymes from the trans-Golgi network. Digestion of haemoglobin has been observed in haemoglobin-containing vesicles prior to, or in the absence of fusion with the digestive vacuole (Abu Bakar *et al.*, 2010). This may indicate precedent for the maturation of vesicles into lytic compartments in the absence of interaction with the main lytic compartment, the digestive vacuole. LysoTracker and LysoSensor probes were used to assess the potential acidification of mCherry-*Pf*ATG8-labelled structures. LysoTracker Red has been shown to accumulate into autophagosomes shortly after their formation in mammalian cells (Kim and Lemasters, 2011). Asynchronous D10 parasites were incubated with LysoTracker Red DND-99 under normal culture conditions before analysis by fluorescence light microscopy (Figure 5.14). LysoTracker, a fluorophore linked to an acidotropic weak base, concentrated to the digestive vacuole in trophozoites and schizonts of wild type parasites. This probe is reported to accumulate in compartments at ~ pH 5.2, which correlates well with pH reported for the digestive vacuole (pH 5.2 – 5.4) (Hayward *et al.*, 2006). With the absence of any staining beyond the digestive

vacuole, it appeared unlikely that mCherry-*Pf*ATG8-labelled structures were acidified to this extent.

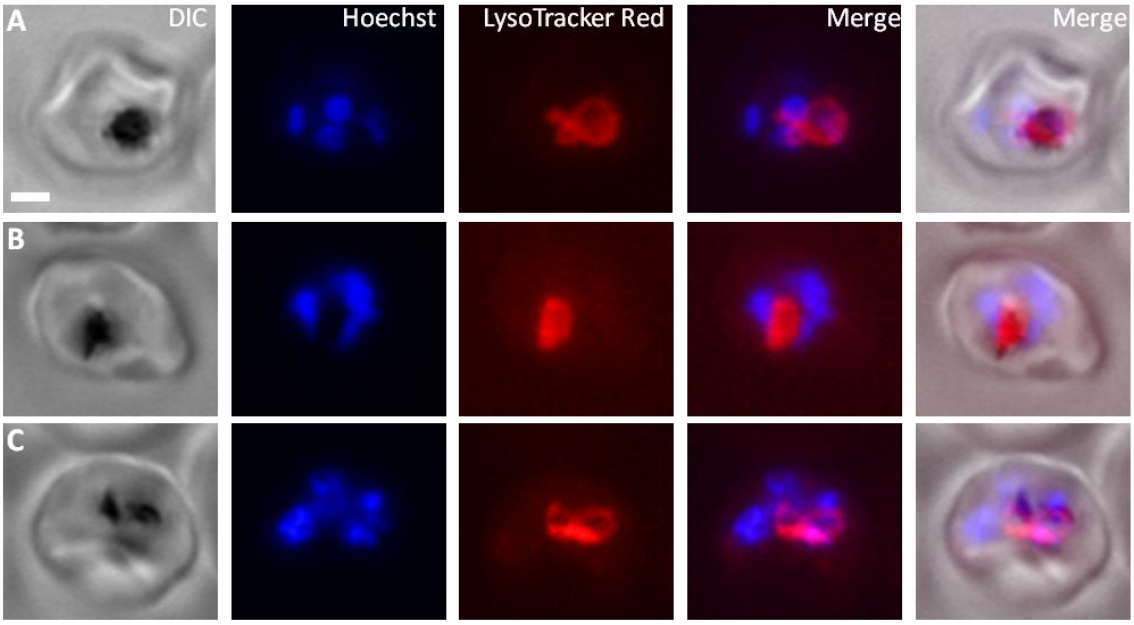

Figure 5.14: Identification of acidic compartments with LysoTracker DND-99.

Asynchronous D10 parasites were incubated with 50 nM LysoTracker DND-99 for 45 min under normal culture conditions. Parasites were analysed by live cell fluorescence light microscopy. Representative images of late trophozoites (B) and early schizonts (A and C) are shown. Scale bar = 2 µm.

An attempt was made to ascribe a rough pH value to mCherry-*Pf*ATG8-labelled structures by using LysoSensor probes. Unlike LysoTracker which maintains its fluorescence independently from pH, LysoSensor probes accumulate in acidic compartments but have differing spectral properties dependent on pH (Life Technologies). LysoSensor Green DND-189 is most fluorescent when in an acidic environment because its fluorescence is quenched until protonation occurs at low pH, whereas LysoSensor Green DND-153 is brightly fluorescent at neutral pH and is reported to concentrate to the membranes of weakly acidic compartments (Life Technologies). Asynchronous parasites expressing mCherry-*Pf*ATG8 were incubated with LysoSensor Green DND-189 and analysed by fluorescence light microscopy. No strong fluorescence was observed in any subcellular structure (including the digestive vacuole), with a weak diffuse signal characteristic of all life cycle stages imaged (Figure 5.15 (A-C)). This cytosolic staining did not overlap with the structures labelled by mCherry-*Pf*ATG8. This suggests that the probe was either unable to accumulate in acidic compartments, or that once in the digestive vacuole it was quickly degraded. Asynchronous parasites expressing

mCherry-*Pf*ATG8 were incubated with LysoSensor Green DND-153 and analysed by fluorescence light microscopy. A strong fluorescence was seen concentrated to subcellular structures in parasites of all stages imaged (Figure 5.15 (D-G)). In late stage parasites in particular, the fluorescence pattern resembled a complex and vast membranous network where apparently very large vacuoles or tubular membrane structures were labelled. This suggested that LysoSensor Green DND-153 concentrates to membranes throughout the parasite and fluoresces strongly while in an environment of near-neutral pH. In some parasites mCherry-*Pf*ATG8-labelled structures overlapped with structures where LysoSensor Green DND-153 had concentrated. This suggested that mCherry-*Pf*ATG8-labelled structures are membrane bound organelles with a near neutral pH.

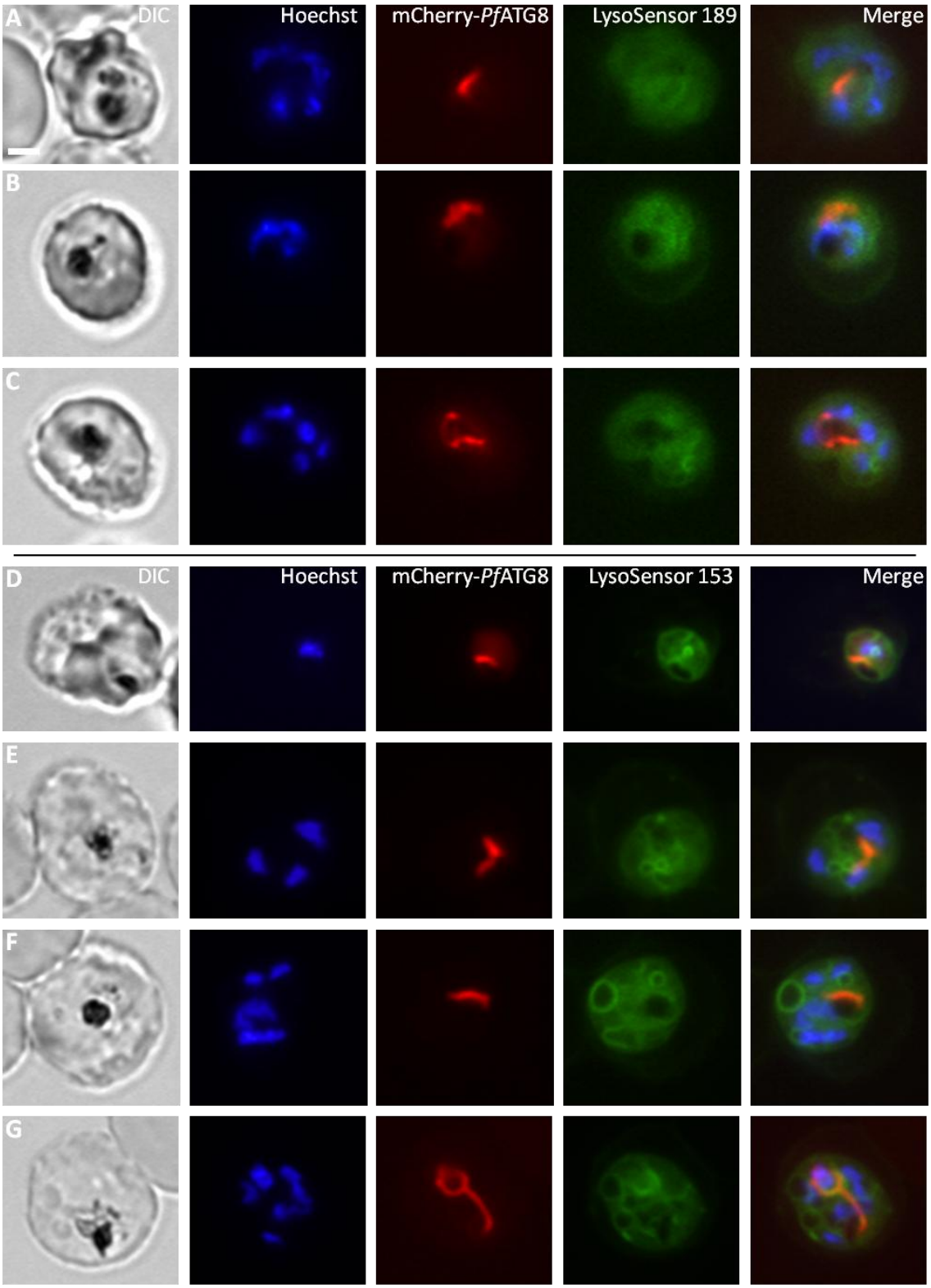

Figure 5.15: Identification of acidic compartments with LysoSensor DND-189 and LysoSensor DND-153.

(Upper panels) Asynchronous parasites transfected with EP-mC-A8 were incubated with 10 nM LysoSensor DND-189 at 37 °C for 5 min before analysis by live cell fluorescence light microscopy. Representative images of trophozoites (B) and schizonts (A and C) are shown. (Lower panels) Asynchronous parasites transfected with EP-mC-A8 were incubated with 10 nM LysoSensor DND-153 at 37 °C for 5 min before analysis by live cell fluorescence light microscopy. Representative images of trophozoites (D and E) and schizonts (F and G) are shown.

Incubation of parasites expressing mCherry-*Pf*ATG8 with each of these probes revealed that mCherry-*Pf*ATG8-labelled structures are unlikely to be acidified. This supported previous findings that suggested that mCherry-*Pf*ATG8-labeled structures were not involved in a canonical autophagic process.

5.2.4.2 Analysis of mCherry-*Pf*ATG8-labelled structures in relation to the mitochondrion and apicoplast

Plasmodium spp. possess a mitochondrion and apicoplast as single copy organelles, which elongate and segment during schizogony to ensure that each daughter merozoite inherits a functional organelle (van Dooren *et al.*, 2005). It has previously been shown by GFP-tagging mitochondrial and apicoplast resident proteins that the expansion and segmentation of these organelles involves striking morphological development with characteristic stages through the intraerythrocytic development of the parasite (McMillan, 2006, McMillan *et al.*, 2005). The appearance of mCherry-*Pf*ATG8-labelled structures resembled the appearance of both the mitochondrion and apicoplast as they develop. Further microscopic analyses were performed to investigate the possible relationship between mCherry-*Pf*ATG8-labelled structures and the mitochondrion and apicoplast.

A range of commercially available mitochondrial-specific probes can be used to identify the mitochondrion in live and fixed cells (Cottet-Rousselle *et al.*, 2011). MitoTracker Green-FM was used to visualise the mitochondrion in live parasites expressing mCherry-*Pf*ATG8. This cell permeable probe accumulates within an active mitochondrion and fluoresces upon conjugation to thiols (Life Technologies). Asynchronous parasites expressing mCherry-*Pf*ATG8 were incubated with MitoTracker Green-FM under normal culture conditions prior to analysis by fluorescence light microscopy. mCherry-*Pf*ATG8-labelled structures did not colocalise with the active mitochondrion reported by MitoTracker in any of the life cycle stages imaged (Figure 5.16 (A-C)).

In the cells of organisms that perform mitophagy, either the whole organelle or damaged portions are selectively incorporated into autophagosomes as cargo destined for degradation (Kim *et al.*, 2007). The precise factors that promote mitophagy have yet to be confirmed but recent work in mammalian cells has

shown that the formation of permeability transition pores which result in the depolarization of mitochondria likely play a role (Kim *et al.*, 2007). By identifying where these pores form, selective turnover of these portions of mitochondrial membrane by mitophagy may facilitate organelle homeostasis in organisms where removal of the entire organelle is not possible. The visualisation of mitochondria with MitoTracker probes is dependent on an active membrane potential. Due to the possibility of the collapse of membrane potential in areas of the mitochondrion that may be labelled by mCherry-*Pf*ATG8, possibly indicating mitophagy, a second method was used in order to assess possible colocalisation of mCherry-*Pf*ATG8 with mitochondrial proteins. If mCherry-*Pf*ATG8 was observed to colocalise with mitochondrial proteins it might indicate a role in turnover of damaged or unnecessary mitochondrial material that would be missed by probing with MitoTracker. In order to facilitate colocalisation with *Pf*ATG8, immunofluorescence assays were performed using a mitochondrial GFP-reporter line. A line already generated by a previous member of the lab had been shown to have a strong GFP signal in the lumen of the mitochondrion (McMillan, 2006). In brief, this line was generated by transfection of D10 parasites with a construct based on pHH2, in which the genomic sequence encoding amino acids 1-33 of *PF*L1550w was cloned in frame with a C-terminal GFP-tag (mE3-GFP-pHH2). Parasites transfected with mE3-GFP-pHH2 and selected with WR99210 exhibit strong fluorescence in the lumen of the mitochondrion in all intraerythrocytic life cycle stages. Approximately 80 – 90 % of parasites analysed by live cell fluorescence light microscopy as part of this study expressed visible levels of mE3-GFP.

Endogenous *Pf*ATG8 was detected in asynchronous parasites expressing mE3-GFP by IFA with rabbit antisera raised against His-*Pf*ATG8 purification B and mouse Alexa Fluor 594-conjugated anti-rabbit polyclonal antibodies (Figure 5.16 (D)). As expected, mE3-GFP appeared to label the mitochondrion similarly to during live cell fluorescent light microscopy; however the labelling was often less homogeneous, suggesting loss of structural integrity during the IFA procedure. As had been seen in IFA analysis of wild type parasites, antisera raised against His-*Pf*ATG8 detected structures similar to those labelled by mCherry-*Pf*ATG8 in live cell microscopy, which often also displayed a slightly fragmented appearance.

No overlap was observed between the structures reported by detection of endogenous *Pf*ATG8 and structures labelled with mE3-GFP.

The lack of colocalisation between *Pf*ATG8-positive structures and either the intact mitochondrion or a mitochondrial resident protein, suggested that it was unlikely that *Pf*ATG8 plays a role in mitochondrial homeostasis in intraerythrocytic stages as no overlap between *Pf*ATG8 and the mitochondrion was observed.

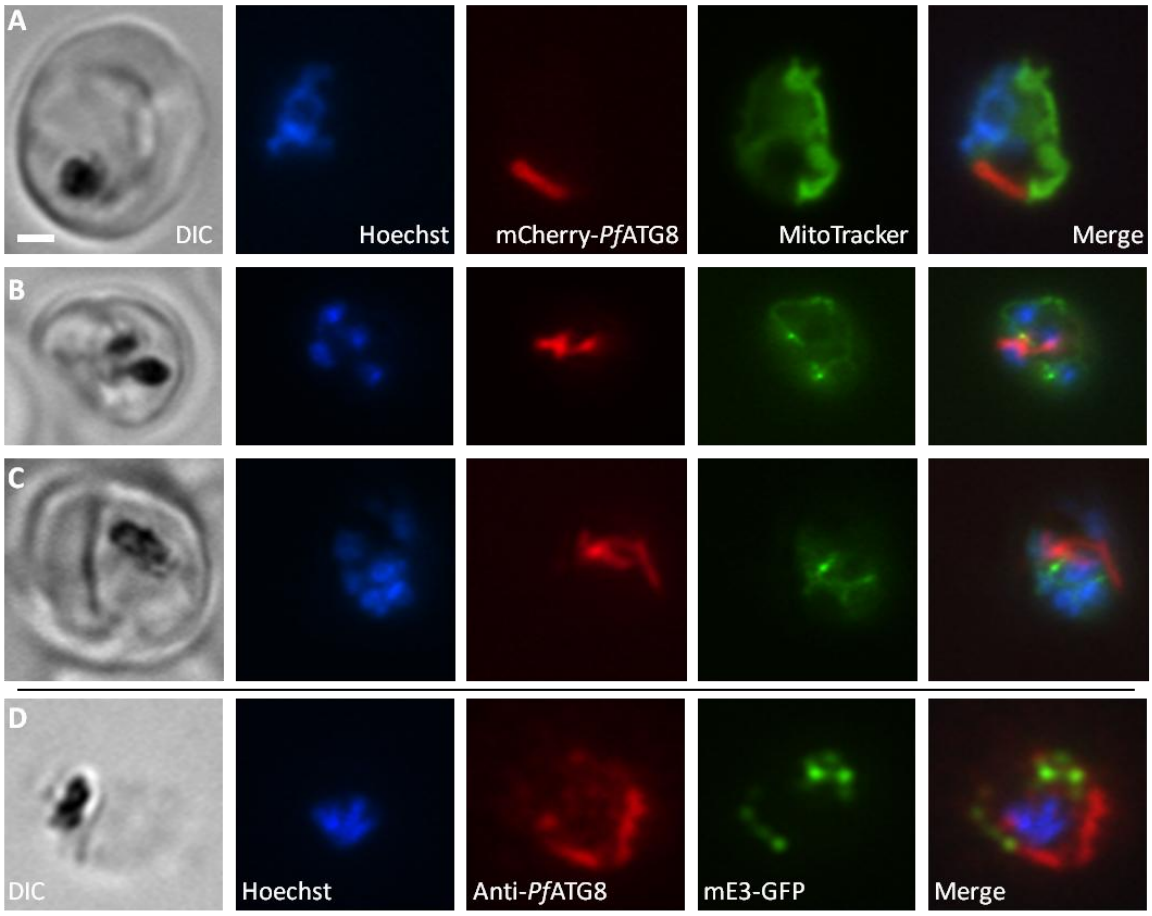

Figure 5.16: Localisation of mCherry-*Pf*ATG8 in relation to the mitochondrion.

(A - C) Asynchronous parasites transfected with EP-mC-A8 were incubated with 25 nM MitoTracker Green-FM for 20 min under normal culture conditions before analysis by live cell fluorescence light microscopy. Representative images of a trophozoite (A), early schizont (B) and late schizont (C) are shown. (D) Asynchronous parasites transfected with mE3-GFP-pHH2 were prepared for IFA with rabbit anti-*Pf*ATG8 antisera (1:1,000) and goat anti-rabbit Alexa Fluor 594-conjugated polyclonal antibodies (1:1,500). A representative image of a trophozoite is shown. Scale bar = 2 µm.

In the absence of commercially available apicoplast-specific probes the possible relationship between the apicoplast and *Pf*ATG8 relied on the use of an apicoplast reporter line, again generated by Dr. P. McMillan (McMillan, 2006). In

brief, the genomic sequence encoding amino acids 1-134 of PF08_0066 was cloned into pHH2 in frame with a C-terminal GFP-tag (aE3-GFP-pHH2). Wild type D10 parasites transfected with aE3-GFP-pHH2 and selected with WR99210 exhibit strong GFP fluorescence in the lumen of the apicoplast in all intraerythrocytic life cycle stages. Approximately 80 – 90 % of parasites analysed by live cell fluorescence light microscopy as part of this study expressed visible levels of aE3-GFP. Asynchronous parasites expressing aE3-GFP were prepared for IFA with rabbit antisera raised against His-*Pf*ATG8 purification B and Alexa Fluor 594-conjugated mouse anti-rabbit monoclonal antibodies (Figure 5.17 (A)). As expected the apicoplast was labelled by aE3-GFP similarly to when examined by live cell fluorescence light microscopy. However, as with the IFA of cells expressing mE3-GFP, it appeared that the apicoplast's structure had been disrupted during the IFA procedure. Most likely the fixation and permeabilisation steps in the preparation of slides were responsible for causing collapse of the organelle's integrity leading to a fragmented appearance. Despite this, it could be seen that there were areas of overlap between the GFP-labelled apicoplast and the structure detected by antisera raised against His-*Pf*TAG8.

To explore the relationship between the apicoplast and *Pf*ATG8 further, a co-expressing parasite line was generated. This required the generation of a new EP-mC-A8 expression vector based on the destination vector pHBlR-3/4, which would allow selection with blasticidin-S-HCl (BLA) in parasites already requiring WR99210 for maintenance of the aE3-GFP-pHH2 construct. For simplicity, this construct is also referred to as EP-mC-A8 (see Table 2.1).

D10 wild type parasites were transfected with the new EP-mC-A8 construct and parasites resistant to BLA were detected 6-8 weeks later. Analysis of mCherry-*Pf*ATG8 localisation by fluorescence light microscopy revealed the same characteristic fluorescence patterns as those previously described. This confirmed that expression of mCherry-*Pf*ATG8 was comparable when driven from either the pHBlR-3/4 or pCHDR-3/4-based constructs. D10 parasites previously transfected with aE3-GFP-pHH2 were then transfected with EP-mC-A8 and parasites resistant to both BLA and WR99210 were detected in Giemsa-stained thin smears after 6-8 weeks. Analysis of the aE3-GFP line transfected with EP-mC-A8 by live cell fluorescence light microscopy following magnetic enrichment showed that in a small (~ 5 %) proportion of parasites, both mCherry-*Pf*ATG8 and

aE3-GFP were expressed (Figure 5.17 (B-D)). Co-expression of mCherry-*Pf*ATG8 had not affected the expression or localisation of aE3-GFP to the apicoplast. Conversely, in the proportion of parasites expressing mCherry-*Pf*ATG8, similar structures were observed to those in parasites expressing mCherry-*Pf*ATG8 only. This showed that the expression of two fusion proteins had not affected the distribution of either in comparison to when they were individually expressed.

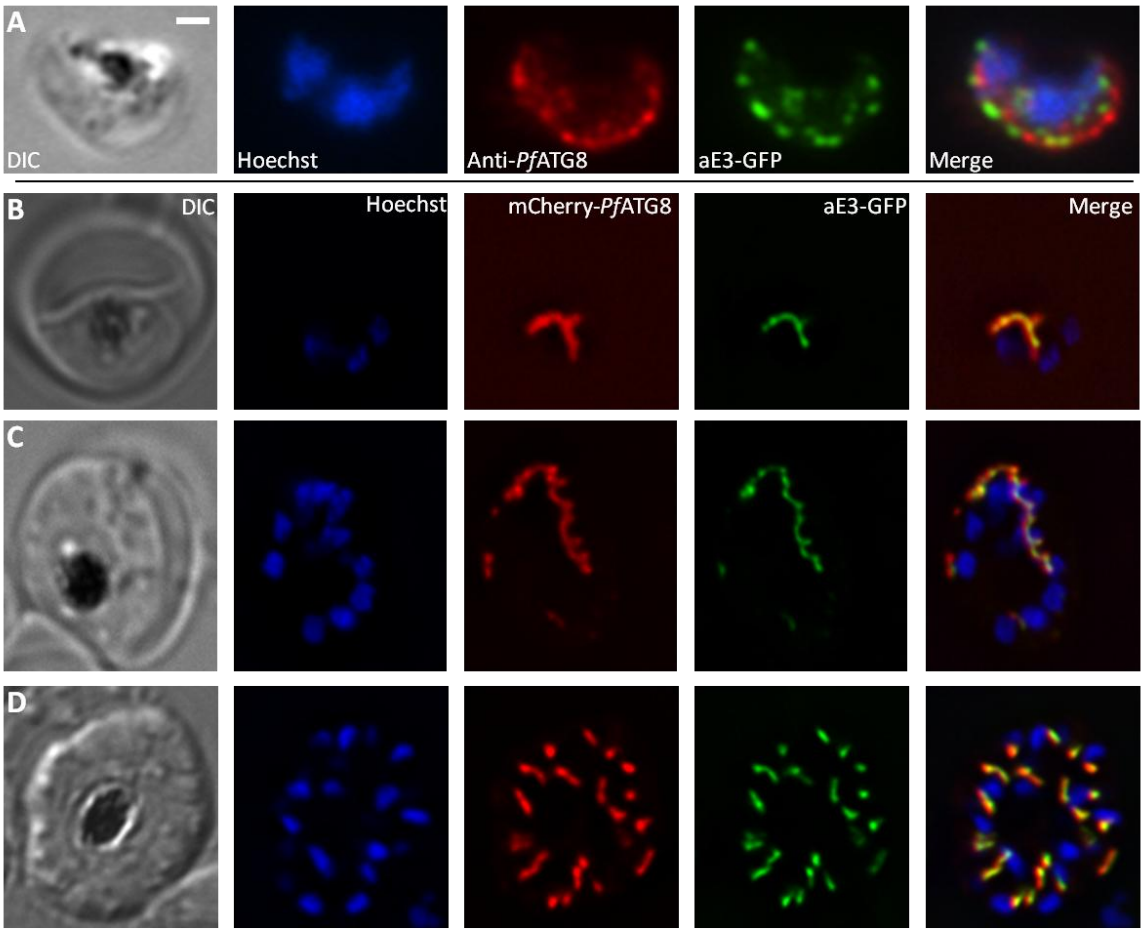

Figure 5.17: Localisation of mCherry-*Pf*ATG8 in relation to the apicoplast.

(A) Endogenous *Pf*ATG8 was detected in parasites transfected with aE3-GFP-pHH2 by IFA with rabbit anti-*Pf*ATG8 antisera (1:1,000) and anti-rabbit Alexa Fluor 594-conjugated polyclonal antibodies (1:1,500). A representative image of a trophozoite is shown.

(B-D) Late stage parasites transfected with both EP-mC-A8 and aE3-GFP-pHH2 were enriched by magnetic isolation and analysed by fluorescence light microscopy using a Delta Vision Core microscope. Representative images of life cycle stages trophozoite (B), schizont (C) and segmenter (D) are shown. Scale bar = 2 µm.

Images were collected of parasites at different stages of intraerythrocytic development. It was found that mCherry-*Pf*ATG8 was closely associated with the apicoplast throughout the life cycle, with a partial overlap between the structures labelled by mCherry-*Pf*ATG8 and the apicoplast lumen, reported by

aE3-GFP. However, a complete co-localisation between the two reporters was not observed. This finding was not surprising considering the aE3-GFP protein resides in the apicoplast lumen, while mCherry-*Pf*ATG8 does not possess a bipartite signal required for entry into the apicoplast lumen and, according to evidence collected in this study, is predicted to be membrane associated due to its lipid modification.

The relationship between mCherry-*Pf*ATG8 and aE3-GFP was analysed by determining the Pearson's coefficient representing co-localisation between the two signals of mCherry and GFP i.e. the overlap of red and green signal in the same pixel, over whole parasites using SoftWoRx software (Applied Precision). The average Pearson's coefficient was found to be 0.69 ± 0.07 (S.D. n = 25). This represents a high degree of correlation with 48 % of variance being linked (Adler and Parmryd, 2010). This can be interpreted as that when a pixel contains signal from aE3-GFP it will also contain signal from mCherry-*Pf*ATG8 in 48 % of cases (http://www.svi.nl/PearsonsInterpretation [last accessed 15/06/2012]). This showed that there was a considerable association between mCherry-*Pf*TAG8 and aE3-GFP but confirmed that the two reporters did not fully co-localise.

This crucial finding added to the characterisation of *Pf*ATG8 and the determination of the identitiy of *Pf*ATG8-positive structures. Data collected to this point suggested that *Pf*ATG8 (and mCherry-*Pf*ATG8) is lipidated and associated with a membrane-bound organelle, which appears to be the apicoplast. This labelling of the apicoplast is entirely dependent on the C-terminal glycine residue of *Pf*ATG8 but is not regulated by the processes known to influence control of the autophagic pathway in other organisms. This left the question, why does *Pf*ATG8 label the apicoplast? In *Toxoplasma gondii*, which possesses an apicoplast, it has recently been shown that an ATG8 homologue plays a role in mitochondrion homeostasis (Besteiro *et al.*, 2011) but no link between *Tg*ATG8 and the apicoplast was alluded to. In order to understand why *Pf*ATG8 labels the apicoplast attempts to explore the relationship between *Pf*ATG8 and the apicoplast were made.

5.2.5 Chemical disruption of the apicoplast

It has recently been shown that production of isoprenoid precursors is the only essential function of the apicoplast in the intraerythrocytic stages of *P. falciparum* (Yeh and DeRisi, 2011). Yeh and DeRisi showed that antibiotic treatment leads to a delayed death phenotype due to perturbation of apicoplast development and subsequent lack of inheritance by daughter merozoites. However, by supplying the parasites with exogenous isopentenyl pyrophosphate (IPP), indefinite continuation of parasite cultures is possible. They show that an apicoplast-targeted acyl carrier protein-GFP fusion protein resides in vesicles scattered throughout the cytosol in parasites that have lost their apicoplast, suggesting that without the presence of an apicoplast, apicoplast-targeted vesicles accumulate. Given the close association of mCherry-*Pf*ATG8 and the apicoplast reporter aE3-GFP, a similar experiment was performed to analyse the localisation of mCherry-*Pf*ATG8 in antibiotic treated, IPP rescued parasites.

Parasites expressing both mCherry-*Pf*ATG8 and aE3-GFP were synchronised to ring stages by a single incubation in 5 % sorbitol. Approximately 16 h later, when cultures mainly contained trophozoite stages, parasites were incubated in culture medium dosed with 50 µM chloramphenicol or an equivalent volume of ethanol as a control. Twenty four hours later the parasites were again fed with chloramphenicol-dosed culture medium. Forty eight and 72 h after the first dose of chloramphenicol, parasites were fed with culture medium dosed with chloramphenicol and supplemented with 200 µM IPP. After a total of 96 h from the initial dose of chloramphenicol, parasites were magnetically enriched and analysed by live cell fluorescence light microscopy (Figure 5.18).

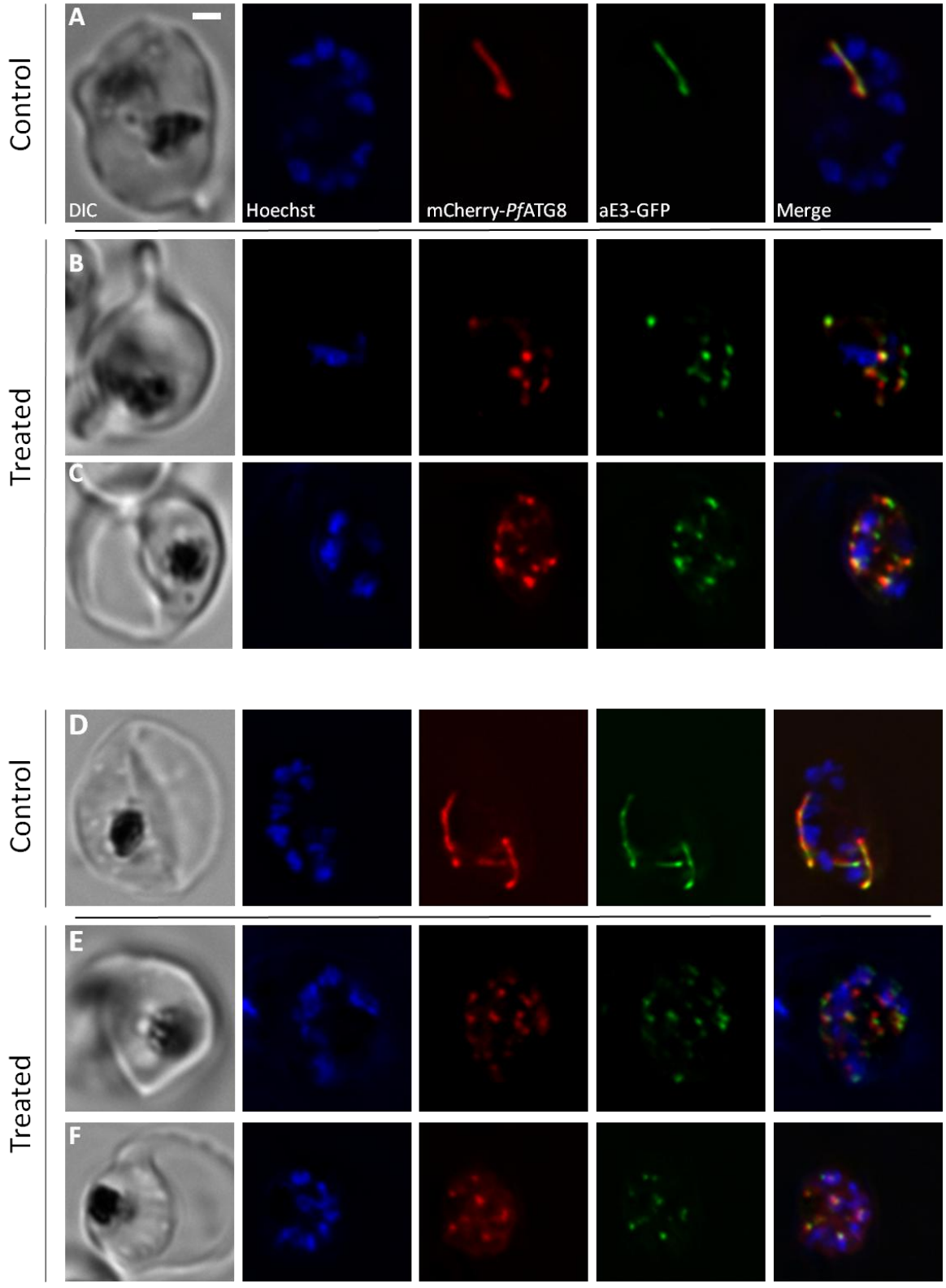

Figure 5.18: Effect of apicoplast loss on mCherry-*Pf*ATG8 and aE3-GFP localisation.

Late stage parasites transfected with both EP-mC-A8 and aE3-GFP-pHH2 were treated with 50 µM chloramphenicol or ethanol (Control) for 96 h and 200 µM IPP for the final 48 h prior to enrichment by magnetic isolation and analysis by live cell fluorescence light microscopy. (A) Representative image of a control trophozoite, (B,C) representative images of chloramphenicol treated trophozoites. (D) Representative image of a control schizont, (E,F) representative images of chloramphenicol treated schizonts. Scale bar = 2 µm.

Similarly to data presented by Yeh and DeRisi, the apicoplast-targeted aE3-GFP protein resided in vesicles scattered throughout the cytosol and no structure resembling an apicoplast was present, confirming that the apicoplast had been lost due to chloramphenicol treatment. The diameter of aE3-GFP labelled vesicles was analysed using SoftWoRx software (Applied Precision). The average diameter of 26 vesicles was 399 ± 99 nm (S.D.). However, these vesicles were often irregular shapes, potentially representing fusion products of multiple vesicles.

In chloramphenicol treated and IPP rescued parasites, mCherry-*Pf*ATG8 also presented a vesicular distribution and the labelling of tubular structures observed in untreated or control parasites was not observed. The localisation of mCherry-*Pf*ATG8 was scored as previously described and while the low proportion of cells displaying vacuolar or cytosolic patterns remained the same following treatment, the proportion of cells displaying a structure(s) pattern had reduced and been replaced by cells displaying a vesicular pattern (Figure 5.19).

EP-mC-A8 + aE3-GFP	Control
No expression	94.5 ± 0.5
Structure(s)	2.7 ± 2.2
Vacuolar	1.1 ± 1.1
Cytosolic	1.7 ± 2.7
Vesicular	0.1 ± 0.1

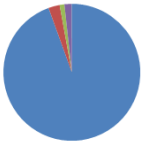

EP-mC-A8 + aE3-GFP	Chloramphenicol
No expression	94.4 ± 1.1
Structure(s)	0.1 ± 0.1
Vacuolar	0.9 ± 1.0
Cytosolic	1.6 ± 1.1
Vesicular	3.3 ± 0.8

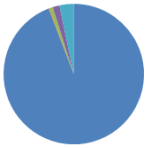

Figure 5.19: Effect of apicoplast loss on mCherry-*Pf*ATG8 expression and localisation.

Late stage parasites transfected with aE3-GFP-pHH2 and EP-mC-A8 were treated with 50 µM chloramphenicol or ethanol (Control) for 96 h and 200 µM IPP for the final 48 h prior to enrichment by magnetic isolation and analysis by live cell fluorescence light microscopy. Treatments were performed four or three times with 2107 (Chloramphenicol) and 1446 (Control) cells being counted, respectively. Numbers indicate percentage of cells counted scored into each category ± S.D.

Similarly to the association observed between mCherry-*Pf*ATG8 and aE3-GFP in untreated cells, there appeared to be a partial overlap between mCherry-*Pf*ATG8 and aE3-GFP-labelled vesicles following chloramphenicol treatment (Figure 5.20). mCherry-*Pf*ATG8-labelled vesicles also appeared to be of various sizes and shapes.

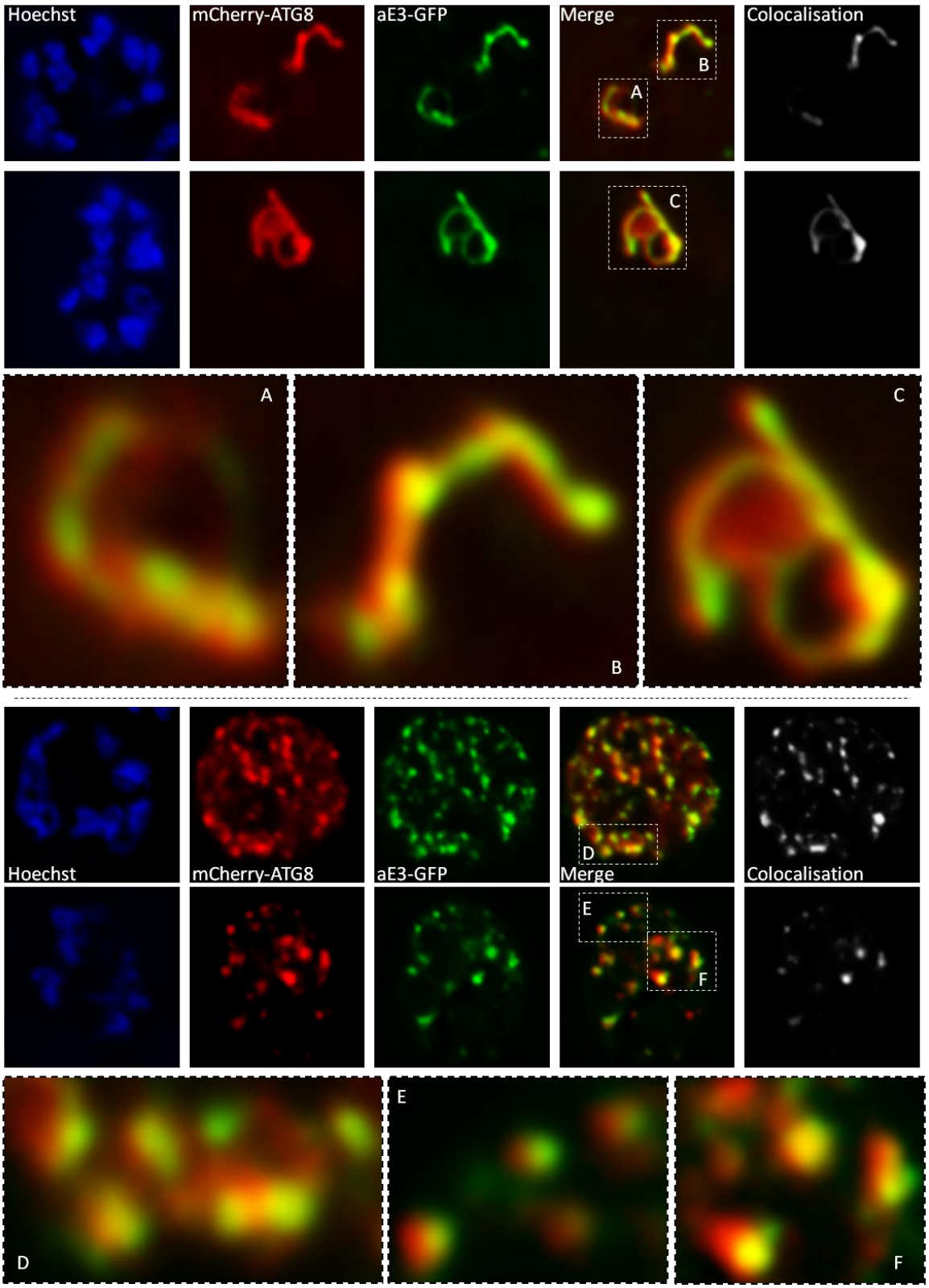

Figure 5.20: Effect of apicoplast loss on mCherry-*Pf*ATG8 and aE3-GFP localisation.

(Upper panels) Two examples of ethanol control parasites are shown. Insets A, B and C show an overlap but not complete colocalisation between mCherry-*Pf*ATG8 (red) and aE3-GFP (green)-labelled structures. (Lower panels) Two examples of chloramphenicol treated parasites are shown. Insets D, E and F show an overlap but not complete colocalisation between mCherry-*Pf*ATG8 (red) and aE3-GFP (green)-labelled vesicles.

The correlation between mCherry-*Pf*ATG8 and aE3-GFP across whole parasites was analysed by determination of the Pearson's coefficient. The average Pearson's coefficient was found to be 0.69 ± 0.07 (S.D. n = 28). As in untreated parasites, this represents a high degree of correlation (Figure 5.21) An indicates that the degree of colocalisation between the two proteins does not differ following apicoplast disruption.

This experiment had shown that in addition to labelling the intact apicoplast, mCherry-*Pf*ATG8 also labelled vesicles containing apicoplast-targeted protein when the intact apicoplast was absent as a result of chloramphenicol treatment. This suggested that the association of mCherry-*Pf*ATG8 to the apicoplast membrane was independent of apicoplast function.

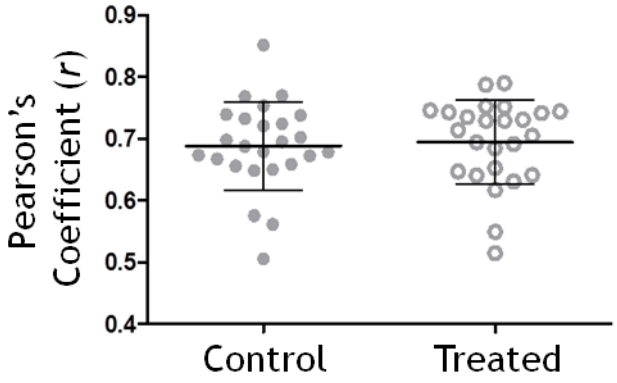

	Coefficient	N	S.D.
Control	0.69	25	0.07
Treated	0.69	28	0.07

Figure 5.21: Analysis of the relationship between mCherry-*Pf*ATG8 and aE3-GFP with or without chemical disruption of the apicoplast.

Deconvolved Z stacks (18 x 0.2 µm) of images obtained from previous experiments were analysed for correlation between mCherry-*Pf*ATG8 and aE3-GFP using SoftWoRx software (Applied Precision). Each data point indicates a whole parasite analysed, solid points indicating ethanol (Control) treated parasites and hollow points indicating chloramphenicol and IPP treated parasites. The average correlation and standard deviation are indicated by bars and whiskers.

Due to the very low proportion of parasites that expressed visible amounts of both mCherry-*Pf*ATG8 and aE3-GFP, chloramphenicol treatment and IPP rescue was also performed on parasites expressing only mCherry-*Pf*ATG8. Visible amounts of mCherry-*Pf*ATG8 are typically seen in ~ 20 % of parasites transfected with EP-mC-A8 only, while only ~ 5 % of co-transfected parasites expressed

visible amounts of both mCherry-*Pf*ATG8 and aE3-GFP. Parasites expressing mCherry-*Pf*ATG8 were treated and analysed as above. As in parasites expressing both mCherry-*Pf*ATG8 and aE3-GFP, the labelling of tubular structures seen in untreated parasites was mostly lost upon chloramphenicol treatment and was replaced by labelling of vesicles throughout the cytosol (Figure 5.22). This large shift in mCherry-*Pf*ATG8 localisation was more apparent in these lines and together with data collected from co-expressing lines, represented the first incidence in which the localisation of mCherry-*Pf*ATG8 has been altered through manipulation of parasites.

EP-mC-A8	Control
No expression	82.4 ± 1.0
Structure(s)	17.3 ± 1.0
Vacuolar	0.3 ± 0.0
Cytosolic	0.0 ± 0.0
Vesicular	0.0 ± 0.0

EP-mC-A8	Chloramphenicol
No expression	86.5 ± 0.4
Structure(s)	1.7 ± 0.3
Vacuolar	0.0 ± 0.0
Cytosolic	0.0 ± 0.0
Vesicular	11.8 ± 0.1

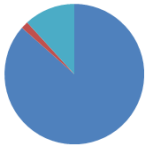

Figure 5.22: Effect of apicoplast loss on mCherry-*Pf*ATG8 expression and localisation.

Late stage parasites transfected with EP-mC-A8 were treated with 50 µM chloramphenicol or ethanol (Control) for 96 h and 200 µM IPP for the final 48 h prior to enrichment by magnetic isolation and analysis by live cell fluorescence light microscopy. Treatments were performed twice with 961 (Chloramphenicol and IPP), 791 (Control) cells being counted. Numbers indicate percentage of cells counted scored into each category ± S.D.

In order to determine whether the vesicular pattern of mCherry-*Pf*ATG8 observed following chloramphenicol treatment was dependent on its lipidation, the same experiment was also performed on parasites expressing mCherry-*Pf*ATG8ΔG. The cytosolic distribution of mCherry-*Pf*ATG8ΔG in untreated parasites was also seen in chloramphenicol treated parasites (Figure 5.23). This showed that the labelling of vesicles by mCherry-*Pf*ATG8 in chloramphenicol treated parasite is entirely dependent on its C-terminal glycine residue, strongly suggesting that this localisation is due to a lipid conjugation and represents a specific association of mCherry-*Pf*ATG8 with vesicular membranes rather than the non-selective packaging of the fusion protein into these vesicles.

EP-mC-A8ΔG	Control
No expression	86.0 ± 0.3
Structure(s)	0.0 ± 0.0
Vacuolar	0.8 ± 0.4
Cytosolic	13.2 ± 0.7
Vesicular	0.0 ± 0.0

EP-mC-A8ΔG	Chloramphenicol
No expression	83.3 ± 0.4
Structure(s)	0.0 ± 0.0
Vacuolar	1.0 ± 0.4
Cytosolic	15.7 ± 0.1
Vesicular	0.0 ± 0.0

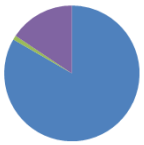

Figure 5.23: Effect of apicoplast loss on mCherry-*Pf*ATG8ΔG expression and localisation.

Late stage parasites transfected with EP-mC-A8ΔG were treated with 50 µM chloramphenicol or ethanol (Control) for 96 h and 200 µM IPP for the final 48 h prior to enrichment by magnetic isolation and analysis by live cell fluorescence light microscopy. Treatments were performed twice with 792 (Chloramphenicol and IPP) and 842 (Control) cells being counted. Numbers indicate percentage of cells counted scored into each category ± S.D.

5.2.6 Characterisation of apicoplast-targeted vesicles

Chemical disruption of the apicoplast leads to the accumulation of apicoplast-targeted vesicles containing proteins such as ACP-GFP (Yeh and DeRisi, 2011) and now reported here, aE3-GFP. The observation that mCherry-*Pf*ATG8 appears to label these vesicles indicated that they display a characteristic of autophagosomes. In order to determine whether aE3-GFP-positive apicoplast-targeted vesicles displayed additional characteristics of autophagosomes in other organisms, IFA analyses were performed using antibodies against *Pf*Rab7. Rab7, a member of the large family of Rab GTPases (Chua *et al.*, 2011) is recruited to mature autophagosomes and facilitates fusion with endolysosomal vesicles prior to autophagolysosome formation (Gutierrez *et al.*, 2004). Parasites expressing aE3-GFP were subjected to chloramphenicol treatment and IPP rescue as above and were prepared for IFA using antibodies against *Pf*Rab7 to detect the endogenous protein (Figure 5.24). In untreated control parasites, the intact apicoplast is reported by aE3-GFP. In these parasites, *Pf*Rab7 localised to punctuate structures representing endolysosomal vesicles (Personal communication with Dr. Gordon Langsley). The degree of correlation as demonstrated by the Pearson's coefficient between aE3-GFP and *Pf*Rab7 was low in all parasites analysed (0.23 ± 0.07 (S.D. n = 3)), indicating that *Pf*Rab7 did not label the intact apicoplast. In treated parasites in which the intact apicoplast was absent, the correlation between aE3-GFP-positive vesicles and *Pf*Rab7-labelled endolysosomes was also low, 0.29 ± 0.04 (S.D. n = 3), indicating that apicoplast-targeted vesicles are not labelled by *Pf*Rab7. This finding suggests that apicoplast-targeted vesicles do not show additional characteristics of

autophagsomes, other than being labelled by mCherry-*Pf*ATG8, providing further evidence that they participate in an anabolic rather than catabolic process.

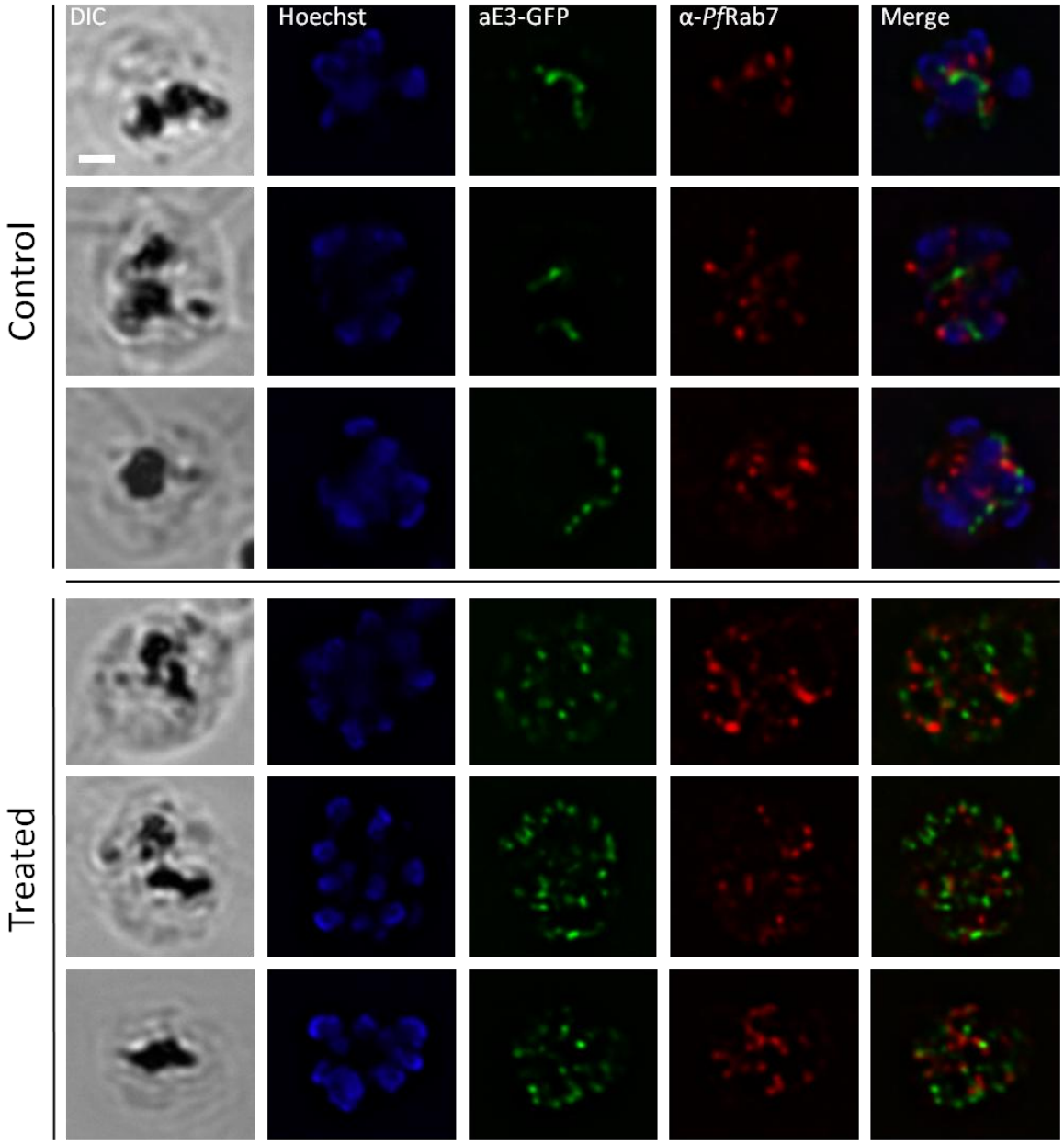

Figure 5.24: Analysis of colocalisation between apicoplast-targeted vesicles and *Pf*Rab7

Late stage parasites transfected with aE3-GFP-pHH2 were treated with 50 µM chloramphenicol or ethanol (Control) for 96 h and 200 µM IPP for the final 48 h prior to analysis by IFA with rat anti-*Pf*Rab7 peptide antibodies (1:300) and anti-rat Alexa Fluor 594-conjugated polyclonal antibodies (1:3,000). Representative images of schizont stage parasites are shown. Scale bar = 2 µm.

The same treatment was also performed on D10 wild type *P. falciparum* in order to assess the localisation of endogenous *Pf*ATG8 and *Pf*Rab7 in the same cells. An IFA using peptide antibodies against *Pf*ATG8 (not those detailed in Chapter 3) and *Pf*Rab7 revealed that as expected, in untreated parasites *Pf*ATG8 and *Pf*Rab7 labelled distinct structures – *Pf*ATG8 labelled a structure resembling the

intact apicoplast while *Pf*Rab7 labelled multiple puncta (as above) believed to represent endolysosomal vesicles (Figure 5.25). In treated parasites, in which the characteristic *Pf*ATG8-labelling of the intact apicoplast was replaced by the labelling of multiple vesicles (as observed in lines expressing mCherry-*Pf*ATG8), the degree of colocalisation between *Pf*ATG8 and *Pf*Rab7 was not notably increased in comparison to untreated parasites (untreated: r = 0.39 ± 0.07 (S.D. n = 2), treated: r = 0.33 ± 0.05 (S.D. n = 2)). This showed that the redistribution of mCherry-*Pf*ATG8 from the intact apicoplast in untreated parasites to apicoplast-targeted vesicles in treated parasites was representative of the same redistribution of the endogenous *Pf*ATG8 protein. It also supported previous findings that *Pf*ATG8-labelled apicoplast-targeted vesicles are not also labelled by *Pf*Rab7, indicating that they do not show additional characteristics of canonical autophagosomes.

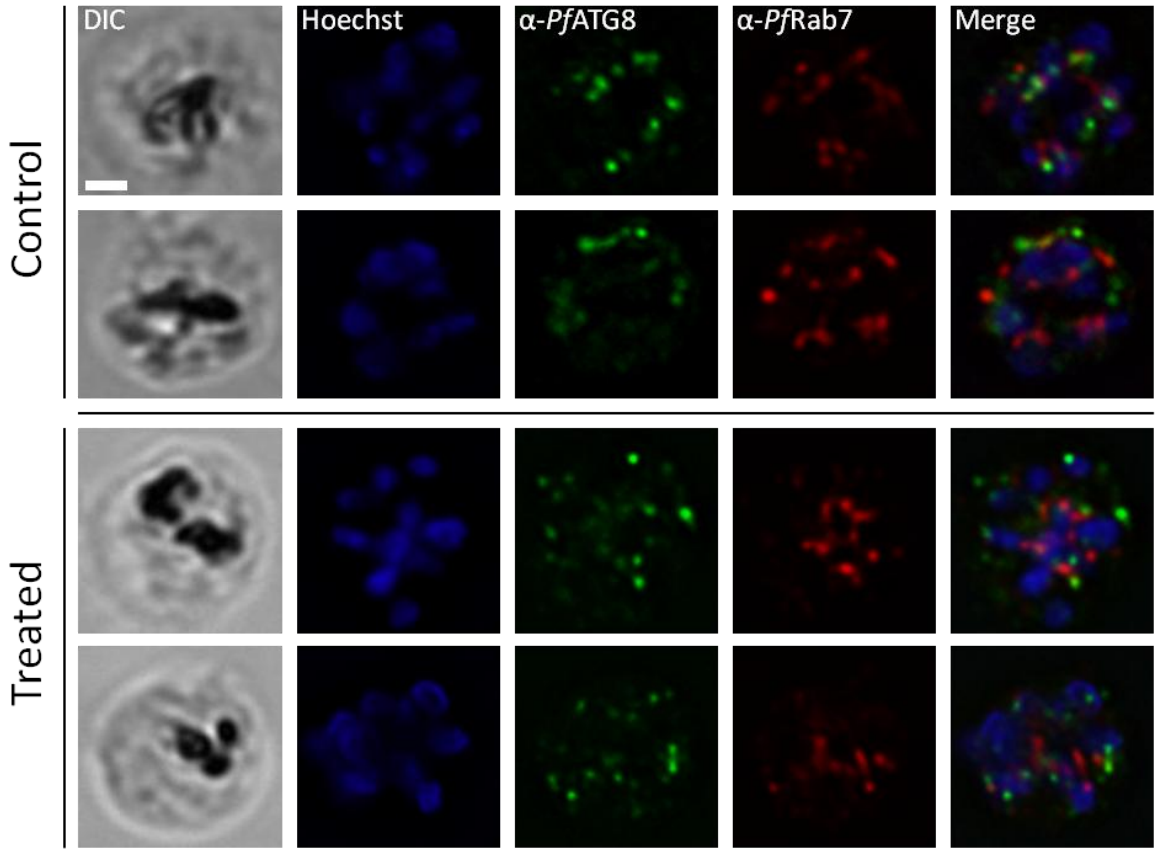

Figure 5.25: Analysis of colocalisation between *Pf*ATG8 and *Pf*Rab7

Late stage D10 *P.falciparum* were treated with 50 µM chloramphenicol or ethanol (Control) for 96 h and 200 µM IPP for the final 48 h prior to analysis by IFA with rat anti-*Pf*Rab7 peptide antibodies (1:300), guinea pig anti-*Pf*ATG8 peptide antibodies (1:3,000), anti-rat Alexa Fluor 594-conjugated polyclonal antibodies (1:3,000) and anti-guinea pig Alexa Fluor 488-conjugated polyclonal antibodies (1:6,000). Representative images of schizont stage parasites are shown. Scale bar = 2 µm.

5.3 Discussion

5.3.1 Characterisation of mCherry-*Pf*ATG8

This chapter has detailed the use of tools to study the localisation of both endogenous *Pf*ATG8 and mCherry-*Pf*ATG8(/*Pf*ATG8ΔG) in wild type or transgenic parasites, respectively. The use of the Gateway cloning platform provided an excellent tool with which to generate a number of constructs for transfection, with minimal cloning steps. Transfection of *P. falciparum* 3D7 and D10 strains yielded parasite lines resistant to WR99210 or BLA in over 90 % of occasions. mCherry or eYFP-tagged fusion proteins were seen to be expressed in all the lines generated, although it appeared that the maintenance of expression of the fusion proteins was limited to ~ 4 weeks after thawing a stabilate, after which point the proportion of parasites seen to express a delectable level of the fusion protein decreased. These effects may stem from the recombination events between the EP-mC-A8 construct and the parasite genome as disscussed in Chapter 4. Nevertheless, these transgenic lines proved to be an invaluable tool in the characterisation of *Pf*ATG8.

This study solely focussed on the use of N-terminal fluorescent tagging of *Pf*ATG8 in order to use the fusion protein as a marker for autophagic structures. The use of a C-terminal tag is certainly one that should be explored in *P. falciparum*. Due to the protein being expressed in a conjugation-competent (*Pf*ATG8-I) form, the initial role of *Pf*ATG4 in the cleavage of residues 3' of the essential glycine is bypassed (Tanida *et al.*, 2004). However, the necessity of processing to deconjugate *Pf*ATG8-II, recycling it back to the conjugation-competent form has yet to be explored. Expression of an N-terminal *and* C-terminally-tagged *Pf*ATG8 in intraerythrocytic stage parasites could highlight potential C-terminal processing. Cleavage of the C-terminal tag could indicate the ability of *Pf*ATG4 or an ATG4-like peptidase to process the C-terminus of *Pf*ATG8, potentially indicating that delipidation of *Pf*ATG8 is also performed. Certainly, the conservation of residues in *Pf*ATG8 shown to be responsible for recognition by ATG4 in other organisms (Amar *et al.*, 2006) and the identification of a putative *Pf*ATG4 homologue in the genome of *P. falciparum* 3D7 strain, suggests that this type of processing might occur. An absence of C-terminal processing of *Pf*ATG8 in *P. falciparum* could indicate a variation in the typical role of *Pf*ATG8. As an

autophagosome forms it engulfs ATG8 conjugated to PE in its inner leaflet. This ATG8 is trapped and destined for degradation along with autophagosome cargo by lysosomal peptidases. ATG8 conjugated to PE on the outer surface of an autophagosome has been suggested to require removal before endolysosomal fusion can occur (Kabeya *et al.*, 2004). If C-terminal processing of *Pf*ATG8 was absent, this may suggest that lipidation of *Pf*ATG8 was permanent. Expression of recombinant *Pf*ATG4 and incubation with protein extracted from parasites expressing mCherry-*Pf*ATG8 could provide additional evidence for de-lipidation of *Pf*ATG8, as a reduction in lipidated mCherry-*Pf*ATG8, similar to that seen following phospholipase D incubation, would indicate a *Pf*ATG8 processing activity for *Pf*ATG4 (Williams *et al.*, 2009).

Based on comparison between localisation of the two proteins, it seemed that mCherry-*Pf*ATG8 was a suitable tool with which to explore the function of endogenous *Pf*ATG8, as has been reported for the use of similar fusion proteins in other organisms (Pankiv *et al.*, 2007, Perry *et al.*, 2009). The observation of a more fragemented appearance of *Pf*ATG8-labelled structures in IFA analysis using *Pf*ATG8-specific antisera (or latterly peptide antibodies) was attributed to partial disruption of subcellular integrity, as demonstrated by the often fragmented appearance of the apicoplast and mitochondrion following fixation and permeabilisation in IFA preparation. For flexability and ease of use, mCherry-*Pf*ATG8 expressing parasites were used in the analysis of *Pf*ATG8 localisation but, when applicable and possible, analysis of endogenous *Pf*ATG8 localisation was also performed.

After establishing that mCherry-*Pf*ATG8 exhibited a localisation similar to that of the endogenous *Pf*ATG8 protein, the next step was to use this tool to elucidate the potential function of *Pf*ATG8 in intraerythrocytic parasites. Detailed analysis of the localisation of mCherry-*Pf*ATG8 revealed that this protein did not appear to label canonical autophagosome-like puncta under normal growth conditions. Instead, the protein localised to distinctive subcellular structures that appeared to elongate and divide during the intraerythrocytic development of the parasite. Time-lapse microscopy of single parasites over the course of their intraerythrocytic development was not attempted as part of this study (Gruring *et al.*, 2011). It would certainly have been interesting to track the temporal development of the mCherry-*Pf*ATG8-labelled structures. From the extensive

analysis performed, it could be concluded that in parasites expressing mCherry-*Pf*ATG8, the labelling of this structure appeared not to be transient as labelling of the structure at all intraerythrocytic stages was observed.

The presence of mCherry-*Pf*ATG8-labelled structures and the absence of any canonical autophagosome-like puncta begged the question as to whether the structures observed represented a novel type of autophagosome-like structure in *P. falciparum*. Autophagy is known to be used in the response to environmental and intracellular stress, as a mechanism to deal with nutrient starvation and during the process of cellular differentiation (Duszenko *et al.*, 2011). Even under conditions of unhindered growth, a dependency on a basal level of autophagy has been shown (Pattison *et al.*, 2011). Inside a host erythrocyte, the developing parasite is relatively well protected from stress and can generate the energy and nutrients it needs for growth from glycolysis and acquirement pathways, respectively (Baumeister *et al.*, 2010). However, as the parasite proceeds through multiple asexual cycles of development, it must undergo vast and successive morphological changes. Remodelling of the cell's architecture, metabolism and biochemistry requires huge turnover of proteins. Indeed, during the asexual cycle, each parasite must not only develop from ring, to trophozoite to schizont forms, expanding as it does so but crucially it must generate multiple invasive merozoites. This requires the generation of a number of invasive organelles *de novo*. Once a merozoite has invaded a new erythrocyte, it must then return itself to a form in which it can develop within the erythrocyte, using haemoglobin as its primary nutrient source. This led to the hypothesis that autophagy might play less of a role in stress response, instead contributing more to differentiation. It would seem logical that as the parasite converts between life cycle stages, it would do so with the minimum of waste by activating autophagy to facilitate the reuse of amino acids and other cellular components that were needed during a precise stage in development but are no longer required during the next. The identification of a large, constitutive structure labelled by mCherry-*Pf*ATG8 suggested that the potential requirement for an autophagic process during cellular differentiation had resulted in a variation on the typical autophagic process in *P. falciparum*. The experiments that followed were intended to determine whether mCherry-*Pf*ATG8, or the structure which it labelled, showed any characteristics of an involvement in an autophagic process.

5.3.2 Effect of autophagy regulators on mCherry-*Pf*ATG8

Through the use of compounds known to inhibit or activate autophagy in other organisms, attempts were made to influence the expression, lipidation or localisation of mCherry-*Pf*ATG8. Firstly, wortmannin was used in order to determine what effect the inhibition of *Pf*PI3K might have on mCherry-*Pf*ATG8. It was predicted that, if the labelling of subcellular structures by mCherry-*Pf*ATG8 was PI3K-dependant, as is the labelling of autophagosomes by ATG8 homologues in other organisms (Fujita *et al.*, 2008), then a decrease in mCherry-*Pf*ATG8 labelling may have been expected. The treatments performed did not have any effect on either the expression of mCherry-*Pf*ATG8, or its lipidation and localisation to subcellular structures. This suggested that the labelling of subcellular structures by mCherry-*Pf*ATG8 is not dependent on *Pf*PI3K activity. This suggests that one of the upstream events known to promote ATG8 lipidation in other organisms does not play a role in the lipidation and localisation of *Pf*ATG8. Parasites expressing mCherry-*Pf*ATG8 were also treated with rapamycin and bafilomycin A1. These two compounds have the effect of increasing the number of autophagosomes in other organisms (Chang *et al.*, 2009, Spencer *et al.*, 2009). Rapamycin inhibits mTOR, which itself is an inhibitor of autophagy initiation (Raught *et al.*, 2001). Therefore rapamycin causes an increase in autophagosome formation, mimicking the triggering of autophagy by environmental or intracellular stresses. Bafilomycin A1 causes an increase in autophagosomes, not by influencing the initiation of autophagy but by preventing the turnover of autophagosomes that have already formed. Treatments were performed with these compounds in order to determine whether mCherry-*Pf*ATG8 could be seen to label canonical punctate autophagosomes, when induced to do so, or to determine what the effect on the mCherry-*Pf*ATG8 labelling of subcellular structures might be. Again, no effect on either mCherry-*Pf*ATG8 expression or its lipidation and localisation was seen. This suggested that either canonical punctate autophagosomes can not be induced by these treatments or that they are not labelled by mCherry-*Pf*ATG8. It also showed that the labelling of subcellular structures was not altered by either of these compounds. Together these results suggested that the subcellular structures labelled by mCherry-*Pf*ATG8 appear to be distinct from canonical autophagic process.

These three treatments are commonly used in the study of autophagy in other organisms (Chang *et al.*, 2009, Klionsky *et al.*, 2008, Ponpuak *et al.*, 2009). However, any effect of these compounds on *Pf*ATG8 in *P. falciparum* would rely not only on the involvement of *Pf*ATG8 in an autophagic process but also the presence and conservation of their targets in an autophagic process. This study involved some of the first work to determine whether *Pf*PI3K, TOR or V-type H^+ATPase play any role in an autophagic process in *Plasmodium spp*. Data collected suggest that these three regulators do not contribute to an autophagic process characterised by effects on mCherry-*Pf*ATG8 expression, lipidation and localisation. However, these treatments may need to be optimised further to exclude the possibility that they are involved in an autophagic process.

From what is known about *Pf*PI3K, TOR and V-type H^+ATPase in *P. falciparum*, it might be predicted that their potential involvement in an autophagic process may not be as straight forward as it appears to be in a number of other organisms. *Pf*PI3K has been shown to be excreted into the host erythrocyte, as well as being indicated in the endocytosis of host cell haemoglobin and its transport to the digestive vacuole (Vaid *et al.*, 2010). The product of *Pf*PI3K, PI3P, has been reported in the membranes of the digestive vacuole, apicoplast and seemingly non-endocytic, single membraned vesicles (Tawk *et al.*, 2010). Together, these findings indicate roles for *Pf*PI3K in multiple membrane-facilitated transport processes. In light of this, inhibition of *Pf*PI3K using wortmannin is likely to have a number of effects in addition to inhibiting a potential autophagic process. Experiments to test additional PI3K inhibitors, such as LY294002 or 3-methyladenine could provide further insight into the involvement of PI3K in the regulation of mCherry-*Pf*ATG8 lipidation. While rapamycin has been shown to have anti-malarial properties, it's supposed target has yet to be identified (Monaghan and Bell, 2005). The *P. falciparum* genome does not encode a protein homologous to TOR. The gene identified as having the highest P-value in the bioinformatic screen performed in this study was PFE0765w, which has since been characterised as *Pf*PI3K (Vaid *et al.*, 2010). Either a TOR kinase of sufficient divergence to escape identification through bioinformatic screening is expressed in *P. falciparum* blood stages, or rapamycin causes death through either an alternative or non-specific mechanism. The IC_{50} value of rapamycin has been shown to be in the low μM range (unpublished data

from this lab and (Bell *et al.*, 1994)). The treatment performed in this study was intended to be a dose equivalent to 5 x IC_{50} but for a brief time period, in an attempt to limit off target effects. It could prove valuable to analyse the effects of additional concentrations of rapamycin on mCherry-*Pf*ATG8 expression, lipidation and localisation. The intended target of bafilomycin A1, a V-type H^+ATPase, has been identified and characterised in *P. falciparum* blood stages (Marchesini *et al.*, 2005). It has been shown to be localised to the membrane of the digestive vacuole suggesting a role in the acidification of this lytic compartment but has also been seen to localise to the plasma membranes of the parasite and the host erythrocyte along with membranous structures within the host erythrocyte, suggesting more universal roles in electrochemical balance (Beyenbach and Wieczorek, 2006). Allen and Kirk showed that a 30 min treatment of both isolated FAF6 and D10 parasites and infected erythrocytes with 100 nM bafilomycin A1 was sufficient to cause a partial depolarisation of parasite membrane potential (Allen and Kirk, 2004). This was therefore considered an appropriate experimental procedure to probe for any effect of V-type H^+ATPase inhibition on the expression and localisation of mCherry-*Pf*ATG8. If autophagosomes were generated in intraerythrocytic stage *P. falciparum* parasites, it would seem likely that their target would be the only lytic compartment described in these stages, the digestive vacuole (Dluzewski *et al.*, 2008). Prevention of the acidification of the digestive vacuole could therefore result in an accumulation of autophagosomes. However, in light of the multiple locations and therefore likely roles of the V-type H^+ATPase in addition to the acidification of the digestive vacuole, the effect of bafilomycin A1 is unlikely to be restricted to the digestive vacuole.

5.3.3 Effect of environmental triggers of autophagy on mCherry-*Pf*ATG8

In addition to the intended compound-based manipulation of autophagy regulation, adjusting environmental conditions was also used as a mechanism predicted to trigger autophagy. Amino acid starvation is generally regarded as the gold standard for autophagy induction (Ni *et al.*, 2011). While triggering autophagy through manipulation of the nutrient sensing pathways with rapamycin is commonly used in the study of autophagy, it is known that amino acid starvation results in a more pronounced autophagic upregulation, at least in

mammalian cells, suggesting that other signalling pathways are also triggered (personal communication with Dr. Patrice Codongo). Therefore, it was predicted that while the use of rapamycin had shown to have no effect on mCherry-*Pf*ATG8 expression, lipidation or localisation, which may have been the result of divergency in the pathways responsible for nutrient sensing, amino acid starvation upstream of any cellular response could provide a trigger to a potential autophagic process.

Unlike in yeast and mammalian cells, where removal of the exogenous supply of amino acids has a starvation effect, due to the fact that intraerythrocytic *P. falciparum* parasites acquire most of the nutrients they need through haemoglobin digestion, a different approach is needed in order to starve them of amino acids (Liu *et al.*, 2006). Experiments performed here, with incubation in amino acid-limited medium and pepstatin A or E64 treatment were intended to make parasites more reliant on haemoglobin digestion, by limiting the exogenous supply of amino acids, before blocking this process by inhibition of proteolysis.

It was initially reported that supplementation of culture medium with cysteine, glutamate, glutamine, isoleucine, methionine, proline, and tyrosine was necessary for continuous culture of *P. falciparum* (Divo *et al.*, 1985). Goldberg and co-workers later reported that parasites cultured in medium supplemented with only methionine, cysteine, isoleucine, glutamine and glutamate grew normally but were more sensitive to an aspartic peptidase inhibitor than the same parasites grown in complete medium (Francis *et al.*, 1994). This indicated that growth in limited medium placed parasites in a state where they relied more heavily on haemoglobin degradation than when supplied with an exogenous source of 20 amino acids in complete medium. Later work from Goldberg and co-workers showed that the doubling time of 3D7 parasites when grown in limited medium for 56 h was approximately 50 % longer than when grown in complete medium (Liu *et al.*, 2005). This was shown to be a result of a decrease in multiplicity rate rather than an increase in developmental time suggesting a lack of material from which to generate daughter merozoites. They also reported IC_{50} values of 7.5 ± 0.5 μM and 1.1 ± 0.02 μM for pepstatin A and E64, respectively, for 3D7 parasites grown in complete medium for 72 h. Goldberg and co-workers then expanded experiments using limited medium further (Liu *et al.*, 2006). They showed that it was in fact only isoleucine for which *P. falciparum* was

auxotropic. They showed that supplementation of medium with 147.5 μM isoleucine as the only amino acid allowed parasites to grow within 86 % of those grown in complete medium over 51 h and that these parasites were viable in culture for over 2 months provided isoleucine was present in the culture medium. They also reported IC_{50} values of 60 μM and 4.4 μM for pepstatin A and E64, respectively, for 3D7 parasites grown in complete medium for 62 h. The large difference in the IC_{50} reported for pepstatin A when compared to that previously reported was attributed to contamination of the older stock of pepstatin A. They also showed that these IC_{50} values were lower in parasites that were grown in isoleucine-supplemented medium, dropping to 31 μM and 2.8 μM, respectively. Sharma and co-workers then showed that treatment of 3D7 parasites grown in complete medium with 30 μM pepstatin A resulted in a ~ 5 % growth defect (Vaid *et al.*, 2010). However, when the same parasites were grown in isoleucine-supplemented medium for 96 h prior to treatment with pepstatin A the growth defect observed over 6 days was as great as ~ 80 %. Taken together, these data show that limiting the availability of exogenous amino acids makes parasites more reliant on haemoglobin degradation in order to acquire necessary nutrients. This therefore increases the susceptibility of these parasites to inhibition of haemoglobin degradation. Certainly, the expansion and maintenance of a large repertoire of haemoglobin-degrading peptidases in *P. falciparum* along with evidence collected from genetic knockouts of key peptidases (Liu *et al.*, 2006) indicates that haemoglobin breakdown is important for parasite growth. These data strongly suggest that haemoglobin degradation plays a role in nutrient acquisition, possibly along with other hypotheses based on the requirement to generate space for development and the maintenance of osmotic stability (Dalal and Klemba, 2007).

Experiments using pepstatin A and E64 treatment on parasites expressing mCherry-*Pf*ATG8 were designed with these data in mind. They appeared to show that amino acid starvation has no effect on mCherry-*Pf*ATG8 expression, lipidation or localisation. This may not be too surprising as parasites residing within host erythrocytes would be unlikely to be exposed to an environment of limited amino acid availability for extended periods of time. While it has been shown that isoleucine levels in the circulation of malnourished individuals in malaria endemic areas can drop as low as 10 μM (Baertl *et al.*, 1974) (complete

culture medium contains 381 μM), the impact of this on parasite growth remains largely unexplored. It is therefore questionable whether an artificially created amino acid starvation environment in culture of *P. falciparum*, would represent what the parasite might experience *in vivo*. The necessity of a potential role of autophagy and *Pf*ATG8 in amino acid starvation-induced turnover of cellular material is therefore uncertain. It is possible that the parasite has lost the ability to up-regulate autophagy in response to amino acid starvation in blood stage parasites. It is known that *Plasmodium* parasites have a limited ability to regulate transcription in response to amino acid availability. They lack a canonical TOR homologue (Brennand *et al.*, 2011) and lack the transcription factors and amino acid synthesis pathways that act downstream of eIF2α kinase signalling. While an orthologue of yeast GCN2, an eIF2α kinase responsible for amino acid sensing has been identified and been found to be expressed in blood stage parasites (Fennell *et al.*, 2009), it has been shown not to be essential.

While strong data sets were generated, experiment design proved difficult and a number of factors may have influenced the potency of the treatments performed. Firstly, a 6 h incubation of parasites in limited medium may not have been long enough to place a substantial need for haemoglobin degradation as the sole source of most amino acids. Cultures were transferred to limited medium when parasites were predominantly trophozoites, as these stages are known to be the most metabolically active (Francis *et al.*, 1997) but longer periods of growth in limited or isoleucine-supplemented medium should be performed in future before addition of pepstatin A or E64. Secondly, due to the discrepancies in reported IC_{50} values for pepstatin A and the fact that the parental line of mCherry-*Pf*ATG8 expressing parasites is D10 rather than 3D7, it would certainly be wise to perform IC_{50} experiments in D10 with the same drug stocks used for treatments of mCherry-*Pf*ATG8 expressing parasites. These experiments were designed to give parasites a short exposure to ~ 10 x IC_{50} concentrations of pepstatin A and E64. However, without determining the IC_{50} value in D10 parasites it is unknown how a treatment with 75 μM pepstatin A or 28 μM E64 might relate to their IC_{50} values. A longer (overnight) incubation was performed with 75 μM pepstatin A on parasites expressing mCherry-*Pf*ATG8 and appeared to have resulted in a complete block of growth, suggesting that this concentration of pepstatin A was at least enough to have a profound effect on

parasite growth over this period. Once a robust experiment design was determined there would be a need for repeated executions bearing in mind the degree of variation observed in other experiments. More standardised assays for amino acid starvation of *P. falciparum* intraerythrocytic stages are beginning to be established (Istvan *et al.*, 2011). Further experimentation making use of these recent developments in our understanding of parasite nutritional needs could provide valuable information of the effect of amino acid starvation on the expression and localisation of mCherry-*Pf*ATG8.

Experiments intended to starve parasites of glucose were of a simpler design than those probing amino acid starvation. Removal of complete culture medium and incubation in EBSS instantly removes the exogenous source of glucose and amino acids and parasites quickly die, identified by a rounded and shrunken appearance under microscopy and a visible lack of digestive vacuole activity in late stage parasites. Therefore, experiments were designed to image parasites after just 30 min starvation to ensure that the majority of parasites were still alive at the time of image collection. Again, there was no change in mCherry-*Pf*ATG8 expression, localisation or lipidation, leading to the conclusion that glucose starvation does not influence these processes. Energy sensing in the parasite is poorly understood. *P. falciparum* possesses upstream components of energy sensing - two adenylate kinases and a GTP:AMP phosphotransferase (Rahlfs *et al.*, 2009) and downstream components – an SNF1-type kinase (Bracchi *et al.*, 1996) and a putative AMPK (Talevich *et al.*, 2011). Quite how these components integrate into an energy sensing mechanism is not clear. It is possible that the adaptation to its specialised niche has disrupted the connection between energy sensing and an autophagic response in *P. falciparum*.

A hindering factor to all treatment experiments performed was the variability in the proportion of parasites expressing visible amounts of mCherry-*Pf*ATG8. This likely stems from the variable copy number and transcriptional regulation of episomally maintained plasmids combined with the integration of the plasmid as seen in Chapter 4 (Kong *et al.*, 2009). As this is a common problem, additional methods for transgene expression have been developed and might be worthwhile to explore for *Pf*ATG8 fusion protein expression.

A novel centromeric sequence-based construct has recently been generated that facilitates expression of a transgene from a singly maintained episomal plasmid (Iwanaga *et al.*, 2012). Inclusion of A/T rich centromeric sequences in the construct *Pf*CEN, promotes efficient segregation, stable maintenance, and low copy number via interaction with the kinetochore, the protein:DNA complex formed during chromosome segregation (Maiato *et al.*, 2004). While a low copy number may limit efforts to over-express a transgene by using a heterologous promoter, this could be used in an attempt to mimic expression of an endogenous protein from its genomic locus. If this construct was used to stably express mCherry-*Pf*ATG8 under control of the endogenous *Pfatg*8 promoter region, it would be predicted that expression levels could closely mimic that of the endogenous protein.

As discussed in Chapter 4.3.2, targeted insertion of plasmid elements driving expression of fusion proteins into a specific locus using *att*P and *att*B sites and expression of Bxb1 integrase, can lead to the maintenance of expression of the fusion protein, whilst reducing the episomal plasmid copy number (Adjalley *et al.*, 2010). The G/C rich nature of the *att*B sites means that integration is unlikely to occur elsewhere in the genome (Nkrumah *et al.*, 2006). This system has been used to generate parasite lines with improved proportions of individual parasites expressing a fluorescently tagged protein of interest, in relation to parasite populations maintaining episomal expression constructs (Adjalley *et al.*, 2010). A more homogeneous parasite population could allow for greater reproducibility between experiments as the variation deriving from plasmid copy number and transgene phenotype variability are eliminated. These systems could be used to supplement and build upon the analysis of *Pf*ATG8 through expression of mCherry-*Pf*ATG8 presented here.

From these, and the preceding experiments, designed to explore commonly used methods to manipulate autophagy in other organisms that might trigger a response in parasites characterised by a change in mCherry-*Pf*ATG8 expression, lipidation or localisation, it was concluded that mCherry-*Pf*ATG8 appears not to be involved in an autophagic process. It appeared instead that mCherry-*Pf*ATG8 is lipidated and associates to a subcellular structure constitutively, regardless of how autophagy control mechanisms are influenced. It remained to be determined what the structure labelled by mCherry-*Pf*ATG8 was. If this structure

was not involved in an autophagic process, why did mCherry-*Pf*ATG8 associate with it? In order to characterise the mCherry-*Pf*ATG8-labelled structure, a series of microscopy-based experiments were designed and performed.

5.3.4 Characterisation of mCherry-*Pf*ATG8-labelled structures

Thorough microscopic analysis was performed in order to determine the localisation of mCherry-*Pf*ATG8 and *Pf*ATG8 within the parasite's subcellular architecture. Through the use of LysoTracker and LysoSensor dyes in wild type *P. falciparum*, or parasites expressing mCherry-*Pf*ATG8 it was found that mCherry-*Pf*ATG8-labelled structures were unlikely to be acidified. Of interest was the complexity of the architecture of intraerythrocytic parasites, as shown by the staining observed using LysoSensor 153. While there did appear to be some degree of overlap between the structures stained using LysoSensor 153 and mCherry-*Pf*ATG8-labelled structures, unfortunately the use of a manually operated epifluorescent microscope rather than an automated deconvolving microscope capable of collecting Z-stacks, meant that quantification of the degree of correlation was not possible in the analysis of these treatments.

Canonical autophagosomes become acidified in order for their contents to be degraded by proteolytic enzymes. This usually occurs as a result of fusion with the lytic compartment (Kawai *et al.*, 2007). Identifying a potential acidification of mCherry-*Pf*ATG8-labelled structures may have indicated a role in an autophagy-like process, however, the use of LysoSensor probes proved too limited to properly characterise potential acidification. Modifying the incubation conditions of LysoSensor in an attempt to reduce background staining were unsuccessful and highlighted a potential limitation of this probe in specifically labelling subcellular compartments within intraerythrocytic parasites. There is also some controversy surrounding analysis of intracellular pH in live parasites by fluorescence light microscopy due to the changes in the parasite that occur as a result to light exposure (Wissing *et al.*, 2002).

The appearance of the mCherry-*Pf*ATG8-labelled structures had initially been remarked to be reminiscent of the mitochondrion and apicoplast (van Dooren *et al.*, 2005). In the absence of any evidence to support the notion that these structures represented a novel autophagic structure, it seemed likely that

mCherry-*Pf*ATG8 may in fact be associated with either of these organelles. Indeed, in *T. gondii*, *Tg*ATG8 has been shown to play a role in mitochondrial homeostasis (Besteiro *et al.*, 2011) and in yeast it has been shown that mitochondria participate in autophagy by providing lipids for autophagosome formation via ATG9 shuttling (Reggiori *et al.*, 2005). Of note was the observation that The transcriptional profiles exhibited by *Pf*ATG8 and *Pf*ATG4 bear similarities to that of many apicoplast or mitochondrion-targeted proteins (Bozdech *et al.*, 2003) and such features have been used to identify apicoplast-targeted nuclear-encoded proteins in *T. gondii* (Sheiner *et al.*, 2011).

Analysis of mCherry-*Pf*ATG8 and *Pf*ATG8-labelled structures in relation to the mitochondrion clearly showed that there was no colocalisation between these two structures. This was in starck contrast to *Tg*ATG8 in *T. gondii*. *T. gondii* is often used as a model organism for *Plasmodium spp.*. This work identifies clear differences between *T. gondii* and *P. falciparum* in the role of their respective ATG8 homologues. The fact that *Pf*ATG8 and *Tg*ATG8 share 83.1 % similarity in their amino acid sequences but appear to be involved in very different processes in the two organisms demonstrates that while *T. gondii* can act as a usefull tool in the study of Apicomplexans as a whole, care must be taken in translating findings in *T. gondii* to *Plasmodium spp.*.

The absence of colocalisation with the mitochondrion left the apicoplast as the likely candidate for the structure labelled by mCherry-*Pf*ATG8. Through IFA using antisera raised against His-*Pf*ATG8 and co-expression of mCherry-*Pf*ATG8 in an aE3-GFP apicoplast reporter parasite line, it was shown that there was a close association between the mCherry-*Pf*ATG8-labelled structure and the apicoplast. From images collected it appeared that mCherry-*Pf*ATG8 may label the outer membrane (or membranes) of the apicoplast while aE3-GFP resides in the lumen. Analysis of mCherry-*Pf*ATG8 or *Pf*ATG8 localisation by immunoelectron microscopy would be needed to provide further evidence of this.

A set of experiments were then performed that involved the chemical removal of the apicoplast via chloramphenicol treatment. The apicoplast does not develop in treated parasites and when daughter merozoites form, they do not inherit an apicoplast (Yeh and DeRisi, 2011). The lethality of this outcome is countered by the supplementation with an exogenous source of IPP. These

experiments showed that not only does mCherry-*Pf*ATG8 label the intact apicoplast but that it also associates to vesicles containing apicoplast-targeted protein. These vesicles have been suggested to be formed following budding from the ER but in the absence of an intact apicoplast, they do not have a target membrane with which to fuse in order to deliver their contents (Personal communication with Dr. Ellen Yeh). The fact that mCherry-*Pf*ATG8 associates with these vesicles suggests that it may play a role in the trafficking of apicoplast material from the ER to the apicoplast. The material being trafficked could be protein and or lipids.

The use of a Delta Vision Core deconvolving microscope facilitated quantification of correlation between mCherry-*Pf*ATG8 and aE3-GFP. The Pearson's Coefficient was calculated from Z stacks of whole parasites or individual vesicles using SoftWoRx. This algorithm calculates the degree of overlap between signals from two channels in each pixel in 3 dimensions and returns a coefficient between 1.0, indicating total colocalisation and -1.0, indicating an inverse relationship (Adler and Parmryd, 2010).

Analysis of the correlation between mCherry-*Pf*ATG8 and aE3-GFP showed that there was a strong correlation with a coefficient of 0.69 ± 0.07 (S.D. n = 25). This was significantly different from the coefficient representing the background i.e. comparing the correlation between mCherry-*Pf*ATG8 and Hoechst 33258 (r = 0.21 ± 0.06 (S.D. n = 28)) (unpaired t-test, P = < 0.0001), and showed that there was a large degree of overlap between mCherry-*Pf*ATG8 and aE3-GFP, but that there was not a complete colocalisation. This supported the subjective observations performed by eye. Quantification of the correlation between mCherry-*Pf*ATG8 and GFP-aE3 also allowed for comparison between untreated parasites and parasites in which the apicoplast had been chemically ablated via chloramphenicol treatment. The coefficient of correlation between mCherry-*Pf*ATG8 and aE3-GFP in entire parasites after chloramphenicol treatment was 0.69 ± 0.07 (S.D. n = 28), indicating that the degree of correlation was unaffected by disruption of the apicoplast. The degree of correlation between mCherry-*Pf*ATG8 and aE3-GFP in chloramphenicol treated and IPP rescued cells was also analysed per individual vesicle. Twenty six vesicles were analysed and an average Pearson's coefficient of 0.65 ± 0.06 (S.D. n = 26) was recorded. While

this was found to be marginally significantly different to that derived from analysis of whole parasites (unpaired t test, P = 0.0290) it was concluded that analysis of the entire parasites was a more reliable method for comparing values against untreated parasites.

Unfortunately, as SoftWoRx software does not generate values representing correlation between the two channels separately, the ratio of singly-labelled vesicles to vesicles apparently positive for aE3-GFP and also labelled with mCherry-*Pf*ATG8 could not be ascertained. Subjective analysis by eye suggests that while the majority of vesicles were positive for both mCherry-*Pf*ATG8 and aE3-GFP, populations of vesicles only positive for mCherry-*Pf*ATG8 or aE3-GFP were also present. This could suggest that the labelling of aE3-GFP-positive vesicles by mCherry-*Pf*ATG8 is transient and, as not all mCherry-*Pf*ATG8-positive vesicles are also positive for aE3-GFP, these vesicles contain different cargo destined for the absent apicoplast. The use of dedicated analytical software such as Volocity 3D Image Analysis (Perkin Elmer) could enable more detailed analysis of the relationship between mCherry-*Pf*ATG8 and aE3-GFP in untreated and chloramphenicol treated parasites (Barlow *et al.*, 2010).

5.3.5 Interpreting the relationship between mCherry-*Pf*ATG8 and the apicoplast

Association of *Pf*ATG8 to the apicoplast throughout the development of the organelle suggests that it may have a role in the processes responsible for its expansion, segmentation and inheritance into daughter merozoites. Quite how *Pf*ATG8 contributes to these processes is worthy of further exploration as the apicoplast and the functions it performs are valid drug targets (Fichera and Roos, 1997, Wiesner *et al.*, 2008). Further elucidation of the role of *Pf*ATG8 in apicoplast homeostasis may expose further approaches to target *Plasmodium* parasites in the symptomatic intraerythrocytic stages of their life cycle. In consideration of the attempts to genetically ablate *Pfatg*8 presented in Chapter 4, it now appears that *Pf*ATG8 could potentially play an essential role apicoplast homeostasis. If this were the case then It might be expected that knockout of *Pfatg*8 in wild type parasites might only be achieved if IPP was supplied to parasites exogenously as this has been shown to facilitate chemical ablation of the apicoplast (Yeh and DeRisi, 2011).

It has been reported that ATG8 homologues can be 'incorrectly' associated with the lipids of non-autophagosomal membranes, and only via the activity of ATG4 is lipidation-competent ATG8-I released into the cytosol ready for autophagosome biogenesis (Nakatogawa *et al.*, 2012a). This could possibly explain the labelling of the apicoplast by mCherry-*Pf*ATG8 but the specificity of apicoplast labelling and the fact that mCherry-*Pf*ATG8 does not appear to be released from the apicoplast following any treatment intended to induce autophagy, suggest that this is not the case. 'Chlorophagy' in plant leaves in response to carbon starvation has been reported in *A. thaliana* (Izumi *et al.*, 2010). In this case, the Rubisco-rich stroma of chloroplasts is selectively targeted for degradation in the food vacuole by a subset of autophagosomes called Rubisco-containing bodies. Again, this more canonical form of autophagic degradation does not appear to explain the localisation of *Pf*ATG8 to the apicoplast membrane(s). No autophagosome formation was seen under basal or induced conditions suggesting that the apicoplast is not selectively turned over by a 'chlorophagy'-like process.

The labelling of what appear to be apicoplast-targeted vesicles by mCherry-*Pf*ATG8 following loss of the apicoplast strongly suggests that the association between *Pf*ATG8 and the apicoplast is of physiological relevance. Yeh and DeRisi made use of an acyl carrier protein-GFP fusion protein as a marker for the apicoplast (Yeh and DeRisi, 2011). By showing a similar localisation of a second apicoplast reporter, aE3-GFP, following apicoplast loss, the hypothesis of apicoplast-targeted proteins being delivered to the organelle by vesicular transport has been further supported in this study. Co-labelling of these vesicles could indicate a variety of roles for *Pf*ATG8. Regarding a more classical view of the role of ATG8, labelling of apicoplast-targeted vesicles by mCherry-*Pf*ATG8 could represent an autophagy-like process. If parasites without an apicoplast still translate nuclear-encoded apicoplast-targeted proteins and package them for vesicular trafficking to their absent apicoplast target, accumulation of these redundant vesicles may trigger their targeting for degradation by an autophagy-like process that requires *Pf*ATG8 labelling. However, the lack of lysosomal targets for these autophagosome-like vesicles and the absence of either mCherry or GFP in the digestive vacuole of chloramphenicol treated cells, suggest that these vesicles are not targeted for lytic degradation. Colocalisation between

ATG8-positive autophagosomes and markers for late endosomes and lysosomes has been used to suggest maturation and subsequent acidification of autophagosomes in mammalian cells (Corcelle *et al.*, 2006, Jager *et al.*, 2004). As demonstrated by the absence of apicoplast-targeted vesicle labelling by *Pf*Rab7, it appears that these vesicles do not mature in an autophagosome-like manner. Additional IFA experiments with antibodies against late endosomal markers responsible for vesicle acidification such as the B subunit of V-type H^+ATPase could be used to support this notion further (Karcz *et al.*, 1994). Presented here, however, is strong evidence that apicoplast-targeted vesicles do not mature in a manner similar to autophagosomes or small haemoglobin-containing vesicles involved in haemoglobin degradation (Abu Bakar *et al.*, 2010).

An autophagy-like process would be unlikely to exist in order to deal with such redundant vesicles as they are unlikely to occur under normal parasite development – loss of the apicoplast would ultimately lead to death of the parasite (Fichera and Roos, 1997) so the opportunity to develop and inherit a mechanism to deal with it is unlikely to have arisen. Also, considering the fact that *Pf*ATG8 labels the intact organelle during normal development, it is unlikely that it would be playing a role in a process of degradation. As the parasite undergoes schizogony, the apicoplast is postulated to be expanded and eventually segmented and incorporated into daughter merozoites via an interaction with centrosomes (Striepen *et al.*, 2000, Waller and McFadden, 2005). During this process the apicoplast must expand enormously and only at the very end of schizogony does it segment, requiring an uncharacterised membrane degradation process that facilitates the 'pinching' of all four apicoplast membranes (van Dooren *et al.*, 2005). The temporal and spatial control of this segmentation must be exquisitely tightly regulated. Each daughter merozoite inherits a single apicoplast while no remaining apicoplast material is left behind in the residual body following egress. Considering the fairly homogeneous association of mCherry-*Pf*ATG8 with the entire apicoplast in all intraerythrocytic stages of parasite development, it would seem unlikely that this protein was involved in a degradative process responsible for segmentation at specific points of the apicoplast during the final stages of schizogony.

Evidence presented here supports a hypothesis that *Pf*ATG8 plays a role in apicoplast homeostasis in an autophagy-independent manner. Labelling of aE3-GFP-positive apicoplast-targeted vesicles by mCherry-*Pf*ATG8 suggests that this protein is involved in the delivery of lipids and nuclear-encoded apicoplast-targeted proteins to the apicoplast. An involvement of *Pf*ATG8 in this process was unexpected and appears to represent a *Plasmodium*-specific role for *Pf*ATG8, not shared by the ATG8 homologue in the closely related parasite *T. gondii* (Besteiro *et al.*, 2011). The delivery of apicoplast-targeted proteins to the apicoplast lumen is not fully understood (Lim *et al.*, 2009). While much is known about the Toc and Tic transporters of chloroplasts and hence transport across the two inner most apicoplast membranes, of cyanobacterial (first) and plant origin (second) (Parsons *et al.*, 2007), less is known about the transit of luminal proteins across the two outer most membranes, of secondary endo-symbiont (third) and parasite (fourth) origin (Tonkin *et al.*, 2008). The limiting membrane of the apicoplast is considered, due to either its transient or continuous connection to the membrane of the ER, to be translocated by apicoplast-targeted proteins co-translationally (Waller and McFadden, 2005). The initial signal peptide of the bipartite leader of apicoplast-targeted proteins promotes co-translational translocation across the ER membrane from the cytosol to the ER lumen. The signal peptide is then cleaved leaving the transit peptide. The next stage of the process is poorly understood (Waller and McFadden, 2005). Multiple methods have been proposed for transfer of ER luminal proteins to the space between the limiting and periplastid membranes of the apicoplast. It has been shown that apicoplast-targeted proteins enter the secretory pathway, as removal of the transit peptide from the bipartite leader fused to GFP results in secretion of GFP into the parasitophorous vacuole (Waller *et al.*, 2000). Whether the apicoplast represents a terminal location for a subpopulation of proteins in the secretory pathway, which would require recognition and separation of apicoplast-targeted proteins from other secreted proteins in the ER, or whether all secreted proteins enter the space between the fourth and third membranes of the apicoplast and non-apicoplast-targeted proteins then continue on to the Golgi, has yet to be elucidated (Tonkin *et al.*, 2008). The presence of mCherry-*Pf*ATG8-labelled aE3-GFP-positive vesicles in chloramphenicol treated parasites would support the hypothesis that sorting of apicoplast-targeted proteins occurs in the ER before reaching the apicoplast. Yeh and DeRisi and now this study have

shown that parasites that have lost their apicoplast are viable provided that an exogenous source of IPP was provided (Yeh and DeRisi, 2011). If the secretory pathway relied on first passing through the apicoplast one might presume that loss of the apicoplast would have profound effects on the ability of parasites to target proteins to the host erythrocyte and to its own digestive vacuole. The viability of antibiotic treated parasites in the presence of IPP suggests this not to be the case. It therefore seems most likely that aE3-GFP-positive, mCherry-*Pf*ATG8-labelled vesicles represent apicoplast-targeted vesicles that are distinct from non-apicoplast-targeted secretory vesicles. The apparent absence of these vesicles under normal growth is likely due to their highly transient nature, budding from the ER and fusing with the limiting membrane of the apicoplast in a short space of time (Karnataki *et al.*, 2007). The fact that the apicoplast can not be synthesised *de novo* shows that a protein or proteins encoded by the small apicoplast genome must be essential to apicoplast function (Biswas *et al.*, 2011). It seems possible that in light of the accumulation of apicoplast-targeted vesicles in parasites that have lost their apicoplast, that an apicoplast-encoded factor facilitates the fusion of these vesicles with the inherited organelle. Indeed, treatment of *P. falciparum* with anti-bacterial compounds in order to block apicoplast-encoded gene translation has been noted to disrupt import of nuclear-encoded proteins (Goodman *et al.*, 2007). Delivery of nuclear-encoded proteins to the chloroplasts of plants may share some similarities to the process suggested here. For many years it was suggested that the chloroplast is not part of the endomembrane system, and that transport of proteins into the chloroplast relies solely on Tic and Toc transporters (Jarvis, 2008). However, recent work has lead to the belief that proteins targeted to the membrane(s)/lumen of the chloroplast may also be delivered by small ER/Golgi-derived vesicles (Li and Chiu, 2010). Whether ATG8 plays a role in delivery of chloroplast-targeted material in plants has yet to be determined.

ATG8 homologues are known to interact with a number of other proteins to provide specificity to cargo selection during autophagosome generation (Johansen and Lamark, 2011) and to provide an anchor for which the completed autophagosome can rely on interaction with the microtubule network (Pankiv *et al.*, 2010) and other proteins to dictate the fate of cargoes (Popovic *et al.*, 2012). It is certainly possible that the labelling of apicoplast-targeted vesicles by

mCherry-*Pf*ATG8 represents a role for *Pf*ATG8 in providing an anchor for interaction of these vesicles with the microtubule network or the apicoplast itself. Microtubules have been shown to play important roles in intracellular transport, organelle dynamism, chromosomal segregation and determination of cell shape (Fennell *et al.*, 2008). *P. falciparum* encodes 2 isoforms of alpha-tubulin, and a single form of beta-tubulin, all three of which are expressed in intraerythrocytic stages, with the two alpha-tubulin forms up-regulated during the schizont stage (Bell, 1998). *P. falciparum* also encodes a single copy of gamma-tubulin, which is primarily associated with nuclear division and microtubule assembly (Maessen *et al.*, 1993). Mammalian ATG8 homologues have been shown to interact with microtubules when in both non-lipidated and lipidated forms (Geeraert *et al.*, 2010). This is thought to facilitate the transport of autophagosomes from the cell periphery towards the core of mammalian cells to promote endolysosomal fusion. The separation of completed autophagosomes and lysosomes to stable microtubules and incomplete, forming autophagosomes to dynamic microtubules is thought to provide a physical separation of incomplete autophagosomes from lysosomes to prevent the initiation of fusion before autophagosome cargo has been fully sequestered (Geeraert *et al.*, 2010). The potential role for *Pf*ATG8 in interaction with microtubules is one that should be explored. Microtubules have been shown to be valid drug targets (Fennell *et al.*, 2008, Kappes and Rohrbach, 2007), understanding the role they play in apicoplast homeostasis could facilitate the exploration of further avenues of therapeutic target discovery.

In addition to interaction with the microtubule network, ATG8 homologues are known to act as an anchor point for a number of protein:protein interactions. As available evidence suggests that apicoplast-targeted vesicles are single membraned and that *Pf*ATG8 does not reside within the ER lumen, it would seem that *Pf*ATG8 plays no role in the selective incorporation of apicoplast-targeted proteins into vesicles that bud from the ER. However, it is possible that *Pf*ATG8 conjugated to PE on the outer leaflet of vesicle membranes provides a platform for interaction with other proteins. A large number of proteins have now been shown to specifically interact with ATG8 homologues (Behrends and Fulda, 2012, Johansen and Lamark, 2011, Popovic *et al.*, 2012). LIR (LC3-interacting motif) containing proteins interact directly with ATG8 and usually with other proteins

forming a bridge between ATG8 and the rest of the proteome. Bioinformatic searches for LIR motifs in the proteome of *P. falciparum* did not identify strong candidates for homologues of the LIR containing proteins found in other organisms detailed in Figure 5.26. However, as more and more interactions are identified the divergence of LIR motifs is expanding rapidly. In fact it has recently been reported that ATG1 actually possesses an LIR, and that in addition to its role in the initiation of autophagy, it specifically interacts with ATG8 and is incorporated into autophagosomes (Nakatogawa *et al.*, 2012b). It is possible that *P. falciparum* possesses divergent LIR motif containing proteins that interact with *Pf*ATG8.

The question as to the physiological relevance of the *Plasmodium* specific loop present in *Pf*ATG8 also remains. The observation that the 9 residue extension between the third beta sheet and alpha helix is conserved in all *Plasmodium spp.* suggests that these residues might contribute an additional binding capacity for these proteins. Bioinformatic identification of proteins that may interact with *Pf*ATG8 will therefore need to take this motif into account. A number of immunoprecipatation choices are available to identify protein interacting partners. Affinity pull down experiments with extracts from parasites expressing either mCherry-*Pf*ATG8 or GST-*Pf*ATG8 using RFP-Trap (Chromotek) or GST Protein Interaction Pull–Down (Thermo Scientific) kits, respectively, followed by mass spectrometry could be used initially to identify *Pf*ATG8 interacting partners. Similar experiments were performed to identify the interaction of ATG8 with the cargo recruitment factor p62 (Pankiv *et al.*, 2007), the Rab7 effector FYCO1 (Pankiv *et al.*, 2010) and an array of Rab GTPase-activating proteins (Popovic *et al.*, 2012). Knowledge of proteins with which *Pf*ATG8 might interact would contribute enormously to the elucidation of the role(s) of *Pf*ATG8 in intraerythrocytic parasites.

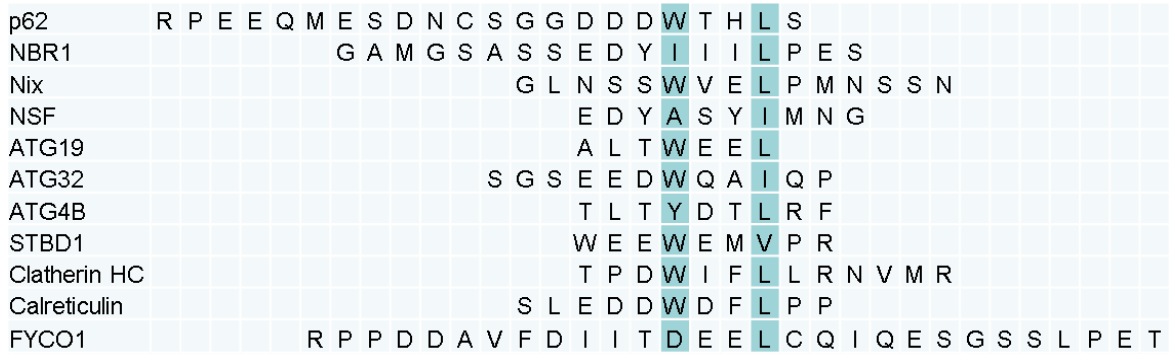

Figure 5.26: Alignment of LC3 Interaction Regions (LIR) of known interaction partners of the yeast and human homologues of ATG8.

The so called WxxL motif (sometimes referred to as an Atg8-family Interaction Motif (AIM)) was first described as forming an interaction with the hydrophobic pocket of ATG8 / LC3 (Noda *et al.*, 2008). As the number of ATG8 / LC3 interacting proteins has grown, so too has the diversity of the WxxL motif (Behrends and Fulda, 2012, Lamark *et al.*, 2009, Noda *et al.*, 2010, Yamaguchi *et al.*, 2010).

The membrane of the apicoplast has been shown to be highly enriched with PE (Personal communication with Prof. Geoffrey McFadden). Another possible function for *Pf*ATG8 in apicoplast biogenesis could be to ensure provision of PE for the membranes of the apicoplast. PE is generated in the ER membrane by CDP-ethanolamine:diacylglycerol ethanolaminephosphotransferase from cytidine diphosphoethanolamine and diacylglycerol (Bisanz *et al.*, 2006) and can also be generated in the mitochondria of mammals from the conversion of phosphatidylserine (PS) by PS decarboxylase (Vance, 2008) . Conjugation of PE by *Pf*ATG8 might sequester PE into the membrane of apicoplast-targeted vesicles budding from the ER. Delivery of these PE-enriched vesicles to the apicoplast would therefore provide PE for the expansion of the apicoplast during schizogony. Neither mCherry-*Pf*ATG8 nor *Pf*ATG8 have been shown to label the ER but in the absence of colocalisation analysis with markers for the ER it can't be discounted that *Pf*ATG8 associates with the membrane of this organelle as well as the apicoplast. However, considering all the images that have been collected showing what appears to be a specific labelling of only the apicoplast or apicoplast-targeted vesicles, it seems more likely that *Pf*ATG8 only associates with apicoplast-targeted vesicles after or very shortly before they bud from the ER. This supports the hypothesis of *Pf*ATG8 playing a role in apicoplast biogenesis dependent on protein:protein interactions, rather than in the supply of PE. However, through protein:protein interactions, *Pf*ATG8 may contribute to the control of the dynamics of the apicoplast limiting membrane. Association of

*Pf*ATG8 to the limiting membrane of the apicoplast may serve as an anchor point for proteins that can alter the properties of this membrane. In other organisms ATG8 itself and through interaction with the ATG12:5:16 complex has been suggested to mediate the curvature of the expanding autophagosomal membrane during the early stages of autophagy (Axe *et al.*, 2008). It is also possible that *Pf*ATG8 may recruit proteins which play roles in membrane curvature, fluidity and rigidity, such as DESAT-1, a lipid desaturase which is suggested to regulate membrane fluidity at the site of autophagosome generation in *Drosophila sp*. (Kohler *et al.*, 2009).

5.3.6 Proposing a model for *Pf*ATG8 function

Based on evidence gathered from biochemical and microscopic analysis of mCherry-*Pf*ATG8 and *Pf*ATG8, a model highlighting the potential roles for *Pf*ATG8 in the intraerythrocytic stages of *P. falciparum* can be drawn (Figure 5.27). Apicoplast-targeted proteins and proteins destined for the secretory pathway which possess a signal peptide are co-translationally transported into the ER lumen. Once within the ER, their signal peptides are cleaved by the signal peptidase complex (Chang *et al.*, 2008, Tuteja *et al.*, 2008). At this point, apicoplast-targeted proteins that possess a transit peptide are recognised and differentially sorted from proteins destined for the secretory pathway. Apicoplast-targeted proteins are recruited to the lumen of single membraned vesicles that bud from the ER. These vesicles may form at sites where the ER membrane is enriched for PE and PI3P. *Pf*ATG8 may also be recruited to forming vesicles shortly before their release, or if not, shortly after. *Pf*ATG8 conjugated to PE on the outer leaflet of apicoplast-targeted vesicles may facilitate their trafficking to the apicoplast through either direct interaction with the microtubule network, or through interaction with proteins that do. *Pf*ATG8 may also play a role in the fusion of vesicles with the apicoplast, either through interaction with *Pf*ATG8 already conjugated to PE on the apicoplast via its ability to promote membrane fusion (Nakatogawa *et al.*, 2007) or through further interaction with other proteins, possibly including an apicoplast-encoded protein. Once fusion has occurred, *Pf*ATG8 remains conjugated to PE on the outer leaflet of the apicoplast's limiting membrane. This might promote fusion of further apicoplast-targeted vesicles or provide a platform for interaction of the apicoplast limiting membrane with other proteins. Proteins targeted to the

apicoplast lumen then cross the remaining three membranes via ERAD-like, TOC and TIC transport (see 1.1.3.3). Once inside the apicoplast lumen, the transit peptide is cleaved by a resident peptidase.

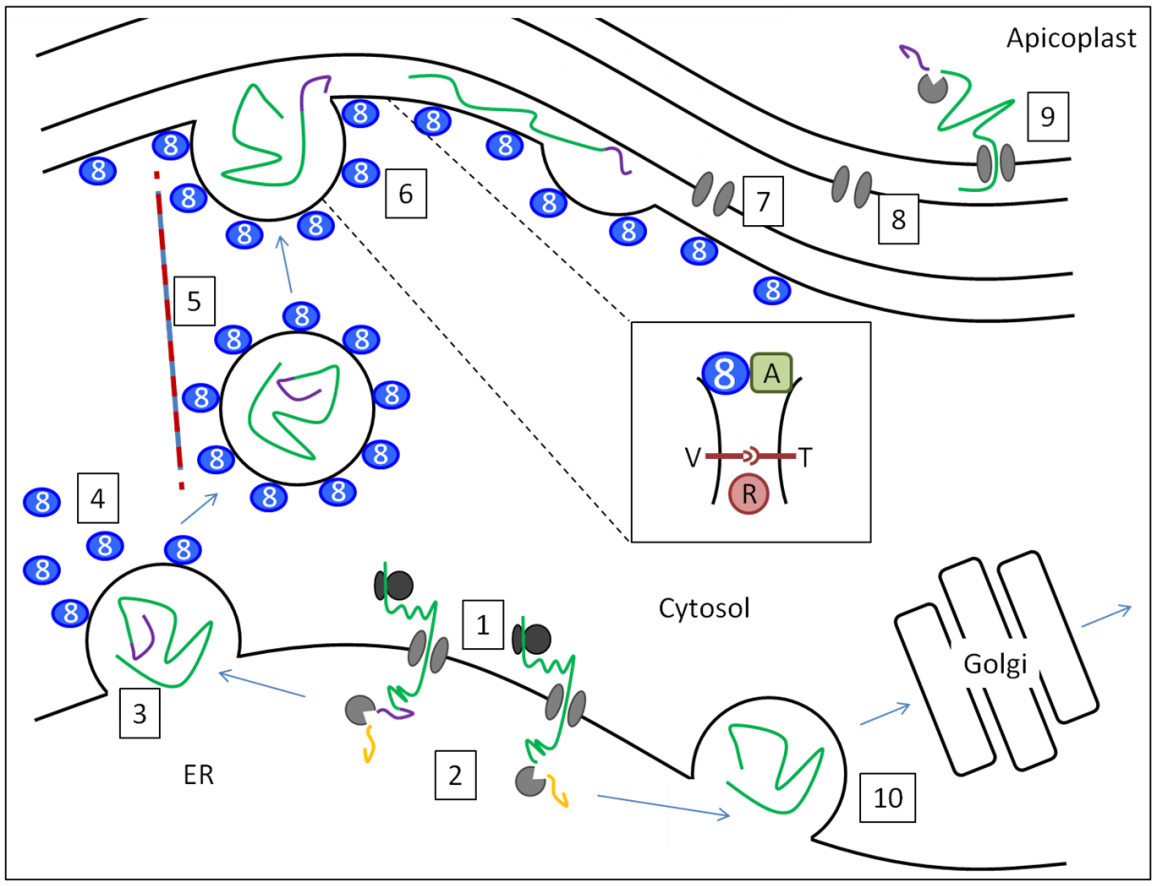

Figure 5.27: Model of *Pf*ATG8 function in apicoplast biogenesis.

1. **Proteins possessing a signal peptide are co-translationally transported to the ER lumen**
2. **The signal peptide is cleaved by ER resident peptidases**
3. **Proteins possessing an transit peptide are recognised and differentially packaged into apicoplast-targeted vesicles**
4. ***Pf*ATG8 is recruited to PE in the outer leaflet of forming or newly formed vesicles**
5. **Apicoplast-targeted vesicles are transported toward the apicoplast, possibly promoted by *Pf*ATG8 interaction with microtubules**
6. **Fusion of the vesicles with the limiting (fourth) membrane of the apicoplast releases the contents into the space between this and the periplastid (third) membrane, possibly facilitated by direct or indirect *Pf*ATG8 interaction with an apicoplast encoded protein (A) (insert) and other nuclear-encoded proteins such as SNAREs (V, T) and Rab GTPases (R)**
7. **Proteins possessing a transit peptide traverse the third membrane via an ERAD-like complex or a TOC apparatus**
8. **Traversal of the second membrane is via a TOC apparatus**
9. **Traversal of the final (first) membrane is via a TIC apparatus. Once inside the apicoplast lumen, the transit peptide is cleaved to produce a mature protein**
10. **ER luminal proteins lacking a transit peptide are packaged into non-apicoplast-targeted vesicles that are not labelled by *Pf*ATG8**

6 Summary and conclusions

This work has been one of the first to explore the potential for an autophagic process in the intraerythrocytic stages of *P. falciparum*. It has added to evidence that autophagy-related proteins, particularly ATG8, may have roles distinct from their involvement in a canonical autophagic process and has opened up an exciting new avenue of research in *P. falciparum*.

Initial identification of potential homologues to a number of ATG and proteins complementary to autophagy suggested that the genome of *P. falciparum* may well encode at least a minimal set of core autophagic genes. This analysis was supported by a later publication (Brennand *et al.*, 2011) which identified a number of the same genes as potential homologues to those in other organisms.

This study went on to focus on one gene in particular, PF10_0193, predicted to encode a homologue to ATG8. Characterisation of the protein product of this gene revealed that *Pf*ATG8 was expressed during intraerythrocytic stages, predominantly during the later stages of parasite development. It was also seen to complement *Sc*ATG8, suggesting that not only was it capable of fulfilling the role of *Sc*ATG8 but also that it was able to interact with the *Sc*ATG8 conjugation machinery present in *S. cerevisiae*. *Pf*ATG8 was seen to localise to subcellular structures in intraerythrocytic stage wild type parasites by IFA. These structures appeared to differ from the classical punctate appearance of autophagosomes observed in other organisms, being elongated and irregularly shaped.

Expression of an mCherry-tagged *Pf*ATG8 fusion protein in *P. falciparum* intraerythrocytic stages was utilised to facilitate further characterisation of *Pf*ATG8. mCherry-*Pf*ATG8 had a similar localisation to endogenous *Pf*ATG8, while a truncated version, mCherry-*Pf*ATG8ΔG was found to be dispersed in the parasite cytosol. It was observed that mCherry-*Pf*ATG8 was processed into a modified form and this processing was dependent on the presence of its C-terminal glycine residue. The modification could also be partially reversed by phospholipase D treatment, shown by a decrease in the more mobile form of mCherry-*Pf*ATG8. These data led to the interpretation that *Pf*ATG8 is modified by conjugation to a lipid, most likely phosphatidylethanolamine. Modification of mCherry-*Pf*ATG8 was required for its localisation to subcellular structures, which

through colocalisation studies was determined to be the apicoplast. It is therefore suggested that endogenous *Pf*ATG8 is also modified via its C-terminal glycine, and that this results in its association with the apicoplast. The processing and localisation of mCherry-*Pf*ATG8 was seen to be unaffected by methods commonly used to manipulate autophagy in other organisms. This suggested that the mechanisms controlling *Pf*ATG8 processing and localisation may be distinct to those usually responsible for the regulation of autophagy in other organisms. Attempts to genetically ablate *Pfatg*8 were inconclusive and the exciting possibility of *Pfatg*8 being an essential gene remains.

Together the findings of this study point to a role for *Pf*ATG8 in apicoplast homeostasis, possibly in membrane-mediated trafficking of apicoplast-targeted components. This could represent a novel role for *Pf*ATG8 but it does not preclude the possibility of *Pf*ATG8 being involved in a canonical autophagy process at other stages of parasite development or under different growth conditions. A role for *Pf*ATG8 in apicoplast homeostasis might also be conserved in other Apicomplexan parasites possessing an apicoplast but has not yet been identified in *T. gondii*. In this closely related organism an association of *Tg*ATG8 with the apicoplast has not been reported, indicating a key difference between teh ATG8 homologues in these two organisms. Further exploration of the involvement of *Pf*ATG8 in this process might give rise to the identification of novel therapeutic targets based around the apicoplast, which has already been proven to be essential and a valid drug target (Wiesner *et al.*, 2008). By targeting *Pf*ATG8, it may be found that parasites can be killed due to defects in the apicoplast. While the amino acid sequence similarity between *Pf*ATG8 and human ATG8 homologues is fairly high, there remains the intriguing presence of the *Plasmodium*-specific loop formed by the 9 amino acid sequence absent in other ATG8 homologues. If *Pf*ATG8 was found to be essential, there is potential scope for design of inhibitors specific for *Pf*ATG8 that would not inhibit the human ATG8 homologues. Also, as the role of *Pf*ATG8 is likely, to some degree, rely on the contribution of proteins involved in its conjugation pathway e.g. ATG3, inhibition of *Pf*ATG8 conjugation may prove to be a valid therapeutic strategy.

While this thesis was being compiled, an article was published entitled ‘Autophagy-Related Atg8 Localizes to the Apicoplast of the Human Malaria

Parasite *Plasmodium falciparum'* (Kitamura *et al.*, 2012). Experiments reported in this article were similar to those performed as a part of this study and reported here. Crucially, the authors of the published article detail similar experimental outcomes and draw conclusions in line with those presented here.

The results of a bioinformatic screen identified the same genes encoding potential homologues for Vps34, ATG18, ATG12, ATG7, ATG5, ATG3, ATG4, ATG7 and ATG8 as those identified in this study.

Similar characterisation of the potential *Pf*ATG8 homologue elucidated that the protein appears to be more abundant later in intraerythrocytic development with a peak in the schizont stages. They discovered that the protein appeared to be present predominantly as a modified form, by comparison to *Pf*ATG8 expressed in mammalian cells which appears not to be modified. They also showed that treatment of intraerythrocytic *P. falciparum* with chloroquine (CQ) did not affect the abundance of *Pf*ATG8 which led to the conclusion that *Pf*ATG8 is not involved in an autophagic process.

Localisation studies then reported that *Pf*ATG8 appeared to be associated with the apicoplast, and by immunoelectron microscopy, they showed that *Pf*ATG8 localised to the membranes of the apicoplast rather than its lumen. Finally they reported that neither CQ nor wortmannin treatment of intraerythrocytic *P. falciparum* affected the localisation of *Pf*ATG8 leading to the conclusion that the association of *Pf*ATG8 to the apicoplast membrane(s) is independent of PI3K function and therefore appears to represent a role distinct from autophagy.

While similar conclusions were expressed in this article, the methodologies used to gain results were, in some cases, very different to those used in this study. This article relied on the use of antibodies raised against *Pf*ATG8, which enabled immunoelectron microscopy aiming to detect *Pf*ATG8 to be performed. This confirmed that *Pf*ATG8 localises to the membrane(s) of the apicoplast and not to its lumen, a conclusion also drawn from the thorough analysis of mCherry-*Pf*ATG8 localisation in this study. The difficulties encountered in generating robust antisera specific for *Pf*ATG8 in this study precluded the possibility of performing immunoelectron microscopy. It is therefore reassuring to see data attained by independent research that supports the conclusions drawn in this

study. While the use of immunoelectron microscopy is often regarded as the gold standard of protein localisation methodologies, a number of key findings presented as part of this study can also add to that of the published article. Complementation of *Sc*ATG8 was crucial to determining that PF10_0193 encodes a functional homologue of *Sc*ATG8. The generation of *P. falciparum* lines expressing mCherry-*Pf*ATG8 and mCherry-*Pf*ATG8ΔG enabled experiments that showed that the C-terminal glycine residue of *Pf*ATG8 is essential for its modification and that the modified form is sensitive to phospholipase D treatment. Chloramphenicol treatment to disrupt the apicoplast in *P. falciparum* intraerythrocytic stages also led to the key finding that mCherry-*Pf*ATG8 and by inference *Pf*ATG8 associates with structures postulated to be apicoplast-targeted vesicles. These vesicles did not show additional features of canonical autophagsomes, such as labelling by *Pf*Rab7, indicating a likely anabolic rather than catabolic role. This led to the conclusion that *Pf*ATG8 might be involved in the processes that provide the apicoplast with proteins and or lipids from the ER. This parasite-specific role for *Pf*ATG8, which may or may not be in addition to its participation in canonical autophagy, was also the main conclusion of Kitamura *et al*. The work presented here therefore appears to be complimentary to and also builds upon that now published.

This work has begun the characterisation of *Pf*ATG8 in *P. falciparum* erythrocytic stages. As is often the case, exploring the role of this protein has created more questions than answers. The original hypothesis of this study was that *P. falciparum* was likely to make use of the conserved eukaryotic process of autophagy to face the differentiation and adaptation challenges encountered during its complex life cycle. It appears that while the autophagy-related protein ATG8, central to autophagy in other organisms, is conserved, along with its ability to become lipidated and associate with membranes, its involvement in an autophagic process in *P. falciparum* erythrocytic stages has not been maintained. The association of this protein to the membranes of the apicoplast or apicoplast-targeted vesicles appears to be independent of the regulatory mechanisms known to modulate autophagy in other organisms. This leaves the questions:-

Is *Pf*ATG8 involved in autophagy in other life cycle stages or under different growth conditions?

- Attempts to inhibit or induce and autophagic response in *P. falciparum* erythrocytic stages did not have an effect on *Pf*ATG8 expression, lipidation or localisation. However, further experimentation is required to exclude the possibility of *Pf*ATG8 contributing to an autophagic response under certain stimuli.

What factors control the lipidation of *Pf*ATG8 and therefore its association to membranes?

- *Pf*ATG8 is translated in a lipidation-competent form. When the temporal regulation of expression was altered by expression of a fusion tagged mCherry-*Pf*ATG8 copy, lipidation of this protein was dependent on cell cycle stage. This suggests that the lipidation of *Pf*ATG8 is not entirely dependent on the temporal control of expression.

With what proteins does *Pf*ATG8 interact?

- ATG8 homologues in other organisms are known to interact with many other proteins, in particular adapter proteins which link ATG8 with the rest of the proteome. Identification of *Pf*ATG8 binding partners could shed light on the function of this protein, particularly in relation to apicoplast homeostasis.

Can *Pf*ATG8 be the focus of a therapeutic strategy?

- Expanding our basic understanding of parasite biology is crucial for the identification of much needed novel drug targets. It appears from this study that the role of *Pf*ATG8 and certain features of the protein itself vary from the ATG8 homologues present in humans. This leads to the exciting proposition that *Pf*ATG8, or the process(es) in which it participates, might prove to be valid drug targets.

This is by no means an exhaustive list of remaining questions but these issues could potentially be resolved by future experimentation exploring the *Pf*ATG8 protein in *P. falciparum* and its homologues in other species of *Plasmodium* parasite.

Bibliography

ABU BAKAR, N., KLONIS, N., HANSSEN, E., CHAN, C. & TILLEY, L. 2010. Digestive-vacuole genesis and endocytic processes in the early intraerythrocytic stages of *Plasmodium falciparum*. *J Cell Sci,* 123**,** 441-50.

ADJALLEY, S. H., LEE, M. C. & FIDOCK, D. A. 2010. A method for rapid genetic integration into *Plasmodium falciparum* utilizing mycobacteriophage Bxb1 integrase. *Methods Mol Biol,* 634**,** 87-100.

ADLER, J. & PARMRYD, I. 2010. Quantifying colocalization by correlation: the Pearson correlation coefficient is superior to the Mander's overlap coefficient. *Cytometry A,* 77**,** 733-42.

AGARRABERES, F. A., TERLECKY, S. R. & DICE, J. F. 1997. An intralysosomal hsp70 is required for a selective pathway of lysosomal protein degradation. *J Cell Biol,* 137**,** 825-34.

AHN, S. Y., SHIN, M. Y., KIM, Y. A., YOO, J. A., KWAK, D. H., JUNG, Y. J., JUN, G., RYU, S. H., YEOM, J. S., AHN, J. Y., CHAI, J. Y. & PARK, J. W. 2008. Magnetic separation: a highly effective method for synchronization of cultured erythrocytic *Plasmodium falciparum*. *Parasitol Res,* 102**,** 1195-200.

ALANO, P. 2007. *Plasmodium falciparum* gametocytes: still many secrets of a hidden life. *Mol Microbiol,* 66**,** 291-302.

ALBERTI, A., MICHELET, X., DJEDDI, A. & LEGOUIS, R. 2010. The autophagosomal protein LGG-2 acts synergistically with LGG-1 in dauer formation and longevity in *C. elegans*. *Autophagy,* 6.

ALLAN, B. B., MOYER, B. D. & BALCH, W. E. 2000. Rab1 recruitment of p115 into a cis-SNARE complex: programming budding COPII vesicles for fusion. *Science,* 289**,** 444-8.

ALLEN, R. J. & KIRK, K. 2004. The membrane potential of the intraerythrocytic malaria parasite *Plasmodium falciparum*. *J Biol Chem,* 279**,** 11264-72.

ALONSO, P. L., BROWN, G., AREVALO-HERRERA, M., BINKA, F., CHITNIS, C., COLLINS, F., DOUMBO, O. K., GREENWOOD, B., HALL, B. F., LEVINE, M. M., MENDIS, K., NEWMAN, R. D., PLOWE, C. V., RODRIGUEZ, M. H., SINDEN, R., SLUTSKER, L. & TANNER, M. 2011. A research agenda to underpin malaria eradication. *PLoS Med,* 8**,** e1000406.

ALVAREZ, V. E., KOSEC, G., SANT'ANNA, C., TURK, V., CAZZULO, J. J. & TURK, B. 2008. Autophagy is involved in nutritional stress response and differentiation in *Trypanosoma cruzi*. *J Biol Chem,* 283**,** 3454-64.

AMAR, N., LUSTIG, G., ICHIMURA, Y., OHSUMI, Y. & ELAZAR, Z. 2006. Two newly identified sites in the ubiquitin-like protein Atg8 are essential for autophagy. *EMBO Rep,* 7**,** 635-42.

ANGRISANO, F., RIGLAR, D. T., STURM, A., VOLZ, J. C., DELVES, M. J., ZUCCALA, E. S., TURNBULL, L., DEKIWADIA, C., OLSHINA, M. A., MARAPANA, D. S., WONG, W., MOLLARD, V., BRADIN, C. H., TONKIN, C. J., GUNNING, P. W., RALPH, S. A., WHITCHURCH, C. B., SINDEN, R. E., COWMAN, A. F., MCFADDEN, G. I. & BAUM, J. 2012. Spatial localisation of actin filaments across developmental stages of the malaria parasite. *PLoS One,* 7**,** e32188.

ARMSTRONG, C. M. & GOLDBERG, D. E. 2007. An FKBP destabilization domain modulates protein levels in *Plasmodium falciparum*. *Nat Methods,* 4**,** 1007-9.

AXE, E. L., WALKER, S. A., MANIFAVA, M., CHANDRA, P., RODERICK, H. L., HABERMANN, A., GRIFFITHS, G. & KTISTAKIS, N. T. 2008. Autophagosome formation from membrane compartments enriched in phosphatidylinositol

3-phosphate and dynamically connected to the endoplasmic reticulum. *J Cell Biol,* 182**,** 685-701.

BABA, M., OSUMI, M., SCOTT, S. V., KLIONSKY, D. J. & OHSUMI, Y. 1997. Two distinct pathways for targeting proteins from the cytoplasm to the vacuole/lysosome. *J Cell Biol,* 139**,** 1687-95.

BABA, M., TAKESHIGE, K., BABA, N. & OHSUMI, Y. 1994. Ultrastructural analysis of the autophagic process in yeast: detection of autophagosomes and their characterization. *J Cell Biol,* 124**,** 903-13.

BABIKER, H. A., ABDEL-MUHSIN, A. M., RANFORD-CARTWRIGHT, L. C., SATTI, G. & WALLIKER, D. 1998. Characteristics of *Plasmodium falciparum* parasites that survive the lengthy dry season in eastern Sudan where malaria transmission is markedly seasonal. *Am J Trop Med Hyg,* 59**,** 582-90.

BAERTL, J. M., PLACKO, R. P. & GRAHAM, G. G. 1974. Serum proteins and plasma free amino acids in severe malnutrition. *Am J Clin Nutr,* 27**,** 733-42.

BAKER, D. A. 2010. Malaria gametocytogenesis. *Mol Biochem Parasitol,* 172**,** 57-65.

BALDACCI, P. & MENARD, R. 2004. The elusive malaria sporozoite in the mammalian host. *Mol Microbiol,* 54**,** 298-306.

BALU, B., SHOUE, D. A., FRASER, M. J., JR. & ADAMS, J. H. 2005. High-efficiency transformation of *Plasmodium falciparum* by the lepidopteran transposable element piggyBac. *Proc Natl Acad Sci U S A,* 102**,** 16391-6.

BANNISTER, L. H., HOPKINS, J. M., FOWLER, R. E., KRISHNA, S. & MITCHELL, G. H. 2000. A brief illustrated guide to the ultrastructure of *Plasmodium falciparum* asexual blood stages. *Parasitol Today,* 16**,** 427-33.

BANNISTER, L. H. & MITCHELL, G. H. 2009. The malaria merozoite, forty years on. *Parasitology,* 136**,** 1435-44.

BARLOW, A. L., MACLEOD, A., NOPPEN, S., SANDERSON, J. & GUERIN, C. J. 2010. Colocalization analysis in fluorescence micrographs: verification of a more accurate calculation of pearson's correlation coefficient. *Microsc Microanal,* 16**,** 710-24.

BAUM, J., PAPENFUSS, A. T., MAIR, G. R., JANSE, C. J., VLACHOU, D., WATERS, A. P., COWMAN, A. F., CRABB, B. S. & DE KONING-WARD, T. F. 2009. Molecular genetics and comparative genomics reveal RNAi is not functional in malaria parasites. *Nucleic Acids Res,* 37**,** 3788-98.

BAUM, J., RICHARD, D., HEALER, J., RUG, M., KRNAJSKI, Z., GILBERGER, T. W., GREEN, J. L., HOLDER, A. A. & COWMAN, A. F. 2006. A conserved molecular motor drives cell invasion and gliding motility across malaria life cycle stages and other apicomplexan parasites. *J Biol Chem,* 281**,** 5197-208.

BAUMEISTER, S., WINTERBERG, M., PRZYBORSKI, J. M. & LINGELBACH, K. 2010. The malaria parasite *Plasmodium falciparum*: cell biological peculiarities and nutritional consequences. *Protoplasma,* 240**,** 3-12.

BEHRENDS, C. & FULDA, S. 2012. Receptor proteins in selective autophagy. *Int J Cell Biol,* 2012**,** 673290.

BEHRENDS, C., SOWA, M. E., GYGI, S. P. & HARPER, J. W. 2010. Network organization of the human autophagy system. *Nature,* 466**,** 68-76.

BELL, A. 1998. Microtubule inhibitors as potential antimalarial agents. *Parasitol Today,* 14**,** 234-40.

BELL, A., WERNLI, B. & FRANKLIN, R. M. 1994. Roles of peptidyl-prolyl cis-trans isomerase and calcineurin in the mechanisms of antimalarial action of cyclosporin A, FK506, and rapamycin. *Biochem Pharmacol,* 48**,** 495-503.

BELLU, A. R. & KIEL, J. A. 2003. Selective degradation of peroxisomes in yeasts. *Microsc Res Tech,* 61**,** 161-70.

BERG, T. O., FENGSRUD, M., STROMHAUG, P. E., BERG, T. & SEGLEN, P. O. 1998. Isolation and characterization of rat liver amphisomes. Evidence for fusion of autophagosomes with both early and late endosomes. *J Biol Chem,* 273**,** 21883-92.

BESTEIRO, S., BROOKS, C. F., STRIEPEN, B. & DUBREMETZ, J. F. 2011. Autophagy protein Atg3 is essential for maintaining mitochondrial integrity and for normal intracellular development of *Toxoplasma gondii* tachyzoites. *PLoS Pathog,* 7**,** e1002416.

BESTEIRO, S., WILLIAMS, R. A., MORRISON, L. S., COOMBS, G. H. & MOTTRAM, J. C. 2006. Endosome sorting and autophagy are essential for differentiation and virulence of *Leishmania major*. *J Biol Chem,* 281**,** 11384-96.

BEYENBACH, K. W. & WIECZOREK, H. 2006. The V-type H+ ATPase: molecular structure and function, physiological roles and regulation. *J Exp Biol,* 209**,** 577-89.

BIRMINGHAM, C. L., SMITH, A. C., BAKOWSKI, M. A., YOSHIMORI, T. & BRUMELL, J. H. 2006. Autophagy controls *Salmonella* infection in response to damage to the *Salmonella*-containing vacuole. *J Biol Chem,* 281**,** 11374-83.

BISANZ, C., BASTIEN, O., GRANDO, D., JOUHET, J., MARECHAL, E. & CESBRON-DELAUW, M. F. 2006. *Toxoplasma gondii* acyl-lipid metabolism: de novo synthesis from apicoplast-generated fatty acids versus scavenging of host cell precursors. *Biochem J,* 394**,** 197-205.

BISSETT, R. E. 2009. *Lipoic Acid Metabolism in Leishmania major*. PhD, University of Glasgow.

BISWAS, S., LIM, E. E., GUPTA, A., SAQIB, U., MIR, S. S., SIDDIQI, M. I., RALPH, S. A. & HABIB, S. 2011. Interaction of apicoplast-encoded elongation factor (EF) EF-Tu with nuclear-encoded EF-Ts mediates translation in the *Plasmodium falciparum* plastid. *Int J Parasitol,* 41**,** 417-27.

BLOMMAART, E. F., KRAUSE, U., SCHELLENS, J. P., VREELING-SINDELAROVA, H. & MEIJER, A. J. 1997. The phosphatidylinositol 3-kinase inhibitors wortmannin and LY294002 inhibit autophagy in isolated rat hepatocytes. *Eur J Biochem,* 243**,** 240-6.

BONILLA, J. A., BONILLA, T. D., YOWELL, C. A., FUJIOKA, H. & DAME, J. B. 2007. Critical roles for the digestive vacuole plasmepsins of *Plasmodium falciparum* in vacuolar function. *Mol Microbiol,* 65**,** 64-75.

BOTTE, C. Y., YAMARYO-BOTTE, Y., JANOUSKOVEC, J., RUPASINGHE, T., KEELING, P. J., CRELLIN, P., COPPEL, R. L., MARECHAL, E., MCCONVILLE, M. J. & MCFADDEN, G. I. 2011. Identification of plant-like galactolipids in *Chromera velia*, a photosynthetic relative of malaria parasites. *J Biol Chem,* 286**,** 29893-903.

BOUQUET, J., RIVAUD, M., CHEVALLEY, S., DEHARO, E., JULLIAN, V. & VALENTIN, A. 2012. Biological activities of nitidine, a potential anti-malarial lead compound. *Malar J,* 11**,** 67.

BOYLE, M. J., WILSON, D. W., RICHARDS, J. S., RIGLAR, D. T., TETTEH, K. K., CONWAY, D. J., RALPH, S. A., BAUM, J. & BEESON, J. G. 2010. Isolation of viable *Plasmodium falciparum* merozoites to define erythrocyte invasion events and advance vaccine and drug development. *Proc Natl Acad Sci U S A,* 107**,** 14378-83.

BOZDECH, Z., LLINAS, M., PULLIAM, B. L., WONG, E. D., ZHU, J. & DERISI, J. L. 2003. The transcriptome of the intraerythrocytic developmental cycle of *Plasmodium falciparum*. *PLoS Biol,* 1**,** E5.

BRACCHI, V., LANGSLEY, G., THELU, J., ELING, W. & AMBROISE-THOMAS, P. 1996. *Pf*KIN, an SNF1 type protein kinase of *Plasmodium falciparum* predominantly expressed in gametocytes. *Mol Biochem Parasitol,* 76**,** 299-303.

BRADFORD, M. M. 1976. A rapid and sensitive method for the quantitation of microgram quantities of protein utilizing the principle of protein-dye binding. *Anal Biochem,* 72**,** 248-54.

BRENNAND, A., GUALDRON-LOPEZ, M., COPPENS, I., RIGDEN, D. J., GINGER, M. L. & MICHELS, P. A. 2011. Autophagy in parasitic protists: unique features and drug targets. *Mol Biochem Parasitol,* 177**,** 83-99.

CAO, Y. & KLIONSKY, D. J. 2008. New insights into autophagy using a multiple knockout strain. *Autophagy,* 4**,** 1073-5.

CARO, F., MILLER, M. G. & DERISI, J. L. 2012. Plate-based transfection and culturing technique for genetic manipulation of *Plasmodium falciparum*. *Malar J,* 11**,** 22.

CARROLL, D. 2011. Zinc-finger nucleases: a panoramic view. *Curr Gene Ther,* 11**,** 2-10.

CHANG, H. H., FALICK, A. M., CARLTON, P. M., SEDAT, J. W., DERISI, J. L. & MARLETTA, M. A. 2008. N-terminal processing of proteins exported by malaria parasites. *Mol Biochem Parasitol,* 160**,** 107-15.

CHANG, Y. Y., JUHASZ, G., GORAKSHA-HICKS, P., ARSHAM, A. M., MALLIN, D. R., MULLER, L. K. & NEUFELD, T. P. 2009. Nutrient-dependent regulation of autophagy through the target of rapamycin pathway. *Biochem Soc Trans,* 37**,** 232-6.

CHAPELAND-LECLERC, F., BOUCHOUX, J., GOUMAR, A., CHASTIN, C., VILLARD, J. & NOEL, T. 2005. Inactivation of the FCY2 gene encoding purine-cytosine permease promotes cross-resistance to flucytosine and fluconazole in Candida lusitaniae. *Antimicrob Agents Chemother,* 49**,** 3101-8.

CHEN, Q., BARRAGAN, A., FERNANDEZ, V., SUNDSTROM, A., SCHLICHTHERLE, M., SAHLEN, A., CARLSON, J., DATTA, S. & WAHLGREN, M. 1998. Identification of *Plasmodium falciparum* erythrocyte membrane protein 1 (*Pf*EMP1) as the rosetting ligand of the malaria parasite *P. falciparum*. *J Exp Med,* 187**,** 15-23.

CHEN, Y. & KLIONSKY, D. J. 2011. The regulation of autophagy - unanswered questions. *J Cell Sci,* 124**,** 161-70.

CHEONG, H. & KLIONSKY, D. J. 2008. Biochemical methods to monitor autophagy-related processes in yeast. *Methods Enzymol,* 451**,** 1-26.

CHRISTOPHER, S. F., J. 1939. Experiments with isolated malaria parasites (Plasmodium knowlesi) free from red cells. *Ann Trop Med Parasitol.,* 1939**,** 161-170.

CHUA, C. E., GAN, B. Q. & TANG, B. L. 2011. Involvement of members of the Rab family and related small GTPases in autophagosome formation and maturation. *Cell Mol Life Sci,* 68**,** 3349-58.

CORCELLE, E., NEBOUT, M., BEKRI, S., GAUTHIER, N., HOFMAN, P., POUJEOL, P., FENICHEL, P. & MOGRABI, B. 2006. Disruption of autophagy at the maturation step by the carcinogen lindane is associated with the sustained mitogen-activated protein kinase/extracellular signal-regulated kinase activity. *Cancer Res,* 66**,** 6861-70.

COTTET-ROUSSELLE, C., RONOT, X., LEVERVE, X. & MAYOL, J. F. 2011. Cytometric assessment of mitochondria using fluorescent probes. *Cytometry A,* 79**,** 405-25.

COWMAN, A. F. & CRABB, B. S. 2006. Invasion of red blood cells by malaria parasites. *Cell,* 124**,** 755-66.

COX, F. E. 2010. History of the discovery of the malaria parasites and their vectors. *Parasit Vectors,* 3**,** 5.

CRABB, B. S. 2002. Transfection technology and the study of drug resistance in the malaria parasite *Plasmodium falciparum*. *Drug Resist Updat,* 5**,** 126-30.

CRABB, B. S., RUG, M., GILBERGER, T. W., THOMPSON, J. K., TRIGLIA, T., MAIER, A. G. & COWMAN, A. F. 2004. Transfection of the human malaria parasite *Plasmodium falciparum*. *Methods Mol Biol,* 270**,** 263-76.

CROSNIER, C., BUSTAMANTE, L. Y., BARTHOLDSON, S. J., BEI, A. K., THERON, M., UCHIKAWA, M., MBOUP, S., NDIR, O., KWIATKOWSKI, D. P., DURAISINGH, M. T., RAYNER, J. C. & WRIGHT, G. J. 2011. Basigin is a receptor essential for erythrocyte invasion by *Plasmodium falciparum*. *Nature,* 480**,** 534-7.

CROWE, J., DOBELI, H., GENTZ, R., HOCHULI, E., STUBER, D. & HENCO, K. 1994. 6xHis-Ni-NTA chromatography as a superior technique in recombinant protein expression/purification. *Methods Mol Biol,* 31**,** 371-87.

DALAL, S. & KLEMBA, M. 2007. Roles for two aminopeptidases in vacuolar hemoglobin catabolism in *Plasmodium falciparum*. *J Biol Chem,* 282**,** 35978-87.

DE KONING-WARD, T. F., JANSE, C. J. & WATERS, A. P. 2000. The development of genetic tools for dissecting the biology of malaria parasites. *Annu Rev Microbiol,* 54**,** 157-85.

DEARNLEY, M. K., YEOMAN, J. A., HANSSEN, E., KENNY, S., TURNBULL, L., WHITCHURCH, C. B., TILLEY, L. & DIXON, M. W. 2012. Origin, composition, organization and function of the inner membrane complex of *Plasmodium falciparum* gametocytes. *J Cell Sci,* 125**,** 2053-63.

DEITSCH, K., DRISKILL, C. & WELLEMS, T. 2001. Transformation of malaria parasites by the spontaneous uptake and expression of DNA from human erythrocytes. *Nucleic Acids Res,* 29**,** 850-3.

DENNEMARKER, J., LOHMULLER, T., MULLER, S., AGUILAR, S. V., TOBIN, D. J., PETERS, C. & REINHECKEL, T. 2010. Impaired turnover of autophagolysosomes in cathepsin L deficiency. *Biol Chem,* 391**,** 913-22.

DENNIS, P. B. & MERCER, C. A. 2009. The GST-BHMT assay and related assays for autophagy. *Methods Enzymol,* 452**,** 97-118.

DEROCHER, A. E., KARNATAKI, A., VANEY, P. & PARSONS, M. 2012. Apicoplast targeting of a *Toxoplasma gondii* transmembrane protein requires a cytosolic tyrosine-based motif. *Traffic,* 13**,** 694-704.

DESAI, M., TER KUILE, F. O., NOSTEN, F., MCGREADY, R., ASAMOA, K., BRABIN, B. & NEWMAN, R. D. 2007. Epidemiology and burden of malaria in pregnancy. *Lancet Infect Dis,* 7**,** 93-104.

DESJARDINS, R. E., CANFIELD, C. J., HAYNES, J. D. & CHULAY, J. D. 1979. Quantitative assessment of antimalarial activity *in vitro* by a semiautomated microdilution technique. *Antimicrob Agents Chemother,* 16**,** 710-8.

DICE, J. F. 1990. Peptide sequences that target cytosolic proteins for lysosomal proteolysis. *Trends Biochem Sci,* 15**,** 305-9.

DIVO, A. A., GEARY, T. G., DAVIS, N. L. & JENSEN, J. B. 1985. Nutritional requirements of *Plasmodium falciparum* in culture. I. Exogenously supplied dialyzable components necessary for continuous growth. *J Protozool,* 32**,** 59-64.

DLUZEWSKI, A. R., LING, I. T., HOPKINS, J. M., GRAINGER, M., MARGOS, G., MITCHELL, G. H., HOLDER, A. A. & BANNISTER, L. H. 2008. Formation of the food vacuole in *Plasmodium falciparum*: a potential role for the 19

kDa fragment of merozoite surface protein 1 (MSP1(19)). *PLoS One,* 3**,** e3085.

DURAISINGH, M. T., TRIGLIA, T. & COWMAN, A. F. 2002. Negative selection of *Plasmodium falciparum* reveals targeted gene deletion by double crossover recombination. *Int J Parasitol,* 32**,** 81-9.

DURAISINGH, M. T., TRIGLIA, T., RALPH, S. A., RAYNER, J. C., BARNWELL, J. W., MCFADDEN, G. I. & COWMAN, A. F. 2003. Phenotypic variation of *Plasmodium falciparum* merozoite proteins directs receptor targeting for invasion of human erythrocytes. *EMBO J,* 22**,** 1047-57.

DUSZENKO, M., GINGER, M. L., BRENNAND, A., GUALDRON-LOPEZ, M., COLOMBO, M. I., COOMBS, G. H., COPPENS, I., JAYABALASINGHAM, B., LANGSLEY, G., DE CASTRO, S. L., MENNA-BARRETO, R., MOTTRAM, J. C., NAVARRO, M., RIGDEN, D. J., ROMANO, P. S., STOKA, V., TURK, B. & MICHELS, P. A. 2011. Autophagy in protists. *Autophagy,* 7**,** 127-58.

ELLIOTT, D. A., MCINTOSH, M. T., HOSGOOD, H. D., 3RD, CHEN, S., ZHANG, G., BAEVOVA, P. & JOINER, K. A. 2008. Four distinct pathways of hemoglobin uptake in the malaria parasite *Plasmodium falciparum*. *Proc Natl Acad Sci U S A,* 105**,** 2463-8.

FEACHEM, R. & SABOT, O. 2008. A new global malaria eradication strategy. *Lancet,* 371**,** 1633-5.

FENGSRUD, M., ERICHSEN, E. S., BERG, T. O., RAIBORG, C. & SEGLEN, P. O. 2000. Ultrastructural characterization of the delimiting membranes of isolated autophagosomes and amphisomes by freeze-fracture electron microscopy. *Eur J Cell Biol,* 79**,** 871-82.

FENNELL, B. J., AL-SHATR, Z. A. & BELL, A. 2008. Isotype expression, post-translational modification and stage-dependent production of tubulins in erythrocytic *Plasmodium falciparum*. *Int J Parasitol,* 38**,** 527-39.

FENNELL, C., BABBITT, S., RUSSO, I., WILKES, J., RANFORD-CARTWRIGHT, L., GOLDBERG, D. E. & DOERIG, C. 2009. *Pf*eIK1, a eukaryotic initiation factor 2alpha kinase of the human malaria parasite *Plasmodium falciparum*, regulates stress-response to amino-acid starvation. *Malar J,* 8**,** 99.

FERBY, I., WAGA, I., KUME, K., SAKANAKA, C. & SHIMIZU, T. 1996. PAF-induced MAPK activation is inhibited by wortmannin in neutrophils and macrophages. *Adv Exp Med Biol,* 416**,** 321-6.

FERGUSON, D. J., HENRIQUEZ, F. L., KIRISITS, M. J., MUENCH, S. P., PRIGGE, S. T., RICE, D. W., ROBERTS, C. W. & MCLEOD, R. L. 2005. Maternal inheritance and stage-specific variation of the apicoplast in *Toxoplasma gondii* during development in the intermediate and definitive host. *Eukaryot Cell,* 4**,** 814-26.

FICHERA, M. E. & ROOS, D. S. 1997. A plastid organelle as a drug target in apicomplexan parasites. *Nature,* 390**,** 407-9.

FIDOCK, D. A. & WELLEMS, T. E. 1997. Transformation with human dihydrofolate reductase renders malaria parasites insensitive to WR99210 but does not affect the intrinsic activity of proguanil. *Proc Natl Acad Sci U S A,* 94**,** 10931-6.

FLORENS, L., WASHBURN, M. P., RAINE, J. D., ANTHONY, R. M., GRAINGER, M., HAYNES, J. D., MOCH, J. K., MUSTER, N., SACCI, J. B., TABB, D. L., WITNEY, A. A., WOLTERS, D., WU, Y., GARDNER, M. J., HOLDER, A. A., SINDEN, R. E., YATES, J. R. & CARUCCI, D. J. 2002. A proteomic view of the *Plasmodium falciparum* life cycle. *Nature,* 419**,** 520-6.

FONAGER, J., FRANKE-FAYARD, B. M., ADAMS, J. H., RAMESAR, J., KLOP, O., KHAN, S. M., JANSE, C. J. & WATERS, A. P. 2011. Development of the

piggyBac transposable system for *Plasmodium berghei* and its application for random mutagenesis in malaria parasites. *BMC Genomics,* 12**,** 155.

FOTH, B. J. & MCFADDEN, G. I. 2003. The apicoplast: a plastid in *Plasmodium falciparum* and other Apicomplexan parasites. *Int Rev Cytol,* 224**,** 57-110.

FOTH, B. J., RALPH, S. A., TONKIN, C. J., STRUCK, N. S., FRAUNHOLZ, M., ROOS, D. S., COWMAN, A. F. & MCFADDEN, G. I. 2003. Dissecting apicoplast targeting in the malaria parasite *Plasmodium falciparum*. *Science,* 299**,** 705-8.

FOTH, B. J., ZHANG, N., CHAAL, B. K., SZE, S. K., PREISER, P. R. & BOZDECH, Z. 2011. Quantitative time-course profiling of parasite and host cell proteins in the human malaria parasite *Plasmodium falciparum*. *Mol Cell Proteomics,* 10**,** M110 006411.

FRANCIS, S. E., GLUZMAN, I. Y., OKSMAN, A., KNICKERBOCKER, A., MUELLER, R., BRYANT, M. L., SHERMAN, D. R., RUSSELL, D. G. & GOLDBERG, D. E. 1994. Molecular characterization and inhibition of a *Plasmodium falciparum* aspartic hemoglobinase. *EMBO J,* 13**,** 306-17.

FRANCIS, S. E., SULLIVAN, D. J., JR. & GOLDBERG, D. E. 1997. Hemoglobin metabolism in the malaria parasite *Plasmodium falciparum*. *Annu Rev Microbiol,* 51**,** 97-123.

FRANKE-FAYARD, B., FONAGER, J., BRAKS, A., KHAN, S. M. & JANSE, C. J. 2010. Sequestration and tissue accumulation of human malaria parasites: can we learn anything from rodent models of malaria? *PLoS Pathog,* 6**,** e1001032.

FUJITA, N., ITOH, T., OMORI, H., FUKUDA, M., NODA, T. & YOSHIMORI, T. 2008. The Atg16L complex specifies the site of LC3 lipidation for membrane biogenesis in autophagy. *Mol Biol Cell,* 19**,** 2092-100.

GALLAGHER, S. R. 2001. Quantitation of DNA and RNA with absorption and fluorescence spectroscopy. *Curr Protoc Immunol,* Appendix 3**,** Appendix 3L.

GARDNER, M. J., HALL, N., FUNG, E., WHITE, O., BERRIMAN, M., HYMAN, R. W., CARLTON, J. M., PAIN, A., NELSON, K. E., BOWMAN, S., PAULSEN, I. T., JAMES, K., EISEN, J. A., RUTHERFORD, K., SALZBERG, S. L., CRAIG, A., KYES, S., CHAN, M. S., NENE, V., SHALLOM, S. J., SUH, B., PETERSON, J., ANGIUOLI, S., PERTEA, M., ALLEN, J., SELENGUT, J., HAFT, D., MATHER, M. W., VAIDYA, A. B., MARTIN, D. M., FAIRLAMB, A. H., FRAUNHOLZ, M. J., ROOS, D. S., RALPH, S. A., MCFADDEN, G. I., CUMMINGS, L. M., SUBRAMANIAN, G. M., MUNGALL, C., VENTER, J. C., CARUCCI, D. J., HOFFMAN, S. L., NEWBOLD, C., DAVIS, R. W., FRASER, C. M. & BARRELL, B. 2002. Genome sequence of the human malaria parasite *Plasmodium falciparum*. *Nature,* 419**,** 498-511.

GARI, E., PIEDRAFITA, L., ALDEA, M. & HERRERO, E. 1997. A set of vectors with a tetracycline-regulatable promoter system for modulated gene expression in *Saccharomyces cerevisiae*. *Yeast,* 13**,** 837-48.

GEERAERT, C., RATIER, A., PFISTERER, S. G., PERDIZ, D., CANTALOUBE, I., ROUAULT, A., PATTINGRE, S., PROIKAS-CEZANNE, T., CODOGNO, P. & POUS, C. 2010. Starvation-induced hyperacetylation of tubulin is required for the stimulation of autophagy by nutrient deprivation. *J Biol Chem,* 285**,** 24184-94.

GENG, J. & KLIONSKY, D. J. 2008. The Atg8 and Atg12 ubiquitin-like conjugation systems in macroautophagy. 'Protein modifications: beyond the usual suspects' review series. *EMBO Rep,* 9**,** 859-64.

GHARBI, S. I., ZVELEBIL, M. J., SHUTTLEWORTH, S. J., HANCOX, T., SAGHIR, N., TIMMS, J. F. & WATERFIELD, M. D. 2007. Exploring the specificity of the PI3K family inhibitor LY294002. *Biochem J,* 404**,** 15-21.

GHOSH, D., WALTON, J. L., ROEPE, P. D. & SINAI, A. P. 2012. Autophagy is a cell death mechanism in Toxoplasma gondii. *Cell Microbiol,* 14**,** 589-607.

GHOSH, P., KIM, A. I. & HATFULL, G. F. 2003. The orientation of mycobacteriophage Bxb1 integration is solely dependent on the central dinucleotide of *attP* and *attB*. *Mol Cell,* 12**,** 1101-11.

GIETZ, R. D. & WOODS, R. A. 2006. Yeast transformation by the LiAc/SS Carrier DNA/PEG method. *Methods Mol Biol,* 313**,** 107-20.

GOLDBERG, D. E., JANSE, C. J., COWMAN, A. F. & WATERS, A. P. 2011. Has the time come for us to complement our malaria parasites? *Trends Parasitol,* 27**,** 1-2.

GOLDBERG, D. E., SLATER, A. F., CERAMI, A. & HENDERSON, G. B. 1990. Hemoglobin degradation in the malaria parasite *Plasmodium falciparum*: an ordered process in a unique organelle. *Proc Natl Acad Sci U S A,* 87**,** 2931-5.

GOODMAN, C. D., SU, V. & MCFADDEN, G. I. 2007. The effects of anti-bacterials on the malaria parasite *Plasmodium falciparum*. *Mol Biochem Parasitol,* 152**,** 181-91.

GRURING, C., HEIBER, A., KRUSE, F., UNGEFEHR, J., GILBERGER, T. W. & SPIELMANN, T. 2011. Development and host cell modifications of Plasmodium falciparum blood stages in four dimensions. *Nat Commun,* 2**,** 165.

GUNTHER, S., MATUSCHEWSKI, K. & MULLER, S. 2009. Knockout studies reveal an important role of *Plasmodium* lipoic acid protein ligase A1 for asexual blood stage parasite survival. *PLoS One,* 4**,** e5510.

GUNTHER, S., MCMILLAN, P. J., WALLACE, L. J. & MULLER, S. 2005. *Plasmodium falciparum* possesses organelle-specific alpha-keto acid dehydrogenase complexes and lipoylation pathways. *Biochem Soc Trans,* 33**,** 977-80.

GUNTHER, S., WALLACE, L., PATZEWITZ, E. M., MCMILLAN, P. J., STORM, J., WRENGER, C., BISSETT, R., SMITH, T. K. & MULLER, S. 2007. Apicoplast lipoic acid protein ligase B is not essential for *Plasmodium falciparum*. *PLoS Pathog,* 3**,** e189.

GUTIERREZ, M. G., MUNAFO, D. B., BERON, W. & COLOMBO, M. I. 2004. Rab7 is required for the normal progression of the autophagic pathway in mammalian cells. *J Cell Sci,* 117**,** 2687-97.

HAASE, S., CABRERA, A., LANGER, C., TREECK, M., STRUCK, N., HERRMANN, S., JANSEN, P. W., BRUCHHAUS, I., BACHMANN, A., DIAS, S., COWMAN, A. F., STUNNENBERG, H. G., SPIELMANN, T. & GILBERGER, T. W. 2008. Characterization of a conserved rhoptry-associated leucine zipper-like protein in the malaria parasite *Plasmodium falciparum*. *Infect Immun,* 76**,** 879-87.

HAILEY, D. W., RAMBOLD, A. S., SATPUTE-KRISHNAN, P., MITRA, K., SOUGRAT, R., KIM, P. K. & LIPPINCOTT-SCHWARTZ, J. 2010. Mitochondria supply membranes for autophagosome biogenesis during starvation. *Cell,* 141**,** 656-67.

HANADA, T., NODA, N. N., SATOMI, Y., ICHIMURA, Y., FUJIOKA, Y., TAKAO, T., INAGAKI, F. & OHSUMI, Y. 2007. The Atg12-Atg5 conjugate has a novel E3-like activity for protein lipidation in autophagy. *J Biol Chem,* 282**,** 37298-302.

HANSON, M. R. & KOHLER, R. H. 2001. GFP imaging: methodology and application to investigate cellular compartmentation in plants. *J Exp Bot,* 52, 529-39.

HANSSEN, E., CARLTON, P., DEED, S., KLONIS, N., SEDAT, J., DERISI, J. & TILLEY, L. 2010. Whole cell imaging reveals novel modular features of the exomembrane system of the malaria parasite, *Plasmodium falciparum*. *Int J Parasitol,* 40, 123-34.

HARA, T., NAKAMURA, K., MATSUI, M., YAMAMOTO, A., NAKAHARA, Y., SUZUKI-MIGISHIMA, R., YOKOYAMA, M., MISHIMA, K., SAITO, I., OKANO, H. & MIZUSHIMA, N. 2006. Suppression of basal autophagy in neural cells causes neurodegenerative disease in mice. *Nature,* 441, 885-9.

HARTLEY, J. L., TEMPLE, G. F. & BRASCH, M. A. 2000. DNA cloning using *in vitro* site-specific recombination. *Genome Res,* 10, 1788-95.

HASENKAMP, S., RUSSELL, K. T. & HORROCKS, P. 2012. Comparison of the absolute and relative efficiencies of electroporation-based transfection protocols for *Plasmodium falciparum*. *Malar J,* 11, 210.

HAYWARD, R., SALIBA, K. J. & KIRK, K. 2006. The pH of the digestive vacuole of *Plasmodium falciparum* is not associated with chloroquine resistance. *J Cell Sci,* 119, 1016-25.

HE, C. & KLIONSKY, D. J. 2009. Regulation mechanisms and signaling pathways of autophagy. *Annu Rev Genet,* 43, 67-93.

HELLMANN, J. K., MUNTER, S., KUDRYASHEV, M., SCHULZ, S., HEISS, K., MULLER, A. K., MATUSCHEWSKI, K., SPATZ, J. P., SCHWARZ, U. S. & FRISCHKNECHT, F. 2011. Environmental constraints guide migration of malaria parasites during transmission. *PLoS Pathog,* 7, e1002080.

HEMPELMANN, E., MOTTA, C., HUGHES, R., WARD, S. A. & BRAY, P. G. 2003. *Plasmodium falciparum*: sacrificing membrane to grow crystals? *Trends Parasitol,* 19, 23-6.

HOCHSTRASSER, M. 2009. Origin and function of ubiquitin-like proteins. *Nature,* 458, 422-9.

HOPKINS, J., FOWLER, R., KRISHNA, S., WILSON, I., MITCHELL, G. & BANNISTER, L. 1999. The plastid in *Plasmodium falciparum* asexual blood stages: a three-dimensional ultrastructural analysis. *Protist,* 150, 283-95.

HUANG, W. P., SCOTT, S. V., KIM, J. & KLIONSKY, D. J. 2000. The itinerary of a vesicle component, Aut7p/Cvt5p, terminates in the yeast vacuole via the autophagy/Cvt pathways. *J Biol Chem,* 275, 5845-51.

HUNDESHAGEN, P., HAMACHER-BRADY, A., EILS, R. & BRADY, N. R. 2011. Concurrent detection of autolysosome formation and lysosomal degradation by flow cytometry in a high-content screen for inducers of autophagy. *BMC Biol,* 9, 38.

ICHIMURA, Y., IMAMURA, Y., EMOTO, K., UMEDA, M., NODA, T. & OHSUMI, Y. 2004. *In vivo* and *in vitro* reconstitution of Atg8 conjugation essential for autophagy. *J Biol Chem,* 279, 40584-92.

ICHIMURA, Y., KIRISAKO, T., TAKAO, T., SATOMI, Y., SHIMONISHI, Y., ISHIHARA, N., MIZUSHIMA, N., TANIDA, I., KOMINAMI, E., OHSUMI, M., NODA, T. & OHSUMI, Y. 2000. A ubiquitin-like system mediates protein lipidation. *Nature,* 408, 488-92.

INOUE, Y. & KLIONSKY, D. J. 2010. Regulation of macroautophagy in *Saccharomyces cerevisiae*. *Semin Cell Dev Biol,* 21, 664-70.

ISTVAN, E. S., DHARIA, N. V., BOPP, S. E., GLUZMAN, I., WINZELER, E. A. & GOLDBERG, D. E. 2011. Validation of isoleucine utilization targets in *Plasmodium falciparum*. *Proc Natl Acad Sci U S A,* 108, 1627-32.

ITAKURA, E., KISHI, C., INOUE, K. & MIZUSHIMA, N. 2008. Beclin 1 forms two distinct phosphatidylinositol 3-kinase complexes with mammalian Atg14 and UVRAG. *Mol Biol Cell,* 19**,** 5360-72.

IWANAGA, S., KATO, T., KANEKO, I. & YUDA, M. 2012. Centromere plasmid: a new genetic tool for the study of *Plasmodium falciparum*. *PLoS One,* 7**,** e33326.

IZUMI, M., WADA, S., MAKINO, A. & ISHIDA, H. 2010. The autophagic degradation of chloroplasts via rubisco-containing bodies is specifically linked to leaf carbon status but not nitrogen status in Arabidopsis. *Plant Physiol,* 154**,** 1196-209.

JAGER, S., BUCCI, C., TANIDA, I., UENO, T., KOMINAMI, E., SAFTIG, P. & ESKELINEN, E. L. 2004. Role for Rab7 in maturation of late autophagic vacuoles. *J Cell Sci,* 117**,** 4837-48.

JARVIS, P. 2008. Targeting of nucleus-encoded proteins to chloroplasts in plants. *New Phytol,* 179**,** 257-85.

JAYABALASINGHAM, B., BANO, N. & COPPENS, I. 2010. Metamorphosis of the malaria parasite in the liver is associated with organelle clearance. *Cell Res,* 20**,** 1043-59.

JOHANSEN, T. & LAMARK, T. 2011. Selective autophagy mediated by autophagic adapter proteins. *Autophagy,* 7**,** 279-96.

JUHASZ, G., HILL, J. H., YAN, Y., SASS, M., BAEHRECKE, E. H., BACKER, J. M. & NEUFELD, T. P. 2008. The class III PI(3)K Vps34 promotes autophagy and endocytosis but not TOR signaling in *Drosophila*. *J Cell Biol,* 181**,** 655-66.

KABEYA, Y., MIZUSHIMA, N., UENO, T., YAMAMOTO, A., KIRISAKO, T., NODA, T., KOMINAMI, E., OHSUMI, Y. & YOSHIMORI, T. 2000. LC3, a mammalian homologue of yeast Apg8p, is localized in autophagosome membranes after processing. *EMBO J,* 19**,** 5720-8.

KABEYA, Y., MIZUSHIMA, N., YAMAMOTO, A., OSHITANI-OKAMOTO, S., OHSUMI, Y. & YOSHIMORI, T. 2004. LC3, GABARAP and GATE16 localize to autophagosomal membrane depending on form-II formation. *J Cell Sci,* 117**,** 2805-12.

KADEKOPPALA, M., CHERESH, P., CATRON, D., JI, D. D., DEITSCH, K., WELLEMS, T. E., SEIFERT, H. S. & HALDAR, K. 2001. Rapid recombination among transfected plasmids, chimeric episome formation and trans gene expression in *Plasmodium falciparum*. *Mol Biochem Parasitol,* 112**,** 211-8.

KAGEYAMA, S., OMORI, H., SAITOH, T., SONE, T., GUAN, J. L., AKIRA, S., IMAMOTO, F., NODA, T. & YOSHIMORI, T. 2011. The LC3 recruitment mechanism is separate from Atg9L1-dependent membrane formation in the autophagic response against Salmonella. *Mol Biol Cell,* 22**,** 2290-300.

KALANON, M., TONKIN, C. J. & MCFADDEN, G. I. 2009. Characterization of two putative protein translocation components in the apicoplast of *Plasmodium falciparum*. *Eukaryot Cell,* 8**,** 1146-54.

KAMADA, Y., FUNAKOSHI, T., SHINTANI, T., NAGANO, K., OHSUMI, M. & OHSUMI, Y. 2000. Tor-mediated induction of autophagy via an Apg1 protein kinase complex. *J Cell Biol,* 150**,** 1507-13.

KAPISHNIKOV, S., WEINER, A., SHIMONI, E., GUTTMANN, P., SCHNEIDER, G., DAHAN-PASTERNAK, N., DZIKOWSKI, R., LEISEROWITZ, L. & ELBAUM, M. 2012. Oriented nucleation of hemozoin at the digestive vacuole membrane in *Plasmodium falciparum*. *Proc Natl Acad Sci U S A,* 109**,** 11188-93.

KAPPES, B. & ROHRBACH, P. 2007. Microtubule inhibitors as a potential treatment for malaria. *Future Microbiol,* 2**,** 409-23.

KARCZ, S. R., HERRMANN, V. R., TROTTEIN, F. & COWMAN, A. F. 1994. Cloning and characterization of the vacuolar ATPase B subunit from *Plasmodium falciparum*. *Mol Biochem Parasitol,* 65**,** 123-33.

KARNATAKI, A., DEROCHER, A., COPPENS, I., NASH, C., FEAGIN, J. E. & PARSONS, M. 2007. Cell cycle-regulated vesicular trafficking of *Toxoplasma* APT1, a protein localized to multiple apicoplast membranes. *Mol Microbiol,* 63**,** 1653-68.

KARUNAMOORTHI, K. 2011. Vector control: a cornerstone in the malaria elimination campaign. *Clin Microbiol Infect,* 17**,** 1608-16.

KAWAI, A., UCHIYAMA, H., TAKANO, S., NAKAMURA, N. & OHKUMA, S. 2007. Autophagosome-lysosome fusion depends on the pH in acidic compartments in CHO cells. *Autophagy,* 3**,** 154-7.

KIEL, J. A. 2010. Autophagy in unicellular eukaryotes. *Philos Trans R Soc Lond B Biol Sci,* 365**,** 819-30.

KIM, I. & LEMASTERS, J. J. 2011. Mitochondrial degradation by autophagy (mitophagy) in GFP-LC3 transgenic hepatocytes during nutrient deprivation. *Am J Physiol Cell Physiol,* 300**,** C308-17.

KIM, I., RODRIGUEZ-ENRIQUEZ, S. & LEMASTERS, J. J. 2007. Selective degradation of mitochondria by mitophagy. *Arch Biochem Biophys,* 462**,** 245-53.

KIM, Y. G., CHA, J. & CHANDRASEGARAN, S. 1996. Hybrid restriction enzymes: zinc finger fusions to Fok I cleavage domain. *Proc Natl Acad Sci U S A,* 93**,** 1156-60.

KIMURA, S., NODA, T. & YOSHIMORI, T. 2007. Dissection of the autophagosome maturation process by a novel reporter protein, tandem fluorescent-tagged LC3. *Autophagy,* 3**,** 452-60.

KIRISAKO, T., BABA, M., ISHIHARA, N., MIYAZAWA, K., OHSUMI, M., YOSHIMORI, T., NODA, T. & OHSUMI, Y. 1999. Formation process of autophagosome is traced with Apg8/Aut7p in yeast. *J Cell Biol,* 147**,** 435-46.

KIRISAKO, T., ICHIMURA, Y., OKADA, H., KABEYA, Y., MIZUSHIMA, N., YOSHIMORI, T., OHSUMI, M., TAKAO, T., NODA, T. & OHSUMI, Y. 2000. The reversible modification regulates the membrane-binding state of Apg8/Aut7 essential for autophagy and the cytoplasm to vacuole targeting pathway. *J Cell Biol,* 151**,** 263-76.

KIRKMAN, L. A., SU, X. Z. & WELLEMS, T. E. 1996. *Plasmodium falciparum*: isolation of large numbers of parasite clones from infected blood samples. *Exp Parasitol,* 83**,** 147-9.

KITAMURA, K., KISHI-ITAKURA, C., TSUBOI, T., SATO, S., KITA, K., OHTA, N. & MIZUSHIMA, N. 2012. Autophagy-Related Atg8 Localizes to the Apicoplast of the Human Malaria Parasite *Plasmodium falciparum*. *PLoS One,* 7**,** e42977.

KLINKEN, S. 2002. Red blood cells. *Int J Biochem Cell Biol,* 34**,** 1513-8.

KLIONSKY, D. J. 2011. For the last time, it is GFP-Atg8, not Atg8-GFP (and the same goes for LC3). *Autophagy,* 7**,** 1093-4.

KLIONSKY, D. J., CREGG, J. M., DUNN, W. A., JR., EMR, S. D., SAKAI, Y., SANDOVAL, I. V., SIBIRNY, A., SUBRAMANI, S., THUMM, M., VEENHUIS, M. & OHSUMI, Y. 2003. A unified nomenclature for yeast autophagy-related genes. *Dev Cell,* 5**,** 539-45.

KLIONSKY, D. J., CUEVA, R. & YAVER, D. S. 1992. Aminopeptidase I of *Saccharomyces cerevisiae* is localized to the vacuole independent of the secretory pathway. *J Cell Biol,* 119**,** 287-99.

KLIONSKY, D. J., ELAZAR, Z., SEGLEN, P. O. & RUBINSZTEIN, D. C. 2008. Does bafilomycin A1 block the fusion of autophagosomes with lysosomes? *Autophagy,* 4**,** 849-950.

KOHLER, K., BRUNNER, E., GUAN, X. L., BOUCKE, K., GREBER, U. F., MOHANTY, S., BARTH, J. M., WENK, M. R. & HAFEN, E. 2009. A combined proteomic and genetic analysis identifies a role for the lipid desaturase Desat1 in starvation-induced autophagy in *Drosophila*. *Autophagy,* 5**,** 980-90.

KOHLI, L. & ROTH, K. A. 2010. Autophagy: cerebral home cooking. *Am J Pathol,* 176**,** 1065-71.

KOMANDER, D. & RAPE, M. 2012. The ubiquitin code. *Annu Rev Biochem,* 81**,** 203-29.

KONG, Q., WU, M., HUAN, Y., ZHANG, L., LIU, H., BOU, G., LUO, Y., MU, Y. & LIU, Z. 2009. Transgene expression is associated with copy number and cytomegalovirus promoter methylation in transgenic pigs. *PLoS One,* 4**,** e6679.

KOOPMANN, R., MUHAMMAD, K., PERBANDT, M., BETZEL, C. & DUSZENKO, M. 2009. *Trypanosoma brucei* ATG8: structural insights into autophagic-like mechanisms in protozoa. *Autophagy,* 5**,** 1085-91.

KOROLCHUK, V. I., MENZIES, F. M. & RUBINSZTEIN, D. C. 2010. Mechanisms of cross-talk between the ubiquitin-proteasome and autophagy-lysosome systems. *FEBS Lett,* 584**,** 1393-8.

KRAFT, C. & MARTENS, S. 2012. Mechanisms and regulation of autophagosome formation. *Curr Opin Cell Biol,* 24**,** 496-501.

KRETTLI, A. U. & DANTAS, L. A. 2000. Which routes do *Plasmodium* sporozoites use for successful infections of vertebrates? *Infect Immun,* 68**,** 3064-5.

KRICK, R., BREMER, S., WELTER, E., ESKELINEN, E. L. & THUMM, M. 2011. Cheating on ubiquitin with Atg8. *Autophagy,* 7**,** 250-1.

KRICK, R., BREMER, S., WELTER, E., SCHLOTTERHOSE, P., MUEHE, Y., ESKELINEN, E. L. & THUMM, M. 2010. Cdc48/p97 and Shp1/p47 regulate autophagosome biogenesis in concert with ubiquitin-like Atg8. *J Cell Biol,* 190**,** 965-73.

KRNAJSKI, Z., GILBERGER, T. W., WALTER, R. D., COWMAN, A. F. & MULLER, S. 2002. Thioredoxin reductase is essential for the survival of *Plasmodium falciparum* erythrocytic stages. *J Biol Chem,* 277**,** 25970-5.

KUMETA, H., WATANABE, M., NAKATOGAWA, H., YAMAGUCHI, M., OGURA, K., ADACHI, W., FUJIOKA, Y., NODA, N. N., OHSUMI, Y. & INAGAKI, F. 2010. The NMR structure of the autophagy-related protein Atg8. *J Biomol NMR,* 47**,** 237-41.

KUNZ, J. B., SCHWARZ, H. & MAYER, A. 2004. Determination of four sequential stages during microautophagy *in vitro*. *J Biol Chem,* 279**,** 9987-96.

LAEMMLI, U. K. 1970. Cleavage of structural proteins during the assembly of the head of bacteriophage T4. *Nature,* 227**,** 680-5.

LAMARK, T., KIRKIN, V., DIKIC, I. & JOHANSEN, T. 2009. NBR1 and p62 as cargo receptors for selective autophagy of ubiquitinated targets. *Cell Cycle,* 8**,** 1986-90.

LAMBROS, C. & VANDERBERG, J. P. 1979. Synchronization of *Plasmodium falciparum* erythrocytic stages in culture. *J Parasitol,* 65**,** 418-20.

LANDY, A. 1989. Dynamic, structural, and regulatory aspects of lambda site-specific recombination. *Annu Rev Biochem,* 58**,** 913-49.

LE ROCH, K. G., JOHNSON, J. R., FLORENS, L., ZHOU, Y., SANTROSYAN, A., GRAINGER, M., YAN, S. F., WILLIAMSON, K. C., HOLDER, A. A., CARUCCI, D. J., YATES, J. R., 3RD & WINZELER, E. A. 2004. Global analysis of

transcript and protein levels across the *Plasmodium falciparum* life cycle. *Genome Res,* 14**,** 2308-18.

LEE, I. H., CAO, L., MOSTOSLAVSKY, R., LOMBARD, D. B., LIU, J., BRUNS, N. E., TSOKOS, M., ALT, F. W. & FINKEL, T. 2008. A role for the NAD-dependent deacetylase Sirt1 in the regulation of autophagy. *Proc Natl Acad Sci U S A,* 105**,** 3374-9.

LELIEVRE, J., BERRY, A. & BENOIT-VICAL, F. 2005. An alternative method for *Plasmodium* culture synchronization. *Exp Parasitol,* 109**,** 195-7.

LEVINE, B. 2005. Eating oneself and uninvited guests: autophagy-related pathways in cellular defense. *Cell,* 120**,** 159-62.

LEVINE, B. & DERETIC, V. 2007. Unveiling the roles of autophagy in innate and adaptive immunity. *Nat Rev Immunol,* 7**,** 767-77.

LEVINE, B. & KLIONSKY, D. J. 2004. Development by self-digestion: molecular mechanisms and biological functions of autophagy. *Dev Cell,* 6**,** 463-77.

LEVINE, B. & KROEMER, G. 2008. Autophagy in the pathogenesis of disease. *Cell,* 132**,** 27-42.

LI, F. J., SHEN, Q., WANG, C., SUN, Y., YUAN, A. Y. & HE, C. Y. 2012a. A role of autophagy in *Trypanosoma brucei* cell death. *Cell Microbiol,* 14**,** 1242-56.

LI, H. M. & CHIU, C. C. 2010. Protein transport into chloroplasts. *Annu Rev Plant Biol,* 61**,** 157-80.

LI, M., HOU, Y., WANG, J., CHEN, X., SHAO, Z. M. & YIN, X. M. 2011a. Kinetics comparisons of mammalian Atg4 homologues indicate selective preferences toward diverse Atg8 substrates. *J Biol Chem,* 286**,** 7327-38.

LI, W., YANG, Q. & MAO, Z. 2011b. Chaperone-mediated autophagy: machinery, regulation and biological consequences. *Cell Mol Life Sci,* 68**,** 749-63.

LI, W. W., LI, J. & BAO, J. K. 2012b. Microautophagy: lesser-known self-eating. *Cell Mol Life Sci,* 69**,** 1125-36.

LIM, L., KALANON, M. & MCFADDEN, G. I. 2009. New proteins in the apicoplast membranes: time to rethink apicoplast protein targeting. *Trends Parasitol,* 25**,** 197-200.

LIM, L. & MCFADDEN, G. I. 2010. The evolution, metabolism and functions of the apicoplast. *Philos Trans R Soc Lond B Biol Sci,* 365**,** 749-63.

LIN, M. G. & ZHONG, Q. 2011. Interaction between small GTPase Rab7 and PI3KC3 links autophagy and endocytosis: A new Rab7 effector protein sheds light on membrane trafficking pathways. *Small Gtpases,* 2**,** 85-88.

LIU, C., CHOE, V. & RAO, H. 2010. Genome-wide approaches to systematically identify substrates of the ubiquitin-proteasome pathway. *Trends Biotechnol,* 28**,** 461-7.

LIU, J., GLUZMAN, I. Y., DREW, M. E. & GOLDBERG, D. E. 2005. The role of *Plasmodium falciparum* food vacuole plasmepsins. *J Biol Chem,* 280**,** 1432-7.

LIU, J., ISTVAN, E. S., GLUZMAN, I. Y., GROSS, J. & GOLDBERG, D. E. 2006. *Plasmodium falciparum* ensures its amino acid supply with multiple acquisition pathways and redundant proteolytic enzyme systems. *Proc Natl Acad Sci U S A,* 103**,** 8840-5.

LOPATICKI, S., MAIER, A. G., THOMPSON, J., WILSON, D. W., THAM, W. H., TRIGLIA, T., GOUT, A., SPEED, T. P., BEESON, J. G., HEALER, J. & COWMAN, A. F. 2011. Reticulocyte and erythrocyte binding-like proteins function cooperatively in invasion of human erythrocytes by malaria parasites. *Infect Immun,* 79**,** 1107-17.

MACASEV, D., WHELAN, J., NEWBIGIN, E., SILVA-FILHO, M. C., MULHERN, T. D. & LITHGOW, T. 2004. Tom22', an 8-kDa trans-site receptor in plants and

protozoans, is a conserved feature of the TOM complex that appeared early in the evolution of eukaryotes. *Mol Biol Evol,* 21**,** 1557-64.

MAESSEN, S., WESSELING, J. G., SMITS, M. A., KONINGS, R. N. & SCHOENMAKERS, J. G. 1993. The gamma-tubulin gene of the malaria parasite *Plasmodium falciparum*. *Mol Biochem Parasitol,* 60**,** 27-35.

MAIATO, H., DELUCA, J., SALMON, E. D. & EARNSHAW, W. C. 2004. The dynamic kinetochore-microtubule interface. *J Cell Sci,* 117**,** 5461-77.

MAIER, A. G., BRAKS, J. A., WATERS, A. P. & COWMAN, A. F. 2006. Negative selection using yeast cytosine deaminase/uracil phosphoribosyl transferase in *Plasmodium falciparum* for targeted gene deletion by double crossover recombination. *Mol Biochem Parasitol,* 150**,** 118-21.

MANDERS, E. M. M., VERBEEK, F. J. & ATEN, J. A. 1993. Measurement of co-localization of objects in dual-colour confocal images. *Journal of Microscopy,* 169**,** 375-382.

MANZANO-ROMAN, R., OLEAGA, A., PEREZ-SANCHEZ, R. & SILES-LUCAS, M. 2012. Gene silencing in parasites: current status and future prospects. *Adv Parasitol,* 78**,** 1-55.

MARCHESINI, N., VIEIRA, M., LUO, S., MORENO, S. N. & DOCAMPO, R. 2005. A malaria parasite-encoded vacuolar H(+)-ATPase is targeted to the host erythrocyte. *J Biol Chem,* 280**,** 36841-7.

MARI, M., GRIFFITH, J., RIETER, E., KRISHNAPPA, L., KLIONSKY, D. J. & REGGIORI, F. 2010. An Atg9-containing compartment that functions in the early steps of autophagosome biogenesis. *J Cell Biol,* 190**,** 1005-22.

MARINO, G., URIA, J. A., PUENTE, X. S., QUESADA, V., BORDALLO, J. & LOPEZ-OTIN, C. 2003. Human autophagins, a family of cysteine proteinases potentially implicated in cell degradation by autophagy. *J Biol Chem,* 278**,** 3671-8.

MARKUS, M. B. 2012. Dormancy in mammalian malaria. *Trends Parasitol,* 28**,** 39-45.

MATTHEWS, T. & BOEHME, R. 1988. Antiviral activity and mechanism of action of ganciclovir. *Rev Infect Dis,* 10 Suppl 3**,** S490-4.

MATUSCHEWSKI, K. 2006. Getting infectious: formation and maturation of *Plasmodium* sporozoites in the *Anopheles* vector. *Cell Microbiol,* 8**,** 1547-56.

MCBRIDE, H. M., NEUSPIEL, M. & WASIAK, S. 2006. Mitochondria: more than just a powerhouse. *Curr Biol,* 16**,** R551-60.

MCDERMOTT, M., WAKELAM, M. J. & MORRIS, A. J. 2004. Phospholipase D. *Biochem Cell Biol,* 82**,** 225-53.

MCFADDEN, G. I., REITH, M. E., MUNHOLLAND, J. & LANG-UNNASCH, N. 1996. Plastid in human parasites. *Nature,* 381**,** 482.

MCMILLAN, P. 2006. *Thioredoxin reductase and dihydrolipoamide dehydrogenases of Plasmodium falciparum*. Doctor of Philosophy, University of Glasgow.

MCMILLAN, P. J., STIMMLER, L. M., FOTH, B. J., MCFADDEN, G. I. & MULLER, S. 2005. The human malaria parasite *Plasmodium falciparum* possesses two distinct dihydrolipoamide dehydrogenases. *Mol Microbiol,* 55**,** 27-38.

MELENDEZ, A., TALLOCZY, Z., SEAMAN, M., ESKELINEN, E. L., HALL, D. H. & LEVINE, B. 2003. Autophagy genes are essential for dauer development and life-span extension in *C. elegans*. *Science,* 301**,** 1387-91.

MIAO, J., LI, J., FAN, Q., LI, X. & CUI, L. 2010. The Puf-family RNA-binding protein *Pf*Puf2 regulates sexual development and sex differentiation in the malaria parasite *Plasmodium falciparum*. *J Cell Sci,* 123**,** 1039-49.

MIKAWA, T., KANOH, J. & ISHIKAWA, F. 2010. Fission yeast Vps1 and Atg8 contribute to oxidative stress resistance. *Genes Cells*.

MIKOLAJCZAK, S. A., SACCI, J. B., JR., DE LA VEGA, P., CAMARGO, N., VANBUSKIRK, K., KRZYCH, U., CAO, J., JACOBS-LORENA, M., COWMAN, A. F. & KAPPE, S. H. 2011. Disruption of the *Plasmodium falciparum* liver-stage antigen-1 locus causes a differentiation defect in late liver-stage parasites. *Cell Microbiol,* 13**,** 1250-60.

MILLER, J. C., HOLMES, M. C., WANG, J., GUSCHIN, D. Y., LEE, Y. L., RUPNIEWSKI, I., BEAUSEJOUR, C. M., WAITE, A. J., WANG, N. S., KIM, K. A., GREGORY, P. D., PABO, C. O. & REBAR, E. J. 2007. An improved zinc-finger nuclease architecture for highly specific genome editing. *Nat Biotechnol,* 25**,** 778-85.

MITCHELL, G. H., THOMAS, A. W., MARGOS, G., DLUZEWSKI, A. R. & BANNISTER, L. H. 2004. Apical membrane antigen 1, a major malaria vaccine candidate, mediates the close attachment of invasive merozoites to host red blood cells. *Infect Immun,* 72**,** 154-8.

MIZUSHIMA, N. 2010. The role of the Atg1/ULK1 complex in autophagy regulation. *Curr Opin Cell Biol,* 22**,** 132-9.

MIZUSHIMA, N. & KLIONSKY, D. J. 2007. Protein turnover via autophagy: implications for metabolism. *Annu Rev Nutr,* 27**,** 19-40.

MIZUSHIMA, N., NODA, T., YOSHIMORI, T., TANAKA, Y., ISHII, T., GEORGE, M. D., KLIONSKY, D. J., OHSUMI, M. & OHSUMI, Y. 1998. A protein conjugation system essential for autophagy. *Nature,* 395**,** 395-8.

MIZUSHIMA, N., OHSUMI, Y. & YOSHIMORI, T. 2002. Autophagosome formation in mammalian cells. *Cell Struct Funct,* 27**,** 421-9.

MIZUSHIMA, N., YAMAMOTO, A., MATSUI, M., YOSHIMORI, T. & OHSUMI, Y. 2004. *In vivo* analysis of autophagy in response to nutrient starvation using transgenic mice expressing a fluorescent autophagosome marker. *Mol Biol Cell,* 15**,** 1101-11.

MIZUSHIMA, N. & YOSHIMORI, T. 2007. How to interpret LC3 immunoblotting. *Autophagy,* 3**,** 542-5.

MIZUSHIMA, N., YOSHIMORI, T. & LEVINE, B. 2010. Methods in mammalian autophagy research. *Cell,* 140**,** 313-26.

MONAGHAN, P. & BELL, A. 2005. A *Plasmodium falciparum* FK506-binding protein (FKBP) with peptidyl-prolyl cis-trans isomerase and chaperone activities. *Mol Biochem Parasitol,* 139**,** 185-95.

MORAHAN, B. J., WANG, L. & COPPEL, R. L. 2009. No TRAP, no invasion. *Trends Parasitol,* 25**,** 77-84.

MORETTI, L., YANG, E. S., KIM, K. W. & LU, B. 2007. Autophagy signaling in cancer and its potential as novel target to improve anticancer therapy. *Drug Resist Updat,* 10**,** 135-43.

MULLIE, C., JONET, A., DESGROUAS, C., TAUDON, N. & SONNET, P. 2012. Differences in anti-malarial activity of 4-aminoalcohol quinoline enantiomers and investigation of the presumed underlying mechanism of action. *Malar J,* 11**,** 65.

MUNAFO, D. B. & COLOMBO, M. I. 2001. A novel assay to study autophagy: regulation of autophagosome vacuole size by amino acid deprivation. *J Cell Sci,* 114**,** 3619-29.

NAIR, S. C. & STRIEPEN, B. 2011. What do human parasites do with a chloroplast anyway? *PLoS Biol,* 9**,** e1001137.

NAIR, U., CAO, Y., XIE, Z. & KLIONSKY, D. J. 2010. Roles of the lipid-binding motifs of Atg18 and Atg21 in the cytoplasm to vacuole targeting pathway and autophagy. *J Biol Chem,* 285**,** 11476-88.

NAIR, U., YEN, W. L., MARI, M., CAO, Y., XIE, Z., BABA, M., REGGIORI, F. & KLIONSKY, D. J. 2012. A role for Atg8-PE deconjugation in autophagosome biogenesis. *Autophagy,* 8.

NAKAMURA, N., MATSUURA, A., WADA, Y. & OHSUMI, Y. 1997. Acidification of vacuoles is required for autophagic degradation in the yeast, *Saccharomyces cerevisiae*. *J Biochem,* 121**,** 338-44.

NAKANISHI, S., KAKITA, S., TAKAHASHI, I., KAWAHARA, K., TSUKUDA, E., SANO, T., YAMADA, K., YOSHIDA, M., KASE, H., MATSUDA, Y. & ET AL. 1992. Wortmannin, a microbial product inhibitor of myosin light chain kinase. *J Biol Chem,* 267**,** 2157-63.

NAKATOGAWA, H., ICHIMURA, Y. & OHSUMI, Y. 2007. Atg8, a ubiquitin-like protein required for autophagosome formation, mediates membrane tethering and hemifusion. *Cell,* 130**,** 165-78.

NAKATOGAWA, H., ISHII, J., ASAI, E. & OHSUMI, Y. 2012a. Atg4 recycles inappropriately lipidated Atg8 to promote autophagosome biogenesis. *Autophagy,* 8**,** 177-86.

NAKATOGAWA, H., OHBAYASHI, S., SAKOH-NAKATOGAWA, M., KAKUTA, S., SUZUKI, S. W., KIRISAKO, H., KONDO-KAKUTA, C., NODA, N. N., YAMAMOTO, H. & OHSUMI, Y. 2012b. The Autophagy-Related Protein Kinase Atg1 Interacts with the Ubiquitin-Like Protein Atg8 via the Atg8 Family Interacting Motif to Facilitate Autophagosome Formation. *J Biol Chem*.

NAKATOGAWA, H. & OHSUMI, Y. 2012. SDS-PAGE techniques to study ubiquitin-like conjugation systems in yeast autophagy. *Methods Mol Biol,* 832**,** 519-29.

NI, H. M., BOCKUS, A., WOZNIAK, A. L., JONES, K., WEINMAN, S., YIN, X. M. & DING, W. X. 2011. Dissecting the dynamic turnover of GFP-LC3 in the autolysosome. *Autophagy,* 7**,** 188-204.

NKRUMAH, L. J., MUHLE, R. A., MOURA, P. A., GHOSH, P., HATFULL, G. F., JACOBS, W. R., JR. & FIDOCK, D. A. 2006. Efficient site-specific integration in *Plasmodium falciparum* chromosomes mediated by mycobacteriophage Bxb1 integrase. *Nat Methods,* 3**,** 615-21.

NODA, N. N., KUMETA, H., NAKATOGAWA, H., SATOO, K., ADACHI, W., ISHII, J., FUJIOKA, Y., OHSUMI, Y. & INAGAKI, F. 2008. Structural basis of target recognition by Atg8/LC3 during selective autophagy. *Genes Cells,* 13**,** 1211-8.

NODA, N. N., OHSUMI, Y. & INAGAKI, F. 2010. Atg8-family interacting motif crucial for selective autophagy. *FEBS Lett,* 584**,** 1379-85.

O'DONNELL, R. A., FREITAS-JUNIOR, L. H., PREISER, P. R., WILLIAMSON, D. H., DURAISINGH, M., MCELWAIN, T. F., SCHERF, A., COWMAN, A. F. & CRABB, B. S. 2002. A genetic screen for improved plasmid segregation reveals a role for Rep20 in the interaction of *Plasmodium falciparum* chromosomes. *EMBO J,* 21**,** 1231-9.

OGWAN'G, R. A., MWANGI, J. K., GITHURE, J., WERE, J. B., ROBERTS, C. R. & MARTIN, S. K. 1993. Factors affecting exflagellation of *in vitro*-cultivated *Plasmodium falciparum* gametocytes. *Am J Trop Med Hyg,* 49**,** 25-9.

OHASHI, Y. & MUNRO, S. 2010. Membrane delivery to the yeast autophagosome from the Golgi-endosomal system. *Mol Biol Cell,* 21**,** 3998-4008.

OKAMOTO, N., SPURCK, T. P., GOODMAN, C. D. & MCFADDEN, G. I. 2009. Apicoplast and mitochondrion in gametocytogenesis of Plasmodium falciparum. *Eukaryot Cell,* 8**,** 128-32.

OMATSU-KANBE, M., YAMAMOTO, T. & MATSUURA, H. 2011. Autophagy is constitutively active in normal mouse sino-atrial nodal cells. *Acta Histochem Cytochem,* 44**,** 223-31.

OTTO, T. D., WILINSKI, D., ASSEFA, S., KEANE, T. M., SARRY, L. R., BOHME, U., LEMIEUX, J., BARRELL, B., PAIN, A., BERRIMAN, M., NEWBOLD, C. & LLINAS, M. 2010. New insights into the blood-stage transcriptome of *Plasmodium falciparum* using RNA-Seq. *Mol Microbiol,* 76**,** 12-24.

PAINTER, H. J., MORRISEY, J. M., MATHER, M. W. & VAIDYA, A. B. 2007. Specific role of mitochondrial electron transport in blood-stage *Plasmodium falciparum*. *Nature,* 446**,** 88-91.

PANKIV, S., ALEMU, E. A., BRECH, A., BRUUN, J. A., LAMARK, T., OVERVATN, A., BJORKOY, G. & JOHANSEN, T. 2010. FYCO1 is a Rab7 effector that binds to LC3 and PI3P to mediate microtubule plus end-directed vesicle transport. *J Cell Biol,* 188**,** 253-69.

PANKIV, S., CLAUSEN, T. H., LAMARK, T., BRECH, A., BRUUN, J. A., OUTZEN, H., OVERVATN, A., BJORKOY, G. & JOHANSEN, T. 2007. p62/SQSTM1 binds directly to Atg8/LC3 to facilitate degradation of ubiquitinated protein aggregates by autophagy. *J Biol Chem,* 282**,** 24131-45.

PAPON, N., NOEL, T., FLORENT, M., GIBOT-LECLERC, S., JEAN, D., CHASTIN, C., VILLARD, J. & CHAPELAND-LECLERC, F. 2007. Molecular mechanism of flucytosine resistance in *Candida lusitaniae*: contribution of the FCY2, FCY1, and FUR1 genes to 5-fluorouracil and fluconazole cross-resistance. *Antimicrob Agents Chemother,* 51**,** 369-71.

PARSONS, M., KARNATAKI, A., FEAGIN, J. E. & DEROCHER, A. 2007. Protein trafficking to the apicoplast: deciphering the apicomplexan solution to secondary endosymbiosis. *Eukaryot Cell,* 6**,** 1081-8.

PATTISON, J. S., OSINSKA, H. & ROBBINS, J. 2011. Atg7 induces basal autophagy and rescues autophagic deficiency in CryABR120G cardiomyocytes. *Circ Res,* 109**,** 151-60.

PATZEWITZ, E. 2009. *Glutathione metabolism of Plasmodium falciparum*. Dipl. Biol., University of Glasgow.

PATZEWITZ, E. M., WONG, E. H. & MULLER, S. 2012. Dissecting the role of glutathione biosynthesis in *Plasmodium falciparum*. *Mol Microbiol,* 83**,** 304-18.

PAYNE, S. H. & LOOMIS, W. F. 2006. Retention and loss of amino acid biosynthetic pathways based on analysis of whole-genome sequences. *Eukaryot Cell,* 5**,** 272-6.

PEI, X., GUO, X., COPPEL, R., BHATTACHARJEE, S., HALDAR, K., GRATZER, W., MOHANDAS, N. & AN, X. 2007. The ring-infected erythrocyte surface antigen (RESA) of *Plasmodium falciparum* stabilizes spectrin tetramers and suppresses further invasion. *Blood,* 110**,** 1036-42.

PEREZ-PEREZ, M. E., FLORENCIO, F. J. & CRESPO, J. L. 2010. Inhibition of target of rapamycin signaling and stress activate autophagy in *Chlamydomonas reinhardtii*. *Plant Physiol,* 152**,** 1874-88.

PERRY, C. N., KYOI, S., HARIHARAN, N., TAKAGI, H., SADOSHIMA, J. & GOTTLIEB, R. A. 2009. Novel methods for measuring cardiac autophagy *in vivo*. *Methods Enzymol,* 453**,** 325-42.

PFANNER, N. & GEISSLER, A. 2001. Versatility of the mitochondrial protein import machinery. *Nat Rev Mol Cell Biol,* 2**,** 339-49.

PFANNER, N. & WIEDEMANN, N. 2002. Mitochondrial protein import: two membranes, three translocases. *Curr Opin Cell Biol,* 14**,** 400-11.

PIZZI, E. & FRONTALI, C. 2001. Low-complexity regions in *Plasmodium falciparum* proteins. *Genome Res,* 11**,** 218-29.

PONPUAK, M., DELGADO, M. A., ELMAOUED, R. A. & DERETIC, V. 2009. Monitoring autophagy during *Mycobacterium tuberculosis* infection. *Methods Enzymol,* 452**,** 345-61.

POPOVIC, D., AKUTSU, M., NOVAK, I., HARPER, J. W., BEHRENDS, C. & DIKIC, I. 2012. Rab GTPase-activating proteins in autophagy: regulation of endocytic and autophagy pathways by direct binding to human ATG8 modifiers. *Mol Cell Biol,* 32**,** 1733-44.

POWIS, G., BONJOUKLIAN, R., BERGGREN, M. M., GALLEGOS, A., ABRAHAM, R., ASHENDEL, C., ZALKOW, L., MATTER, W. F., DODGE, J., GRINDEY, G. & ET AL. 1994. Wortmannin, a potent and selective inhibitor of phosphatidylinositol-3-kinase. *Cancer Res,* 54**,** 2419-23.

PREISER, P., KAVIRATNE, M., KHAN, S., BANNISTER, L. & JARRA, W. 2000. The apical organelles of malaria merozoites: host cell selection, invasion, host immunity and immune evasion. *Microbes Infect,* 2**,** 1461-77.

PROTO, W., RICHARD. 2010. *Characterisation of autophagy and a metacaspase in Trypanosoma brucei*. Thesis (PhD), University of Glasgow.

PRUDENCIO, M., RODRIGUEZ, A. & MOTA, M. M. 2006. The silent path to thousands of merozoites: the *Plasmodium* liver stage. *Nat Rev Microbiol,* 4**,** 849-56.

PUTRIANTI, E. D., SCHMIDT-CHRISTENSEN, A., ARNOLD, I., HEUSSLER, V. T., MATUSCHEWSKI, K. & SILVIE, O. 2010. The *Plasmodium* serine-type SERA proteases display distinct expression patterns and non-essential *in vivo* roles during life cycle progression of the malaria parasite. *Cell Microbiol,* 12**,** 725-39.

QUINTO-ALEMANY, D., CANERINA-AMARO, A., HERNANDEZ-ABAD, L. G., MACHIN, F., ROMESBERG, F. E. & GIL-LAMAIGNERE, C. 2012. Yeasts acquire resistance secondary to antifungal drug treatment by adaptive mutagenesis. *PLoS One,* 7**,** e42279.

RADOSHEVICH, L., MURROW, L., CHEN, N., FERNANDEZ, E., ROY, S., FUNG, C. & DEBNATH, J. 2010. ATG12 conjugation to ATG3 regulates mitochondrial homeostasis and cell death. *Cell,* 142**,** 590-600.

RAHLFS, S., KONCAREVIC, S., IOZEF, R., MAILU, B. M., SAVVIDES, S. N., SCHIRMER, R. H. & BECKER, K. 2009. Myristoylated adenylate kinase-2 of *Plasmodium falciparum* forms a heterodimer with myristoyltransferase. *Mol Biochem Parasitol,* 163**,** 77-84.

RAIBORG, C. & STENMARK, H. 2009. The ESCRT machinery in endosomal sorting of ubiquitylated membrane proteins. *Nature,* 458**,** 445-52.

RAJAWAT, Y., HILIOTI, Z. & BOSSIS, I. 2010. Autophagy: a target for retinoic acids. *Autophagy,* 6**,** 1224-6.

RAUGHT, B., GINGRAS, A. C. & SONENBERG, N. 2001. The target of rapamycin (TOR) proteins. *Proc Natl Acad Sci U S A,* 98**,** 7037-44.

RAVIKUMAR, B., MOREAU, K., JAHREISS, L., PURI, C. & RUBINSZTEIN, D. C. 2010. Plasma membrane contributes to the formation of pre-autophagosomal structures. *Nat Cell Biol,* 12**,** 747-57.

REED, M. B., SALIBA, K. J., CARUANA, S. R., KIRK, K. & COWMAN, A. F. 2000. Pgh1 modulates sensitivity and resistance to multiple antimalarials in *Plasmodium falciparum*. *Nature,* 403**,** 906-9.

REGGIORI, F., SHINTANI, T., NAIR, U. & KLIONSKY, D. J. 2005. Atg9 cycles between mitochondria and the pre-autophagosomal structure in yeasts. *Autophagy,* 1**,** 101-9.

REGGIORI, F., TUCKER, K. A., STROMHAUG, P. E. & KLIONSKY, D. J. 2004a. The Atg1-Atg13 complex regulates Atg9 and Atg23 retrieval transport from the pre-autophagosomal structure. *Dev Cell,* 6**,** 79-90.

REGGIORI, F., WANG, C. W., NAIR, U., SHINTANI, T., ABELIOVICH, H. & KLIONSKY, D. J. 2004b. Early stages of the secretory pathway, but not endosomes, are required for Cvt vesicle and autophagosome assembly in *Saccharomyces cerevisiae*. *Mol Biol Cell,* 15**,** 2189-204.

REHLING, P., MODEL, K., BRANDNER, K., KOVERMANN, P., SICKMANN, A., MEYER, H. E., KUHLBRANDT, W., WAGNER, R., TRUSCOTT, K. N. & PFANNER, N. 2003. Protein insertion into the mitochondrial inner membrane by a twin-pore translocase. *Science,* 299**,** 1747-51.

REININGER, L., GARCIA, M., TOMLINS, A., MULLER, S. & DOERIG, C. 2012. The *Plasmodium falciparum*, Nima-related kinase *Pf*nek-4: a marker for asexual parasites committed to sexual differentiation. *Malar J,* 11**,** 250.

RIGDEN, D. J., MICHELS, P. A. & GINGER, M. L. 2009. Autophagy in protists: Examples of secondary loss, lineage-specific innovations, and the conundrum of remodeling a single mitochondrion. *Autophagy,* 5**,** 784-94.

ROEHL, H., BOSENBERG, M., BLELLOCH, R. & KIMBLE, J. 1996. Roles of the RAM and ANK domains in signaling by the *C. elegans* GLP-1 receptor. *EMBO J,* 15**,** 7002-12.

ROWE, J. A., MOULDS, J. M., NEWBOLD, C. I. & MILLER, L. H. 1997. *P. falciparum* rosetting mediated by a parasite-variant erythrocyte membrane protein and complement-receptor 1. *Nature,* 388**,** 292-5.

RUSSELL, J. S. A. D. W. 2001. *Molecular Cloning A Laboratory Manual,* New York, Cold Spring Harbour Laboratory Press.

RUSSO, I., OKSMAN, A., VAUPEL, B. & GOLDBERG, D. E. 2009. A calpain unique to alveolates is essential in *Plasmodium falciparum* and its knockdown reveals an involvement in pre-S-phase development. *Proc Natl Acad Sci U S A,* 106**,** 1554-9.

SANGLARD, D. 2002. Clinical relevance of mechanisms of antifungal drug resistance in yeasts. *Enferm Infecc Microbiol Clin,* 20**,** 462-9; quiz 470, 479.

SANTOS, J. M., FERGUSON, D. J., BLACKMAN, M. J. & SOLDATI-FAVRE, D. 2011. Intramembrane cleavage of AMA1 triggers *Toxoplasma* to switch from an invasive to a replicative mode. *Science,* 331**,** 473-7.

SCHIFFMAN, M. H., BAUER, H. M., LORINCZ, A. T., MANOS, M. M., BYRNE, J. C., GLASS, A. G., CADELL, D. M. & HOWLEY, P. M. 1991. Comparison of Southern blot hybridization and polymerase chain reaction methods for the detection of human papillomavirus DNA. *J Clin Microbiol,* 29**,** 573-7.

SCHWARTEN, M., STOLDT, M., MOHRLUDER, J. & WILLBOLD, D. 2010. Solution structure of Atg8 reveals conformational polymorphism of the N-terminal domain. *Biochem Biophys Res Commun,* 395**,** 426-31.

SCHWARTZ, L., BROWN, G. V., GENTON, B. & MOORTHY, V. S. 2012. A review of malaria vaccine clinical projects based on the WHO rainbow table. *Malar J,* 11**,** 11.

SCOTT, S. V., HEFNER-GRAVINK, A., MORANO, K. A., NODA, T., OHSUMI, Y. & KLIONSKY, D. J. 1996. Cytoplasm-to-vacuole targeting and autophagy employ the same machinery to deliver proteins to the yeast vacuole. *Proc Natl Acad Sci U S A,* 93**,** 12304-8.

SHANER, N. C., CAMPBELL, R. E., STEINBACH, P. A., GIEPMANS, B. N., PALMER, A. E. & TSIEN, R. Y. 2004. Improved monomeric red, orange and yellow fluorescent proteins derived from *Discosoma sp.* red fluorescent protein. *Nat Biotechnol,* 22**,** 1567-72.

SHANER, N. C., STEINBACH, P. A. & TSIEN, R. Y. 2005. A guide to choosing fluorescent proteins. *Nat Methods,* 2**,** 905-9.

SHEINER, L., DEMERLY, J. L., POULSEN, N., BEATTY, W. L., LUCAS, O., BEHNKE, M. S., WHITE, M. W. & STRIEPEN, B. 2011. A systematic screen to discover and analyze apicoplast proteins identifies a conserved and essential protein import factor. *PLoS Pathog,* 7**,** e1002392.

SHERMAN, I. W. 2005. *Molecular Approaches to Malaria,* Washington, DC., ASM Press American Society for Microbiology.

SHINTANI, T. & KLIONSKY, D. J. 2004. Autophagy in health and disease: a double-edged sword. *Science,* 306**,** 990-5.

SHINTANI, T., MIZUSHIMA, N., OGAWA, Y., MATSUURA, A., NODA, T. & OHSUMI, Y. 1999. Apg10p, a novel protein-conjugating enzyme essential for autophagy in yeast. *EMBO J,* 18**,** 5234-41.

SILVA, F., QUEIROZ, J. A. & DOMINGUES, F. C. 2012. Evaluating metabolic stress and plasmid stability in plasmid DNA production by *Escherichia coli*. *Biotechnol Adv,* 30**,** 691-708.

SILVIE, O., MOTA, M. M., MATUSCHEWSKI, K. & PRUDENCIO, M. 2008. Interactions of the malaria parasite and its mammalian host. *Curr Opin Microbiol,* 11**,** 352-9.

SIMONSEN, A. & TOOZE, S. A. 2009. Coordination of membrane events during autophagy by multiple class III PI3-kinase complexes. *J Cell Biol,* 186**,** 773-82.

SINDEN, R. E., HARTLEY, R. H. & WINGER, L. 1985. The development of *Plasmodium* ookinetes *in vitro*: an ultrastructural study including a description of meiotic division. *Parasitology,* 91 (Pt 2)**,** 227-44.

SINGER, M. & FRISCHKNECHT, F. 2012. Understanding parasite transmission through imaging approaches. *Methods Enzymol,* 506**,** 19-33.

SINGH, S. B., DAVIS, A. S., TAYLOR, G. A. & DERETIC, V. 2006. Human IRGM induces autophagy to eliminate intracellular mycobacteria. *Science,* 313**,** 1438-41.

SLAVIKOVA, S., SHY, G., YAO, Y., GLOZMAN, R., LEVANONY, H., PIETROKOVSKI, S., ELAZAR, Z. & GALILI, G. 2005. The autophagy-associated Atg8 gene family operates both under favourable growth conditions and under starvation stresses in *Arabidopsis* plants. *J Exp Bot,* 56**,** 2839-49.

SMITH, J. D., KYES, S., CRAIG, A. G., FAGAN, T., HUDSON-TAYLOR, D., MILLER, L. H., BARUCH, D. I. & NEWBOLD, C. I. 1998. Analysis of adhesive domains from the A4VAR *Plasmodium falciparum* erythrocyte membrane protein-1 identifies a CD36 binding domain. *Mol Biochem Parasitol,* 97**,** 133-48.

SORBER, K., DIMON, M. T. & DERISI, J. L. 2011. RNA-Seq analysis of splicing in *Plasmodium falciparum* uncovers new splice junctions, alternative splicing and splicing of antisense transcripts. *Nucleic Acids Res,* 39**,** 3820-35.

SPENCER, B., POTKAR, R., TREJO, M., ROCKENSTEIN, E., PATRICK, C., GINDI, R., ADAME, A., WYSS-CORAY, T. & MASLIAH, E. 2009. Beclin 1 gene transfer activates autophagy and ameliorates the neurodegenerative pathology in alpha-synuclein models of Parkinson's and Lewy body diseases. *J Neurosci,* 29**,** 13578-88.

SPORK, S., HISS, J. A., MANDEL, K., SOMMER, M., KOOIJ, T. W., CHU, T., SCHNEIDER, G., MAIER, U. G. & PRZYBORSKI, J. M. 2009. An unusual ERAD-like complex is targeted to the apicoplast of *Plasmodium falciparum*. *Eukaryot Cell,* 8**,** 1134-45.

SRIVASTAVA, A., SINGH, S., DHAWAN, S., MAHMOOD ALAM, M., MOHMMED, A. & CHITNIS, C. E. 2010. Localization of apical sushi protein in *Plasmodium falciparum* merozoites. *Mol Biochem Parasitol,* 174**,** 66-9.

STORM, J., PERNER, J., APARICIO, I., PATZEWITZ, E. M., OLSZEWSKI, K., LLINAS, M., ENGEL, P. C. & MULLER, S. 2011. *Plasmodium falciparum* glutamate

dehydrogenase a is dispensable and not a drug target during erythrocytic development. *Malar J,* 10**,** 193.

STRIEPEN, B., CRAWFORD, M. J., SHAW, M. K., TILNEY, L. G., SEEBER, F. & ROOS, D. S. 2000. The plastid of *Toxoplasma gondii* is divided by association with the centrosomes. *J Cell Biol,* 151**,** 1423-34.

STUDIER, F. W., ROSENBERG, A. H., DUNN, J. J. & DUBENDORFF, J. W. 1990. Use of T7 RNA polymerase to direct expression of cloned genes. *Methods Enzymol,* 185**,** 60-89.

STURM, A., AMINO, R., VAN DE SAND, C., REGEN, T., RETZLAFF, S., RENNENBERG, A., KRUEGER, A., POLLOK, J. M., MENARD, R. & HEUSSLER, V. T. 2006. Manipulation of host hepatocytes by the malaria parasite for delivery into liver sinusoids. *Science,* 313**,** 1287-90.

SU, X., HAYTON, K. & WELLEMS, T. E. 2007. Genetic linkage and association analyses for trait mapping in *Plasmodium falciparum*. *Nat Rev Genet,* 8**,** 497-506.

SUGAWARA, K., SUZUKI, N. N., FUJIOKA, Y., MIZUSHIMA, N., OHSUMI, Y. & INAGAKI, F. 2004. The crystal structure of microtubule-associated protein light chain 3, a mammalian homologue of *Saccharomyces cerevisiae* Atg8. *Genes Cells,* 9**,** 611-8.

SUMMERS, R. L., NASH, M. N. & MARTIN, R. E. 2012. Know your enemy: understanding the role of PfCRT in drug resistance could lead to new antimalarial tactics. *Cell Mol Life Sci,* 69**,** 1967-95.

SUN, Q., FAN, W., CHEN, K., DING, X., CHEN, S. & ZHONG, Q. 2008. Identification of Barkor as a mammalian autophagy-specific factor for Beclin 1 and class III phosphatidylinositol 3-kinase. *Proc Natl Acad Sci U S A,* 105**,** 19211-6.

SUZUKI, K., KIRISAKO, T., KAMADA, Y., MIZUSHIMA, N., NODA, T. & OHSUMI, Y. 2001. The pre-autophagosomal structure organized by concerted functions of APG genes is essential for autophagosome formation. *EMBO J,* 20**,** 5971-81.

TAHERBHOY, A. M., TAIT, S. W., KAISER, S. E., WILLIAMS, A. H., DENG, A., NOURSE, A., HAMMEL, M., KURINOV, I., ROCK, C. O., GREEN, D. R. & SCHULMAN, B. A. 2011. Atg8 transfer from Atg7 to Atg3: a distinctive E1-E2 architecture and mechanism in the autophagy pathway. *Mol Cell,* 44**,** 451-61.

TALEVICH, E., MIRZA, A. & KANNAN, N. 2011. Structural and evolutionary divergence of eukaryotic protein kinases in Apicomplexa. *BMC Evol Biol,* 11**,** 321.

TAMURA, N., OKU, M. & SAKAI, Y. 2010. Atg8 regulates vacuolar membrane dynamics in a lipidation-independent manner in *Pichia pastoris*. *J Cell Sci,* 123**,** 4107-16.

TANIDA, I., MIZUSHIMA, N., KIYOOKA, M., OHSUMI, M., UENO, T., OHSUMI, Y. & KOMINAMI, E. 1999. Apg7p/Cvt2p: A novel protein-activating enzyme essential for autophagy. *Mol Biol Cell,* 10**,** 1367-79.

TANIDA, I., SOU, Y. S., EZAKI, J., MINEMATSU-IKEGUCHI, N., UENO, T. & KOMINAMI, E. 2004. HsAtg4B/HsApg4B/autophagin-1 cleaves the carboxyl termini of three human Atg8 homologues and delipidates microtubule-associated protein light chain 3- and GABAA receptor-associated protein-phospholipid conjugates. *J Biol Chem,* 279**,** 36268-76.

TAWK, L., CHICANNE, G., DUBREMETZ, J. F., RICHARD, V., PAYRASTRE, B., VIAL, H. J., ROY, C. & WENGELNIK, K. 2010. Phosphatidylinositol 3-phosphate, an essential lipid in *Plasmodium*, localizes to the food vacuole membrane and the apicoplast. *Eukaryot Cell,* 9**,** 1519-30.

TILLEY, L., DIXON, M. W. & KIRK, K. 2011. The *Plasmodium falciparum*-infected red blood cell. *Int J Biochem Cell Biol,* 43**,** 839-42.

TONKIN, C. J., KALANON, M. & MCFADDEN, G. I. 2008. Protein targeting to the malaria parasite plastid. *Traffic,* 9**,** 166-75.

TONKIN, C. J., VAN DOOREN, G. G., SPURCK, T. P., STRUCK, N. S., GOOD, R. T., HANDMAN, E., COWMAN, A. F. & MCFADDEN, G. I. 2004. Localization of organellar proteins in *Plasmodium falciparum* using a novel set of transfection vectors and a new immunofluorescence fixation method. *Mol Biochem Parasitol,* 137**,** 13-21.

TOOZE, S. A. & YOSHIMORI, T. 2010. The origin of the autophagosomal membrane. *Nat Cell Biol,* 12**,** 831-5.

TRA, T., GONG, L., KAO, L. P., LI, X. L., GRANDELA, C., DEVENISH, R. J., WOLVETANG, E. & PRESCOTT, M. 2011. Autophagy in human embryonic stem cells. *PLoS One,* 6**,** e27485.

TRAGER, W. & JENSEN, J. B. 1976. Human malaria parasites in continuous culture. *Science,* 193**,** 673-5.

TRANG, D. T., HUY, N. T., KARIU, T., TAJIMA, K. & KAMEI, K. 2004. One-step concentration of malarial parasite-infected red blood cells and removal of contaminating white blood cells. *Malar J,* 3**,** 7.

TUTEJA, R., PRADHAN, A. & SHARMA, S. 2008. *Plasmodium falciparum* signal peptidase is regulated by phosphorylation and required for intra-erythrocytic growth. *Mol Biochem Parasitol,* 157**,** 137-47.

VAID, A., RANJAN, R., SMYTHE, W. A., HOPPE, H. C. & SHARMA, P. 2010. *Pf*PI3K, a phosphatidylinositol-3 kinase from *Plasmodium falciparum,* is exported to the host erythrocyte and is involved in hemoglobin trafficking. *Blood,* 115**,** 2500-7.

VAN DOOREN, G. G., MARTI, M., TONKIN, C. J., STIMMLER, L. M., COWMAN, A. F. & MCFADDEN, G. I. 2005. Development of the endoplasmic reticulum, mitochondrion and apicoplast during the asexual life cycle of *Plasmodium falciparum*. *Mol Microbiol,* 57**,** 405-19.

VAN DOOREN, G. G., REIFF, S. B., TOMOVA, C., MEISSNER, M., HUMBEL, B. M. & STRIEPEN, B. 2009. A novel dynamin-related protein has been recruited for apicoplast fission in Toxoplasma gondii. *Curr Biol,* 19**,** 267-76.

VAN DOOREN, G. G., STIMMLER, L. M. & MCFADDEN, G. I. 2006. Metabolic maps and functions of the *Plasmodium* mitochondrion. *FEMS Microbiol Rev,* 30**,** 596-630.

VAN DOOREN, G. G., SU, V., D'OMBRAIN, M. C. & MCFADDEN, G. I. 2002. Processing of an apicoplast leader sequence in *Plasmodium falciparum* and the identification of a putative leader cleavage enzyme. *J Biol Chem,* 277**,** 23612-9.

VAN SCHALKWYK, D. A., CHAN, X. W., MISIANO, P., GAGLIARDI, S., FARINA, C. & SALIBA, K. J. 2010. Inhibition of *Plasmodium falciparum* pH regulation by small molecule indole derivatives results in rapid parasite death. *Biochem Pharmacol,* 79**,** 1291-9.

VANCE, J. E. 2008. Phosphatidylserine and phosphatidylethanolamine in mammalian cells: two metabolically related aminophospholipids. *J Lipid Res,* 49**,** 1377-87.

VARSHAVSKY, A. 2012. The ubiquitin system, an immense realm. *Annu Rev Biochem,* 81**,** 167-76.

VAUGHAN, A. M., O'NEILL, M. T., TARUN, A. S., CAMARGO, N., PHUONG, T. M., ALY, A. S., COWMAN, A. F. & KAPPE, S. H. 2009. Type II fatty acid synthesis is essential only for malaria parasite late liver stage development. *Cell Microbiol,* 11**,** 506-20.

VELLAI, T. & TAKACS-VELLAI, K. 2010. Regulation of protein turnover by longevity pathways. *Adv Exp Med Biol,* 694**,** 69-80.

VELLAI, T., TAKACS-VELLAI, K., SASS, M. & KLIONSKY, D. J. 2009. The regulation of aging: does autophagy underlie longevity? *Trends Cell Biol,* 19**,** 487-94.

VERMES, A., GUCHELAAR, H. J. & DANKERT, J. 2000. Flucytosine: a review of its pharmacology, clinical indications, pharmacokinetics, toxicity and drug interactions. *J Antimicrob Chemother,* 46**,** 171-9.

VOLKMAN, S. K., NEAFSEY, D. E., SCHAFFNER, S. F., PARK, D. J. & WIRTH, D. F. 2012. Harnessing genomics and genome biology to understand malaria biology. *Nat Rev Genet,* 13**,** 315-28.

WALLER, R. F., KEELING, P. J., DONALD, R. G., STRIEPEN, B., HANDMAN, E., LANG-UNNASCH, N., COWMAN, A. F., BESRA, G. S., ROOS, D. S. & MCFADDEN, G. I. 1998. Nuclear-encoded proteins target to the plastid in *Toxoplasma gondii* and *Plasmodium falciparum*. *Proc Natl Acad Sci U S A,* 95**,** 12352-7.

WALLER, R. F. & MCFADDEN, G. I. 2005. The apicoplast: a review of the derived plastid of apicomplexan parasites. *Curr Issues Mol Biol,* 7**,** 57-79.

WALLER, R. F., REED, M. B., COWMAN, A. F. & MCFADDEN, G. I. 2000. Protein trafficking to the plastid of *Plasmodium falciparum* is via the secretory pathway. *EMBO J,* 19**,** 1794-802.

WEI, H., THERRIEN, C., BLANCHARD, A., GUAN, S. & ZHU, Z. 2008. The Fidelity Index provides a systematic quantitation of star activity of DNA restriction endonucleases. *Nucleic Acids Res,* 36**,** e50.

WEICHHART, T. 2012. Mammalian target of rapamycin: a signaling kinase for every aspect of cellular life. *Methods Mol Biol,* 821**,** 1-14.

WEIDBERG, H., SHVETS, E., SHPILKA, T., SHIMRON, F., SHINDER, V. & ELAZAR, Z. 2010. LC3 and GATE-16/GABARAP subfamilies are both essential yet act differently in autophagosome biogenesis. *EMBO J,* 29**,** 1792-802.

WHO 2011. Eliminating Malaria: Learning From the Past, Looking Ahead.

WIESNER, J., REICHENBERG, A., HEINRICH, S., SCHLITZER, M. & JOMAA, H. 2008. The plastid-like organelle of apicomplexan parasites as drug target. *Curr Pharm Des,* 14**,** 855-71.

WILLIAMS, R. A., SMITH, T. K., CULL, B., MOTTRAM, J. C. & COOMBS, G. H. 2012. ATG5 Is Essential for ATG8-Dependent Autophagy and Mitochondrial Homeostasis in *Leishmania major*. *PLoS Pathog,* 8**,** e1002695.

WILLIAMS, R. A., WOODS, K. L., JULIANO, L., MOTTRAM, J. C. & COOMBS, G. H. 2009. Characterization of unusual families of ATG8-like proteins and ATG12 in the protozoan parasite *Leishmania major*. *Autophagy,* 5**,** 159-72.

WILSON, R. J., DENNY, P. W., PREISER, P. R., RANGACHARI, K., ROBERTS, K., ROY, A., WHYTE, A., STRATH, M., MOORE, D. J., MOORE, P. W. & WILLIAMSON, D. H. 1996. Complete gene map of the plastid-like DNA of the malaria parasite *Plasmodium falciparum*. *J Mol Biol,* 261**,** 155-72.

WIRTH, D. F. 2002. Biological revelations. *Nature,* 419**,** 495-6.

WISSING, F., SANCHEZ, C. P., ROHRBACH, P., RICKEN, S. & LANZER, M. 2002. Illumination of the malaria parasite *Plasmodium falciparum* alters intracellular pH. Implications for live cell imaging. *J Biol Chem,* 277**,** 37747-55.

WONG, E. & CUERVO, A. M. 2010. Integration of clearance mechanisms: the proteasome and autophagy. *Cold Spring Harb Perspect Biol,* 2**,** a006734.

WOODS, K. L. 2009. *Regulators of Autophagy in Leishmania major*. PhD Thesis, University of Glasgow.

WU, Y., SIFRI, C. D., LEI, H. H., SU, X. Z. & WELLEMS, T. E. 1995. Transfection of *Plasmodium falciparum* within human red blood cells. *Proc Natl Acad Sci U S A,* 92**,** 973-7.

WU, Y. T., TAN, H. L., SHUI, G., BAUVY, C., HUANG, Q., WENK, M. R., ONG, C. N., CODOGNO, P. & SHEN, H. M. 2010. Dual role of 3-methyladenine in modulation of autophagy via different temporal patterns of inhibition on class I and III phosphoinositide 3-kinase. *J Biol Chem,* 285**,** 10850-61.

XIA, H. G., ZHANG, L., CHEN, G., ZHANG, T., LIU, J., JIN, M., MA, X., MA, D. & YUAN, J. 2010. Control of basal autophagy by calpain1 mediated cleavage of ATG5. *Autophagy,* 6**,** 61-6.

XIE, Z., NAIR, U. & KLIONSKY, D. J. 2008. Atg8 controls phagophore expansion during autophagosome formation. *Mol Biol Cell,* 19**,** 3290-8.

YAMADA, Y., SUZUKI, N. N., HANADA, T., ICHIMURA, Y., KUMETA, H., FUJIOKA, Y., OHSUMI, Y. & INAGAKI, F. 2007. The crystal structure of Atg3, an autophagy-related ubiquitin carrier protein (E2) enzyme that mediates Atg8 lipidation. *J Biol Chem,* 282**,** 8036-43.

YAMAGUCHI, M., NODA, N. N., NAKATOGAWA, H., KUMETA, H., OHSUMI, Y. & INAGAKI, F. 2010. Autophagy-related protein 8 (Atg8) family interacting motif in Atg3 mediates the Atg3-Atg8 interaction and is crucial for the cytoplasm-to-vacuole targeting pathway. *J Biol Chem,* 285**,** 29599-607.

YAMAMOTO, A., TAGAWA, Y., YOSHIMORI, T., MORIYAMA, Y., MASAKI, R. & TASHIRO, Y. 1998. Bafilomycin A1 prevents maturation of autophagic vacuoles by inhibiting fusion between autophagosomes and lysosomes in rat hepatoma cell line, H-4-II-E cells. *Cell Struct Funct,* 23**,** 33-42.

YANG, Z. & KLIONSKY, D. J. 2009. An overview of the molecular mechanism of autophagy. *Curr Top Microbiol Immunol,* 335**,** 1-32.

YEH, E. & DERISI, J. L. 2011. Chemical rescue of malaria parasites lacking an apicoplast defines organelle function in blood-stage *Plasmodium falciparum*. *PLoS Biol,* 9**,** e1001138.

YEOH, S., O'DONNELL, R. A., KOUSSIS, K., DLUZEWSKI, A. R., ANSELL, K. H., OSBORNE, S. A., HACKETT, F., WITHERS-MARTINEZ, C., MITCHELL, G. H., BANNISTER, L. H., BRYANS, J. S., KETTLEBOROUGH, C. A. & BLACKMAN, M. J. 2007. Subcellular discharge of a serine protease mediates release of invasive malaria parasites from host erythrocytes. *Cell,* 131**,** 1072-83.

YOSHIMORI, T. 2004. Autophagy: a regulated bulk degradation process inside cells. *Biochem Biophys Res Commun,* 313**,** 453-8.

YU, M., KUMAR, T. R., NKRUMAH, L. J., COPPI, A., RETZLAFF, S., LI, C. D., KELLY, B. J., MOURA, P. A., LAKSHMANAN, V., FREUNDLICH, J. S., VALDERRAMOS, J. C., VILCHEZE, C., SIEDNER, M., TSAI, J. H., FALKARD, B., SIDHU, A. B., PURCELL, L. A., GRATRAUD, P., KREMER, L., WATERS, A. P., SCHIEHSER, G., JACOBUS, D. P., JANSE, C. J., AGER, A., JACOBS, W. R., JR., SACCHETTINI, J. C., HEUSSLER, V., SINNIS, P. & FIDOCK, D. A. 2008. The fatty acid biosynthesis enzyme FabI plays a key role in the development of liver-stage malarial parasites. *Cell Host Microbe,* 4**,** 567-78.

YUAN, H., BARNES, K. R., WEISSLEDER, R., CANTLEY, L. & JOSEPHSON, L. 2007. Covalent reactions of wortmannin under physiological conditions. *Chem Biol,* 14**,** 321-8.

ZHANG, X. & STUDIER, F. W. 1997. Mechanism of inhibition of bacteriophage T7 RNA polymerase by T7 lysozyme. *J Mol Biol,* 269**,** 10-27.

ZHANG, Y. 2008. I-TASSER server for protein 3D structure prediction. *BMC Bioinformatics,* 9**,** 40.

ZHANG, Y. & SKOLNICK, J. 2005. TM-align: a protein structure alignment algorithm based on the TM-score. *Nucleic Acids Res,* 33**,** 2302-9.

ZHONG, Y., WANG, Q. J., LI, X., YAN, Y., BACKER, J. M., CHAIT, B. T., HEINTZ, N. & YUE, Z. 2009. Distinct regulation of autophagic activity by Atg14L and Rubicon associated with Beclin 1-phosphatidylinositol-3-kinase complex. *Nat Cell Biol,* 11**,** 468-76.